Synthesis of GnRH and Somatostatin Cytotoxic Drug Conjugates

Sabine Schuster

PhD thesis

Supervisor

Prof. Dr. Gábor Mező

Head of the Research Group of Peptide Chemistry

Doctoral School of Chemistry

Head of Doctoral School: Dr. Attila Császár

Doctoral Program:

Synthetic Chemistry, Materials Science and Biomolecular Chemistry

Director of the Program: Prof. Dr. András Perczel

Department of Organic Chemistry

MTA-ELTE Research Group of Peptide Chemistry

Eötvös Loránd University, Faculty of Science

Budapest, 2019

»Wir müssen lernen, magische Kugeln zu gießen, die gleichsam wie Zauberkugeln des Freischützen nur die Krankheitserreger treffen.«

Paul Ehrlich (1854 – 1915)

List of abbreviations

All applied three-letter and one-letter codes for α-amino acids are in agreement with the recommendations from the IUPAC-IUB Commission on Biochemical Nomenclature.

5-FU	fluorouracil
Aaa	amino acid
Ab	antibody
ADC	antibody drug conjugate
AcOH	acetic acid
AM-resin	aminomethyl-polystyrene resin
Aoa	aminooxyacetic acid
>=Aoa	isopropylidene protected Aoa
Boc	*tert*-butyloxycarbonyl
Boc_2O	di-*tert*-butyl dicarbonate (Boc-anhydride)
Bu	butyryl
cAMP	cyclic adenosine monophosphate
CLSM	confocal laser scanning microscopy
CPP	cell penetrating peptide
Dab	L-1,4-diaminobutyric acid
DAPI	4′,6-diamidine-2-phenylindole dihydrochloride
Dau	daunorubicin
DBU	1,8-diazabicyclo[5.4.0]undec-7-ene
DCC	*N,N'*-dicyclohexylcarbodiimide
DCM	dichloromethane
Dde	1-(4,4-dimethyl-2,6-dioxocyclohex-1-ylidene)ethyl
DDS	drug delivery system
DIC	*N,N'*-diisopropylcarbodiimide
DIPEA	*N,N*-diisopropylethylamine
DM-1	mertansine, N_2'-deacetyl-N_2'-(3-mercapto-1-oxopropyl)-maytansine
DME	1,2-dimethoxyethane
DMEM	Dulbecco's Modified Eagle Medium
DMF	*N,N*-dimethylformamide
DMSO	dimethyl sulfoxide
DOTA	1,4,7,10-tetraazacyclododecane-1,4,7,10-tetraacetic acid

DOTATE	1,4,7,10-tetraazacyclododecane-1,4,7,10-tetraacetic acetyl octreotate
Dox	doxorubicin
DTPA	pentetic acid, diethylenetriaminepentaacetic acid
DTT	1,4-DL-dithiothreitol
DTX	docetaxel
E2	17β-estradiol
EA	ethylamide
EBRT	external beam radiotherapy
ECD	electronic circular dichroism
EDT	1,2-ethanedithiol
EDTA	ethylenediaminetetraacetic acid
EEDQ	2-ethoxy-2*H*-quinoline-1-carboxylic acid ethyl ester
EG_2	diethylene glycol
EGF	epidermal growth factor
EMC	6-maleimidohexanoyl
eq	equivalent
ER	estrogen receptor
ESI	electrospray ionization
EtOAc	ethyl acetate
Et_2O	diethyl ether
EtOH	ethanol
FACS	fluorescence-activated cell sorting
FAM	5(6)-carboxyfluorescein
FBS	fetal bovine serum
FDA	Food and Drug Administration
Fmoc	9-fluorenylmethoxycarbonyl
FSH	follicle stimulating hormone
GEP-NET	gastroenteropancreatic neuroendocrine tumors
GH	growth hormone
Glp	pyroglutamic acid
GnRH-III	gonadotropin releasing hormone-III
GnRH-R	gonadotropin releasing hormone-receptor
GPCR	G protein-coupled receptor
GSH	glutathione

HATU	1-[bis(dimethylamino)methylene]-1-*H*-1,2,3-triazolo[4,5-*b*]pyridinium 3-oxid hexafluorophosphate
HCl	hydrochloric acid
HEPES	4-(2-hydroxyethyl)-1-piperazineethanesulfonic acid
HOBt	1-hydroxybenzotriazole hydrate
HOSu	*N*-hydroxysuccinimide
HRP	horseradish peroxidase
HMPI	HEPES-buffered medium RPMI-1640
IC_{50}	half maximal inhibitory concentration
IGF	insulin-like growth factors
LH	luteinizing hormone
LC-MS	liquid chromatography-mass spectrometry
mAb	monoclonal antibody
MBHA	4-methylbenzhydrylamine
MeCN	acetonitrile
MeOH	methanol
MMAE	monomethyl auristatin E
MS	mass spectrometry
MTT	3-(4,5-dimethylthiazol-2-yl)-2,5-diphenyltetrazolium bromide
Mtt	4-methyltrityl
MTX	methotrexate
NCD	noncommunicable disease
NEAA	non-essential amino acids
NSCLC	non-small cell lung cancer
OCT	octreotide
OOI	National Institute of Oncology (Országos Onkológiai Intézet)
OtBu	*tert*-butyl ester
P(VP-co-MA)	poly(vinylpyrrolidone-co-maleic acid)
PABC	*para*-aminobenzyloxycarbonyl
PAB-OH	4-aminobenzyl alcohol, *para*- aminobenzyl alcohol
PBS	phosphate buffered saline
Pcp	pentachlorophenyl
PDA	pancreatic ductal adenocarcinoma
PEG	polyethylene glycol

Pnp	*para*-nitrophenyl
PTX	paclitaxel
PVDP	polyvinylidene difluoride
pyDau	2-pyrrolino-daunorubicine
RP-HPLC	reversed-phase high-performance liquid chromatography
RMPI	Roswell Park Memorial Institute
RT	room temperature
R_t	retention time
sat.	saturated
SMCC	*N*-succinimidyl-4-(*N*-maleimidomethyl)-cyclohexane-1-carboxylate
SMDC	small molecule drug conjugate
SDS	sodium dodecyl sulfate
SPPS	solid phase peptide synthesis
SST	somatostatin
SSTR	somatostatin receptor
TBS	Tris buffered saline
TBST	Tris buffered saline with 0.1% Tween 20
tBu	*tert*-butyl
TCEP	tris-(2-carboxyethyl)-phosphine
T-DM1	Trastuzumab emtansine
TEMED	*N*,*N*,*N*',*N*'-tetramethyl ethylenediamine
Thr-ol	L-threoninol
TFA	trifluoroacetic acid
THF	tetrahydrofuran
TNBC	triple negative breast cancer
Tic	1,2,3,4-tetrahydroisoquinoline-3-carboxylic acid
Tis	triisopropylsilane
Tris	tris-(hydroxymethyl)-aminomethane
Trt	triphenylmethyl/trityl
VEGF	vascular endothelial growth factor

Table of Contents

1. Introduction

1.1 Cancer

In the last century, the average life expectancy was rapidly increasing and even between 2000 and 2016, the median lifespan was enhanced by 5.5 years. Negatively associated with the higher life expectancy is the growing incidence of noncommunicable diseases (NCDs) which are responsible for 71% of all deaths globally [1]. Next to cardiovascular diseases, cancer is the second leading cause of death worldwide, whereby 18.1 million new cases and 9.6 million deaths were estimated to account in 2018 [2]. The rising burdens of cancer in the developing world are not only caused by population growth and ageing, but also environmental factors and lifestyle, reproductive and hormonal factors, as well as infections play an important role [3–6]. The most common types of cancer in men are lung, prostate, colorectal, stomach and liver cancer, while in women breast, colorectal, lung, cervix and thyroid cancer occur most frequently [2]. Cancer in general can arise in any part of the body and thus, comprise a large group of diseases. All kinds of cancer are defined by a rapid and abnormal cell growth with the potential to invade surrounding tissue and to spread to other organs [2,7]. According to Hanahan and Weinberg, eight hallmarks of cancer and two 'enabling characteristics' have been identified which facilitate tumor growth and metastatic dissemination (**Figure 1**) [8,9]. The acquisition of these distinctive and complementary biological capabilities is required for the malignant

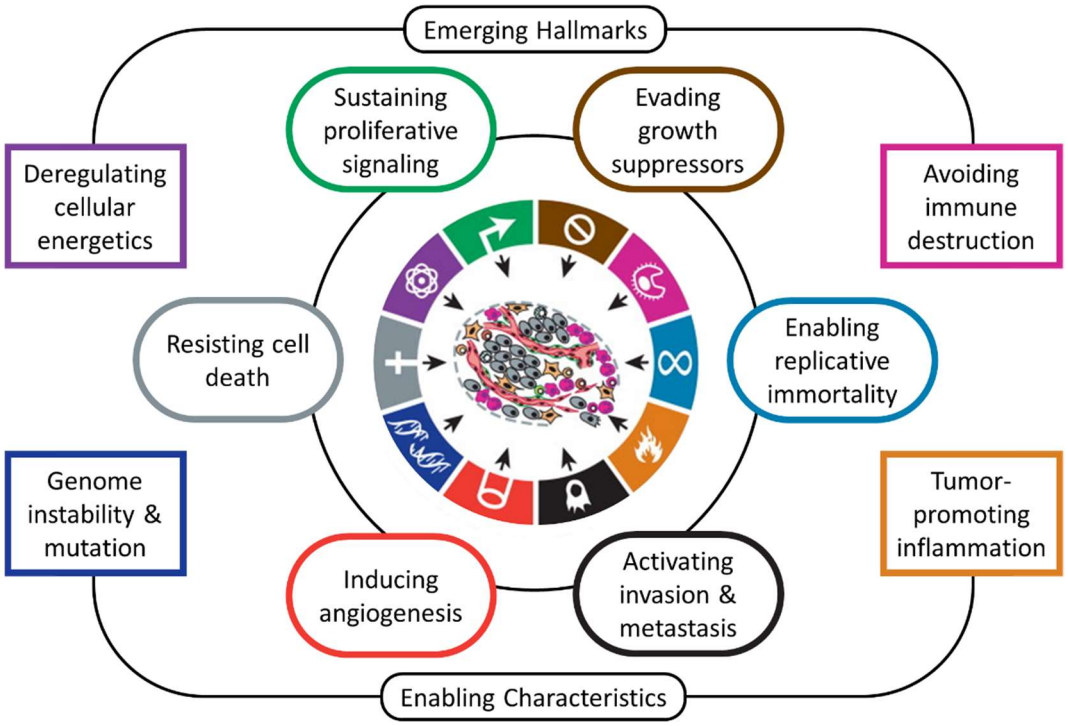

Figure 1. The ten hallmarks of cancer adapted from Hanahan and Weinberg [8,9], comprising six biological capabilities, two emerging hallmarks of potential generality and two characteristics which enable cancer.

transformation of normal cells. The two enabling characteristics which have been described facilitate these acquisitions during the multistep development of human tumors. One is genome instability which is responsible for random mutations, such as chromosomal rearrangement [9–12], the other characteristic is tumor-promoting inflammation which is driven by the immune system and involves the inflammatory state of premalignant or malignant lesion [9,13–18]. Moreover, it is assumed that each core hallmark is regulated by a number of parallel signaling pathways which elucidate the complexities of neoplastic diseases and might be partially responsible for the ability of tumors to survive with residual function permitting renewed tumor growth and clinical relapse [9,19]. Drugs that interfere with at least one of the hallmark capabilities are considered as promising candidates for cancer therapy and numerous drug candidates with different molecular targets and mode of actions are under research.

1.2 Cancer therapy

In order to treat and cure cancerous diseases, a variety of treatment options and therapies have been investigated. Since the malignant transformation of cells is not reversible, the removal and/or destruction of tumorous tissue represents the basis of cancer treatment. Classical options include surgical resection, radiation therapy, chemotherapy and hormone therapy [20–24]. Already at the end of the 19th century, the first milestone in cancer therapy was achieved by William S. Halsted, who pioneered surgical approaches for cancer by establishing radical mastectomy to cure breast cancer and to reduce recurrence [25]. The removal of both, the tumor and the surrounding tissue, is still an important treatment option for cancer and the most effective treatment of localized primary tumors [26]. Nowadays, a broader range of innovative therapies is available including targeted therapy, immunotherapy, bone marrow transplantation and gene therapy [26–38]. Considering that tumorous diseases possess a high diversity and differ strongly from each other, depending on their tissue origin, cell types and genetic profile, individual specific treatment regimes and combined therapies are often applied according to the kind of tumor, the stage of cancer and specific genetic feature of the tumor [39–41].

1.2.1. Radiation therapy

The next milestone subsequent to cancer surgery was the successful use of radiation therapy to treat cancer. Already five years after Marie Curie's discovery of radium in 1898, it was used to treat two Russian patients with basal cell carcinoma of the skin, resulting in an eradication of the disease in both patients [42,43], while the first histological

cure of a similar skin cancer from X-ray treatment was already documented in 1899 [43,44]. Since that moment, radiation therapy represents one of the main treatment options for cancer. In general, there are two ways to apply radiation to the cancerous tissue. The most common approach in clinics is the use of external beam radiotherapy (EBRT) which is delivered from the outside of the body to the location of the tumor by using high energy rays, like photon or proton beams [24,45–47]. Another treatment option is internal radiation or brachytherapy which is delivered from inside the body by radioactive sources. Brachytherapy has been already used since the early 20th century and although its application became less common with the advanced progress in EBRT, this treatment modality has benefited from technological advances and is particularly used to treat prostate and cervical cancer due to its exceptional effectiveness [48,49]. In the last decades, radiation therapy techniques improved significantly which was mainly caused by advances in imaging techniques, computerized treatment planning systems and the improved understanding of radiobiology and radiation therapy [23,24,50–52]. According to the rapid progress in this field, a variety of radiation therapy techniques are available nowadays, such as linear accelerators, 3-dimensional conformal radiotherapy, proton therapy, image guided radiation therapy, stereotactic body radiation therapy, and intensity modulated radiation therapy [24,53]. Due to its high efficiency and the immense technical advances, nearly half of all cancer patients receive radiation therapy, whereby it is often used in combination with other treatment strategies, such as surgery, immunotherapy and chemotherapy [26,54–58].

1.2.2. Chemotherapy

The term chemotherapy was coined and initiated in the beginning of the last century by a German chemist named Paul Ehrlich who is often considered as ‘the founder of chemotherapy’ [21,59–61]. His idea was the use of chemical substances or substances endowed with chemical groups which provide a pharmacologic or toxicologic effect at a distinct part of the body to treat a certain disease [59,60]. Another important achievement of his work was his theory of a ‘magic bullet’, a drug which specifically attacks a particular pathogen without harming healthy/host cells. Initially, he attempted this concept on infectious diseases and his first magic bullet (Salvarsan) provided the first effective treatment for syphilis until penicillin was discovered [62–64]. In general, Paul Ehrlich presumed that his idea of a ‘magic bullet’ can be also applied to other kinds of pathogens also to cancer and his accomplishments provide the fundament of a new era of anticancer therapies.

A selection of historical and commonly used chemotherapeutics is shown in **Figure 2**. The first remission of a cancerous disease by administration of a synthetic compound was reported by Sidney Faber in 1948, who treated children with acute leukemia by intramuscular injection of the folic acid antagonist aminopteroylglutamic acid (aminopteine) [65]. This achievement was facilitated by the observation that the injection of folic acid conjugates lead to an 'acceleration phenomenon' in the leukemic process and the following conclusion that antimetabolic drugs with structural similarity might cause blocking of the processes [65,66]. Another folic acid analogue which was also developed for the treatment of acute leukemia is methotrexate (MTX, also amethopterin or 4-amino-10-methyl-pteroylglutamic acid) [67]. Initially, MTX has been approved by the Food and Drug Administration (FDA) for the treatment of served, recalcitrant, disabling psoriasis in 1972 [68]. Later on, an additional approval was granted for its use in malignant neoplastic diseases, such as acute lymphoblastic leukemia, non-Hodgkin lymphoma, gestational choriocarcinoma, but also head and neck, breast and lung cancers [68–70].

In 1949, the FDA approved nitrogen mustard (mustine, chlormethine, mechlorethamine) as the first chemotherapeutical drug. Nitrogen mustard, which was originally developed as a weapon gas, was used for the treatment of non-Hodgkin lymphoma [71,72]. The cytotoxic effect is based on its ability to modify DNA by guanine alkylation, which led to the development of several related alkylating compounds, such as chlorambucil and cisplatin [73–75].

Apart from alkylating agents, different strategies have been investigated causing inhibition of DNA replication. One approach is the application of DNA unit analogs. The first candidate of the new class of tumor inhibiting compounds, 5-fluorouracil (5-FU) has been described already four years after the discovery of the double-helical structure of DNA by James Watson and Francis Crick in 1953 [76,77]. This pyrimidine antimetabolite possesses different modes of action including the disruption of RNA processing and functions by incorporation into RNA and DNA and the depletion of thymidine triphosphate (TTP) by inhibition of the thymidylate synthase [78]. 5-FU is widely used for the treatment of cancer, particularly for colorectal cancer, where it is often used in combination with other anticancer drugs, like MTX or cisplatin [79]. Another efficient DNA unit surrogate is gemcitabine, a cytidine analog which is used for the treatment of various carcinomas, and it is the standard chemotherapy for patients with advanced pancreatic cancer [80–82].

Furthermore, another group of chemotherapeutics has been discovered that affect DNA

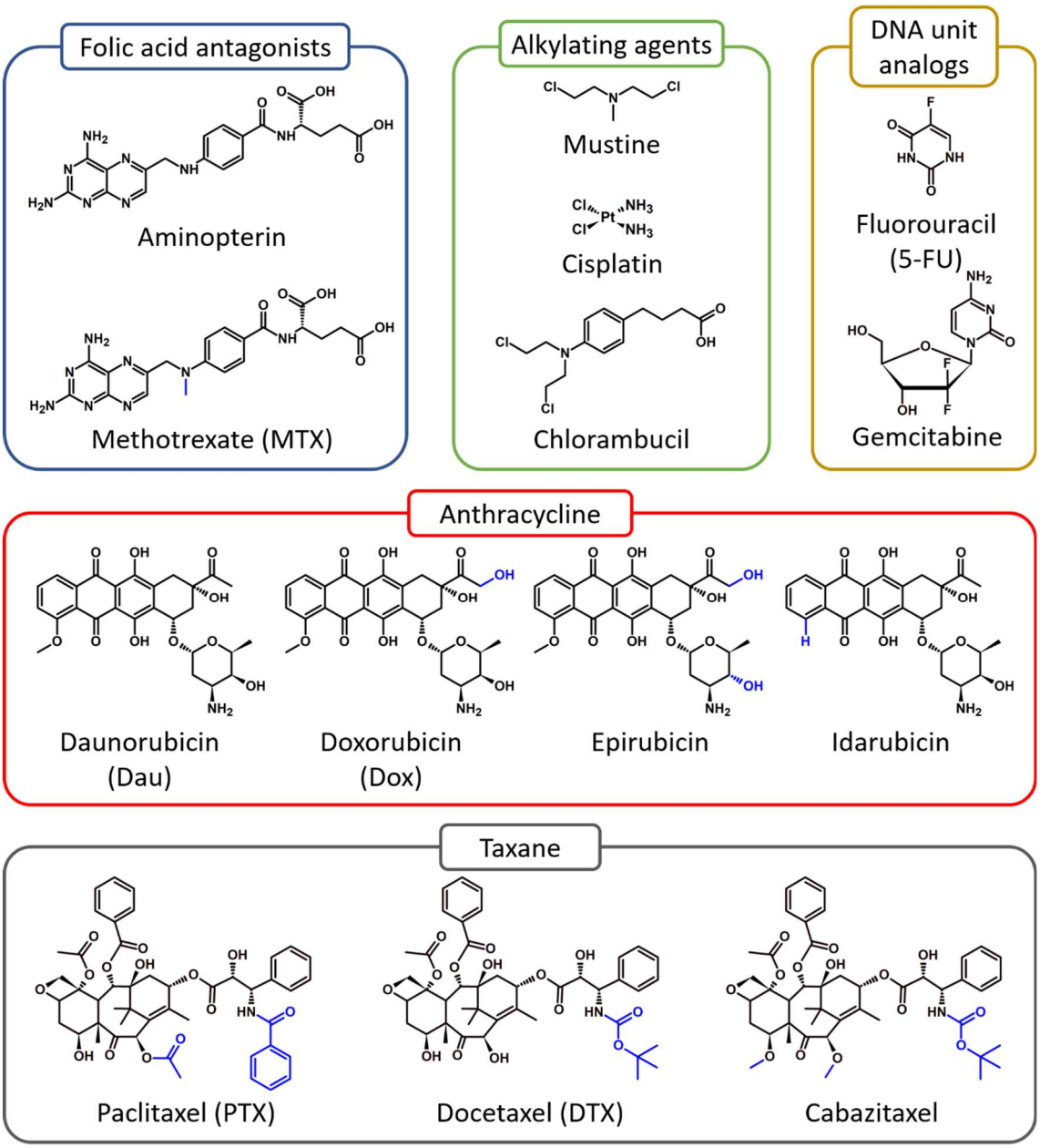

Figure 2. Selection of historical and common chemotherapeutics.

replication, called anthracyclines. The first discovered anthracycline was daunorubicin (Dau) in the early 1960, followed by its 14-hydroxyl derivative doxorubicin (Dox, Andramycin®). Both drugs were isolated from *Streptomyces peucetius* and exhibit a strong antitumor activity by inhibiting protein biosynthesis and DNA replication *via* intercalation between DNA bases (G and C) [83]. Dox and Dau were granted FDA approval in the 1970th, whereby Dox is commonly applied in a broad range of malignancies, including leukemia, lymphomas and breast cancer, while Dau is mainly used to treat acute myelogenous leukemia and acute lymphocytic leukemia [84]. Due to the great success of Dox and Dau for chemotherapy, a huge variety of anthracycline analogs have been produced, while only epirubicin and idarubicin gained clinical relevance [84,85].

In the beginning of the 1990s, a new family of highly efficient anticancer substances, called taxanes, gained importance in clinical cancer treatment [86]. The first discovered member of this group was paclitaxel (PTX, Taxol®) which is a naturally derived substance, isolated from the bark of the western yew tree (*Taxus brevifolia*) [84,86]. PTX is a widely used treatment option for malignant diseases, like head and neck, ovarian, breast and lung cancers [86]. Moreover, it is also often used in combination with other anticancer dugs, for instance together with gemcitabine as first-line therapy of pancreatic adenocarcinomas [81,87–90]. A semi-synthetic analog of PTX is docetaxel (DTX, Taxotere®) which is used, like PTX, for the treatment of various cancer diseases, including advanced breast cancer, non-small cell lung, prostate, gastric and head and neck cancers [84]. The activity of PTX and DTX is based on their high tubulin binding affinity which promotes the formation of excessively stable microtubules and inhibits their disassembly [91]. The second generation taxane, cabazitaxel possesses a similar mechanism of action, but in contrast to PTX and DTX, it is more effective in multidrug-resistant tumor cells and provides the ability to penetrate the blood–brain barrier *in vivo* [92,93]. Due to the promising results of clinical phase III on advanced prostate cancer, it has been approved in 2010 for the treatment of hormone-refractory prostate cancer [92,93]. In the last decades, chemotherapy has been developed continuously, and although there are many novel treatment options, it still plays a key role. Today, single-agent therapy occurs very rarely, because of the heterogeneity of cell chemosensitivity within a single cancer. To overcome this problem, various anticancer drugs are commonly used in combination.

1.2.3. Hormone therapy

Considering that the growth of some types of malignancies strongly depend on the presence of certain hormones, hormonal cancer therapy offers another effective option to treat cancer. Commonly, hormone therapy is applied to tumors of the reproductive system, like breast, ovarian and prostate cancer. The impact of hormones on cancerous diseases has been already demonstrated in the end of the 19th century, when oophorectomy was performed to treat breast cancer in women [94]. Nowadays, the application of drugs which prevent the production of certain hormones or inhibit their action are much more common. In breast cancer therapy, aromatase inhibitors (AIs) and selective estrogen receptor modulators (SERM), like tamoxifen are frequently used (**Figure 3**) [27,29]. Tamoxifen possesses a dual agonist-antagonist activity and acts by binding to estrogen receptors (ER) which prevent the binding of coactivators by

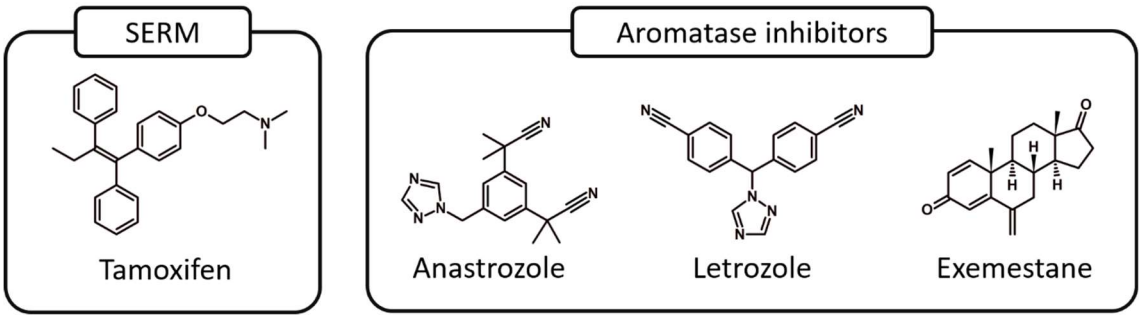

Figure 3. Selection of selective estrogen receptor modulators (SERM) and aromatase inhibitors (AIs) for hormone therapy of breast cancer.

conformational change of the receptor. This leads to an impediment of estrogen mediated transcriptional activity [95]. Another treatment option for post-menopausal and non-pregnant women, is the application of AIs, which lead to a subsequent decrease of estradiol levels by preventing the peripheral conversion of androgens to estrogens. New generation AIs, such as anastrozole, letrozole and exemestane, have rapidly become first line therapy, since they are more efficient than tamoxifen, and their lack of agonistic activity leads to a reduced risk for thrombotic or endometrial cancer [26,27].

1.2.3.1. Gonadotropin-releasing hormone (GnRH) analogs

Another sufficient hormonal treatment alternative, in particular for breast and prostate cancer, is the administration of gonadotropin-releasing hormone (GnRH) analogs that cause a central endocrine ablation. The natural GnRH, also known as GnRH-I or luteinizing hormone releasing hormone (LH-RH), regulates the production of sex steroids by inducing a hormonal cascade, and was discovered by Andrew V. Schally and coworkers in 1971 [96]. This hormonal decapeptide (Glp-His-Trp-Ser-Tyr-Gly-Leu-Arg-Pro-Gly-NH_2, where Glp is pyroglutamic acid) is synthesized in specialized neurons of the hypothalamus and released in the hypophysial portal bloodstream by pulsatile secretion [97]. Hence, it reaches the anterior pituitary, where it binds to special G-protein-coupled seven-transmembrane receptors (GPCRs) called gonadotropin-releasing hormone-receptors (GnRH-R). This stimulates the production of luteinizing hormone (LH) and follicle stimulating hormone (FSH). The release of these gonadotropins triggers gametogenesis, as well as the secretion of androgens and estrogens. In case of GnRH-based cancer therapy, this hormonal signaling pathway is disrupted, whereby two different strategies can be applied. Initially, it has been demonstrated that the continuous exposure and high doses of human GnRH-I or its agonists result in the suppression of gonadotropin and sex-steroid secretion by desensitization of gonadotropic cells and the downregulation of pituitary GnRH receptors. Considering that the *in vivo* half-life of

GnRH-I is very short and varies between 2-5 minutes, synthetic GnRH agonists have been developed which possess a higher stability in the circulation [98,99]. Studies on the primary amino acid sequence of naturally occurring GnRHs revealed that the residues 5 till 8 are quite variable, while the *C*-and the *N*-terminal regions of GnRH are highly conserved in vertebrates [100]. Moreover, it could be shown that the active conformation of mammalian GnRH exhibits a β-turn structure, whereby the *N*- and *C*-termini face each other. This illustrates that the *N*-and *C*-terminal residues are crucial for the receptor binding and activity, while changes of the β-turn forming amino acids 5 to 8 are mostly well tolerated [100,101]. Taking this into account, as well as the fact that glycine in position 6 is highly prone to degradation during circulation, ^{6}Gly was often exchanged by D-amino acids, providing highly potent GnRH-agonists, like triptorelin [^{6}D-Trp] and nafarelin [^{6}D-(2-naphtyl)alanine (Nal)] [102,103]. The modification in position six was often combined with the *C*-terminal variations Pro-ethylamide (Pro-NHEt or Pro-EA) and Pro-Azgly-NH_2, yielding further superagonists, such as leuprolide [^{6}D-Leu, ^{9}Pro-EA], buserelin [^{6}D-Ser(tBu), ^{9}Pro-EA] and goserelin [^{6}D-Ser(tBu), ^{9}Pro-^{10}Azagyl-NH_2] [104–106]. It could be shown that the increased activity of the compounds is caused by an enhanced durability in the bloodstream, as well as an improved β-turn conformation of the ^{6}D-amino acid substituted compounds [100]. GnRH agonists, like buserelin, goserelin, leuprolide and triptorelin, are often used to treat hormonal prostate or breast cancer, and are commonly administered intramuscular, subcutaneous or by subcutaneous depots which release the drug over a certain period [28,99]. Although this kind of therapy can cause several side effects, like initial tumor flares, hot flashes, erectile dysfunction, gynecomastia and chemical castration, the treatment with GnRH analogs is often the first choice for the pharmacological treatment for advanced, metastatic prostate cancer due to its good tolerance and the reversibility of sex steroid suppression [28,98]. Furthermore, GnRH agonists are not only used for cancer therapy, but also for the treatment of other hormonal diseases, like endometriosis and precocious puberty or for *in vitro* fertilization [99]. The most commonly used GnRH-agonists and their therapeutic applications are summarized in **Table 1** [98,99].

Another strategy to interrupt the hormonal cascade of sex steroid release, is the administration of GnRH antagonists, which cause a reversible blockage of the pituitary receptor without gonadotropin release. These synthetic GnRH derivatives bind to the receptor with high affinity and avoid in that way, the activation of the receptor by the native peptide hormone. One of the main advantages of GnRH antagonist therapy over

Table 1: Summary of approved GnRH-agonist and their therapeutic application in human [102,103].

	GnRH-analogs	Sequence and therapeutic application
GnRH-agonists	**Buserelin acetate** Superfact®, Cinnafact®	Glp-His-Trp-Ser-Tyr-**D-Ser(tBu)**-Leu-Arg-Pro-**EA** Treatment of hormone dependent prostate cancer
	Goserelin acetate Zoladex®	Glp-His-Trp-Ser-Tyr-**D-Ser(tBu)**-Leu-Arg-Pro-**Azagly-NH_2** Treatment of hormone dependent prostate and breast cancer, endometriosis, uterine fibroids, central precocious puberty and in *in vitro* fertilization
	Histrelin acetate Vantas®, Suprelin LA®,	Glp-His-Trp-Ser-Tyr-**D-His(N^{τ}-Bzl)**-Leu-Arg-Pro-**EA** Treatment of hormone dependent prostate cancer, treatment of central precocious puberty in children
	Leuprolide acetate (Leuprorelin) Lupron®, Eligard®	Glp-His-Trp-Ser-Tyr-**D-Leu**-Leu-Arg-Pro-**EA** Treatment of hormone dependent prostate and breast cancer, endometriosis, uterine fibroids, central precocious puberty
	Nafarelin acetate Synarel®	Glp-His-Trp-Ser-Tyr-**D-Nal**-Leu-Arg-Pro-Gly-NH_2 Treatment of endometriosis, uterine fibroids, central precocious puberty and in *in vitro* fertilization
	Triptorelin acetate or pamoate Decapeptyl®, Gonapeptyl Depot®	Glp-His-Trp-Ser-Tyr-**D-Trp**-Leu-Arg-Pro-Gly-NH_2 Treatment of hormone dependent prostate and breast cancers, endometriosis, uterine fibroids, central precocious puberty and in *in vitro* fertilization
GnRH-antagonists	**Abarelix** Plenaxis®[a]	Ac-D-Nal-D-Cpa-D-Pal-Ser-*N*-MeTyr-D-Asn-Leu-Lys(iPr)-Pro-D-Ala-NH_2 Palliative treatment of advanced prostate cancer
	Cetrorelix acetate Cetrotide®	Ac-D-Nal-D-Cpa-D-Pal-Ser-Tyr-D-Cit-Leu-Arg-Pro-D-Ala-NH_2 Used in *in vitro* fertilization
	Degarelix acetate Firmagon®	Ac-D-Nal-D-Cpa-D-Pal-Ser-Aph(Hor)-D-Aph(Cba)-Leu-Lys(iPr)-Pro-D-Ala-NH_2 Treatment of advanced hormone dependent prostate cancer
	Ganirelix acetate Antagon®, Orgalutran®	Ac-D-Nal-D-Cpa-D-Pal-Ser-Tyr-D-hArg(Et_2)-Leu-hArg(Et_2)-Pro-D-Ala-NH_2 Used in fertility treatment to prevent premature ovulation

Aph(Cba): 4-ureido-phenylalanyl, Aph(Hor): 4-[2,6-dioxohexahydropyrimidin-4(S)-ylcarboxamido]-L-phenylalanyl, Azagly-NH_2: hydrazine carboxamide, Cit: citrulline, Cpa: 4-chlorophenylalanine, EA: ethylamide, Glp: pyroglutamic acid, hArg(Et_2):N^6-[bis(ethylamino)methylene]-lysine, iPr: isopropyl, Nal: 2-naphtylalanine, *N*-MeTyr: *N*-methyltyrosine, N^{τ}-Bzl: benzyl protection on N^{τ}-imidazol of His, Pal: 3-pyridylalanine.
[a] voluntarily withdrawing the drug from the market in 2006

the treatment with GnRH agonist, is the prevention of an initial surge of LH and FSH, which excludes the risk of flare effects and ensures a direct inhibition of gonadotropin and sex steroid secretion [107,108]. The therapeutic use of GnRH antagonists is similar to that of GnRH agonists, whereby the main applications in clinics are *in vitro* fertilization and treatment of prostate cancer [109]. In general, four peptide-based GnRH antagonists were granted FDA approval, including abarelix, cetrorelix, degarelix and ganirelix, whereby abarelix was voluntarily withdrawn from the marked (**Table 1**) [98,99].

Next to peptidic GnRH antagonists, a 'second generation' of GnRH modulators has been recently discovered, which are nonpeptide, small molecule GnRH antagonists [108,110,111]. In comparison to peptide GnRH analogs that are commonly administrated parenterally, this new class of GnRH antagonists possesses the potential for an oral administration, simplifying the treatment and represents a more convenient way of drug application for the patients. In 2018, the first non-peptidic and orally administrated GnRH antagonist called elagolix (Orilissa®) has been approved for the treatment of moderate to severe pain, associated with endometriosis in women (**Figure 4**) [112]. Besides, other highly promising small molecule GnRH modulators are in clinical development, such as relugolix (Relumina®) and linzagolix (**Figure 4**). Although non-peptide GnRH modulators represent attractive alternatives, the administration of peptide-based GnRH analogs remains the mainstay for the treatment of hormone dependent cancer.

In addition to the natural GnRH-R occurrence in pituitary, GnRH-R expression has been also identified in various reproductive system related cancers, such as breast, prostate and ovarian cancers, but also in non-reproductive cancers, like pancreatic and lung cancer [113–115]. It could be shown that GnRH-agonists induce a dose- and time-dependent growth inhibitory effect on cancer cells by GnRH-R activation [100,116–120]. Moreover, also classical GnRH antagonists act on tumor cells like GnRH-agonist and their binding to locally expressed GnRH-Rs elicits a similar direct antitumor effect [120–125]. This effect seems to be mediated by the interaction of GnRH receptors with G-protein α_i which occurs after ligand binding and induces activation of phosphotyrosine phosphatase-dependent transducing mechanism preventing mitogenic signal transduction and reduces the expression of growth factor receptors [80,126–128]. In comparison, GnRH-R activation at the pituitary level by GnRH agonists leads to an interaction with G-protein α_q which induces activation of phospholipase C pathway [80,98,117]. This indicates that the signaling mechanisms which are triggered by GnRH-R binding, differ in pituitary and in cancer cells, though the extra-pituitary GnRH-Rs possess the same DNA nucleotide sequence like pituitary GnRH-Rs, and also the expressed mRNA and receptor protein are of

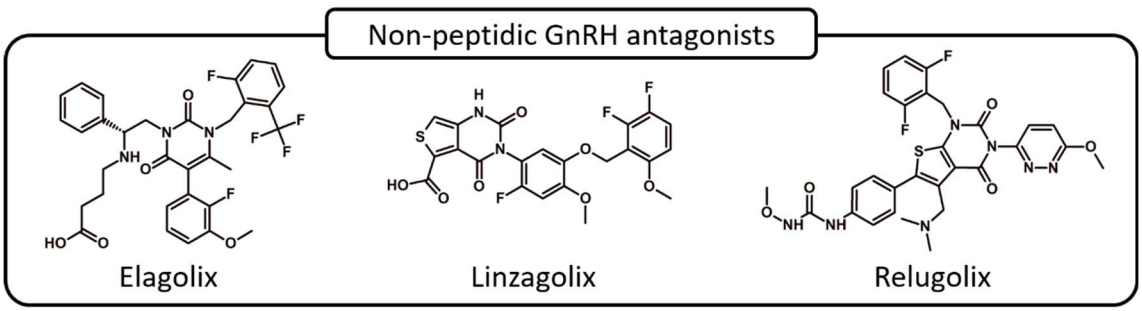

Figure 4. Chemical structure of three non-peptidic GnRH antagonists.

identical size [98,129,130]. The exact cause for this phenomenon is not yet completely understood, but one possible explanation provides the concept of ligand-induced selective signaling which was proposed by Millar and coworkers [125,131,132]. It is assumed that different active receptor conformations are existing depending on the cell type which are able to activate distinct signaling complexes and in that way, induce various cellular effects. This assumption is further supported by the fact that natural isoforms of GnRH-I are able to bind GnRH-Rs on cancer cells. Thus, GnRH-II (**Figure 5**), a second form of GnRH which was initially identified in chicken brain, but occurs ubiquitous in vertebrates including human, has been shown to reveal an improved cell growth inhibitory effect in comparison to GnRH-I, while its ability to induce the gonadotropin secretion pathway is less effective [125]. In contrast to GnRH-I, GnRH-II expression was verified significantly outside of the brain, whereby it could be detected predominantly in the kidney, but also in bone marrow and prostate [133]. Due to the widespread expression, multiple functions might be exerted by GnRH-II, but its exact role is not yet fully elucidated. A second GnRH receptor type (GnRH-IIR) which might mediate the biological effect of GnRH-II could be identified in few species including nonhuman primates, while it is not present in several mammals including human, chimpanzee, cow, horse, rat and mouse [100]. Although mRNA expression of GnRH-IIRs could be identified in human tumor cells, the existence of the functional full-length protein could not be verified, which might be mainly related to a frameshift in exon 1 and a premature stop codon in exon 2 [98,134]. This observation, but also other data, support the assumption that the biological activity of GnRH-I, GnRH-II and their derivatives is mediated exclusively by type I GnRH-R [125,132,135].

Another natural isoform of GnRH-I is the sea lamprey (*Petromyzon marinus*) analog GnRH-III which was identified and characterized by Sower *et al* [136]. This weak GnRH agonist binds to GnRH-Rs on cancer cells and induces like GnRH-I and II a direct antitumor activity on several cancer cell lines, while its gonadotropin releasing activity is strongly reduced *in vitro* and *in vivo* [137,138]. However, further studies pointed out that GnRH-III can act as a GnRH agonist and stimulates LH and FSH release in a dose-dependent manner, but GnRH-I induces gonadotropin secretion at a 1000-fold lower dose

GnRH-I	**Glp – His – Trp – Ser – Tyr – Gly – Leu – Arg – Pro – Gly – NH_2**
GnRH-II	**Glp – His – Trp – Ser – His – Gly – Trp – Tyr – Pro – Gly – NH_2**
GnRH-III	**Glp – His – Trp – Ser – His – Asp – Trp – Lys – Pro – Gly – NH_2**

Figure 5. Primary amino acid sequence of different GnRH isoforms. Conserved *N*- and *C*-terminal residues are highlighted in grey.

[139]. Moreover, it has been shown that GnRH-III binds to the GnRH-R on human breast cancer cells with higher affinity than GnRH-I. Furthermore, the results indicated specific binding to two binding sites, a high and a low affinity binding site, which could be also observed for GnRH-I agonists, like Triptorelin, but not for native GnRH-I [137,140]. Considering other studies, it is expected that there are two GnRH binding sites in cancer, one with low affinity and high capacity and another one with high affinity and low capacity [80]. This cancer specific low affinity-high capacity binding site seems to be important for the direct anticancer activity of GnRH derivatives. To enhance the anticancer potency of GnRH-III, a series of structure-related activity studies have been conducted [138,141–143]. One general result is the conformational difference between GnRH-I and GnRH-III. While GnRH-I exposes a well-defined U-shape conformation, GnRH-III is characterized by an extended backbone structure [142,143]. Besides, the studies revealed that amino acid substitutions in the peptide sequence can have a positive impact on the cancer growth inhibitory effect [141,142]. In conclusion, GnRH-III represents a valuable candidate for affecting cancer cells selectively without causing an endocrine effect which might lower the risk of chemical castration and other gonadotropin releasing activity related side-effects.

1.2.3.2. Somatostatin analogs

Another group of therapeutic peptides which are used clinically for cancer therapy are somatostatin analogs. Native somatostatin (SST) is an important regulatory-inhibitory neuropeptide with autocrine, paracrine and endocrine activity [144]. This cyclic peptide hormone is secreted by neuroendocrine neurons of the hypothalamus and by paracrine cells in different parts of the gastrointestinal tract, but mainly in the pancreas [145–147]. Somatostatin is expressed as a 116 amino acid-containing precursor molecule called preprosomatostatin, and the two biologically active forms which contain either 14 or 28 amino acids (SST-14 and SST-28), are produced by alternate proteolysis [148]. Both forms are key regulators of several biological functions, including suppression of growth hormone (GH), thyroid stimulating hormone and adrenocorticotropic hormone secretion, inhibition of growth factor synthesis (*e.g.* insulin-like growth factor (IGF), epidermal growth factor (EGF), vascular endothelial growth factor (VEGF)), and inhibition of pancreatic and gastrointestinal hormone secretion (*e.g.* glucagon and insulin) [99]. The exocrine and endocrine activity of SST is mediated by binding to a distinct family of GPCRs consisting of five somatostatin receptors (SSTR1-5) [149]. These receptors are not only expressed in specific healthy tissues (brain, pancreatic islets, adrenal gland,

gastrointestinal tract, liver, lung, and thyroid), but also in various tumor types including neuroendocrine tumors, gastrointestinal and pancreatic cancer, breast cancer, prostate cancer, lung cancer and hepatocellular carcinoma [99,147]. It could be shown that somatostatin and its derivatives possess an antitumoral activity which is exerted by direct and indirect mechanisms. The direct antineoplastic action is based on antimitotic and apoptotic effects [99]. Thus, cell cycle arrest is caused by the inhibition of cyclic adenosine monophosphate (cAMP) activity, followed by downregulation of phosphorylation through activation of phosphotyrosine phosphatase and inhibition of tyrosine kinase leading to the suppression of mitogenic hormones and cytokines, while SST mediated apoptosis is caused by intracellular acidification, endonuclease activation and p53 induced Bax upregulation [147,150]. Additionally, an indirect antiproliferative effect of SST is induced by suppression of growth factors (IGF and EGF), inhibition of tumor angiogenesis (VEGF) and immune modulating activity (*e.g.* lymphocyte proliferation, immunoglobulin synthesis) [99,147,151]. Similar to native GnRH, the clinical application of native SST is limited by its very short plasma half-life ($t_{1/2}$ = 2-3 minutes) caused by proteolytic degradation. In order to overcome this limitation, various D-amino acid-containing, synthetic SST analogs have been developed which possess an improved metabolic stability and increased SSTR affinity and/or selectivity. Nowadays, two FDA approved SST analogs are commonly used in cancer therapy, namely octreotide (OCT, Sandostatin®) and lanreotide (Somatuline®) (**Figure 6**). Both somatostatin analogs are used for the treatment of acromegaly and symptoms caused by neuroendocrine tumors,

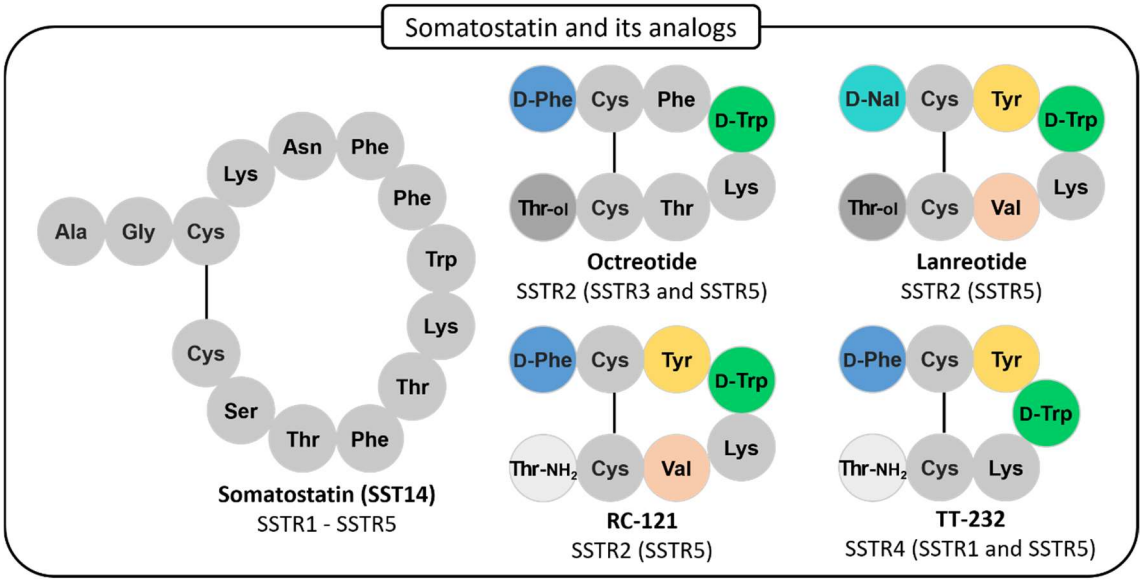

Figure 6. Structure of native somatostatin (SST14), clinically used SST analogs octreotide and lanreotide and the SST derivatives RC-121 and TT-232. The preference of the SST analogs to the somatostatin receptors (SSTR) is mentioned according to their binding affinities. The given SSTRs are bound with high affinities, while the SSTRs in parentheses represent moderate affinities. Diverse colors highlight structural similarities and differences. Nal: 2-naphtylalanine

whereby slow release formulations are available enabling a monthly injection interval [99,147,152]. Although a decrease in tumor size occurs only rarely by somatostatin analogs, their medication provides clinical benefits for the treatment of accompanying symptoms of cancer, such as carcinoid syndrome. Lanreotide has been also approved by the FDA for the treatment of patients with unresectable, well- or moderately-differentiated, locally advanced or metastatic gastroentero-pancreatic neuroendocrine tumors (GEP-NETs) to improve progression-free survival [152].

At this point, it might be worthy to state that another somatostatin derivative gained FDA approval, called pasireotide (Signifor®) [153]. This 'head-to-tail' cyclic SST analog is used for the treatment of Cushing's disease, a rare endocrine disease, and exerts its activity by binding to SSTR1-3 and SSTR5 [99]. However, since it is commonly not used for cancer therapy, further details will not be mentioned here.

Besides OCT and lanreotide, a variety of potent somatostatin derivatives for cancer therapy have been developed, including RC-121 and TT-232 (**Figure 6**). RC-121 which was initially synthesized by Schally's group, possesses a highly enhanced potency and a longer duration of action for inhibition of GH release, and also the suppression of insulin and glucagon release was improved, but here the potency was much lower compared to GH release [154]. Moreover, RC-121 exhibits a significant *in vitro* and *in vivo* inhibitory effect on cancer cells and binds to SSTR2 with high affinity and to SSTR5 with moderate affinity [155,156]. Next to cyclic octapeptides, the heptameric SST analog TT-232 which contains a five-residue ring and differs from RC-121 only by the deletion of ^{5}Val, has no GH release inhibitory activity, but it exerts a strong tyrosine kinase inhibitory activity inducing antiproliferative and apoptotic effects *in vitro* and *in vivo* [157–160]. Thus, TT-232 elicits a strong antineoplastic activity on a wide range of malignant tumors, like breast, prostate and colon cancer. It has been proven that TT-232 induces its activity by preferential binding to SSTR4, but also to SSTR1 and SSTR5 [161].

1.2.4. Targeted tumor therapy

Although classical approaches for cancer treatment provide valuable advantages, each of these treatment options has its limitations and disadvantages [162]. Conventional surgery offers an efficient treatment of localized tumors, but does not affect the formation and progression of metastases. Moreover, the surgical removal of tumor tissue is accompanied by damages to heathy tissue and/or the removal of organs or parts of organs which might cause other health-related problems and limits the patients' quality of life. In comparison, radiation therapy provides an effective treatment option to destroy large proportions of

cancer cells and offers the ability to shrink tumors without organ removal. However, radiation therapy is not efficient in treating metastatic neoplastic diseases, and it might causes damages to surrounding tissue, and especially in case of larger tumors, a complete eradication of tumor cells cannot be achieved, hence, it is commonly used as supplementary treatment strategy. In order to affect also metastases, chemotherapy is widely used as systemic therapy, but the lack of selectivity, drug-specific side effects and toxicity to healthy tissues can lead to various complications.

A promising alternative is represented by targeted tumor therapy. Already 100 years ago, the principle of targeted tumor therapy was described by Paul Ehrlich, who received the Nobel Prize for Medicine in 1908. He coined the term 'Magic bullet' for a drug which is highly specific for its target and thus, do not cause toxic side effects in healthy tissue [66]. In the recent decades, a major advance has been achieved, and nowadays a wide selection of targeted treatment modalities against cancer are available. In general, targeted tumor therapy is directed to specific cancer associated targets, while standard chemotherapy acts on all rapidly dividing cells whether cancerous or not [162]. Moreover, drugs for targeted cancer therapy can be mostly categorized into two main groups, namely molecularly targeted drugs and targeted drug delivery systems (DDS), whereby both groups can be also divided into small molecule drugs and monoclonal antibodies (mAb) [163]. In molecularly targeted therapy, the applied drugs or substances interact selectively with a specific target which interferes with at least one hallmark of cancer necessary for tumor growth and progression. Prominent examples for molecularly targeted drugs are small molecule kinase inhibitors, such as imatinib (Gleevec®) and sorafenib (Nexavar®) or mAbs, such as rituximab (Rituxan®) and trastuzumab (Herceptin ®) [164,165]. Trastuzumab was approved by the FDA for the treatment of human epidermal growth factor 2 (HER2) receptor positive breast cancer in 1998 [166]. Although the exact mechanisms of trastuzumab mediated antibody-dependent cellular cytotoxicity (ADCC) are not yet fully elucidated, recent studies pointed out that trastuzumab inhibits downstream signaling cascades and promotes in that way cell cycle arrest and apoptosis [167–169]. In addition, it has been shown that trastuzumab exerts an antiangiogenic activity *in vitro* and *in vivo* [169–172]. Thus, treatment with Herceptin leads to a significantly improved disease free and overall survival in patient with HER2 positive metastatic breast cancer [173]. Today, a myriad of antibody therapeutics are approved and over 570 mAb are in various clinical phases for both cancer and non-cancer indications, whereby 33 are in late stage clinical studies for cancer diseases [174].

Another form of targeted therapy, is ligand-mediated drug delivery which is also called active drug targeting (**Figure 7A**). This approach is based on the fact that receptors for many regulatory ligands are overexpressed on the surface of various cancer cells. These ligands can be used as carriers for anticancer drugs. After binding of the ligand, the receptors are internalized into the cancer cell and consequently the attached drugs can enter tumor cells *via* receptor-mediated endocytosis. The release of the drugs or small drug-containing metabolites is commonly facilitated by distinct intracellular mechanisms or conditions, such as high glutathione (GSH) concentration, acidic pH in lysosomes or degradation by lysosomal enzymes which ensure that the drug gets to its site of action (**Figure 7A**). The main advantages of receptor mediated targeting compared to the application of free drugs is the selective delivery of potent cytotoxic agents to cancer cells and the accompanied decreased toxicity to normal tissue. In general, the transition between some targeting cancer therapies are blurred, and therapeutics which are applied in molecularly targeted therapy might be also used as ligand for the delivery of drugs. Thus, mAbs, like trastuzumab, have been used as carriers for the delivery of cytotoxic payloads and were classified as antibody drug conjugates (ADC). Next to macromolecules, also small molecule ligands, such as folic acid, carbohydrates or peptides, can be used as targeting moieties, whereby peptide hormone analogs of GnRH or somatostatin represent promising homing devices for targeted tumor therapy.

1.2.4.1. Antibody-drug conjugates (ADC)

The concept to link an anticancer drug to a cell targeting antibody was firstly implemented in at the end of the 1950s. Mathe and coworkers linked MTX to polyclonal gamma globulins from hamster in order to achieve a combinatory effect on mouse leukemia [175,176]. However, the progress in ADC research, from the initial magic bullet concepts of Paul Ehrlich up to FDA approved ADCs, is strongly connected to the achievements in antibody technology. A key step for the success of therapeutic antibodies and ADCs, was the development of the hybridoma technology which enables the production of mAb [177]. In 1983, the first human clinical trial with an ADC was conducted, whereby an anti-carcinoembryonic antigen antibody-vindesine conjugate, derived from sheep, has been used [178]. Other clinical trials with murine mAbs pointed out that the foreign proteins were rapidly cleared from the body as a result of an immune response and the development of human anti-mouse antibodies [179]. An efficient remedy of this problem could be provided by another important advancement in antibody engineering, the development of chimeric and humanized antibodies [180]. The first FDA approved mAb

for cancer treatment was rituximab (Rituxan®), a chimeric antibody which is administrated to treat CD-20 expressing B-cell lymphomas [176]. The final breakthrough was the discovery of phage display technology and the creation of transgenic mice which enable the production of fully human antibodies [181,182]. Due to these advances, the immune response which has been observed for murine mAb, could be minimized, while the circulation half-life was significantly prolonged [179]. Encouraged by these improvements, a first generation of ADCs have been developed and tested in the 1990s [176]. Unfortunately, these ADCs exerted insufficient results in clinical trials which was mainly related to the low *in vivo* potency of the conjugated drugs, inefficient target internalization, side product prone drug coupling and imperfect linker design [179]. Additional refinements of the cytotoxic payload, as well as the linker system and the conjugation reaction led to improved ADCs with superior targeting characteristics, high durability in circulation, combined with efficient drug release inside the cancer cell and low systemic toxicity. Up to now, four ADCs have been approved by the FDA for cancer treatment (**Figure 7B**). Gemtuzumab ozogamicin (Mylotarg®) was the first ADC which entered the market. Molotarg® consists of a CD-33 targeting mAb and the highly cytotoxic, DNA breaking drug *N*-acetyl-gamma-calicheamicin which is conjugated to lysine side chains of the mAb by a combined reducible-acid labile disulfide bond-hydrazone linker. From 2000 to 2010, Mylotarg® was used to treat patients over 60 years with relapsed acute myeloid leukemia, who were not suitable candidates for standard chemotherapy [183]. Due to insufficient survival improvement and raised toxicity concerns, Mylotarg® was voluntarily withdrawn from the market in 2010. Based on additional extensive clinical studies and an improved understanding of drug dosing, Mylotarg® was relaunched into the market in 2017 [184]. Brentuximab vedotin (Adcetris®) and trastuzumab emtansine (also called T-DM1, Kadcyla®), two ADCs equipped with microtubule polymerization blocking agents, gained market approval in the early 2010s [185,186]. Adetris® which targets CD-30, is administered in Hodgkin lymphoma and anaplastic large cell lymphoma. The antimitotic drug monomethyl auristatin E (MMAE) is linked to cysteine side chains of the mAb by thioether bond formation with a 6-maleimidohexanoyl (EMC) spacer which is adjacent to a protease labile dipeptide and a self-immolative *para*-aminobenzyloxycarbonyl (PABC) spacer. This linker system facilitates the release of the free drug within the cancer cell after cleavage by lysosomal enzymes (mainly cathepsin B) (**Figure 7B**) [187,188]. In comparison, Kadcyla® which is used to treat metastatic breast cancer by HER2 targeting, is equipped

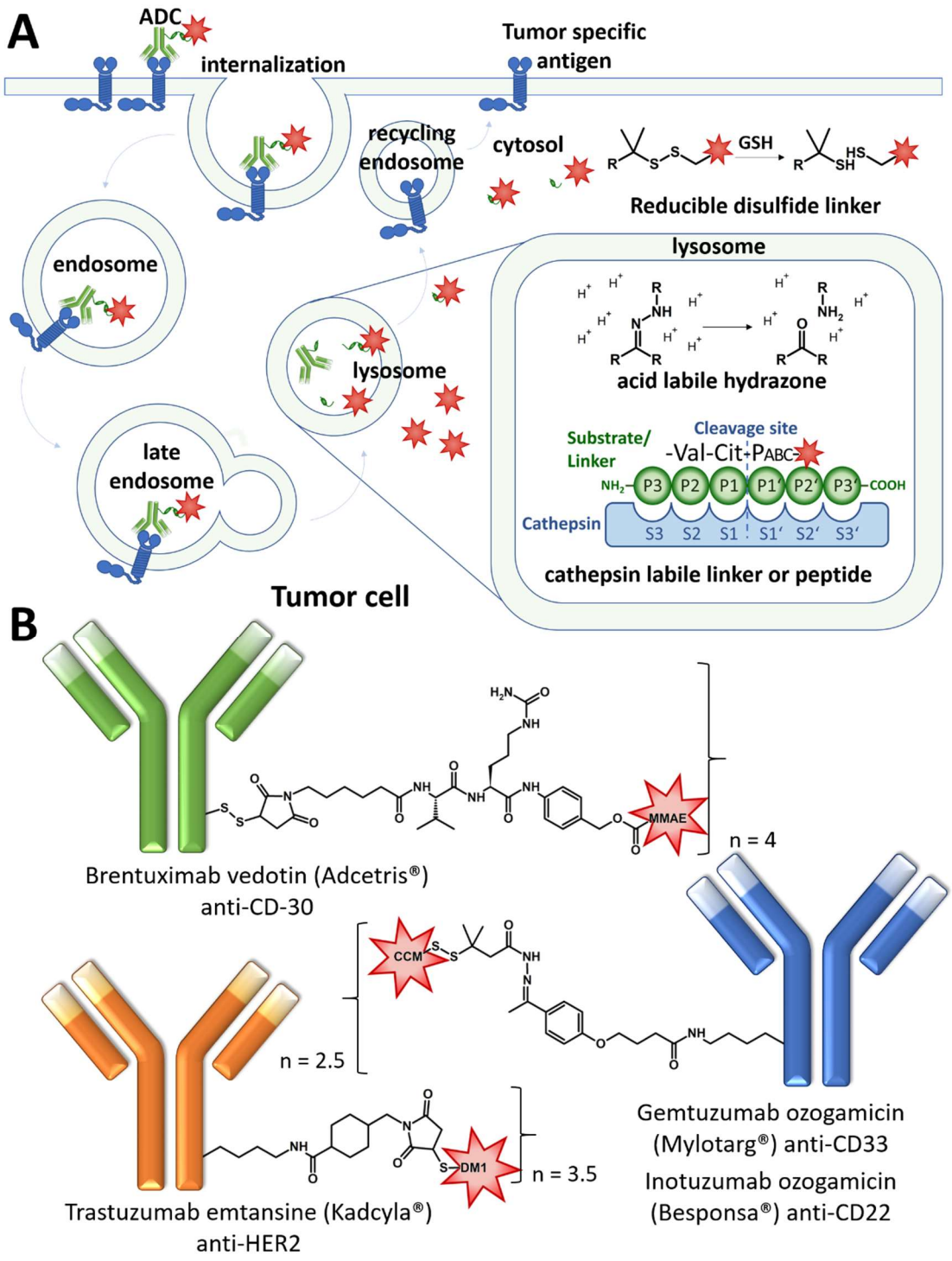

Figure 7. **A.** Schematic structure of FDA approved antibody-drug conjugates (ADC). **B.** Endocytic uptake of ADCs and intracellular drug releasing mechanisms, including disulfide reduction by glutathione (GSH), hydrazone cleavage by acidic pH and peptide(-linker), degradation by lysosomal cathepsins. n: drug-to-antibody ratio, CCM: *N*-acetyl-gamma-calicheamicin, MMAE: monomethyl auristatin E, DM1: mertansine, S3-S3': substrate binding site, P3-P3' substrate residues that bind to the active center, S1-S1' cleavage site (substrate and enzyme binding site according to Schecher and Berger nomenclature [189]).

with a non-cleavable SMCC linker (*N*-succinimidyl-4-(*N*-maleimidomethyl)-cyclo-hexane-1-carboxylate) to link the drug mertansine (also called maytansinoid or DM1) to surface exposed lysine residues of the mAb [190]. In this case, active lysine-linked drug metabolites are released, when the mAb is entirely degraded by lysosomal enzymes [187].

The newest ADC on the market, inotuzumab ozogamicin (Besponsa®), is applied to treat relapsed or refractory acute lymphoblastic leukemia, and consists of a humanized CD-22 targeting mAb and the same drug linker system which was used for Mylotarg® [191,192]. Due to the success of the approved ADCs, nearly 60 ADCs are in clinical pipelines to date, whereby nine ADCs are already in late-stage clinical trials [174,193].

Although ADCs achieved a great success and are considered as excellent DDSs, there are also certain drawbacks which might cause some limitations. A major problem is the heterogenicity of the conjugation reaction which causes positional and stoichiometric diversity. This might lead to serious analytical and therapeutic problems, especially for conjugates with a relatively narrow therapeutic window [194]. A substantial improvement offers the THIOMAB^{TM} antibody technology which allows the site-specific conjugation of a thiol-reactive drug-linker system to a substituted cysteine of the mAb, which was incorporated by site-directed mutagenesis [195–197]. However, due to the complex nature of the ADCs, large scale production is still difficult to achieve, and requires special conditions which is accompanied with high production costs [198]. Additionally, the large size of the ADCs has a negative impact on the extravasation and the penetration into solid tumors [199]. This limitations might be overcome by small molecule drug conjugates (SMDC).

1.2.4.2. Small molecule drug conjugates

In comparison to protein-based biopharmaceutics, like ADCs, SMDCs, in particular peptide-drug conjugates, possess valuable properties, like excellent tissue permeability, low immunogenicity and structural simplicity. Moreover, peptide-based DDS can be produced cost-efficiently in large scale by chemical synthesis [200,201]. Especially, the good progress in peptide technology, solid phase synthesis and chemical ligation techniques facilitates the synthesis and modification of peptides [202,203]. The main limitation of native peptides is their relatively short plasma half-life and the accompanied low *in vivo* stability, as well as the rapid renal clearance [204]. However, as shown for GnRH and somatostatin derived peptide therapeutics (1.2.3.), these limitations can be overcome by sequence modifications with unnatural amino acids, like D-amino acids, and modified-release dosage, such as depot formulation [99]. Due to the success story of GnRH and somatostatin analogs for hormonal (targeted) therapy, both peptide hormones are promising targeting moieties for targeted tumor therapy. Thus, a variety GnRH and somatostatin DDS are under research and will be outlined in the upcoming sections. In order to provide a wider picture of the topic SMDC, it is worth to mention that also other

peptides or small molecules with specific binding activity to cell surface receptors or cell membrane permeability are extensively studied. Prominent examples for peptide DDSs are bombesin [205–209], RGD and *iso*DGR peptides [210–216], NGR peptides [217–220], TAU-protein derived peptides [221,222] and cell penetrating peptides (CPP) [223–225], but also small ligand carriers are used for targeted cancer therapy, like folic acid (analogs) or prostate-specific membrane antigen (PSMA) ligands [226–229].

Daunorubicin, doxorubicin and paclitaxel as payload

Traditional anticancer agents, such as Dau, Dox and PTX, are often used as cytotoxic payloads for SMDC. The anthracyclines Dau and Dox consists of a planar tetracyclic anthracyclinone body which is glycosylated at the C7-OH with the deoxy pyranose sugar daunosamine. The structure of Dau provides two suitable conjugation sites, either the C13 carbonyl function or the amino group of the daunosamine sugar, whereas Dox can be additionally linked to its C14-OH group (**Figure 8**). The anticancer activity of Dau and Dox is elicited by non-covalent intercalation between DNA-base pairs which inhibits DNA topoisomerase II activity and thus, affects polymerase activity. It is known that anthracyclines stabilized the DNA-topoisomerase II cleavage complex, resulting in highly lethal DNA breaks which might lead to apoptosis when DNA cuts become irreversible at genomic regions of active DNA synthesis in proliferating cancer cells [230]. Moreover, also redox-processes which are mediated by the quinone structure, are responsible for toxicity. The production of reactive oxygen species can damage DNA, cell-membranes and proteins, but it is also assumed that these oxygen species are responsible for the cardiotoxic side effects of the drug [231].

The naturally-derived antimitotic drug PTX, is another valuable candidate for targeted drug therapy, since it provides an exceptionally strong anticancer activity and can be linked by its hydroxyl groups (**Figure 8**). The C2'-OH group of PTX is often used for the ligation to linker systems which enable an intracellular release of the free PTX, since the exposure of the free C2'-OH group is highly important for the activity of PTX. In that way, the drug is less active until it enters tumor cells where the free drug is released by distinct mechanisms. Although the high potential of PTX was already discovered in the early 1960s, it needed nearly 30 years until PTX entered the market [86]. The major challenge for the distribution and wide use of PTX was its large scale production, since the extraction from the primary source afforded only low yield which was not economical, and the total synthesis of PTX is quite demanding due to its complex structure with eleven stereocenters. A breakthrough was achieved with the establishment of the semisynthetic

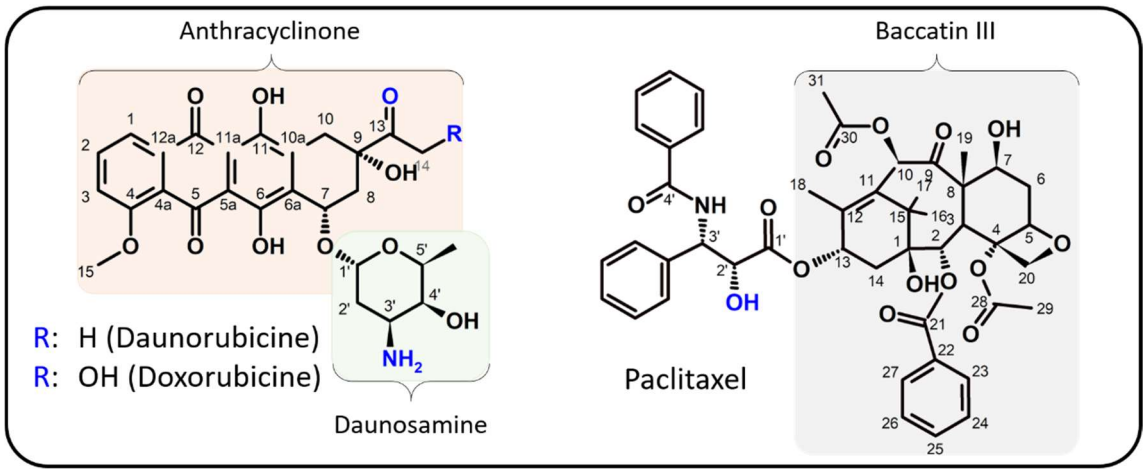

Figure 8. Structure of daunorubicin, doxorubicin and paclitaxel. The functional groups used as conjugation sites are colored in blue.

route which facilitates the large scale production of PTX from the natural precursor 10-deacetyl baccatin III. This precursor is extracted from the renewable and more readily available leaves of the European yew tree.

GnRH-based drug delivery systems

At the end of the 1980s, the first cytotoxic GnRH-I derivatives have been developed in Schally's laboratories, thereby agonistic and antagonistic GnRH carriers have been used as targeting moiety, and the alkylating agents cisplatin or melphalan (Mel), the phenylalanine derivative of nitrogen mustard, were incorporated [232–234]. In cases of GnRH agonists, the drug was inserted in position 6, either directly in the peptide sequence (^{6}D-Mel) or conjugated to the side chain of ^{6}D-Lys. Moreover, further GnRH-I-[^{6}D-Lys]-drug conjugates have been designed, where MTX or Dox were applied as cytotoxic payload [235,236]. In order to link Dox to the lysine side chain, a glutaric acid linker was inserted, enabling an ester bond formation with the primary hydroxyl group at the C-14 of Dox. The antitumor activity of this conjugate, called zoptarelin-doxorubicin (Zoptrex™, AEZS-108, previously AN-152) (**Figure 9A**), was intensively studied. It could be demonstrated that AEZS-108 internalizes selectively in GnRH-R expressing cells, and that the drug is released intracellularly by tumor specific carboxylesterases, revealing a significant tumor growth inhibition on several tumor types *in vitro* and *in vivo* [113,237–239]. Based on these promising results, AEZS-108 was the first cytotoxic GnRH-I derivative which entered preclinical and clinical trials [240]. Unfortunately, AEZS could not achieve its primary endpoint in clinical phase III studies on endometrial cancer, which was caused by the lack of a significant difference in the median period of overall survival of patients treated with Zoptrex™ as compared to patients treated with Dox [241]. The main reason for this might be the poor enzymatic stability of the conjugate in circulation.

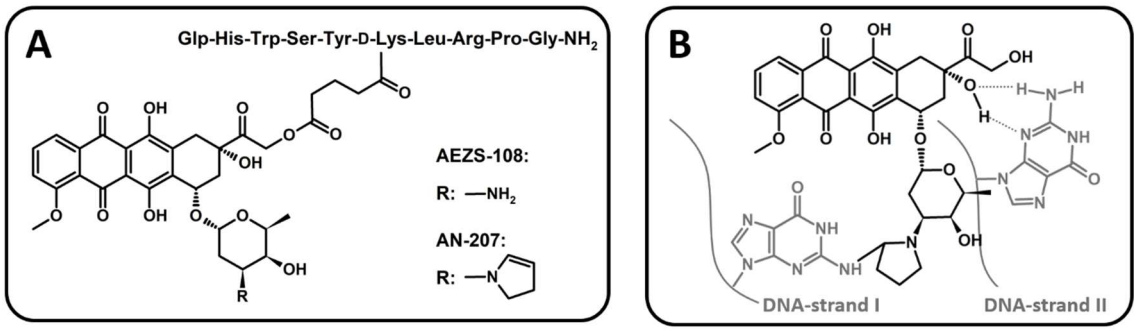

Figure 9. **A.** Structure of ester bond-linked doxorubicin (AEZS-108) and 2-pyrrolino-doxorubicin (AN-207) GnRH-I-[^{6}D-Lys] **B.** Structure of 2-pyrrolino-DOX–DNA adduct (guanine DNA interstrand cross-links) [113,244]

It has been demonstrated that the ester bond is rapidly hydrolyzed by carboxylesterases of mouse ($t_{1/2}$ = 19 minutes) and human ($t_{1/2}$ = 126 minutes) blood serum [242]. Together with the development of AEZS-108, modified Dox-analogs have been studied with the aim to generate compounds with higher potency [243]. In this occasion, 2-pyrrolino-Dox (pyDox, 3'-deamino-3'-(2"pyrroline-1"-yl)-doxorubicin) was discovered which is 500-1000-times more active than Dox. Further studies indicated that the improved potency of pyDox is mainly related to the alkylating ability of pyDox. Thus, pyDox blocks not only topoisomerase II activity by intercalation, but also forms cross-links in double-stranded DNA by covalent and hydrogen bonding with guanine bases (**Figure 9B**) [113,244]. Due to its effectiveness, pyDox was used to prepare the highly active AEZS-108 analog AN-207 (**Figure 9A**) [236]. Initial *in vitro* studies revealed highly promising results leading to a series of preclinical studies to analyze the antitumor activity of AN-207 [113,236,245–248]. Although these preclinical studies demonstrated a lower toxicity and an improved efficacy of AN-207 than the free drug, AN-207 was not further investigated in clinical trials. This might be explained by more harmful side effects of pyDox in comparison to Dox, caused by a premature release of the drug by carboxylesterases [113]. However, due to the initial encouraging results of AEZS-108 and AN-207, further GnRH-I-[^{6}D-Lys] drug conjugates have been designed and evaluated. Aggrawal *et al*. conjugated curcumin, a diarylheptanoid of turmeric, *via* ester bond to the glutaryl spacer. The resulting conjugate revealed an apoptotic effect, and a significant reduction of pancreatic cancer cell growth could be obtained *in vitro* and *in vivo* [249]. Comparable results have been reported for GnRH-I-[^{6}D-Lys-gemcitabine] conjugates on prostate cancer cells and tumor-bearing mice [250].

Apart from that, also the potential of GnRH-I-PTX derivatives has been verified. Vanek and coworkers utilized a truncated GnRH agonist (Glp-His-Trp-Ser-Tyr-D-Cys-Leu-OH) and linked PTX *via* its C2'-OH group to the carboxylic function of a thiol-reactive

maleimide spacer which was conjugated to ^{6}D-Cys. The resulting PTX conjugates exerted a GnRH-R mediated anticancer activity [251]. Moreover, the GnRH-I antagonist degarelix was employed as a targeting moiety for PTX. A carbonate function was formed to link PTX to a thiol-containing bifunctional spacer which was attached to degarelix (modified with 3-sulfanylpropanoic acetyl moiety) in different positions by disulfide bond formation. *In vitro* studies revealed that all conjugates possess a cancer cell growth inhibitory effect, and were more stable in human serum than AEZS-108 [252].

Considering that the sea lamprey GnRH analog, GnRH-III, elicits a GnRH-R-mediated inhibitory effect on the growth of various human cancer cell types, while the hormone releasing effect is substantially reduced, GnRH-III represents a valuable targeting moiety for targeted tumor therapy. One of the first GnRH-III conjugates contained a non-degradable poly(vinylpyrrolidone-co-maleic acid) (P(VP-co-MA)) moiety which was linked through the enzyme labile tetrapeptidyl spacer GFLG to ^{8}Lys. This GnRH-III-P(VP-co-MA) conjugate revealed a higher antiproliferative activity on human ERα positive and negative breast cancer, as well as on endometrial and prostate cancer cells than the unconjugated GnRH-III. Moreover, the *in vivo* antitumor activity on estrogen independent human breast cancer xenograft in nude mice was improved [253]. It was proposed that this improvement might be related to a higher proteolytic resistance of the compound accompanied with an elongated receptor occupancy and an intracellular cytotoxic effect, caused by the non-degradable copolymer [253,254]. Due to these encouraging outcomes, also biodegradable, branched polypeptide carriers have been devolved, but the obtained results were not satisfying, which was either related to an insufficient synthetic reproduction (polylysine backbone GnRH-III conjugates) or an insignificant antiproliferative effect (tuftsin-derived polypeptide backbone GnRH-III conjugates) [254].

Furthermore, Mező and coworkers developed a huge variety of GnRH-III-based DDS, whereby different series of studies have been performed to systematically refine the properties of the GnRH-III conjugates and to improve the antitumor activity. In the first set of GnRH-III-drug conjugates, the anticancer agents MTX, Dox and Dau have been used as payload. In all cases, the lysine in position 8 was utilized as ligation site, whereby different linkage systems have been compared [254]. Thus, Dox was attached to the GnRH-III carrier, either by ester bond to a glutaryl spacer, by hydrazone bond to a monohydrazide succinyl linker, by oxime bond to an aminooxyacetyl (Aoa) -GFLG spacer or by amide bond formation to a glutaryl and glutaryl-GFLG moiety. Moreover,

equivalent oxime and amide bond-containing GnRH-Dau conjugates have been synthesized. Cell viability studies on human breast and murine colon cancer cells exposed that the applied linkage systems have a significant impact on the anticancer activity. The ester and hydrazone linked conjugates possess the highest activity which might be related to the intracellular release of the free anthracycline. However, also the oxime bond-linked conjugates displayed a substantial *in vitro* cytostatic effect, although this system does not facilitate the release of the free drug. It is worth mentioning, that the direct comparison of oxime-linked Dox and Dau revealed that the Dau conjugates possess a slightly improved cytostatic effect over the Dox conjugates on breast and colon cancer cells. This effect could be confirmed in latter studies, indicating the advantage of Dau for this ligation system [255,256]. Interestingly, none of the conjugates which were linked *via* amide bond to the amino sugar of Dox or Dau, revealed a significant cancer cell growth inhibitory effect. It has been proposed that this is related to a reduced intercalation ability, caused by the amide bond which might disturb the interaction of Dau/Dox with DNA bases. Considering that the relatively short half-life of the ester bond under physiological conditions might limit the efficacy of the conjugates and cause toxic side effects, also the stability of hydrazone and oxime bond-linked GnRH-III conjugates have been verified [255]. According to the literature, the hydrazone bond should be stable in circulation (pH ~ 7.4), while the acidic conditions in lysosomes (4.5-5) should lead to linker degradation and release of the drug. The pH sensitivity studies displayed that the hydrazone linker is not fully stable at pH 7.4 which might cause a partial release of the drug before it can reach the tumor tissue and enter cancerous cells [255]. In comparison, the oxime bond is more stable under physiological conditions and thus represents an attractive and alternative linkage system, even if the lack of free drug release might limit the potency of the DDS. In order to improve the anticancer activity of the highly stabile oxime bond-linked GnRH-III-Dau conjugates, different concepts have been established, including the influence of cathepsin cleavable peptide linkers between Dau=Aoa and the sidechain of ^{8}Lys [257]. These studies pointed out that the incorporation of an enzyme labile linker (GFLG or YRRL) did not lead to an improved antitumor activity compared to the GnRH-III conjugate where Dau=Aoa was directly linked to the ε-NH_2 group of ^{8}Lys **(K1)**. Similar antitumor activities could be also obtained *in vivo* on colon carcinoma-bearing mice [258]. This was mainly related to the degradation profiles of the conjugates caused by lysosomal enzymes, revealing for all conjugates the presence of the smallest Dau-containing metabolite. Moreover, DNA binding studies provided valuable information

about the intercalation ability of the active Dau=Aoa-metabolites. Although the DNA affinity of the metabolites was slightly reduced in comparison to the free drug, all Dau=Aoa-fragments interacted efficiently with DNA, whereby the Gly- and Lys-containing Dau-metabolites exposed enhanced binding properties over the Tyr-fragment [257]. Due to these outcomes, the attention was turned to modifications in the targeting sequence. Manea *et al*. reported that an exchange of the ^{4}Ser by ^{4}Lys within the GnRH-III sequence causes an improved cytostatic effect of the conjugates on human breast and colon cancer cells [259]. In order to enhance the stability towards proteases with the preference to cleave between basic amino acids, the impact of lysine acetylation (Lys(Ac)) has been studied, demonstrating that the initially improved cytostatic effect of the ^{4}Lys compound was not affected by the side chain modification. Moreover, the acetylation led to an increased cellular uptake rate, compared to the native ^{4}Ser and the free ^{4}Lys-containing GnRH-III derivatives. The positive effect of the ^{4}Lys(Ac) exchange on the antitumor activity of GnRH-III-Dau conjugates was further verified by *in vivo* studies on murine colon carcinoma-bearing mice [259]. Additional studies by Hegedüs *et al*. demonstrated that this effect could be further improved using other short chain fatty acids for acylation. The best cytostatic effect was detected for the compound with butyrylated ^{4}Lys (^{4}Lys(Bu)) (**K2**). The improved growth inhibitory effect on human colon cancer and ER(+) breast cancer cells could be explained by an increased cellular uptake of the GnRH-III-Dau derivative. Moreover, the higher potential of **K2** in comparison to the GnRH-III-[^{4}Lys(Ac),^{8}[Lys(Dau=Aoa)] conjugate, could be further confirmed by *in vivo* studies on human colon carcinoma bearing mice [260].

Apart from that, the beneficial exchange of ^{4}Ser to ^{4}Lys paved the way for the development of multifunctional GnRH-III conjugates. Leurs *et al*. reported on an improved cancer cell growth inhibitory effect of the dual drug conjugate GnRH-III-[^{4}Lys(MTX),^{8}Lys(Dau=Aoa)] on non-reproductive system related colon cancer cells in comparison to the mono-drug conjugates GnRH-III-[^{4}Lys(MTX),^{8}Lys(Ac)] and GnRH-III-[^{8}Lys(Dau=Aoa)] (**K1**) [261]. Considering that the compound GnRH-III-[^{4}Lys(MTX),^{8}Lys(Ac)] did not display a cytotoxic effect under the applied assay conditions, the authors concluded that the exerted cytostatic effect of the dual drug conjugates might be synergetic. Furthermore, a similar effect could be obtained for the dual drug conjugate, where both drugs were attached to ^{8}Lys, namely GnRH-III-[^{8}Lys(MTX-Lys(Dau=Aoa)]. However, it needs to be mentioned that both dual-drug conjugates displayed a similar anticancer activity as **K1** on steroid hormone receptor

expressing breast and prostate cancer cells [261]. In addition, a related study has been published, where Dau was used twice (di-Dau) instead of MTX and Dau in combination [262]. In this case, GnRH-III-[^{4}Lys(Dau=Aoa),^{8}Lys(Dau=Aoa)] and GnRH-III-[^{8}Lys(Dau=Aoa-Lys(Dau=Aoa))] revealed a significant enhanced anticancer activity on all analyzed cancer cell lines over **K1**, whereby the improvement on prostate and colon cancer cells was more remarkable than on estrogen dependent breast cancer cells. Further studies on di-Dau-containing GnRH-III conjugates have been reported by Hegedüs *et al.*, whereby the targeting sequence was equivalent to that of **K2** and both Dau molecules have been inserted at ^{8}Lys by adding an additional Lys to the side chain [263]. In total, four different GnRH-III-[^{8}Lys(Dau=Aoa-X-Lys(Dau=Aoa-X) conjugates have been developed. Next to the initial conjugate without any spacer, X represents either GFLG, diethylene glycol (EG_2) or GFLG-EG_2. Cell viability studies on human ER(+) breast cancer cells pointed out that all spacer-containing derivatives exerted a higher cytostatic activity than the non-spacer conjugate, whereby the GFLG-EG_2 compound exposed the best biological activity. Moreover, it has been shown that the improved cell growth inhibitory effect was related to the release of mono-Dau metabolites which could be observed for the three spacer-containing GnRH-III-di-Dau conjugates. It worth mentioning that the insertion of diethylene glycol spacer enhanced significantly the water solubility of the conjugates.

However, although most of the GnRH-III-di-Dau conjugates revealed an improved cytostatic effect, the mono-Dau conjugate **K2** represents the most promising candidate for GnRH-III-based targeted tumor therapy, since it possesses a comparable cytostatic effect and provides a better ratio between drug-content and achieved anticancer activity [262–264].

Somatostatin-based drug delivery systems

Similar to the GnRH-drug conjugates, the first cytotoxic somatostatin derivatives have been developed in the mid 1980s by Schally and coworkers [154]. Different somatostatin analogs have been tested for their ability as efficient targeting moieties, whereby RC-121 was identified as highly promising candidate. Due to this, Dox and pyDox were linked to RC-121 using the same drug linker system as for the GnRH-Dox conjugates AEZS-108 and AN-207, resulting in the Dox conjugate AN-162 and the pyDox compound AN-238 [265]. Both conjugates exhibit a strong antitumor effect *in vitro* and *in vivo* on a wide range of tumor types, including prostate, breast, ovarian, pancreatic, colon and lung cancers [206,248]. These promising outcomes led to preclinical studies of AN-162 [266,267]. Although

many promising results for both conjugates have been published, to date there is no hint for performed or ongoing clinical trials which might be a result of the premature drug release by carboxylesterases as already mentioned for the GnRH conjugate AEZS-108. A promising alternative was reported by Mező and coworkers, who linked Dau to RC-121 by oxime bond formation to an *N*-terminally inserted Aoa spacer [268]. This conjugate revealed a substantial inhibitory effect on the growth of breast, non-small cell lung cancer (NSCLC) and colon cancer cells *in vitro*.

Next to RC-121, OCT has been extensively used as homing device to target SSTR positive cancer. For instance, the tubulin binder PTX was linked to its C2'-OH function by ester bond formation with a succinyl linker that was attached to the *N*-terminus of OCT [269]. This conjugate displayed a selective cell growth inhibitory effect on SSTR expressing ER(+) breast cancer cells. Moreover, the same PTX-OCT conjugate was used to overcome taxol-resistance in human ovarian tumor xenograft [270]. Another PTX-OCT conjugate was reported by Huo *et al*. which consists of the same PTX-linker system, but here a polyethylene glycol spacer (PEG) was inserted between the succinyl moiety and OCT to increase the solubility of the compound [271]. The *in vitro* and *in vivo* antitumor activity on NSCLC was investigated, revealing a significant and stronger antitumor efficacy, combined with a lower toxicity in comparison to PEGylated PTX which was used as control. This effect could be further improved by incorporating the redox sensitive 3,3'-dithiodipropionyl spacer between PTX and the PEGylated OCT instead of succinyl linker [272]. The authors proposed that these positive results are related to an accelerated release of the free PTX and exposure of the free C2'-OH group. The fast intracellular release of the less-hindered PTX-propionyl-SH prodrug by GSH seems to be the key step and facilitates an increased ester hydrolysis.

Apart from that, a variety of other PTX-OCT systems have been reported which exert a significant antitumor activity *in vitro* and *in vivo*, including di-PTX-OCT conjugates and OCT-modified-PTX-loaded micelles [273–275]. Furthermore, also lanreotide has been used as targeting peptide of PTX-loaded micelles which provokes apoptosis and a tumor growth inhibition in human lung cancer bearing mice [276].

Next to PTX, many other drugs have been linked to octreotide, such as Dox, bufalin, periplocymarine and proteasome inhibitor [277–280]. As an example, Lelle *et al*. used a dithiol functionalized glutamate linker which contains oxime-linked Dox at the N^{α}-group (Dox=Aoa-Glu(O-mercaptamine)-O-mercaptamine). This linker was intercalated between the disulfide bridge of OCT, resulting in an OCT-DOX conjugate with two

disulfide bonds and an enlarged ring size [277]. It has been shown that a GSH mediated release of the Dox-linker caused an *in vitro* cytostatic effect on pancreatic and breast cancer cells.

Although radiolabeled derivatives are not the main focus of the present thesis, it should be noted that somatostatin derivatives have been successfully used as targeting moieties for diagnosis and radiotherapy [[99]]. The first and most commonly used radiotracer for somatostatin receptor scintigraphy was ^{111}In-DTPA-octreotide (^{111}In-Pentetreotide, OctreoScan®; where pentetic acid (DTPA) is used as chelator for ^{111}In) which has been approved by the FDA in 1994 [99]. However, some weaknesses of OctreoScan®, like the limited image quality and spatial resolution encouraged the development of more efficient chelator-conjugated SST-analogs [281]. A superior alternative is ^{68}Ga-DOTATATE (GaTate, NETSPOT®), where octreotate is used as targeting moiety and 1,4,7,10-tetraazacyclododecane-1,4,7,10-tetraacetic acid (DOTA) as chelator. In comparison to octreotide, octreotate, possesses a carboxylic *C*-terminus instead of the alcohol. Due to the enhanced diagnostic efficacy, GaTate has been recently approved by the FDA [282]. Moreover, the ^{177}Lu chelated equivalent ^{177}Lu-DOTATAE ((LuTate, Lutatheran®) entered the US market in January 2018, and is used for targeted radiotherapy of somatostatin receptor-positive GEP-NETs, including foregut, midgut, and neuroendocrine tumors in adults [283].

2. Aims and objectives

Although the progress in cancer research leads to a constant improvement of anticancer drugs and increasing median survival rates, there are still urgent needs for more effective therapies. One worthwhile strategy is represented by targeted cancer therapy, and the use of drug delivery systems. Considering that receptors for GnRH and somatostatin are highly expressed on the surface of various cancer cells, both peptide hormones and their analogs can be used as homing devices for targeted drug delivery.

Recent studies demonstrated that oxime-linked daunorubicin GnRH-III bioconjugates exert an efficient *in vitro* and *in vivo* antitumor activity and possess a high stability in circulation. However, the lack of free drug release might limit the potency of the conjugates. To compensate this effect, different strategies should be pursued to increase the antitumor activity of the GnRH-III drug delivery system.

Besides, somatostatin-drug conjugates represent an attractive drug delivery system, especially for tumors which lack GnRH-receptor expression. In the last years, many different somatostatin analogs have been investigated which elicit an antineoplastic activity by binding to different somatostatin receptors. Recent studies highlight the value of the two somatostatin analogs RC-121 and TT-232.

Due to this fact, the central goal of the present thesis was the development and evaluation of efficient GnRH- and somatostatin-based drug delivery systems for targeted tumor therapy. Moreover, certain main objectives have been defined:

1. Improvement of the antitumor activity of oxime bond-linked GnRH-III-Dau conjugates:

- synthesis and characterization of oxime bond-linked GnRH-III-Dau conjugates with various unnatural amino acids in the GnRH-III sequence, using solid phase peptide synthesis (SPPS) and ligation of Dau in solution
- evaluation of the cytostatic effect of the compounds on GnRH expressing human breast and colon cancer cells in comparison to **K2** by cell viability assays
- additional analyses of (best) candidates to analyze the cellular uptake (flow cytometry) and localization (confocal laser scanning microscopy (CLSM)), stability in plasma and in presence of lysosomal enzymes (LC-MS assay) and GnRH receptor affinity by radio ligand binding studies in order to validate the results of the cell viability assays and to prove the mechanism of action of the conjugates

2. Development of cleavable linker-containing GnRH-drug conjugates:

- synthesis of targeting moieties by SPPS (best carriers from the 1. objective) and synthesis of PTX and Dau-containing linker systems in solution consisting of Val-Ala or Val-Cit cathepsin B cleavage site and a PABC self-immolative spacer, followed by attachment to carrier
- synthesis of non-cleavable counterparts as controls
- evaluation of cytostatic effect of the conjugates on human cancer cells to gain information about the impact of the linker system and comparison of the anticancer activity to the oxime-linked GnRH-III-Dau conjugates
- proof of linker concept by lysosomal degradation studies and receptor binding studies

3. Comparison of different SST carriers and linker systems to establish a new SST lead compound:

- synthesis of 5(6)-carboxyfluorescein (FAM) labeled SST-compounds by SPPS, using RC-121 and TT-232 as targeting moiety, as well as a new type of somatostatin derivative which is cyclized by thioether bond instead of a disulfide bridge
- cellular uptake studies of the FAM compounds by CLSM and flow cytometry to compare the potential of the derivatives as homing device for targeted drug delivery
- synthesis of equivalent oxime bond-linked SST-Dau conjugates and analysis of the cytostatic effect on human SSTR-expressing cancer cells to select the best targeting moiety
- synthesis of additional SST-conjugates with different linker systems and evaluation of their cytostatic effect to investigate the impact of these linker systems on the anticancer activity
- synthesis of 2-pyrrolino-Dau (pyDau) SST conjugate using the best carrier-linker combination to deliver the highly potent daunorubicin analog pyDau to SSTR-expressing cancer cells and evaluation of the antitumor activity

3. Results and discussion

Targeted tumor therapy represents a promising strategy for the selective and efficient treatment of tumors and their metastases. Next to monoclonal antibodies, peptide ligands, such as GnRH or somatostatin, can be used as carriers for cytotoxic payloads. Encouraged by the success of the first GnRH- and somatostatin-based drug delivery systems which have been established in the laboratories of the Nobel laureate A. V. Schally, a large number of cytotoxic GnRH and somatostatin derivatives has been synthesized and evaluated.

In the present thesis, novel derivatives of the regulatory peptides GnRH-III and somatostatin have been developed and used as carrier for therapeutic agents, whereby different linker systems and anticancer payloads have been applied (**Scheme 1**). The resulting cytotoxic DDSs were characterized, and different biochemical studies have been performed, including the analysis of the growth inhibitory effect of all designed peptide-drug conjugates on different human cancer cells.

3.1. GnRH-III-drug conjugates

The natural sea lamprey analog of GnRH, GnRH-III represents a promising starting compound for the development of new types of SMDC. With the aim to achieve an improved cytostatic effect on human cancer cells, the influence of sequence modification within the GnRH-III sequence has been studied. To ensure the comparability of the results, ^{8}Lys was constantly used as ligation site, whereby Dau was initially attached to an incorporated Aoa moiety by formation of an oxime bond. In total, 20 novel GnRH-III-Dau conjugates were synthesized and analyzed for their cytostatic effect on MCF-7 and HT-29 human cancer cells. The best candidates were chosen for further biochemical evaluations, including cellular uptake and localization studies, radioligand binding studies and analysis of stability/degradation in presence of cell culture medium, human blood plasma or lysosomal homogenate.

Moreover, the most promising GnRH-III carriers of these studies were selected as targeting moiety for the development of new drug conjugates, containing a cathepsin B cleavable dipeptide linker and a self-immolative spacer. As a payload, the classical anticancer drugs Dau and PTX have been used. For a better comparison, non-cleavable linker-containing GnRH-drug conjugates were also synthesized. The resulting compounds have been studied for their growth inhibitory effects on A-2780 ovarian and Panc-1 pancreatic cancer cells. These cell lines were selected according to their receptor

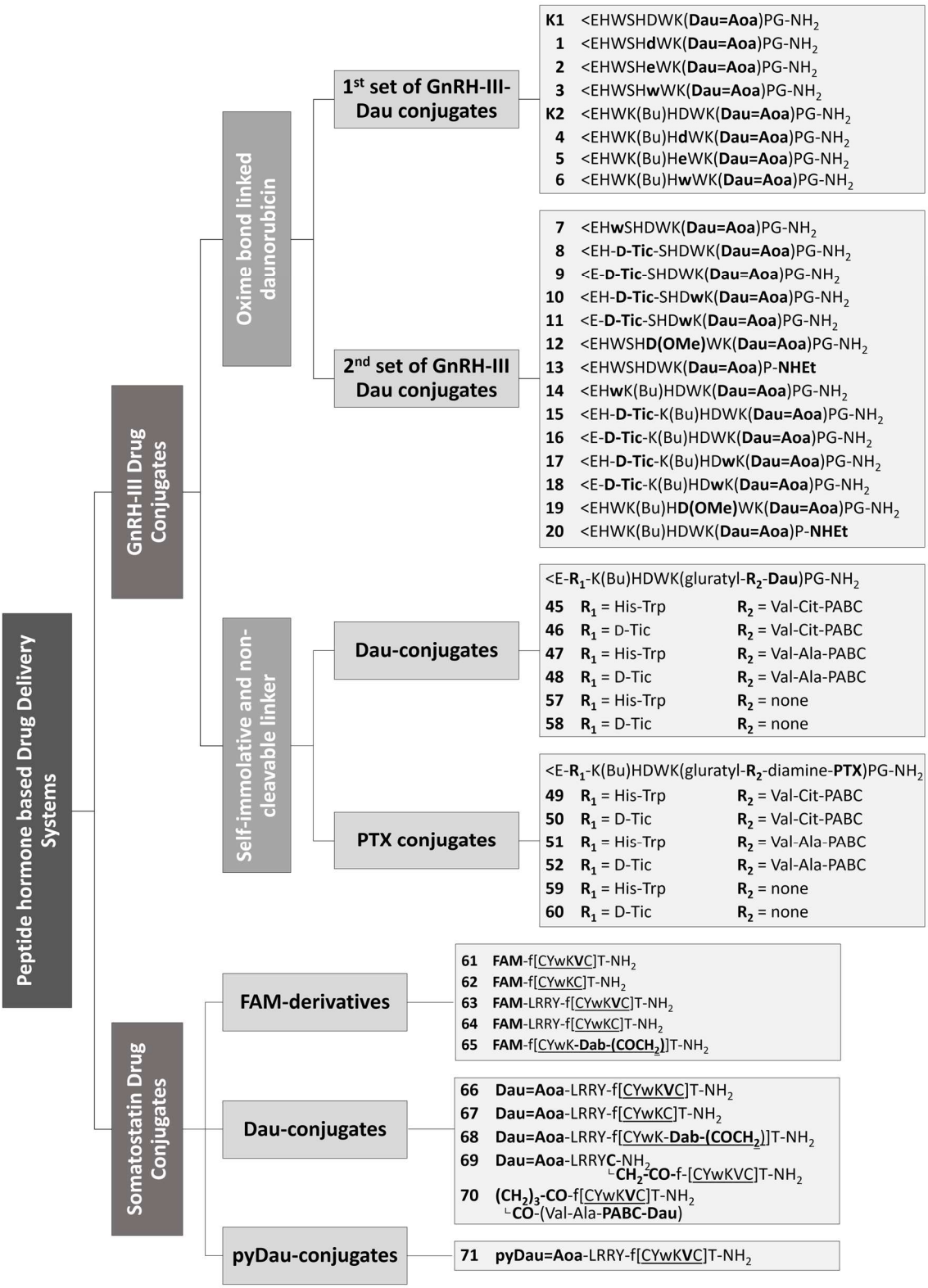

Scheme 1. Overview of all synthesized GnRH-III and somatostatin conjugates. **Aoa**: aminooxyacetic acid, **Dab**: 1,4-diaminobutyric acid, **Dau**: daunorubicin, **diamine**: *N*,*N*'-dimethylethylene diamine, **FAM**: 5(6)-carboxyfluorescein, **Tic**: 1,2,3,4-tetrahydroisoquinoline-3-carboxylic acid, **PABC**: *para*-aminobenzyloxycarbonyl, **PTX**: paclitaxel, **pyDau**: pyrrolino-daunorubicin.

expression level which was determined by western blot studies. In order to prove the concept, the cleavage of the peptide linker and the corresponding release of the drug were

investigated in presence of lysosomal enzymes and the affinity of the conjugates to the GnRH-R was examined by radioligand competition assay.

3.1.1. Oxime bond-linked daunorubicin–GnRH-III conjugates

Many different linker systems, such as ester, hydrazine, oxime or amide bonds have been investigated in our laboratories to link anthracyclines, like Dox and Dau, to GnRH-based targeting moieties [254–257,284]. Since the oxime linkage provides distinct advantages, like its formation in aqueous solution using unprotected peptide carriers, as well as its high chemical and enzymatic stability, this ligation method was chosen to study the impact of sequence modification in the GnRH-III sequence on the efficiency of tumor targeting. Apart from that, two different groups of compounds have been designed, one with the native serine in position 4 and a second group where the ^{4}Ser was replaced by ^{4}Lys(Bu) (**Scheme 2**). This modification was selected due to the promising *in vivo* and *in vitro* results of our lead compound **K2** [260,264].

3.1.1.1. Synthesis of oxime bond-linked daunorubicin–GnRH-III conjugates

All oxime-linked GnRH-III-Dau derivatives were synthesized as shown in **Scheme 2**. The peptide carriers were prepared by standard solid phase peptide synthesis (SPPS) using orthogonal lysine protecting groups. With exception of compound **19**, Fmoc-

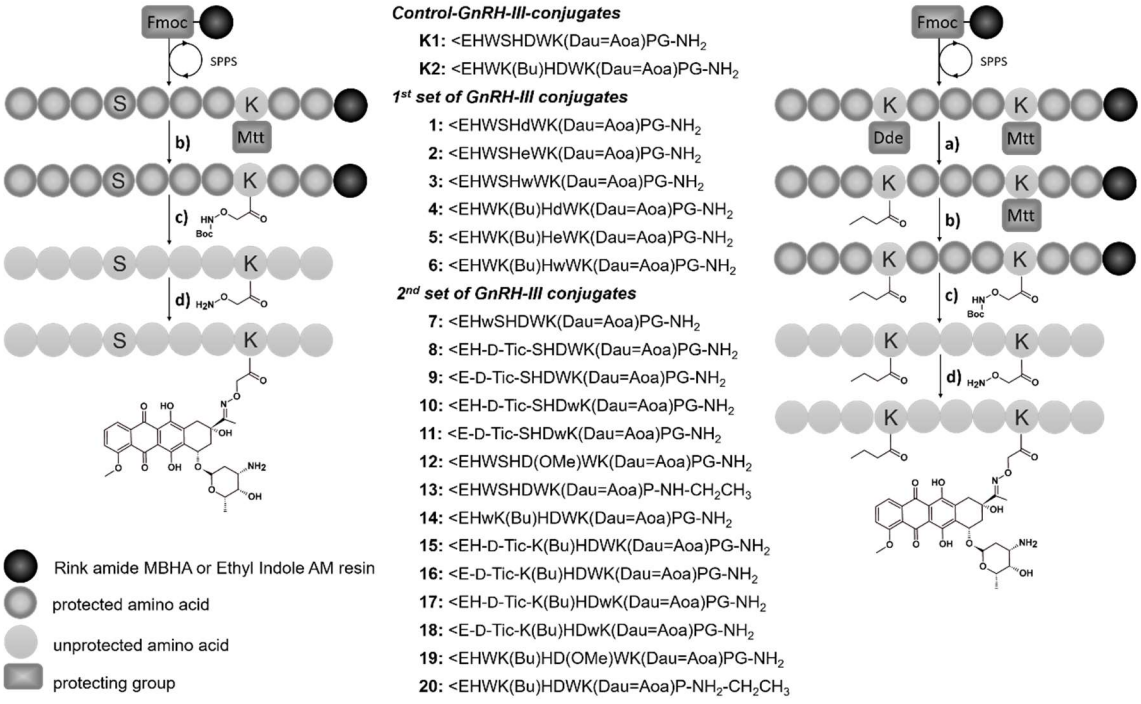

Scheme 2. Synthesis of GnRH-III-Dau conjugates. (a) (1) 2% hydrazine in DMF 12 × 5 min; (2) 3 eq butyric anhydride, 3 eq DIPEA in DMF, 2 h, (b) (1) 2% TFA in DCM, 6 × 5 min; (2) 10% DIPEA in DCM, 3 × 5 min; (3) 3 eq Boc-Aoa-OH, 3 eq HOBt, 3 eq DIC in DMF, 1 h, (c) 95% TFA, 2.5% TIS, 2.5% H_2O, 10 eq H-Aoa-OH, 2 h, (d) 1.3 eq Dau in 0.1 M NH_4OAc buffer (pH 5), overnight. Fmoc: 9-fluorenylmethoxycarbonyl, SPPS: solid phase peptide synthesis, Dde: 1-(4,4-dimethyl-2,6-dioxocyclohex-1-ylidene)ethyl, Mtt: 4-methyltrityl, Bu: butyryl; Aoa: aminooxyacetyl, Dau: daunorubicin.

Ser(tBu)-OH or Fmoc-Lys(Dde)-OH was coupled in position four and Fmoc-Lys(Mtt)-OH in position eight. The Dde group was cleaved after peptide chain elongation and then the ^{4}Lys was butyrylated. In the next step, the Mtt group was removed under mild acidic condition and Boc-Aoa-OH was coupled to the lysine side chain. The peptide moieties were cleaved from the resin using an appropriate TFA-scavenger mixture, followed by RP-HPLC purification. Immediately afterwards, the ligation of Dau by oxime bond formation was carried out in solution and the resulting conjugates were purified again by preparative RP-HPLC.

Synthesis of 1st set of GnRH-III-Dau-conjugates – modification in position 6

Initially, GnRH-III analogs were investigated where ^{6}Asp was replaced by D-Asp, D-Glu and D-Trp. These modifications were chosen since it has been reported that an insertion of D-amino acids in position 6 of GnRH-I and GnRH-II can produce highly efficient analogs with an improved receptor binding affinity and an enhanced anticancer activity [99,101,284,285]. After synthesis, the corresponding GnRH-III-Dau conjugates **1**-**6**, as well as the control peptides **K1** and **K2** were characterized by analytical RP-HPLC and mass spectrometry (**Table 2**, Appendix 10.2.1.1. Figure A1-A8). All bioconjugates revealed a high purity of at least 95% and were obtained in yields up to 27% over all synthesis and purification steps. The reduced yields of the ^{6}D-Aaa-containing compounds, especially for the D-Trp derivatives **3** and **6,** might be mainly related to their decreased solubility in buffered aqueous solution used for chemoselective ligation. Furthermore, the unprotected aminooxyacetyl group is prone to react with aldehydes and ketones. Unwanted side-products can be easily formed through the reaction of the peptide precursors with traces

Table 2: Chemical characteristics of 1st set of GnRH-III-Dau bioconjugates

Code	[^{8}Lys(Dau=Aoa)]-GnRH-III compound	Purity [%]	RP-HPLC R_t [min][a]	ESI-MS MW_{cal} /MW_{exp} [g/mol][b]	Yield [%][c]
K1	-	≥97	27.8	1841.89/1841.66	22
K2	[^{4}Lys(Bu)]	≥97	29.3	1953.07/1952.79	27
1	[^{6}D-Asp]	≥96	28.0	1841.89/1841.60	8
2	[^{6}D-Glu]	≥98	29.2	1855.91/1855.70	14
3	[^{6}D-Trp]	≥95	32.5	1913.01/1912.80	7
4	[^{4}Lys(Bu),^{6}D-Asp]	≥98	29.5	1953.07/1952.90	9
5	[^{4}Lys(Bu),^{6}D-Glu]	≥96	29.7	1966.93/1966.70	7
6	[^{4}Lys(Bu),^{6}D-Trp]	≥97	32.6	2024.03/2023.70	6

[a]Column: Phenomenex Luna C18 column (250 mm x 4.6 mm) with 5 µm silica (100 Å pore size); gradient: 0 min 0% B, 5 min 0% B, 50 min 90% B; eluents: 0.1% TFA in water (A) and 0.1% TFA in acetonitrile-water (80:20, v/v) (B); flow rate: 1 mL/min; detection at 220 nm. [b]Bruker Daltonics Esquire 3000+ ion trap mass spectrometer. [c]Yield over all synthetic and purification steps

of acetone or formaldehyde in plastic tubes (from softeners) or laboratory air, whereby the reaction environment, as well as the RP-HPLC purification conditions can have a high impact on the yields.

Synthesis of 2nd set of GnRH-III-Dau-conjugates – advanced sequence modification

Next to the modification of ^{6}Aaa, an additional set of GnRH-III-Dau conjugates was developed based on previously reported antiproliferative activity studies of drug-free GnRH-III derivatives [142]. My research was focused particularly on amino acid substitutions in position 3 and/or 7 by D-Aaa, alkylation of the ^{6}Asp side chain and the modification of the *C*-terminus were carried out. The synthesized bioconjugates were characterized by analytical RP-HPLC and mass spectrometry (**Table 3**, Appendix 10.2.2.1. Figure A11-A26). To ensure the absence of free Dau, two different analytical RP-HPLC column types (C4 and C18) have been applied. The final products could be obtained in moderate yields up to 42% over all steps. In case of compound **19**, the overall yield was drastically reduced, which was mainly related to the enhanced reactivity of the methyl ester of the ^{6}Asp side chain. Due to the side-reaction of hydrazine with the ^{6}Asp(OMe) during Dde cleavage, the synthesis strategy needed to be changed (see

Table 3: Chemical characteristics of 2nd set of GnRH-III-Dau bioconjugates

Code	GnRH-III-[^{8}Lys(Dau=Aoa)] compound	Purity [%]	RP-HPLC R_t [min][a]	ESI-MS MW_{cal} /MW_{exp} [g/mol][b]	Yield [%][c]
K1	-	≥97	21.37	1841.89/1841.66	22
K2	[^{4}Lys(Bu)]	≥97	22.41	1953.07/1952.79	27
7	[^{3}D-Trp]	≥98	21.43	1841.89/1841.65	14
8	[^{3}D-Tic]	≥98	21.22	1814.86/1814.65	17
9	[^{2}ΔHis, ^{3}D-Tic]	≥95	22.98	1677.72/1677.54	41
10	[^{3}D-Tic, ^{7}D-Trp]	>97	21.58	1814.86/1814.62	16
11	[^{2}ΔHis, ^{3}D-Tic, ^{7}D-Trp]	≥95	23.10	1677.72/1677.53	42
12	[^{6}Asp(OMe)]	≥95	21,85	1855.91/1855.64	7
13	[^{10}ΔGly-NHEt]	≥97	21.18	1812.88/1812.82	8
14	[^{3}D-Trp, ^{4}Lys(Bu)]	≥98	22.83	1953.07/1952.65	16
15	[^{3}D-Tic, ^{4}Lys(Bu)]	≥97	22.57	1926.05/1925.73	19
16	[^{2}ΔHis, ^{3}D-Tic, ^{4}Lys(Bu)]	≥96	24.27	1788.91/1788.64	35
17	[^{3}D-Tic, ^{4}Lys(Bu), ^{7}D-Trp,]	≥96	22.77	1926.05/1925.81	25
18	[^{2}ΔHis, ^{3}D-Tic, ^{4}Lys(Bu), ^{7}D-Trp]	≥98	24.27	1788.91/1788.68	16
19	[^{4}Lys(Bu), ^{6}Asp(OMe)]	≥98	22.92	1967.10/1966.68	1
20	[^{4}Lys(Bu), ^{10}ΔGly-NHEt]	≥97	23.17	1924.07/1923.72	10

[a]Column: Vydac 214TP5 C4 column (250 mm x 4.6 mm) with 5 µm silica (300 Å pore size); gradient: 0 min 0% B, 5 min 0% B, 40 min 90% B; eluents: 0.1% TFA in water (A) and 0.1% TFA in acetonitrile-water (80:20, v/v) (B); flow rate: 1 mL/min; detection at 220 nm. [b]Bruker Daltonics Esquire 3000+ ion trap mass spectrometer. [c]Yield over all synthetic and purification steps.

5.2.1.3.1.) and >=Aoa-OH has been used instead of Boc-Aoa-OH. This coupling reaction was insufficient even after the second repetition which had a decisive impact on the total yield. Moreover, for both Asp(OMe) compounds (**12**, **19**), the formation of the succinimide ring-containing side-product could be detected which also reduced the overall yields of the compounds. However, the obtained amount of the conjugates was sufficient for the conducted experiments, wherefore the synthesis strategy was not optimized further.

3.1.1.2. Biochemical evaluation of 1st set of GnRH-III-Dau-conjugates

To evaluate the influence of sequence modification in position 6, a variety of biochemical studies have been carried out, whereby the novel GnRH-III-Dau compounds were systematically compared with the lead compounds **K1** and/or **K2**. Next to the stability in cell culture medium and the degradation in presence of rat liver lysosomal homogenate, the *in vitro* cytostatic effect, the receptor binding affinity, the cellular uptake, as well as the subcellular localization of the conjugates **1**-**6** have been examined.

3.1.1.2.1. Stability and degradation of the 1st set of GnRH-III-Dau conjugates

In order to verify the efficient activity of the GnRH-III-based drug delivery system, the stability under physiological conditions and the release of the drug in tumor cells is of great importance. Next to stability studies in presence of gastrointestinal enzymes and human serum, the durability under biological assay conditions and the degradation in presence of lysosomal enzymes provide beneficial information. Previously, it has been reported that the conjugates GnRH-III-[^{8}Lys(Dau=Aoa)] (**K1**) and GnRH-III-[^{4}Lys(Ac), ^{8}Lys(Dau=Aoa)] reveal a high stability in human serum, as well as in presence of trypsin, thereby both conjugates stayed intact for at least 24 hours at 37 °C [257,259]. Moreover, it could be shown that the modification in position 4 from Ser to Lys(Ac) enhanced the durability in presence of α-chymotrypsin, which was mainly related to a decelerated cleavage of the ^{3}Trp-^{4}Lys(Ac). A further improvement of the resistance towards chymotrypsin could be observed with increasing chain length of the acyl moiety on the ^{4}Lys [264]. Thus, the butyrylated conjugate **K2** revealed a two-times higher stability than GnRH-III-[^{4}Lys(Ac), ^{8}Lys(Dau=Aoa)] [259,264]. Considering the satisfactory stability of the ^{4}Lys(Bu)-containing GnRH-III conjugates in presence of chymotrypsin and trypsin, an oral administration of the compounds might be feasible. Since the ^{4}Ser of GnRH-peptides are highly susceptible to enzymatic cleavage, the replacement by an acylated lysine leads to an increased stability under physiological conditions and extents the

application possibilities of the GnRH-III-based DDS [264,286,287].

Apart from that, it can be assumed that the ^{6}D-Aaa-containing GnRH-III derivatives reveal a similar or improved durability in presence of gastrointestinal enzymes and human serum. Therefore, the focus was turned to the stability of the compounds in cell culture medium and in presence of rat liver lysosomal homogenate. Both experiments were performed at 37 °C and the compounds were incubated up to 24 hours. For a direct comparison, **K1** and **K2** were included in the experiments and all collected samples were analyzed by LC-MS. All bioconjugates remained intact in cell culture medium, which is in line with our previous studies [264]. Within 24 hours of incubation, only the full bioconjugates could be detected, displaying that no free Dau or any Dau-containing metabolite was produced under conditions used for biological assays.

Next to the stability of the compounds, the release of the drug within the cancer cell is of high importance. Therefore, the digestion of the GnRH-III-Dau analogs (**1**-**6**, **K1**, **K2**) in presence of rat liver lysosomal homogenate has been studied. Since the oxime bond possesses a high chemical and enzymatic stability, no release of free Dau was detected, which is in agreement with previous results [259,264]. However, recent studies point out that also small Dau-containing metabolites such as H-Lys(Dau=Aoa)-OH can interact with DNA by intercalation and inhibit the topoisomerase II activity which leads to reduced cell proliferation [257]. The results of the degradation study demonstrate that all applied GnRH-III conjugates were digested by lysosomal enzymes resulting in various fragments (**Figure 10A**, Appendix 10.2.1.2.), whereby the degradation profile and cleavage sites vary depending on their amino acid sequence. Though, the cleavage of the *C*-terminal part of the conjugate (H-Gly-NH_2 and H-Pro-Gly-NH_2) could be observed already within the first 5 minutes for all eight conjugates indicating the presence of enzymes with carboxymono- and dipeptidase activity. Besides that, the smallest Dau-containing metabolite H-Lys(Dau=Aoa)-OH (**Figure 10B**) was most efficiently released in case of the ^{6}L-Asp-containing control derivatives. This fragment could be detected after one (**K2)** and two (**K1**) hours of incubation which is consistent with previous results [259,264]. In contrast, the ^{6}D-Asp-containing counterpart **1** and **4** displayed an increased resistance to lysosomal enzymes which avert the release of the H-Lys(Dau=Aoa)-OH. Despite this fact, a small amount of the bioactive metabolite could be obtained after 24 hours lysosomal digestion of the ^{6}D-Glu-containing conjugates **2** and **5**. Interestingly, from all D-Aaa-containing compounds, the ^{6}D-Trp derivatives were most efficiently degraded revealing the presence of the smallest Dau-metabolite already within two (**6**) or four (**3**) hours and

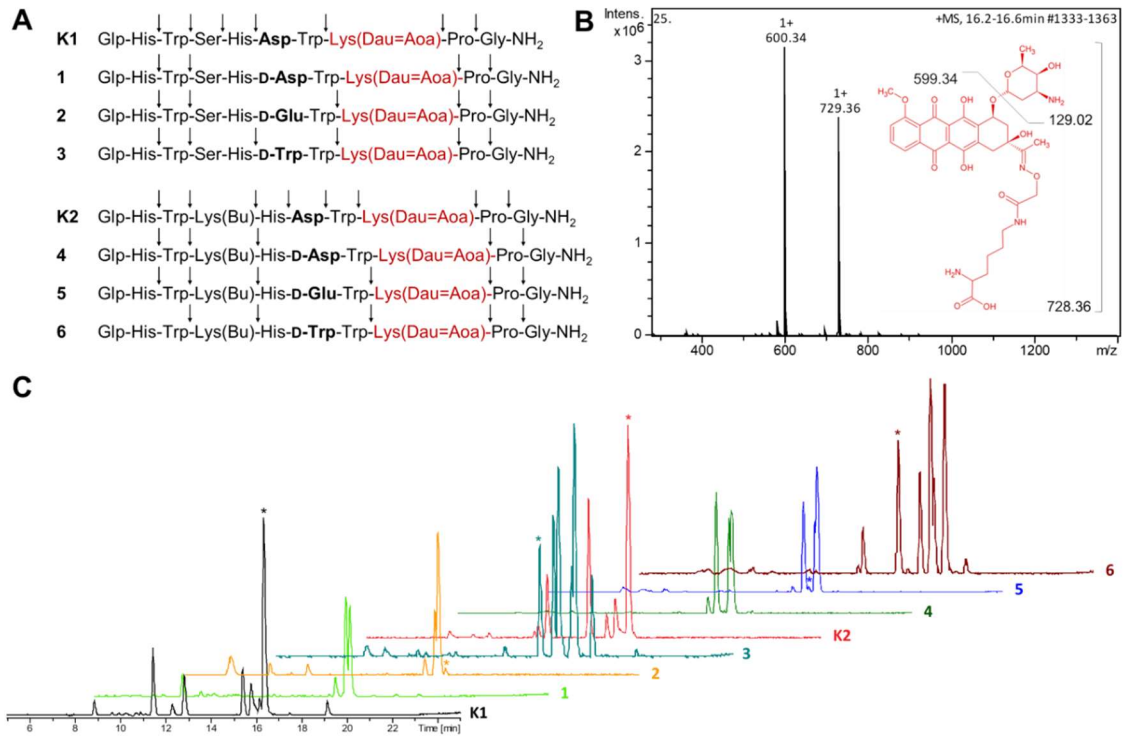

Figure 10. Degradation of 1st set of GnRH-III-Dau bioconjugates by rat liver lysosomal homogenate. **A**: Detectable cleavage sites of lysosomal enzymes, **B**: mass spectrum and structure of the smallest Dau-containing metabolite (H-K(Dau=Aoa)-OH). **C**: RP-HPLC chromatogram of the bioconjugates after 24 h incubation with lysosomal homogenate at 37 °C (*peak of H-K(Dau=Aoa)-OH).

in higher amount (**Figure 10C**: labeled peaks). Moreover, the obtained fragment H-wWK(Dau=Aoa) indicates that the ^{6}D-Trp of compound **3** was accepted by the S1' site of at least one lysosomal protease which might promote the release of the active fragment. It can be assumed that also the ^{6}D-Trp of bioconjugate **6** was accepted at this site, but due to a prior hydrolysis of the peptide bond between ^{7}Trp- and ^{8}Lys(Dau=Aoa)-OH, an evidential fragment could not be detected. Another explanation for this diversity might be the substrate specificity of the proteases whereby not only the S1 and S1' but also adjacent binding sites can have an impact on the proteolysis of the substrate [288]. In general, lysosomal cysteine proteases also known as cathepsins show a broad substrate specificity with the preference to cleave their substrate after basic or hydrophobic residues [289]. Nearly all human cysteine proteases exhibit an endopeptidase activity, whereas cathepsin B possesses an additional carboxydipeptidase activity and cathepsin X acts as carboxymono- and dipeptidase [289–293]. In contrast, cathepsin H possesses both an endopeptidase and a strong monoaminopeptidase activity different from cathepsin C which acts as a diaminopeptidase [290,294]. Considering all identified proteolytical fragments, it can be supposed that the applied rat liver homogenate contains a mixture of enzymes with comparable activities. Besides, the obtained results indicate that the

exomono- and/or dipeptidase activity was not substantially affected by the amino acid replacement, while the incorporation of ^{6}D-Aaa in combination with ^{4}Ser reduced the endopeptidase activity. Interestingly, the analysis of the ^{4}Lys(Bu) conjugates (**4**-**6**, **K2)** leads to the assumption that the replacement of ^{4}Ser by ^{4}Lys(Bu) supports the acceptability of the GnRH-III-Dau compounds as substrate for lysosomal endopeptidases. Thus, the insertion of ^{4}Lys(Bu) has not only a positive impact on the stability under physiological conditions, but also on the degradation of the compounds by lysosomal enzymes. This might be of high relevance for the release of the drug or bioactive metabolites within cancer cells and might enhance the selectivity of these conjugates to tumor cells.

3.1.1.2.2. In vitro cytostatic effect

To determine the biological activity of the novel conjugates, the *in vitro* cytostatic effect of the GnRH-III-Dau conjugates **1**-**6** was studied on reproductive system related MCF-7 human breast cancer and unrelated HT-29 human colon cancer cells. The well-studied bioconjugates **K1** and **K2** were used as internal standards for a better and direct comparison, since immortal cell lines can differ in their genotypic and phenotypic characteristics depending on the passage and state of confluence [295,296]. However, due to their easy handling, cost-effectiveness and a high level of reproducibility, cancer cell lines are often the first method of choice to study the antiproliferative activity of novel anticancer drugs or drug conjugates [296].

It could be shown that GnRH-R expression occurs in cancers related to the reproduction system, like breast, endometrial, prostate and ovarian cancer, but also in tumors unrelated to the reproductive system, such as lung, melanoma and colorectal cancer [114,297–302]. Based on these findings, one cell line from each group, namely MCF-7 and HT-29 was chosen to study the growth inhibitory effect of the GnRH-III-Dau conjugates on cancer cells. Many different studies evidence that both cell lines express GnRH-receptors and that they are particularly suitable for *in vitro* characterization of GnRH and its derivatives [80,116,252,302]. Apart from that, the GnRH-R expression was confirmed for both human cancer cell lines by western blot analysis (Appendix 10.2.2.3.). In order to investigate the influence of sequence modification in position 6, a resazurin-based cell viability assay was performed[a] and the corresponding IC_{50} values were calculated by nonlinear regression (sigmoidal dose-response) (**Table 4**, Appendix 10.2.1.3.). Due to the fact that

[a] Experiments were performed in close collaboration with Beáta Biri-Kovács

Table 4: *In vitro* cytostatic effect of 1st set of GnRH-III-Dau bioconjugates on HT-29 human colon cancer and MCF-7 human breast cancer cells

Code	GnRH-III-[^{8}Lys(Dau=Aoa)] compound	IC_{50} [µM] HT-29	IC_{50} [µM] MCF-7
K1	-	1.5 ± 0.5	3.2 ± 0.1
K2	[^{4}Lys(Bu)]	1.9 ± 0.7	2.7 ± 0.1
1	[^{6}D-Asp]	8.9 ± 1.3	13.0 ± 0.5
2	[^{6}D-Glu]	10.1 ± 1.4	6.8 ± 0.2
3	[^{6}D-Trp]	n.d.[a]	n.d.[a]
4	[^{4}Lys(Bu),^{6}D-Asp]	9.3 ± 1.1	6.2 ± 0.2
5	[^{4}Lys(Bu),^{6}D-Glu]	13.7 ± 2.6	7.0 ± 1.2
6	[^{4}Lys(Bu),^{6}D-Trp]	n.d.	n.d.

n.d. – not determined, [a] compound **3** and **6** precipitated in medium at concentrations higher than 20 µM – no dose response), all values represent mean ± SE

the D-Trp-containing compounds **3** and **6** started to precipitate in cell culture medium at higher concentrations, the maximum concentration of these compounds was limited to 10 µM. Unfortunately, the precipitation could not be avoided using DMSO instead of water. Thus, it can be assumed that the reduced solubility is mainly related to the presence of inorganic salts, sugars, amino acids or other components of the medium. Though 10 µM was not sufficient to obtain the maximal biological response of the compounds, but both compounds revealed a growth inhibitory effect at this concentration. The cell viability was reduced down to 58% (**3**) or rather 55% (**6**) in case of HT-29 cells, while 69% (**3**) and 53% (**6**) cell viability has been determined on MCF-7 cells. For the other novel bioconjugates, IC_{50} values between 6.2-13.7 µM were obtained on both cell lines. Except compound **1**, all new GnRH-III-Dau analogs display a higher cytostatic effect on MCF-7 than on HT-29 cells which is in line with previous studies [259,264]. Moreover, all analyzed compounds exhibit a moderate *in vitro* cytostatic effect, although the replacement of ^{6}Asp by D-Asp, D-Glu or D-Trp did not lead to an improved biological activity on the examined cell lines. This might be explained by the enhanced stability of the new conjugates **1**-**6** towards lysosomal enzymes and the associated release of the active drug-metabolite within the cancer cell.

Apart from that, there was no substantial difference regarding the anticancer activity of the ^{4}Ser and ^{4}Lys(Bu)-containing derivatives which is not in accordance with former studies [264]. A possible explanation for this observation might be the extended treatment time which was adjusted from six hours to 24 hours. This modification was necessary to achieve the maximal biological response of the novel DDSs. Thus, it can be assumed that the ^{4}Ser bioconjugates require a longer treatment period to display their full biological

activity. Besides that, the ^{6}D-Glu conjugates **2** and **5** exhibit slightly higher IC_{50} values on HT-29 cells than the D-Asp compounds, although the release of the smallest Dau-containing metabolite was observed only in case of the D-Glu analogs. Considering these findings, it can be supposed that not only the formation of the smallest drug metabolite, but also other factors, like the cellular uptake or the receptor affinity of the drug-conjugates have an impact on the biological activity.

3.1.1.2.3. Radioligand binding studies

To gain a further insight into the role of ^{6}Asp on the anticancer activity, the receptor binding affinity of the GnRH-III-Dau derivatives was investigated by an *in vitro* radioligand competition assay. The experiments were performed at the research group of Gábor Halmos (Department of Biopharmacy, Faculty of Pharmacy, University of Debrecen). Hence, the displacement of radiolabeled triptorelin (GnRH-I-[^{6}D-Trp]) by the Dau conjugates (**K1**, **K2**, **1**, **2**, **4**, **5**) has been studied on human pituitary and GnRH-R positive human prostate cancer tissues. The obtained IC_{50} values (**Table 5**) are in the low nanomolar range indicating that all applied compounds replace [^{125}I]-triptorelin efficiently from cancer, as well as pituitary tissue. In agreement with previous studies, the majority of the analyzed GnRH-III-Dau analogs displayed a slightly higher binding affinity on human prostate cancer than on pituitary tissue [264,284]. The highest binding affinity was obtained for the control **K2** (3.9 nM on pituitary and 3.0 nM on human prostate cancer), followed by its ^{6}D-Asp-containing counterpart **4** (6.1 nM on pituitary and 4.0 nM on human prostate cancer). In general, the ^{4}Lys(Bu) conjugates bind GnRH-Rs with higher affinity than their ^{4}Ser equivalent, whereas the selectivity of ^{4}Ser conjugates towards cancer tissue was more favorable. Besides that, the results indicate that the incorporation of D-Glu in position 6 reduces the binding affinity with a higher extent than D-Asp. Nevertheless, all determined IC_{50} values are within a narrow, low nanomolar range and vary, especially on cancer tissue (3.0-11.6 nM), only slightly from each other, indicating that the incorporation of D-Asp and D-Glu has no crucial effect on the receptor binding affinity. Furthermore, the investigated GnRH-III-Dau conjugates displaced the radiolabeled triptorelin completely by using rising compound concentrations (1 pM to 1 μM). This is comparable to the reported results of the high affinity GnRH-R ligands cetrorelix and buserelin, whereas GnRH unrelated peptides, like SST-14 or bombesin, could not inhibit triptorelin binding at concentrations up to 1 μM [303,304]. Comparing the obtained results with findings from the literature, it can be supposed that all analyzed conjugates bind to the GnRH-receptor in a specific manner.

Table 5: Competitive inhibition of [^{125}I][^{6}D-Trp]-GnRH-I binding to membranes of human pituitary and human prostate cancer specimens by GnRH-III-Dau conjugates.

Code	GnRH-III-[^{8}Lys(Dau=Aoa)] compound	IC_{50} [nM]	
		pituitary	prostate cancer
K1	-	6.5 ± 0.7	5.2 ± 0.6
K2	[^{4}Lys(Bu)]	3.9 ± 0.7	3.0 ± 1.1
1	[^{6}D-Asp]	19.4 ± 2.8	8.9 ± 1.6
2	[^{6}D-Glu]	23.5 ± 2.1	10.4 ± 1.3
3	[^{6}D-Trp]	n.d.	n.d.
4	[^{4}Lys(Bu),^{6}D-Asp]	6.1 ± 0.1	4.0 ± 1.3
5	[^{4}Lys(Bu),^{6}D-Glu]	7.9 ± 1.1	11.6 ± 2.0
6	[^{4}Lys(Bu),^{6}D-Trp]	n.d.	n.d.

n.d. – not determined, all values represent mean ± SE

3.1.1.2.4. Cellular uptake of the bioconjugates by flow cytometry

Flow cytometry studies were carried out[b] to investigate the cellular uptake of the GnRH-III-Dau conjugates on HT-29 and MCF-7 cancer cells, whereby only living cells have been considered to determine the cellular uptake rates (**Figure 11**). Because of the reduced solubility of compound **3** and **6** in cell culture medium, they were not included in this experiment. The cancer cells were treated with different concentrations of the new conjugates **1**, **2**, **4** and **5**, as well as the controls **K1** and **K2** for six hours. Both controls revealed a higher cellular uptake rate on HT-29 cells than the D-Aaa-containing compounds, whereby the cellular uptake at 10 µM compound concentration was higher for **K2 (**27.2%) than for **K1 (**17.8%) which is in line with previous data [259,264]. At 40 µM, the uptake rates for **K1** (94.1%) and **K2** (94.7%) were comparable, whereby the uptake of novel compounds varied between 13.1% (**5**) and 55.2% (**1**). In addition, all bioconjugates except **5** (84%) displayed a cellular uptake rate over 90% on HT-29 cells at 160 µM concentration. A similar effect could be observed on MCF-7 cells, while compound **5** was taken up by 76.8% of living cells. Furthermore, ^{6}D-Asp bioconjugate **1** revealed with 3.5% the best uptake rate at 10 µM and with 48.4% the second best at 40 µM concentration, though **K2** was taken up more efficiently with 61.2%. Considering all obtained uptake rates, compound **1** exposed the best uptake profile of the ^{6}D-Aaa-containing compounds with even higher uptake rates on MCF-7 than its ^{6}L-Asp counterpart **K1**, while both ^{6}D-Glu derivatives showed a clearly declined cellular uptake rate on both cell lines. Additionally, the uptake rates of the ^{4}Ser analogs **1** and **2** were substantially higher than for the ^{4}Lys(Bu) counterparts **4** and **5**, although an opposite

[b] Flow cytometry studies were performed by Beáta Biri-Kovács

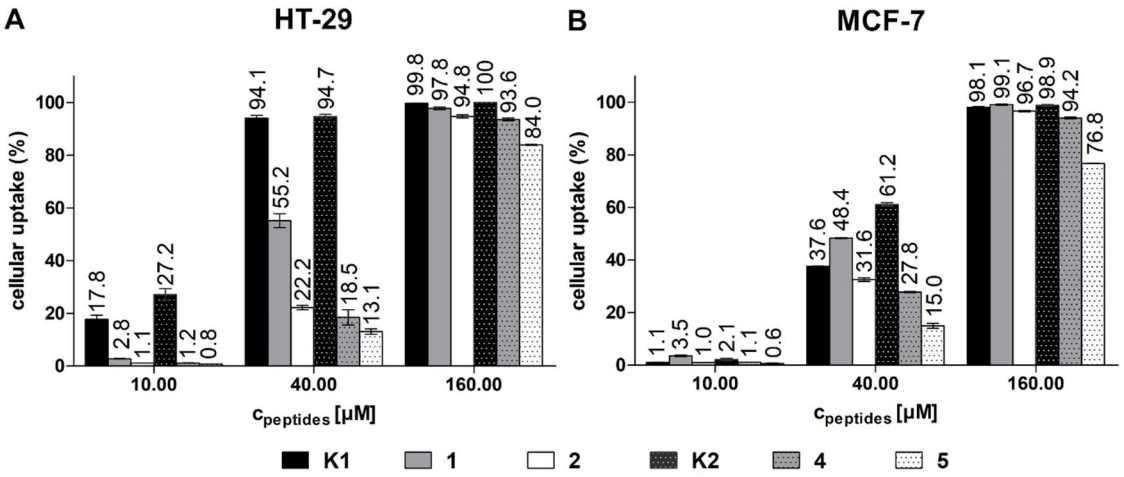

Figure 11. Cellular uptake of 1st set of GnRH-III-Dau conjugates by flow cytometry. **A**: HT-29 and **B**: MCF-7 cancer cells after 6 h treatment. Experiments were performed in duplicates. Error bars represent SD.

effect could be observed for the ^{6}L-Asp controls **K1** and **K2**. Taking into account that the receptor binding was not essentially disturbed by the incorporation of D-Aaa in position 6, it might be possible that the internalization of the receptor is influenced by these sequence modifications.

Considering all these findings, it can be concluded that the cytostatic effect is not only influenced by the cellular uptake of the bioconjugates, but also the release of the smallest Dau-containing metabolites is of high relevance. This becomes particularly obvious in case of bioconjugate **1** which was taken up more efficiently than the other D-Aaa compounds, while its IC_{50} value was comparable to the ones from the other derivatives or even higher. This might be a result of the enhanced stability of bioconjugate **1** in presence of lysosomal enzymes which prevents the release of the bioactive metabolite H-Lys(Dau=Aoa)-OH.

3.1.1.2.5. Confocal laser scanning microscopy (CLSM) studies[c]

In order to visualize the cellular uptake and the sub-cellular localization of the bioconjugates (**1**, **2**, **4**, **5**, **K1** and **K2**) on MFC-7 cells, confocal fluorescence microscopy studies were carried out. In the initial experiment, 10 µM, 40 µM and 160 µM compound concentrations were used and after six hour treatment, the cells were fixed and prepared for CLSM imaging. Due to the fact that Dau assimilates in the nuclei and intercalates with DNA, nuclei were stained with DAPI to verify the presence of the drug on its site of action by co-localization. All presented CLSM images are depicted in BestFit mode to

[c] All CLSM samples were prepared by Beáta Biri-Kovács (MTA-ELTE Research Group of Peptide Chemistry, ELTE Budapest) and images were recorded by Bálint Szeder (MTA Research Centre for Natural Science, Institute of Enzymology, Budapest)

ensure an improved illustration of low signals and to enhance image quality. In general, the recorded images should not be considered in a quantitative manner, but they provide valuable qualitative information of the intracellular localization of the bioconjugates. All analyzed compounds and concentrations displayed the Dau-signal predominantly in the nuclei but also in small cytosolic compartments (**Figure 12A**, Appendix 10.2.1.4) demonstrating that the conjugated Dau gets to its site of action.

In order to gain a deeper insight into the intracellular localization directly after internalization, an additional CLSM experiment was carried out in a time-dependent manner. Based on the fact, that bioconjugate **K2** provides the highest biological activity on MCF-7 cells and was taken up most efficiently according to the flow cytometry studies, it was selected for further investigation, whereby a constant compound

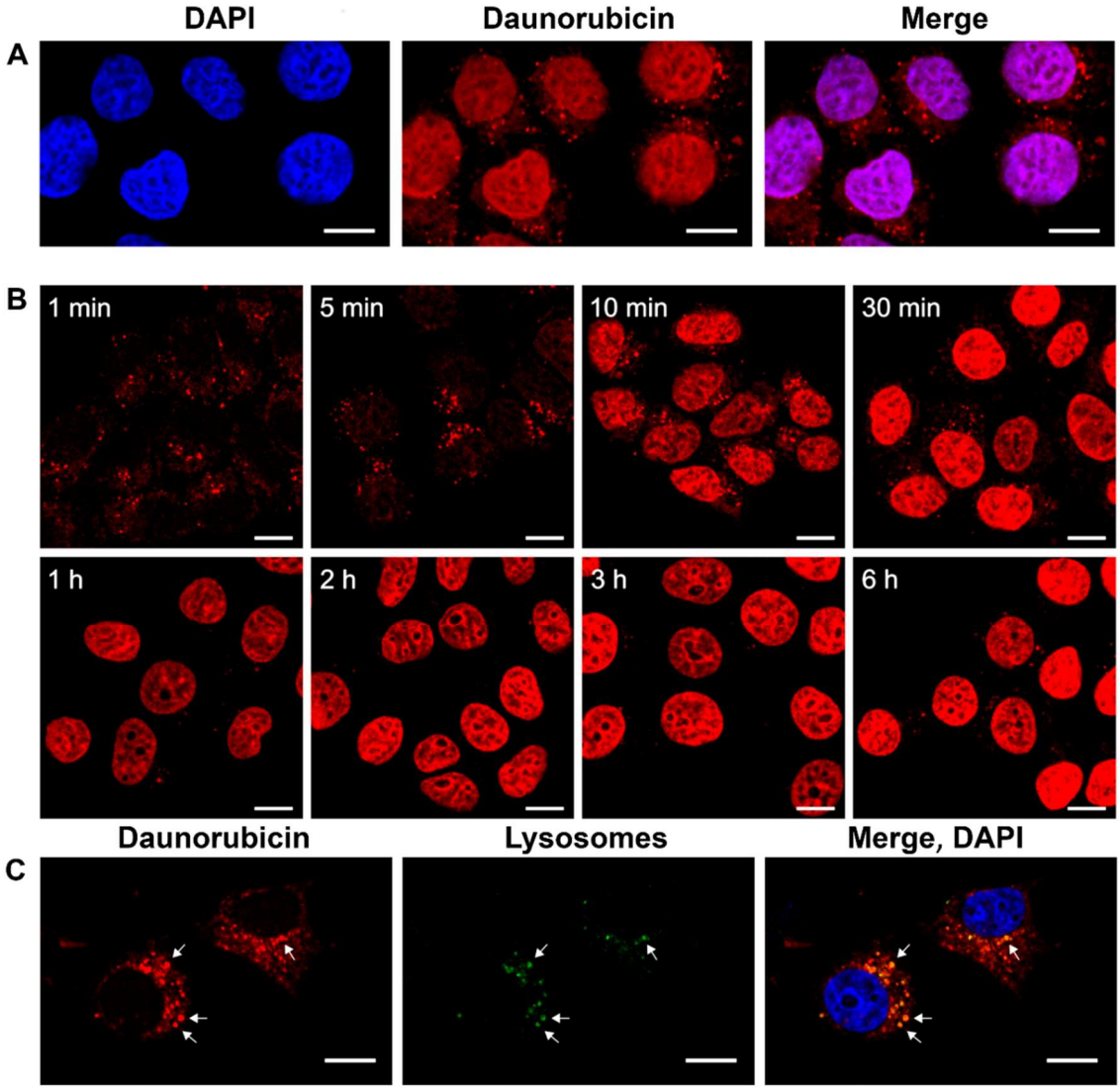

Figure 12. Cellular localization of conjugate **K2** (40 µM) visualized by confocal laser scanning microscopy (CLSM). **A**: Co-localization of Dau-signal with nuclei (stained by DAPI) after 6 h incubation. **B**: Time-dependent localization of **K2** after 1, 5, 10, 30 minutes and 1, 2, 3, 6 hours incubation. **C**: Co-localization of **K2** with lysosomes (stained with CytoPainter Lysosomal staining Kit) after 5 minutes incubation. Scale bars represent 10 µm.

concentration of 40 µM was applied. The obtained results (**Figure 12B**) demonstrate the presence of Dau in the nuclei already after 10 to 30 minutes, while after a short treatment period of 1 and 5 minutes, the Dau-signal was mainly detected in small cytosolic vesicles. Due to the fact that it is assumed that the GnRH-III derivatives, like **K2,** enter cancer cells by a receptor-mediated endocytic pathway, the small cell compartments at early time points might be lysosomes. To validate this assumption, a lysosomal co-localization study was carried out with bioconjugate **K2** on MCF-7 cells. For this purpose, the cells were preincubated with a lysosomal stain, followed by five minutes treatment with **K2**. As shown in **Figure 12C**, the obtained signal of the lysosomal stain corresponds largely to the monitored Dau-signal. Considering that a higher amount of intracellular vesicles was monitored by Dau than by the lysosomal staining kit, it can be assumed that the remaining vesicles belong to other compartments of the endocytic pathway and display early and late endosomes.

3.1.1.2.6. Receptor blockage by triptorelin

The obtained results from CLSM studies support the proposed endocytic internalization of the GnRH-III conjugates. To ensure that the cellular uptake occurs in a receptor-mediated manner, the uptake rate of **K2** was studied by flow cytometry in presence of the GnRH superagonist triptorelin. The ligand competition assay was performed by Beáta Biri-Kovács and carried out on MCF-7 cells using a constant concentration of **K2** (40 µM) and ascending doses of triptorelin. This highly effective GnRH-I analog was already successfully used to verify the receptor mediated pathway of the GnRH-I-Dox conjugate AN-152 [237]. Since recently reported data pointed out that triptorelin can cause an enhanced GnRH-R density on MCF-7 cells, a shorter treatment time might be favorable for the competition study [297]. Due to this and the results of the CLSM which indicate that one to two hours of treatment are sufficient enough to obtain a substantial uptake of **K2**, the treatment time was adjusted to 100 min, whereby the cells were incubated simultaneously with **K2** and triptorelin. The obtained results evident that the cellular uptake of **K2** can be inhibited in a concentration dependent manner by triptorelin which confirms the assumption that the GnRH-III-Dau conjugates can enter GnRH-R positive cancer cells in a receptor mediated manner (**Figure 13**).

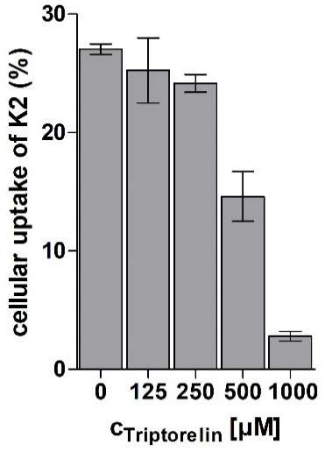

Figure 13. Competitive inhibition of **K2** on MCF-7 cells in presence of triptorelin (125-1000 µM) by flow cytometry.

3.1.1.3. Biochemical evaluation of 2nd set of GnRH-III-Dau conjugates

Considering the fact that the incorporation of ^{6}D-Aaa did not lead to an improved antitumor activity of the GnRH-III-Dau conjugates, further amino acid substitutions, and their effect on cancer cell proliferation have been investigated. The applied sequence modifications have been selected based on the findings of previously reported structure-related activity studies of unconjugated GnRH-III derivatives [142]. Due to the results of Pappa *et. al*., 14 novel GnRH-III-Dau conjugates with modified peptide sequence have been prepared and evaluated. Similar to the 1st set of GnRH-III-Dau-conjugates, all synthesized compounds have been studied for their inhibitory effect on the growth of GnRH-R expressing HT-29 colon cancer and MCF-7 breast cancer cells. For a better interpretation of the results, the cytostatic effect of a distinct group of compounds was also analyzed on MDA-MB-231 breast cancer cells. Afterwards, the best candidates were selected for further studies, including the stability in presence of human blood plasma and lysosomal enzymes, the cellular uptake and sub-cellular localization, as well as the affinity to GnRH-Rs.

3.1.1.3.1. In vitro cytostatic effect

At the outset of the cell viability studies, GnRH-R expression was confirmed on HT-29, MCF-7 and MDA-MB-231 cancer cells by western blot analysis. In case of all three cell lines, a distinct band at approximately 38 kDa was identified, which can be considered as full-length human GnRH-R (Appendix 10.2.2.3. Figure A30). In addition, further bands at higher molecular weight (55-70 kDa) were detected which is in line with previous findings and might represent the glycosylated forms of the GnRH-Rs [305–307]. In the next step, the *in vitro* cytostatic effect of the modified GnRH-III-Dau derivatives was determined on MCF-7 and HT-29 human cancer cells by a resazurin-based cell viability assay, performed by Beáta Biri-Kovács. To ensure the comparability with previous results, the well-established compounds **K1** and **K2** were used as internal standards and positive controls [259,264]. As it is shown in **Table 6**, all investigated GnRH-III-Dau conjugates revealed an inhibitory effect on cancer cell growth, whereby the obtained IC_{50} values vary between 0.14 and 6.64 µM on MCF-7 cells and 3.31-18.00 µM on HT-29 cells. The slightly lower anticancer activity on HT-29 is in line with previous data [259,264]. With exception of compound **16**, the cytostatic effect of the bioconjugates was not substantially different from that of the controls **K1** and **K2**. However, the exchange of ^{3}Trp by ^{3}D-Tic in combination with ^{4}Lys(Bu) and the deletion of ^{2}His led to a remarkable improved cytostatic effect of bioconjugate **16** on both cell lines, whereby its IC_{50} value

Table 6: *In vitro* cytostatic effect of 2nd set of GnRH-III-Dau bioconjugates on HT-29 human colon cancer, MCF-7 and MDA-MB-231 human breast cancer cells

Code	[GnRH-III-^{8}Lys(Dau=Aoa)]-compound	IC_{50} [µM] HT-29	IC_{50} [µM] MCF-7	IC_{50} [µM] MDA-MB-231
K1	-	13.89±3.62	2.54±0.67	8.22±0.13
K2	[^{4}Lys(Bu)]	15.93±0.99	2.36±0.07	9.00±1.33
7	[^{3}D-Trp]	15.25±2.51	3.60±0.28	n.d.
8	[^{3}D-Tic]	8.75±0.86	2.89±0.62	n.d.
9	[^{2}ΔHis, ^{3}D-Tic]	10.32±1.32	2.75±0.17	9.35±1.93
10	[^{3}D-Tic, ^{7}D-Trp]	15.34±2.63	3.42±0.39	n.d.
11	[^{2}ΔHis, ^{3}D-Tic, ^{7}D-Trp]	10.70±0.95	1.90±0.58	7.88±1.24
12	[^{6}Asp(OMe)]	10.66±1.76	4.81±0.72	n.d.
13	[^{10}ΔGly-NHEt]	14.18±3.59	4.88±0.01	14.33±1.18
14	[^{3}D-Trp, ^{4}Lys(Bu)]	15.03±2.51	6.64±1.58	n.d.
15	[^{3}D-Tic, ^{4}Lys(Bu)]	12.73±3.10	2.56±0.51	n.d.
16	[^{2}ΔHis, ^{3}D-Tic, ^{4}Lys(Bu)]	3.31±0.90	0.14±0.01	2.49±0.53
17	[^{3}D-Tic, ^{4}Lys(Bu), ^{7}D-Trp,]	16.83±0.66	2.57±0.47	n.d
18	[^{2}ΔHis, ^{3}D-Tic, ^{4}Lys(Bu), ^{7}D-Trp]	16.55±0.30	2.81±0.04	8.18±0.18
19	[^{4}Lys(Bu), ^{6}Asp(OMe)]	18.00±0.13	3.44±0.51	n.d.
20	[^{4}Lys(Bu), ^{10}ΔGly-NHEt]	17.84±0.08	2.23±0.40	12.41±2.30

n.d. – not determined, all values represent mean ± SE

on MCF-7 cells was more than 15-times lower, and on HT-29 cells around five-times lower than that of compound **K2**. Furthermore, the *C*-terminal modification ^{10}ΔGly-NHEt (**13**, **20**) did not cause a notable change in the anticancer activity compared to the controls. These results are in line with reported results of drug-free GnRH-III derivatives [141], while in case of GnRH-I, the substitution of Gly-NH_2 by ethyl amide leads to an enhanced biological activity of the GnRH-I agonist fertirelin [308,309]. This effect could be further improved by combining the *C*-terminal modification ^{9}Pro-^{10}ΔGly-NHEt with ^{6}D-Aaa resulting in GnRH-I superagonists, like buserelin (^{6}D-Ser(tBu),^{10}ΔGly-NHEt) or leuprolide (^{6}D-Leu,^{10}ΔGly-NHEt), with much higher biological activity than GnRH-I or fertirelin [99,309]. It has been shown that the improved activity of these GnRH-I agonists is mainly related to an enhanced β-turn conformation which is caused by the D-Aaa substitution in position 6 [100]. Regarding the results of the 1st set of GnRH-Dau conjugates, it could be demonstrated that an adaption of this concept to GnRH-III derivatives is not leading to a similar positive effect on the activity of GnRH-III derivatives. Beyond that, divergent results about the importance of ^{6}Asp on the anticancer activity of GnRH-III have been published [138,142,310]. According to Pappa *et al.*, who studied the antitumor activity of GnRH-III peptide derivatives without drug molecule, the

negative charge in position six is not essential for the antiproliferative activity of GnRH-III derivatives, whereby especially methylation of ^{6}Asp might lead to an increased activity [142]. On the other hand, previous studies pointed out that this aspartate plays a crucial role on the activity of GnRH-III and its derivatives [142,310]. To investigate the impact of ^{6}Asp on the antitumor activity of GnRH-III-[^{8}Lys(Dau=Aoa)] conjugates, Asp(OMe) was incorporated instead of ^{6}Asp yielding compound **12** and **19**. The obtained results confirm that the acidic character is not mandatory for the anticancer activity of the Dau conjugates, though the methylation did not lead to an improved *in vitro* cytostatic effect. Considering these results, as well as the findings from the literature, it can be assumed that not the negative charge directly, but rather the general structure of the side chain and the corresponding different intramolecular interactions are responsible for the biological activity.

In addition, the *N*-terminal residues ^{2}His and ^{3}Trp might be of high importance for the receptor binding and the antiproliferative activity of GnRH-I and GnRH-III [101]. In case of GnRH-I derivatives, it could be shown that an exchange of ^{3}Trp to ^{3}D-Trp and ^{3}D-Tic led to a reduced receptor binding affinity, while the antiproliferative activity of the compounds was increased on MCF-7 cells [311]. A similar inhibitory effect on the cell growth of LNCaP human prostate cancer cells could be observed for ^{3}D-Trp and ^{3}D-Tic-containing GnRH-III derivatives which could be further improved by a coincidental ^{7}D-Trp insertion [142]. Due to these findings, the influence of ^{2}His-^{3}Trp sequence modification was analyzed, whereby also the combination with ^{7}D-Trp was examined. In accordance with previous studies, none of the applied modifications led to a substantial decline of the cytostatic effect of the GnRH-III-Dau conjugates [142]. In the first step, ^{3}D-Trp or ^{3}D-Tic was incorporated within the peptide sequence resulting in a slightly enhanced activity for the D-Tic compounds **8** and **15** on HT-29 cells. To achieve a more pronounced reduction of the cancer cell viability, the effect of ^{2}His deletion with or without ^{7}D-Trp substitution was studied in combination with ^{3}D-Tic. In contrast to the results from Pappa *et al.*, the replacement of ^{7}Trp to ^{7}D-Trp did not lead to an improved anticancer activity which might be the result of an enhanced stability of the conjugates towards lysosomal enzymes. Thus, one possible explanation is that the insertion of ^{7}D-Trp adjacent to ^{8}Lys(Dau=Aoa), could lead to a decelerated release of the smallest Dau-containing metabolite which might overcompensate an advantageous inherent anticancer activity. Apart from that, the deletion of ^{2}His in combination with ^{3}D-Tic-^{4}Lys(Bu) produced a GnRH-III-Dau conjugate (**16**) with a clearly increased anticancer activity on both cell lines, whereby the

improvement on MCF-7 cell was notably higher than on HT-29. This effect might be related to the fact that GnRH-receptor signaling can interfere with estrogen receptor signaling [80]. For instance, it was shown that the GnRH agonist triptorelin inhibited 17β-estradiol (E2)-induced cell proliferation in MFC-7 and other ERα+/ERβ- cancer cells while ERα-/ERβ+ cancer cell lines remained unaffected [298]. This example clearly indicates that GnRH-analogs can affect estrogen-induced cell proliferation. To verify the obtained results, the *in vitro* cytostatic effect of compound **16** was additionally investigated on GnRH-R positive but ERα negative MDA-MB-231 breast cancer cells. For a better interpretation, all ^{2}ΔHis-^{3}D-Tic-containing conjugates (**9**, **11**, **16**, **18**), as well as the *C*-terminal modified conjugates (**13**, **20**) were included in this study. The tendency of the growth inhibitory effect on MDA-MB-231 cells was comparable to that of MCF-7 and HT-29 cells, whereby bioconjugate **16** revealed on all three cell lines a higher activity than **K2** (**Figure 14**) or any other applied GnRH-Dau conjugate. This clearly indicates that compound **16** is highly efficient on ERα+ and ERα- breast cancer cells, as well as on reproduction system unrelated colon cancer cells, which might lead to an enlarged scope of application. The promising results, especially on MDA-MB-231 cells which are not only ERα-, but also progesterone receptor (PgR) and human epidermal growth factor receptor 2 (HER-2) negative, illustrate the great potential of compound **16** [80,297]. Since these so called triple negative breast cancer (TNBC) cells are known to be more aggressive and lack the ability to use specific targeted treatment options, like Herceptin

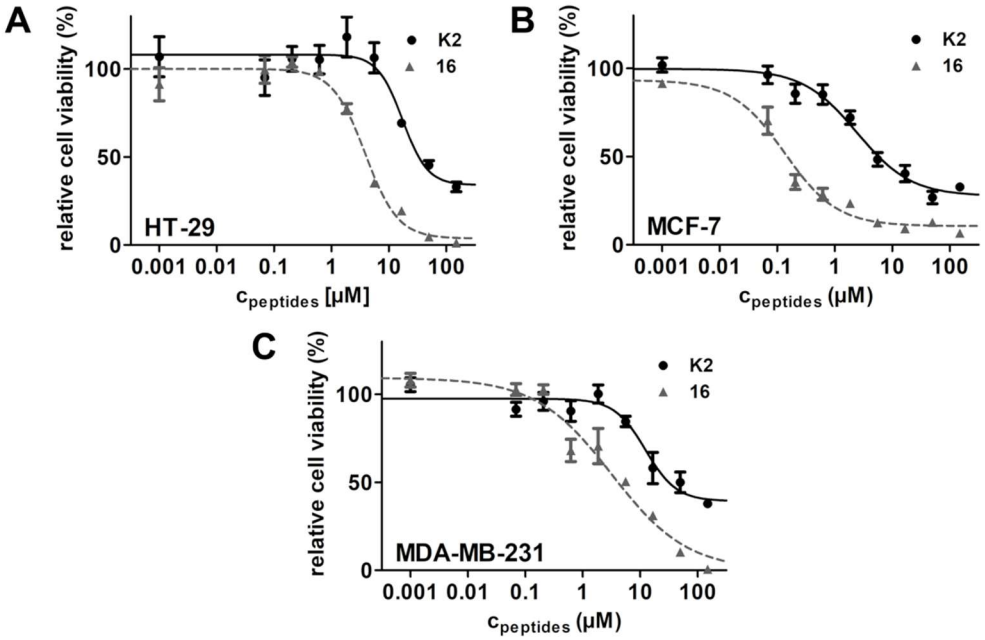

Figure 14. Cytostatic effect of the GnRH-III conjugate **K2** and **16** on **A**: HT-29, **B**: MFC-7 and **C**: MDA-MB-231 human cancer cells after 72 h (24 h treatment and an additional 48 h incubation). Curves obtained by non-linear regression (sigmoidal dose response, error bars represent the standard deviation of four parallels, the measurements were repeated twice).

(Her-2 targeted chemotherapy), alternative approaches are necessary to affect these cancer cells [312]. Since GnRH-R expression occurs in more than 50% of human breast cancer, GnRH-Rs might represent a potential target to overcome these limitations and offer a possibility to treat TNBC more efficiently. Considering that the GnRH-III-Dau conjugate **16** provides the highest inhibitory effect on the growth of various cancer cell lines, further studies were carried out in direct comparison to **K2** to verify its potential as GnRH-based DDS.

3.1.1.3.2. Stability in human and mice plasma

To ensure an efficient and selective delivery of the drug to cancer cells, the stability of DDSs under physiological conditions is of high relevance. Initially, the stability of compound **16** and **K2** was investigated in human blood plasma. Both conjugates were incubated up to 24 hours at 37 °C in 90% plasma and appropriate samples were analyzed by LC-MS. In accordance with previous results of related GnRH-III-Dau conjugates, no degradation or cleavage could be observed within one day plasma exposure (Appendix 10.2.2.4, Figure A31A) [259,313]. This indicates that both compounds possess a high stability towards plasma-specific enzymes providing a reliable durability during circulation. Moreover, it might be possible that the incorporation of ^{3}D-Tic causes an even higher stability of compound **16** than that of **K2**. However, since the elimination half-life ($t_{1/2e}$) of GnRH-I agonists, like triptorelin ($t_{1/2e}$ = 2.8 hours), or antagonists, like cetrorelix ($t_{1/2e}$ = 11-12 hours), is commonly below 24 hours after intravenous application, the incubation time was restricted to 24 hours [314–316]. Taking into account that preclinical studies of anticancer drugs are mainly carried out using xenograft mouse models, the durability of **16** and **K2** was also determined in mouse blood plasma revealing that both compounds are stable for at least 24 hours (Appendix 10.2.2.4, Figure A31B). Both *in vitro* studies provide valuable information and are helpful to avoid misinterpretation of preclinical results which might be caused by differences between the enzymatic activity of laboratory animals and humans [242,317].

3.1.1.3.3. Lysosomal degradation in presence of rat liver lysosomal homogenate

Next to the durability in blood plasma, the degradation of compound **16** and **K2** in presence of rat liver lysosomal homogenate was analyzed. In accordance with previous findings and the results of the 1st set of GnRH-III-Dau conjugates, no free Dau could be detected [259,264]. However, both bioconjugates were digested by lysosomal enzymes, whereby various fragments could be detected (**Figure 15**, Appendix 10.2.2.5. Table A2).

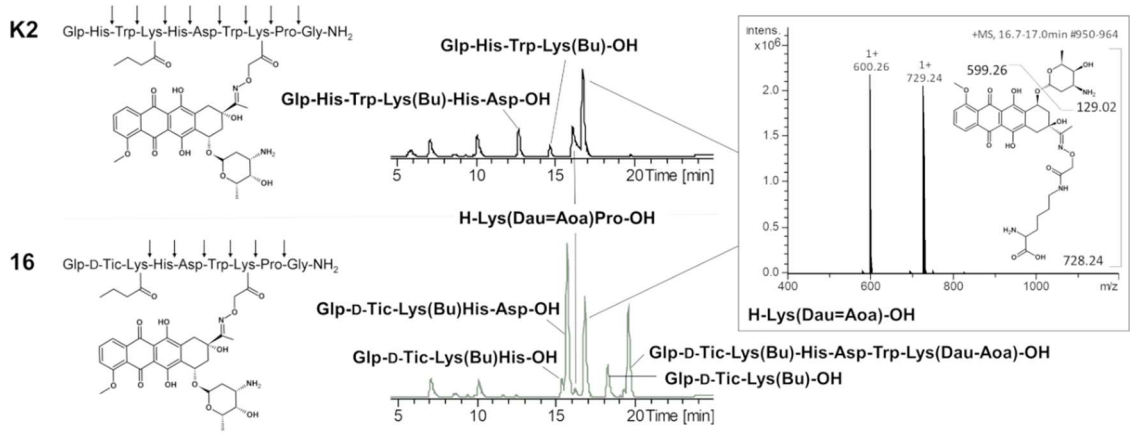

Figure 15. Degradation of the GnRH-III conjugates **K2** and **16** in presence of lysosomal rat liver homogenate. Cleavage sites produced by lysosomal enzymes are shown by full line arrows (left). LC chromatograms of **K2** and **16** after 24 h degradation (middle) and MS spectra of the active metabolite H-Lys(Dau=Aoa)-OH (right).

In general, the degradation profile of **K2** was similar to the previous study (3.1.1.2.2.) which verifies a comparable enzyme activity of the used lysosomal homogenates. The *N*-terminal fragment Glp-His-Trp-Lys(Bu)-OH and the *C*-terminal fragment H-His-Asp-Trp-Lys(Dau=Aoa)-Pro-Gly-NH_2 were already detected after five minutes incubation which clearly indicates the presence of a lysosomal enzyme with endopeptidase activity. Apart from that, the obtained results displayed that the novel compound **16** possesses an enhanced stability towards lysosomal enzymes than **K2**, whereby especially the *N*-terminal region Glp-D-Tic-Lys(Bu) provides a higher resistance. Despite this, the enzymatic hydrolysis of the *C*-terminal amino acids H-Gly-NH_2 and H-Pro-Gly-NH_2 was not influenced by the sequence modification and also the release of the smallest Dau-containing metabolite H-Lys(Dau=Aoa)-OH could be observed for both conjugates within one hour. Based on these findings, it can be proposed that the rapid formation of the active Dau metabolite is mainly mediated by lysosomal enzymes which possess carboxymono- and/or dipeptidase activity. In summary, the applied amino acid modifications of conjugate **16** lead to an enhanced stability of the *N*-terminus, while the degradation of the *C*-terminus and the corresponding release of the smallest Dau-metabolite is not disrupted which is of high relevance for the biological activity of oxime bond-containing GnRH-III-Dau conjugates.

3.1.1.3.4. Cellular uptake of the bioconjugates by flow cytometry

Based on the fact that anthracyclines, like Dau, have autofluorescent properties, the cellular uptake, as well as the subcellular localization of GnRH-III-Dau conjugates can be studied without changing the inherent properties of the DDSs. Thus, flow cytometry studies were performed to determine the cellular uptake rates of **K2** and **16** on HT-29 and

MCF-7 human cancer cells. After six hours treatment with different compound concentrations, both cell lines displayed an enhanced cellular uptake rate for compound **16** in comparison to **K2** while considering only the fluorescence emission of living cells (**Figure 16**). In case of HT-29, the uptake rate at low concentrations (3.125 µM, 6.25 µM and 12.5 µM) was approximately 2.7-times higher for **16** than for **K2**. At 25 µM concentration, 55.7% (**K2**) and 89.5% (**16**) of HT-29 cells were Dau positive, while the cellular uptake rates at 50 µM were 92.3% and 99.3%. A similar tendency could be obtained on MCF-7 cells, whereby the cellular uptake at 3.125 µM was already 4-times higher for compound **16** (14.6%) than for **K2** (3.3%). At the two highest concentrations, uptake rates between 96.5 and 100% could be observed. Due to these results, it can be assumed that the enhanced anticancer activity is mainly caused by the improved cellular uptake of compound **16**. Especially the results at low concentrations indicate that the cellular uptake of **16** is accelerated which might provide the high potency of the compound. Moreover, the higher uptake rates on MFC-7 are in line with the lower IC_{50} values, which might be related with a higher GnRH-R level on the cell surface.

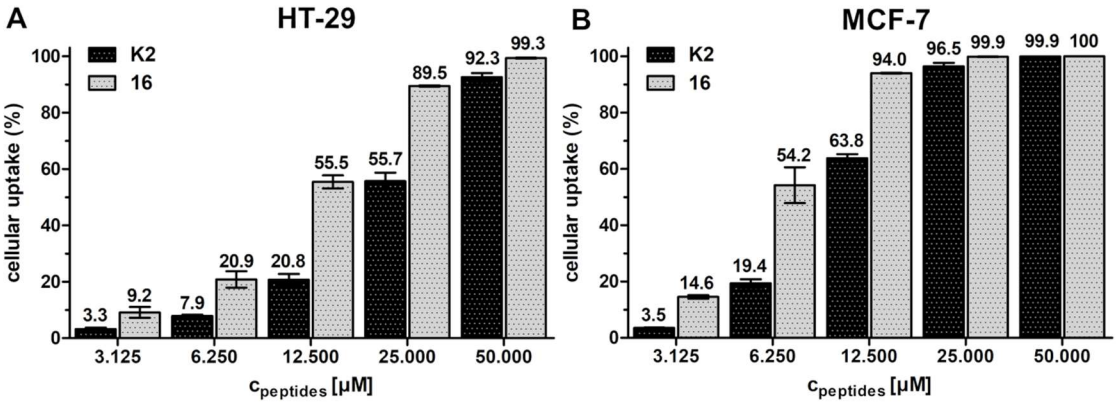

Figure 16. Cellular uptake of GnRH-III-Dau conjugates **K2** and **16** by flow cytometry. **A**: HT-29 and **B**: MCF-7 cancer cells after 6 h treatment. Experiments were performed in duplicates. Error bars represent SD.

3.1.1.3.5. Confocal laser scanning microscopy (CLSM) studies[d]

Aside from quantitative flow cytometry studies, the cellular uptake and the subcellular localization of compound **16** was investigated in a time-dependent manner by CLSM. For this study, MCF-7 cells were treated with **16** for different periods of time from five seconds up to one hour, followed by fixation and preparation for image recording. To ensure the comparability with the study of **K2** (3.1.1.2.5.), 40 µM compound concentration was used and images were depicted in BestFit mode (**Figure 17**). Moreover, nuclei were stained with DAPI to verify the presence of Dau or Dau-containing

[d] All CLSM samples were prepared by Beáta Biri-Kovács and images were recorded by Bálint Szeder

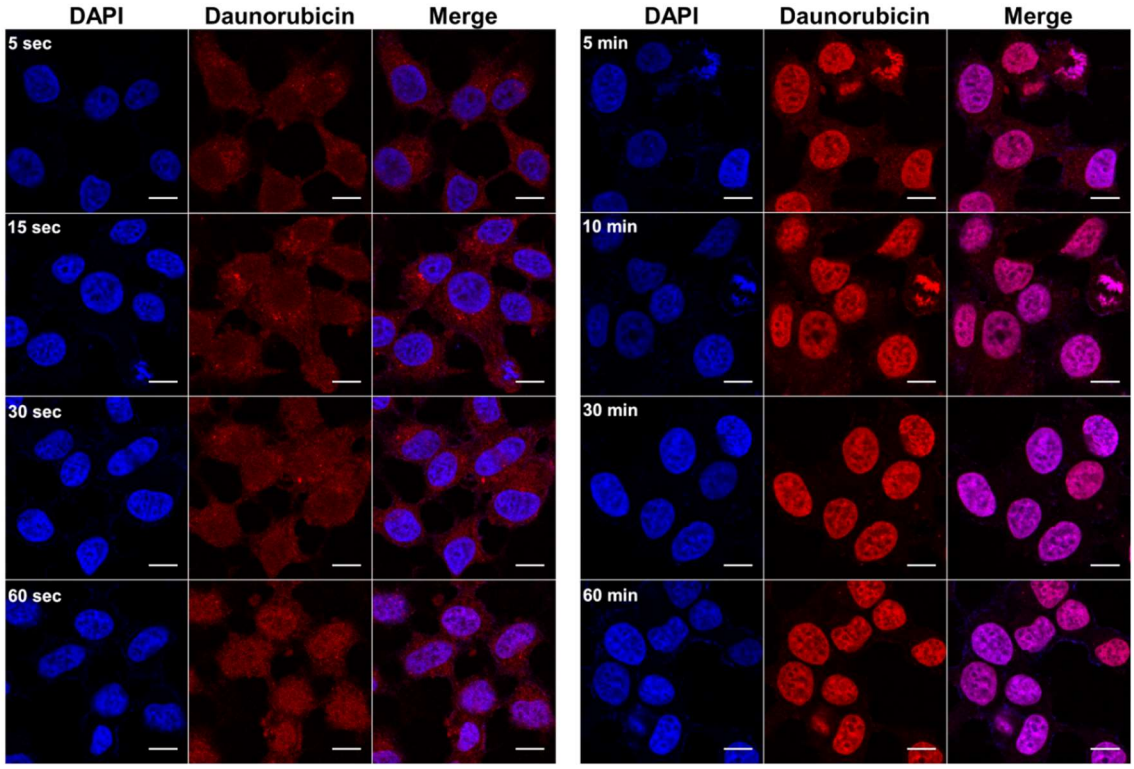

Figure 17. Time-dependent cellular uptake and co-localization with nuclei (stained by DAPI) of GnRH-III conjugate **16** (Daunorubicin signal) on MCF-7 breast cancer cells after 5, 15, 30 and 60 seconds (left), as well as 5, 10, 30 and 60 minutes (right) incubation. Scale bars represents 10 µm.

derivatives on the site of action. The recorded images illustrate an accumulation of Dau in the nuclei after five minutes, while within the first minute, the Dau-signal was predominantly detected in the cytosol and in small cytosolic vesicles which are assumed to represent endosomes and lysosomes. Similar studies of **K2** showed after five minutes the Dau-signal only in small cytosolic vesicles, and a treatment period of 10 minutes was necessary to verify the accumulation of Dau in the nuclei. This indicates that the GnRH-III-Dau conjugate **16** was taken up more efficiently by MCF-7 cell than **K2**. Moreover, it can be assumed that the delivery of the drug to the site of action is accelerated. Beyond that, the images of **16** at five and ten minutes display dividing cells, where the chromatin was already condensed and chromosomes became visible. This illustrates not only the presence of Dau in nuclei, but also the rapid intercalation of the drug into DNA.

3.1.1.3.6. Radioligand binding studies

In order to prove that the novel bioconjugate enters cancer cells by receptor mediated endocytosis, the binding affinity of **16** and **K2** to GnRH-Rs was determined by radioligand displacement assay. The experiments were performed at the research group of Gábor Halmos (Department of Biopharmacy, Faculty of Pharmacy, University of Debrecen). Increasing compound concentrations were used to replace [^{125}I]-triptorelin

from GnRH-Rs on human pituitary and human prostate cancer tissues. The results evident that both compounds bind to the receptors with similar affinities in low nanomolar range. In case of human pituitary tissues, IC_{50} values of 3.59 ± 2.17 nM (**K2**) and 3.53 ± 0.96 nM (**16**) were obtained, while 3.43 ± 2.01 nM (**K2**) and 2.79 ± 1.24 nM (**16**) were achieved for human prostate cancer tissue (Appendix 10.2.2.6. Figure A32). Considering that no substantial difference could be detected between the compounds, it can be presumed that the receptor binding is not affected by the *N*-terminal modification of compound **16**. In comparison to GnRH, unrelated peptides, like SST-14 or bombesin, are not able to displace triptorelin using concentrations up to 1 μM, **K2** and **16** replace triptorelin efficiently in a competitive manner by applying increasing concentrations of 1 pm to 1 μM. Due to these findings, it can be assumed that both GnRH-III compounds bind to the GnRH-receptor in a specific manner which enables a receptor mediated uptake by endocytosis.

3.1.2. Self-immolative and non-cleavable linker-containing GnRH-III-Dau and -PTX conjugates

DDSs are promising tools for targeted tumor therapy providing a selective delivery of cytotoxic drugs to malignant cells, while side-effects and systemic toxicity are reduced. To ensure these beneficial features, the stability of the linkage between the targeting moiety and the cytotoxic agent, but also the specific release of the anticancer agent or bioactive drug-metabolites within the cancer cell plays a crucial role. Thus, many different linker systems have been developed to link cytotoxic drug molecules to tumor homing ligands [318–321]. A prominent example for the use of non-selective stable linker is the ADC Trastuzumab emtansine (T-DM1), where the cytotoxic payload DM-1 is covalently connected to the antibody by a heterobifunctional SMCC crosslinker forming a stable thioether-maleimide bond between linker and drug, and an amide bond between linker and Lys-residues of the mAb [322]. Similarly to the oxime-linked GnRH-III-Dau conjugates (3.1.1) where the drug remains covalently linked to the lysine side chain, the bioactive DM1-containing Lys adducts are released by lysosomal enzymes which can efficiently bind to tubulin and thereby prevent microtubule assembly [190,323]. Next to stable non-cleavable linkers, a variety of labile linkers have been designed which are relatively stable outside, but degradable inside the cancer cell [255,318–320]. These linkages are cleaved by specific intracellular mechanisms or pathways which result in the release of the free drug. Commonly used linker systems for ADCs and SMDCs are mainly acid-labile linkers (drug release caused by acidic environment of late endosomes and

lysosomes), reducible disulfide linkers (release by high intracellular GSH concentration) or enzymatic degradable peptide linkers (hydrolysis by carboxylesterases or lysosomal cathepsins) [255,318,324–326]. In order to promote the accessibility of cleavage sites adjacent to sterically bulky payloads, additional spacer and linker systems are often incorporated which undergo rapid and irreversible disassembly directly after cleavage, leading to a subsequent release of the free drug [252,324,327–330]. Thus, enzyme cleavable peptide linker have been successfully used in combination with a self-immolative PABC spacer to conjugate anticancer drugs, like Dox, MMAE or PTX to tumor specific homing devices [210,320,331–333]. In case of the FDA approved ADC brentuximab vedotin, the cytotoxic payload MMAE is connected to the mAb by the cathepsin B cleavable, self-immolative linker system EMC-Val-Cit-PABC-MMAE which contains a maleimide moiety for the attachment of the linker to Cys side chains of the mAb by thioether bond formation [332,334–336]. The Val-Cit-PABC linker system was initially applied for the conjugation of Dox to a chimeric mAb resulting in an ADC which revealed excellent stability in human plasma and rapid release of free Dox by cathepsin B and in lysosomal preparation [320]. Due to these promising results, related Val-Cit-PABC linker systems have been used for a variety of DDSs [337–341]. Other frequently used cathepsin B cleavable dipeptides are Phe-Lys and Val-Ala, whereby Val-Cit and Val-Ala are the most successfully used cleavable linkers which might be related to the reduced plasma half-life of the Phe-Lys linker [176,211,255,320,342–346]. In comparison to non-cleavable linker systems, it could be shown that ADCs with cleavable linker systems reveal not only toxic effects on antigen-positive cancer cells, but also on antigen-negative cancer cells in the direct proximity to these cells. This so called bystander effect, is probably caused by direct diffusion of the free drug across the plasma membrane to adjacent cells and/or by extracellular matrix proteins of the microenvironment of the tumor [319,347,348]. Especially for tumors with a heterogeneous population of antigen-positive and antigen-negative cells, the application of DDSs which exhibit significant bystander killing are assumed to enhance the chances of tumor relapse with a monotherapy [348]. Encouraged by these promising findings, novel GnRH-III drug conjugates were developed and synthesized which contain the cathepsin B cleavable dipeptidyl linker Val-Ala or Val-Cit, and the self-immolative PABC moiety. Considering the favorable results of **16** and **K2**, the corresponding peptide sequences have been selected as targeting moieties for the novel conjugates and the classical anticancer drugs Dau and PTX were used as payloads. In the past, a variety of PTX prodrugs have been designed to ligate PTX to different targeting moieties, and to improve the solubility

of PTX [211,212,324,349–353]. Moreover, it could be shown that an elongated linker between the cathepsin B cleavage site and PTX might be favorable for a rapid enzymatic cleavage of the dipeptide linker [353]. To achieve an adequate stability of the GnRH-III-PTX conjugates, the well-known *N,N'*-dimethylethylene diamine spacer has been incorporated between the PABC moiety and the PTX by carbamate formation [210,211,353]. For a better comparison and to demonstrate the proof of concept, equivalent non-cleavable GnRH-III-Dau and PTX conjugates have also been developed. All synthesized GnRH-III-Dau and PTX conjugates were studied for their anticancer activity in A2780 ovarian and Panc-1 pancreatic cancer cells. In addition, the release of the drug was studied in presence of lysosomal enzymes and the GnRH-R binding affinity was examined for some compounds.

3.1.2.1. Synthesis of self-immolative linker-containing GnRH-III-Dau and -PTX conjugates

In general, the synthesis of the Val-Aaa-PABC-containing GnRH-III-drug conjugates was carried out as described recently [211,320,353,354]. The appropriate peptide carriers **43** and **44** were synthesized by standard Fmoc-SPPS, while the dipeptidyl-PABC-drug linkers were synthesized in solution as shown in **Scheme 3**. Initially, the intermediates Fmoc-Val-Cit-OH (**22**) and Fmoc-Val-Ala-OH (**34**) were prepared in accordance to Dubowchik *et al*. and Hochdörffer *et al.*, whereby the obtained yields were comparable to the reported ones [320,354]. In the next step, 4-aminobenzyl alcohol was coupled affording compound **23** and **35** in adequate yield. Afterward, the hydroxyl group was activated by formation of *para*-nitrophenyl carbonate intermediates (**24**, **36**). For the synthesis of the Dau-containing linkers, Dau·HCl was coupled to **24** and **36** yielding 47% of Fmoc-Val-Cit-PABC-Dau (**25**) and 34% of Fmoc-Val-Ala-PABC-Dau after flash chromatography. The yield of **25** is in line with the reported yield of Z-Val-Cit-PABC-Dox [320], while compound **37** was obtained in lower yield which is mainly related to the insufficient separation during flash chromatography. The isolation of product and side products might be improved by starting the purification with a higher percentage of the nonpolar eluent hexane and performance of a gradient elution. However, since the obtained amount of **37** was sufficient to complete the synthesis of the GnRH-III-Val-Ala-PABC-Dau conjugates, this purification step was not optimized. In the following, the Fmoc-group was removed in solution and products were isolated after DMF evaporation by precipitation in ether and centrifugation. The crude compounds were used for the coupling with glutaric anhydride without further purification. The obtained products were

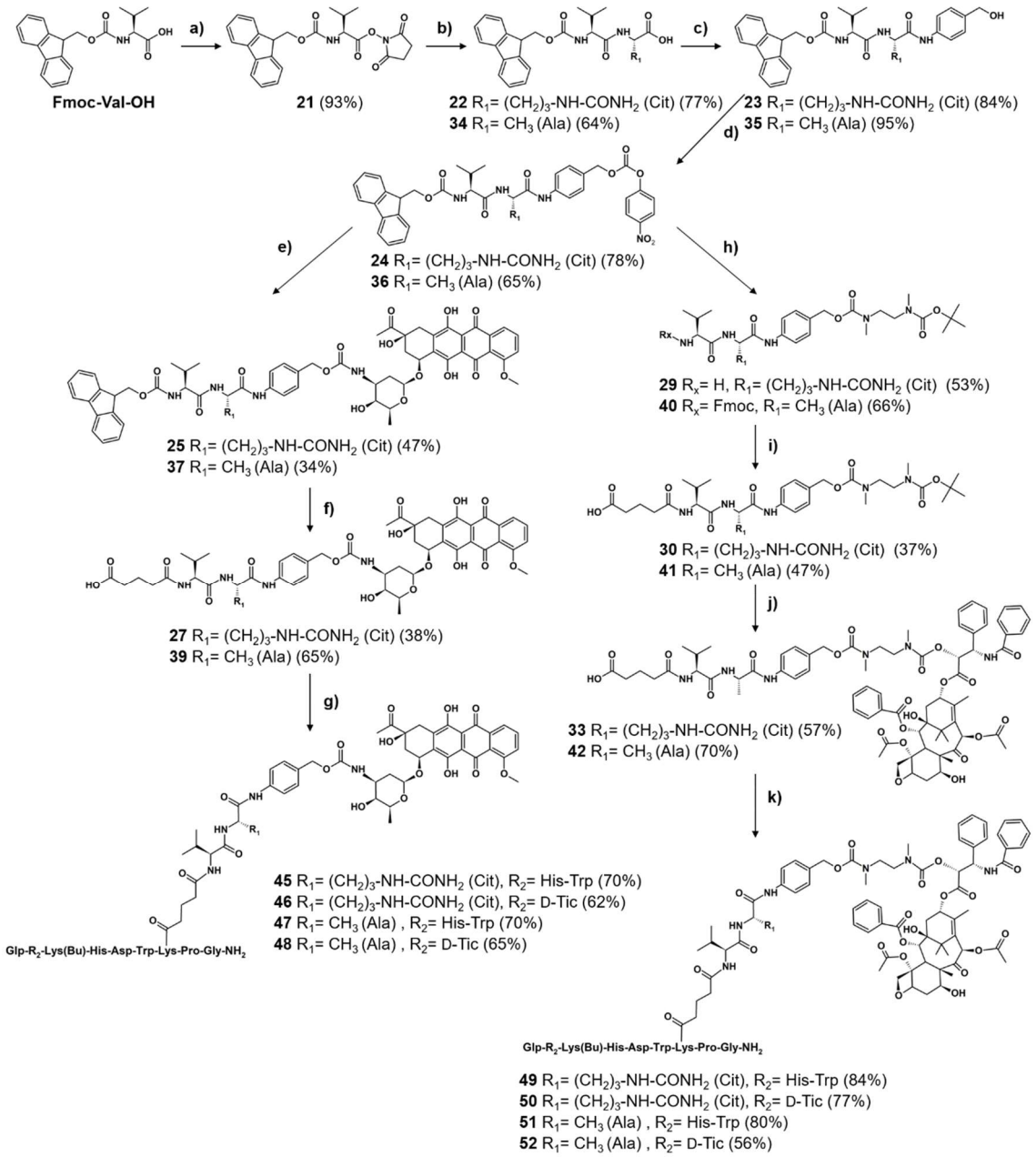

Scheme 3. Synthesis of self-immolative linker-containing GnRH-III-Dau and -PTX conjugates (**a**) 1 eq HOSu, 1 eq DCC in THF, overnight, RT, (**b**) **22:** 1.05 eq L-citrulline, 1.05 eq $NaHCO_3$ in H_2O/DME (1:1), overnight, RT, **34:** 1.1 eq L-Ala-OH, 1.1 eq $NaHCO_3$ in H_2O/DME (3:2), overnight, RT, (**c**) 2 eq PAB-OH, 2 eq EEDQ in DCM/MeOH (2:1), overnight, RT, (**d**) 2 eq $(Pnp)_2CO$, 2eq DIPEA in DMF, overnight, RT, (**e**) **25:** 1 eq **24**, 1.1 eq Dau, 1.5 eq DIPEA in DMF, overnight, RT, **27:** 1.5 eq **36**, 1 eq Dau, 1.9 eq DIPEA in DMF, overnight, RT, (**f**) [1.)] 5 eq piperidine in DMF, [2.)] 2 eq glutaric anhydride, 2 eq DIPEA in DMF, 2 h, RT, (**g**) [1.)] 1 eq **27** or **39**, 0.9 eq HATU, 2 eq DIPEA in DMF 30 min, [2.)] 1 eq peptide carrier **43** or **44**, overnight, RT, (**h**) 2.5 eq **28**, 2.5 eq DIPEA in DMF, overnight, RT, (**i**) **29**: 3 eq glutaric anhydride, 3 eq DIPEA in DMF, 4 h, RT, **40**: [1.)] 5 eq piperidine in DMF, [2.)] 2 eq glutaric anhydride, 2 eq DIPEA in DMF, overnight, RT, (**j**) [1.)] TFA/DCM (1:2), 45 min, RT, [2.)] 1.3 eq activated PTX (**31**), 4 eq DIPEA in DMF, overnight, RT, (**k**) [1.)] 1 eq **33** or **42**, 0.9 eq HATU, 2 eq DIPEA in DMF 30 min, [2.)] 1 eq peptide carrier **43** or **44**, overnight, RT.

purified by RP-HPLC which afforded both linkers (**27**, **39**) in moderate yield. For the conjugation reaction, the appropriate linker was preincubated with HATU to form the activated glutaryl ester and after 30 minutes, the peptide carrier was added. The final GnRH-III-Val-Aaa-PABC-Dau conjugates (**45**-**48**) were isolated by semipreparative RP-

HPLC and characterized by analytical RP-HPLC and ESI-MS (**Table 7**, Appendix 10.2.3.1.). For the synthesis of the PTX conjugates, the intermediate *N*-Boc-*N,N'*-dimethylethylene diamine (**28**) and the activated 2'-(*para*-nitrophenoxycarbonyl)-PTX were needed (**31**). Intermediate **28** was prepared from commercially available dimethylethylene diamine as recently reported by Meyer *et al*. [355], and the regioselective activation of PTX in the C2-OH' position was carried out in accordance to the previously described synthetic route [211]. The synthesis of the PTX conjugates was continued by the reaction of the *para*-nitrophenyl carbonate compounds (**24**, **36**) with *N*-Boc-*N,N'*-dimethylethylene diamine (**28**) yielding the Fmoc-protected compound **40** (Ala) and the deprotected compound **29** (Cit). In case of the citrulline-containing linker intermediate, the Fmoc group was removed during reaction. Nevertheless, the coupling of the diamine spacer proceeded successfully, and by taking into account that the Fmoc removal was intended as the next step, the synthesis strategy was not modified. After Fmoc-deprotection of compound **40**, both intermediates were treated with glutaric anhydride yielding compounds **33** and **42**. In contrast to the described synthetic route for RGD-PTX conjugates, the linker synthesis was continued by Boc deprotection and coupling of the 2'-(*para*-nitrophenoxycarbonyl)-PTX to the diamine moiety. After purification by preparative RP-HPLC, the final drug-linkers **33** and **42** were obtained in satisfactory yields and were used for the conjugation to the peptide carriers. As described for the ligation of the Dau-conjugates, the PTX-peptidyl linkers were preactivated with HATU and then coupled to the corresponding peptide moiety. The resulting GnRH-III-PTX conjugates (**49**-**52**) were purified by RP-HPLC and analyzed by analytical RP-HPLC and ESI-MS (**Table 7**; Appendix 10.2.3.1.). All cleavable GnRH-III drug conjugates (**45**-**52**)

Table 7: Chemical characteristics of self-immolative GnRH-III-Dau and -PTX bioconjugates

Code	GnRH-III-[^{4}Lys(Bu), ^{8}Lys(linker-drug)]	Linker	Purity [%]	RP-HPLC R_t [min][a]	ESI-MS MW_{cal} /MW_{exp} [g/mol][b]
45	[^{2}His-^{3}Trp]	Val-Cit	≥97	27.45	2399.57/2398.63
46	[^{2}ΔHis-^{3}D-Tic]	Val-Cit	≥98	28.88	2235.40/2234.45
47	[^{2}His-^{3}Trp]	Val-Ala	>99	27.92	2313.47/2312.74
48	[^{2}ΔHis-^{3}D-Tic]	Val-Ala	≥98	28.53	2149.31/2148.35
49	[^{2}His-^{3}Trp]	Val-Cit	≥99	27.10	2840.10/2839.30
50	[^{2}ΔHis-^{3}D-Tic]	Val-Cit	≥98	28.53	2675.66/2675.28
51	[^{2}His-^{3}Trp]	Val-Ala	≥98	27.58	2754.01/2753.38
52	[^{2}ΔHis-^{3}D-Tic]	Val-Ala	≥97	29.13	2589.84/2589.30

[a]Column: Macherey-Nagel Nucleosil C18 column (250 mm x 4.6 mm) with 5 µm silica (100 Å pore size gradient: 0 min 0% B, 5 min 0% B, 30 min 90% B; eluents: 0.1% TFA in water (A) and 0.1% TFA i acetonitrile-water (80:20, v/v) (B); flow rate: 1 mL/min; detection at 220 nm. [b]Bruker Daltonics Esqui 3000+ ion trap mass spectrometer.

were obtained in high purities of at least 97% and the final conjugation to the targeting moiety proceeded well with yields up to 84%.

3.1.2.2. Synthesis of non-cleavable linker-containing GnRH-III-Dau and -PTX conjugates

The non-cleavable linker-containing GnRH-III-drug conjugates were prepared by the synthetic route shown in **Scheme 4**. To obtain Dau-linker **53**, Dau·HCl was treated with glutaric anhydride and purified (preparative RP-HPLC). For the synthesis of PTX-linker **56**, mono-Boc protected diamine (**28**) was reacted with glutaric anhydride yielding compound **54** in high yield. Then, the Boc group was removed in solution and activated PTX (**31**) was coupled. The PTX linker **56** was obtained in good yield (75%) over two steps and further RP-HPLC purification. The conjugation of the drug-linker to the GnRH-III-carrier was coupled with HATU as described for the cleavable counterparts. The non-cleavable GnRH-III-drug conjugates (**57**-**60**) were obtained in moderate yields (50-72%). Analytical RP-HPLC and ESI-MS analyses evidenced the high purity of the compounds (**Table 8**, Appendix 10.2.3.2).

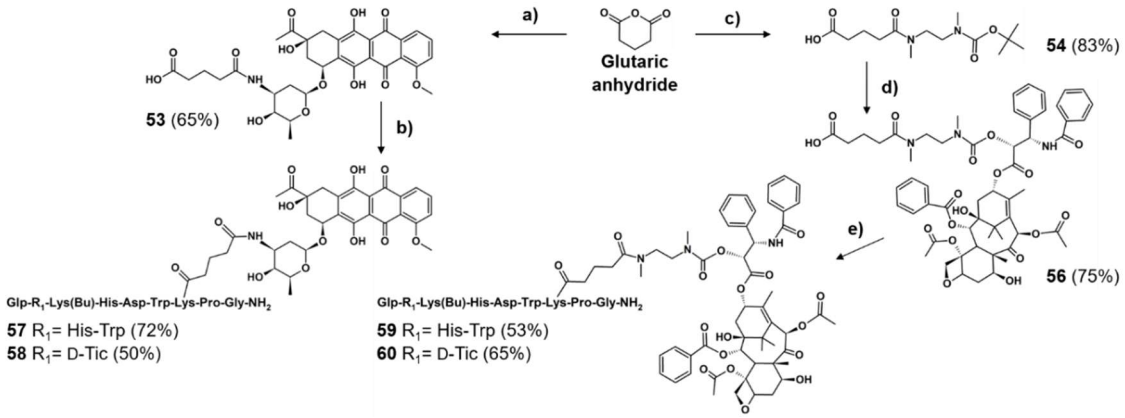

Scheme 4. Synthesis of non-cleavable linker-containing GnRH-III-Dau and -PTX conjugates (**a**) 1 eq Dau, 3 eq DIPEA in DMF, 3 h, RT, (**b**) [1.)] 1 eq **53**, 0.9 eq HATU, 2 eq DIPEA in DMF 30 min, [2.)] 1 eq peptide carrier **43** or **44**, overnight, RT, (**c**) 1 eq **28**, 2 eq DIPEA in DMF, 6 h, RT, (**d**) [1.)] TFA/DCM (1:2), 45 min, RT, [2.)] 1 eq activated PTX (**31**), 30 eq DIPEA in DMF, overnight, RT, (**e**) [1.)] 1 eq **56**, 0.9 eq HATU, 2 eq DIPEA in DMF 30 min, [2.)] 1 eq peptide carrier **43** or **44**, overnight, RT.

Table 8: Chemical characteristics of non-cleavableGnRH-III-Dau and -PTX bioconjugates

Code	GnRH-III-[^{4}Lys(Bu), ^{8}Lys(glutaryl-linker-drug)]	Purity [%]	RP-HPLC R_t [min][a]	ESI-MS MW_{cal} /MW_{exp} [g/mol][b]
57	[^{2}His-^{3}Trp]	≥99	25.15	1994.12/1993.49
58	[^{2}ΔHis-^{3}D-Tic]	≥98	27.10	1829.95/1829.75
59	[^{2}His-^{3}Trp]	>98	26.83	2434.65/2434.11
60	[^{2}ΔHis-^{3}D-Tic]	≥99	28.57	2270.49/2270.04

[a]Column: Macherey-Nagel Nucleosil C18 column (250 mm x 4.6 mm) with 5 µm silica (100 Å pore size); gradient: 0 min 0% B, 5 min 0% B, 30 min 90% B; eluents: 0.1% TFA in water (A) and 0.1% TFA in acetonitrile-water (80:20, v/v) (B); flow rate: 1 mL/min; detection at 220 nm. [b]Bruker Daltonics Esquire 3000+ ion trap mass spectrometer.

3.1.2.3. Biochemical evaluation of GnRH-III-Dau and PTX conjugates

In order to investigate the biological activity of the cleavable and non-cleavable linker-containing GnRH-III drug conjugates, cell viability studies have been performed on A2780 ovarian cancer and Panc-1 pancreatic cancer cells. Apart from that, the release of the free Dau and PTX was studied in presence of rat liver lysosomal homogenate and the receptor binding affinity of distinct compounds was investigated and compared to our oxime bond-containing lead compound **16**.

3.1.2.3.1. In vitro cytostatic effect

In collaboration with the research group of Dr. József Tóváry from the National Institute of Oncology in Budapest (OOI), our lead compounds **16** and **K2** have been intensively studied for their *in vitro* cytostatic effect on more than 20 cancer cell lines, and a variety of these cell lines were further analyzed in terms of their GnRH-R expression level [356]. The results revealed that A2780 ovarian cancer cells possess high basal protein level of GnRH-R, as well as a high GnRH-R surface expression level, while Panc-1 pancreatic cancer cells revealed an adequate GnRH-R surface expression level, but the basal protein level of GnRH-R was substantially reduced. Apart from the studies of the OOI, the GnRH-R expression of A2780, Panc-1 and seven other cell lines was additionally studied by western blot analysis (**Figure 18**). In case of A2780 cells, a broad band at approximately 38 kDa could be detected which can be considered as full-length human GnRH-R. In contrast, the signal intensity of the 38 kDa band was much lower for Panc-1 pancreatic cancer cells. Based on these results, the high GnRH-R expressing cell line A2780 and the low GnRH-R expressing cell line Panc-1 were selected to study the anticancer activity of the self-immolative and non-cleavable GnRH-drug conjugates. Taking into account that the release of the free Dau and PTX can be assumed, both drugs were used as controls. The two cell lines were treated 24 hours in case of the Dau

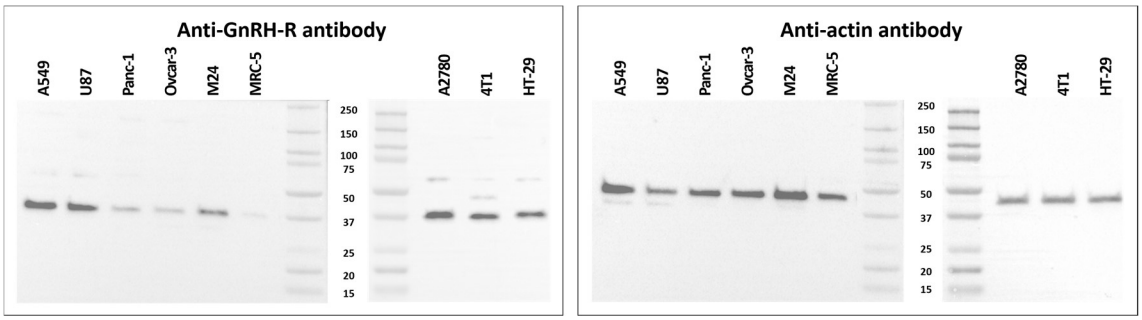

Figure 18. Western blot performed on whole cell lysates of A549, U87, Panc-1, Ovcar-3, M24, MRC-5, A2780, 4T1 and HT-29 cells. Anti-GnRH-R antibody (Proteintech, 19950-1AP) (left) was used to detect GnRH-R. Actin expression was evaluated as loading control (Santa Cruz Biotechnology, sc-1616 (right). Band at 38 kDa represents the full length human GnRH-R; the signals at higher molecular weight (55-70 kDa) are assumed to be glycosylated forms of the receptor.

conjugates and six hours for the PTX compounds, followed by additional incubation with fresh growth medium until 72 hours after treatment initiation. The obtained results which are shown in **Table 9** reveal that the non-cleavable linker-containing conjugates possess a reduced anticancer activity in comparison to the cleavable conjugates. Moreover, all compounds displayed a lower biological activity on Panc-1 cells than on A2780. In case of the cleavable GnRH-III-Dau conjugates, the IC_{50} values varied between 2.85-11.18 µM on A2780 cells, whereby the best activity was obtained for compound **48** (2.85 µM) which contains the cathepsin B cleavage site Val-Ala and the modified GnRH-III carrier. In general, the IC_{50} values of the Dau-conjugates on A2780 cells emphasize that the novel targeting moiety GnRH-III-[^{2}ΔHis-^{3}D-Tic-^{4}Lys(Bu)] (**46**, **48**) has a beneficial impact on the antitumor activity with IC_{50} values 2.5-times lower than that of the GnRH-III-[^{2}His-^{3}Trp-^{4}Lys(Bu)] conjugates (**45**, **47**). Furthermore, the outcomes indicate that the Val-Ala linker-containing conjugates provide a slightly improved cytotoxic effect in comparison to the Val-Cit-containing conjugates. This effect might be related to an accelerated release of Dau within the tumor cell. Apart from that, it needs to be mentioned that the activity of the free Dau was lower in comparison to previous studies from Ivan Ranđelović (OOI) [356] which might be explained by the fact that the experiments were performed at different times and in different laboratories using different cell viability assays (MTT- and resazurin-based assays), but also the passage number and confluence of the A2780 cells

Table 9: *In vitro* cytostatic effect of self-immolative GnRH-III-Dau and -PTX bioconjugates on A2780 human ovarian cancer and Panc-1 human pancreatic cancer cells

Code	GnRH-III-[^{4}Lys(Bu), ^{8}Lys(linker-drug)]	Linker	IC_{50} [µM] A2780	IC_{50} [µM] Panc-1
Dau			0.21 ± 0.01	2.43 ± 0.58
45	[^{2}His-^{3}Trp]	Val-Cit	11.18 ± 0.38	85.57 ± 24.33
46	[^{2}ΔHis-^{3}D-Tic]	Val-Cit	4.24 ± 1.09	> 100
47	[^{2}His-^{3}Trp]	Val-Ala	7.48 ± 0.66	56.19 ± 17.28
48	[^{2}ΔHis-^{3}D-Tic]	Val-Ala	2.85 ± 0.90	> 100
57	[^{2}His-^{3}Trp]	non-cleavable	67.88 ± 25.36	> 100
58	[^{2}ΔHis-^{3}D-Tic]	non-cleavable	48.14 ± 0.47	>100
PTX			0.02 ± 0.001	0.17 ± 0.01
49	[^{2}His-^{3}Trp]	Val-Cit	0.67 ± 0.07	5.03 ± 1.91
50	[^{2}ΔHis-^{3}D-Tic]	Val-Cit	0.51 ±0.11	6.44 ± 1.22
51	[^{2}His-^{3}Trp]	Val-Ala	0.66 ± 0.18	4.89 ± 1.08
52	[^{2}ΔHis-^{3}D-Tic]	Val-Ala	0.77 ± 0.08	8.15 ± 3.22
59	[^{2}His-^{3}Trp]	non-cleavable	41.52 ± 9.83	> 100
60	[^{2}ΔHis-^{3}D-Tic]	non-cleavable	> 100	> 100

all values represent mean ± SE

might have an impact on the cytostatic effects [295,296]. In order to facilitate a direct comparison of the anticancer activities of the cleavable, self-immolating GnRH-III conjugates and the best oxime bond-linked GnRH-III-Dau conjugates (**K2** and **16**), an additional cell viability experiment was performed. Both oxime bond-containing conjugates revealed a higher cell growth inhibitory effect than the best cleavable compound **48** (Appendix 10.2.3.2. Figure A47). The IC_{50} value of the lead compound **16** was around 50% lower and the value of **K2** was more than 30% lower than that of **48**. Since it has been reported, that the free Dau binds DNA with higher affinity and thus possesses a higher potential than the H-Lys(Dau-Aoa)-OH metabolite [257], further studies are needed to interpret the results. In contrast to the Dau-conjugates, all cleavable PTX-conjugates displayed nearly the same activity on A2780 cells (0.51-0.77 μM). This might be related to the releasing mechanism of the PTX. It has been reported that by using the PABC spacer in combination with the diamine linker, initially the diamine linker-containing prodrug is released [211,353]. The following cyclization of the diamine-linker to 1,3-dimethyl-2-imidazolidinone and the corresponding release of PTX has been reported to be the rate-limiting step of the self-immolative process [353]. Taking this into account, it can be assumed that the stability of the prodrug and the release of the free PTX have a higher impact on the antitumor activity of the GnRH-III conjugates than the targeting sequence or the cathepsin cleavable dipeptide spacer. Apart from that, the non-cleavable linker-containing GnRH-III-drug conjugates exhibited a clearly decreased growth inhibitory effect on both cell lines. Thus, it can be assumed that the decreased biological activity of these conjugates is related to the fact that the free drug is not released. Moreover, the acylation of the amino sugar moiety of Dau might have an impact on the DNA intercalation properties, since it has been shown that a hydrogen bond is formed between this amino group and the DNA [357–359]. This assumption is supported by recent studies which demonstrated that the *in vitro* antitumor activity of GnRH-III conjugates is remarkably decreased when the amino function of the daunosamine sugar was used for amide bond formation to a glutaryl-spacer [254]. In comparison to the activity on A2780 ovarian cancer cells, all applied conjugates revealed substantially decreased cytostatic effect on Panc-1 pancreatic cancer cells. Since the reduced activity of the conjugates is in correlation with a lower GnRH-R expression level, it can be assumed that the anticancer activity is mediated by a receptor mediated uptake of the compounds. On the contrary, also the free drugs Dau and PTX revealed a decreased anticancer activity on Panc-1 cells. This reduced potency might be related to a resistance of the Panc-1 cells to these

chemotherapeutic agents. In general, it is well known that pancreatic cancers commonly possess several cellular mechanisms which lead to strong resistance towards a variety of classical anticancer drugs [360–365]. This fact, together with the high invasive and metastatic behavior of pancreatic cancer, as well as the difficult diagnosis at early stages result in a bad prognosis and high lethality rate of the disease [364–367]. One reason for the poor response of pancreatic ductal adenocarcinoma (PDA) to cytotoxic drugs is the expression of membrane-bound transporter proteins which mediate the efflux of cytotoxic drugs out of the cytosol. Miller *et al.* determined that the multidrug resistance (MDR) of Panc-1 cells is mainly related to the presence of the multidrug resistance-associated protein (MRP) [368,369]. Moreover, it has been shown that MRP mediates the ATP-dependent efflux of anthracyclines, like Dau and other anticancer agents [370–373]. Based on these findings, it can be assumed that the low activity of the free Dau is mainly related to the efflux of the drug from cytosol directly after passive diffusion. In contrast to that, it has been reported that MRP-transfected cells exhibit just a low resistance level to PTX [370–372]. Nonetheless, different studies pointed out that taxanes do not display a significant antitumor activity towards PDA which might be caused by other cellular processes [361,374,375]. Although the specific mechanisms for taxane resistance in pancreatic cancer are not fully elucidated yet, it can be assumed that the membrane transporter protein P-glycoprotein 1 (P-gp, also known as multidrug resistance protein 1 (MDR1)) is at least partially involved [361,376]. MDR1 expression results in a similar ATP-mediated resistance like MRP and causes an enhanced drug efflux which leads to a reduced intracellular drug accumulation. Despite the similarities, P-gp exhibits a different substrate selectivity than MRP and mediates the effective cytosolic efflux of paclitaxel [377–380]. Although studies on patient-derived pancreatic tumor tissue pointed out that a majority of pancreatic carcinomas express P-gp, it could be shown that PTX resistance is not only mediated by MDR1 [361,381,382]. Other mechanisms which might provoke PTX resistance, include changes in the assembly, organization and dynamics of microtubules [361,382,383]. A direct evidence for the correlation of taxol sensitivity and class III β-tubulin (TUBB3) isotype level has been reported by Kavallaris *et al*. [384]. Initially, it has been shown in human lung cancer cells that the increased resistance to PTX is associated with an increased expression of TUBB3 [385]. This relationship could be further confirmed in taxol-resistant ovarian, prostate and also pancreatic carcinomas [385–389]. Related studies evidenced that the PDA cell line Panc-1 expresses TUBB3 in high level [389]. Considering these findings and the fact that Panc-1 cells exhibit no or just low expression of the drug efflux pump

MDR1 [368,390], it can be assumed that the reduced activity of PTX is mainly related to changes of the microtubule composition caused by high TUBB3 expression.

In order to verify whether the reduced anticancer activity of the GnRH-III compounds is related to the decreased receptor mediated uptake or caused by the MDR of Panc-1 cells, the cytotoxic effect of Dau conjugated cell penetrating peptides (CPP) have been studied. CPPs are defined as short peptides (up to 30 amino acids) which can pass the cell membrane independently and deliver conjugated cargos to the cell without targeting a cell surface protein [391–393]. The translocation mechanism of CPPs is not completely defined yet. It can be assumed that the main uptake pathway for CPPs is endocytosis mediated, but also direct penetration through the membrane or simultaneous translocation by different routes can facilitate the internalization depending on the conditions [394]. Moreover, the uptake mechanism of CPPs can depend on a variety of factors, such as the peptide sequence of the CPP, the attached cargo, as well as the cell line of interest and the corresponding lipid structure [395]. Next to classical CPPs, like TAT, penetratin or oligoarginine, a novel CPP with excellent drug delivery properties has been described by Neundorf and coworkers [391,396–401]. This CPP is called sC18 and is derived from the 16 *C*-terminal amino acids of the cationic antimicrobial peptide CAP18 [400]. It could be shown that sC18 is able to form a helical structure by contact with the lipid membrane, whereby the internalization is mainly caused by endocytosis [402]. Due to this, sC18 might represent an excellent alternative to reflect and simulate the intracellular action of drug-conjugates after cellular uptake in drug resistant Panc-1 cells. Therefore, two sC18-based Dau conjugates have been developed and analyzed. These studies were designed and performed by Lucia Feni from the Research Group of Ines Neundorf (University of Cologne). Based on the fact that the oxime bond-containing compounds provide a slightly improved activity on A2780 cells and a comparable low activity on Panc-1 (IC_{50} **K2** >100 and **16** >50 µM) than the self-immolating compounds, Dau was linked to the sC18 *via* oxime bond. The Aoa-linker was either directly incorporated at the side chain of lysine in position eight or by an Aoa-GFLG peptide spacer in the same position. The antitumor activity of both compounds was investigated on Panc-1 cells and compared to free Dau and **K2** (**Table 10**) [224]. In contrast to the evaluation of the oxime bond and self-immolative linker-containing GnRH-III-Dau conjugates, the treatment time was drastically shortened from 24 hours down to 15 minutes. The obtained results clearly show that both Dau-containing sC18-Dau conjugates reveal a higher anticancer activity than the GnRH-III conjugate **K2**. The best activity could be obtained for sC18(Dau=Aoa-

Table 10: Structure and i*n vitro* cytostatic effect of sC18 and **K2** on Panc-1 human pancreatic cancer cells after 15 min treatment and 72 hours incubation

Code	Structure	IC_{50} Panc-1 [µM]
Dau		13.8 ± 8.9
K2	<EHWK(Bu)HDWK(Dau=Aoa)PG-NH_2	>140
sC18(Dau=Aoa)	GLRKRLRK(Dau=Aoa)FRNKIKEK-NH_2	79.9 ± 56.4
sC18(Dau=Aoa-GFLG)	GLRKRLRK(Dau=Aoa-GFLG)FRNKIKEK-NH_2	9.4 ± 0.9

GFLG), which has an 8-times higher growth inhibitory effect than the non linker counterpart sC18(Dau=Aoa). Since it has been described that both smallest Dau-containing metabolites (Dao=Aoa-Gly-OH and H-Lys(Dau=Aoa)-OH) show similar DNA-binding properties, there should be another reason for the diversity of the results [257]. Considering the findings from the lysosomal degradation studies (3.1.1.2.2.) which prove that the lysosomal enzymes possess high amino- and carboxypeptidase activity, it can be assumed that the release of the smallest Dau-containing metabolite Dau=Aoa-Gly-OH is accelerated in comparison to the release of H-Lys(Dau=Aoa)-OH). In case of GnRH-III conjugates, the insertion of a Dau=Aoa-GFLG spacer at the side chain of ^{8}Lys did not lead to an improved cytostatic effect, but this might be explained by the localization of the Lys(Dau=Aoa) close to the *C*-terminus. On the contrary, in sC18(Dau=Aoa) the ligation site is in the middle of the peptide which might slow down the release [257]. Moreover, the structure of GnRH-III-derivatives is characterized by an extended backbone conformation which might facilitate an enzymatical degradation, while the helical backbone structure of sC18 could hamper the lysosomal formation of the H-Lys(Dau=Aoa)-OH. In case of sC18(Dau=Aoa-GFLG), the Dau=Aoa-GFLG-linker is not involved in the helix which probably enhances the access of the cleavage site to enzymes. Besides, compound sC18(Dau=Aoa-GFLG) displays an even higher cytostatic effect on Panc-1 cells than the free Dau indicating that the MDR of Panc-1 cells can be obviated when Dau enters the cell by endocytosis and not by passive diffusion. Comparable results could be obtained by *Zheng et al.,* whereby doxorubicin was bound noncovalently to a CPP with a drug binding motive [403]. In that way, the free Dox could enter leukemia cells by endocytosis and was directed into the perinuclear area and the nucleus. Therefore, it can be suggested that the Dau/Dox resistance of Panc-1 and other PDA cells can be reduced when the drug enters the cells by an endocytic route and not by passive diffusion. Moreover, considering all obtained results, it can be concluded that the reduced activity of the GnRH-III conjugates is caused by the low GnRH-receptor level and the

accompanied decreased cellular uptake of the compounds, and not by the MDR. However, since the novel self-immolative linker-containing Dau conjugates possess a lower cytostatic effect than the oxime bond-containing lead compounds, additional experiments are necessary to draw a final conclusion on biological activity of the novel compounds.

3.1.2.3.2. Lysosomal degradation in presence of rat liver lysosomal homogenate

In order to get a deeper insight into the mode of action of the self-immolative GnRH-III conjugates and to understand why the activity of these compounds is lower than the activity of the two oxime bond-linked compounds **K2** and **16**, lysosomal degradation studies have been carried out. According to the literature, the release of the free drug should occur as described in **Scheme 5** [211,320]. In case of the Val-Aaa-PABC-Dau-conjugates, the free Dau should be released together with carbon dioxide after enzymatical hydrolysis and 1,6-elimination of the PABC-moiety to 4-methylene-2,5-cyclohexadien-1-imine. Considering that the His-Trp-containing self-immolative compounds revealed a better solubility in acidic aqueous buffer than the ΔHis-D-Tic compounds, the degradation studies were performed with conjugates **45** and **47**, as well as the non-cleavable linker conjugates **57** and **58**. For both non-cleavable linker-containing derivatives, no release of free Dau could be detected, only the smallest Dau-containing metabolite H-Lys(Dau-glutaryl)-OH (**Figure 19**, peaks labeled by #). This result supports the assumption that the substantially reduced anticancer activity of the non-cleavable GnRH-III compounds is caused by the stable acylation at the amino group of the daunosamine sugar moiety which might prevent an efficient intercalation of the Dau-derivative with the minor groove of the DNA [254,404]. In contrast, for both cleavable linker-bearing compounds, the release of free Dau and the formation of various peptide fragments could be proven (**Figure 19**), whereby the Val-Cit linker was cleaved slightly faster than the Val-Ala linker and a small portion of Dau could be already detected after

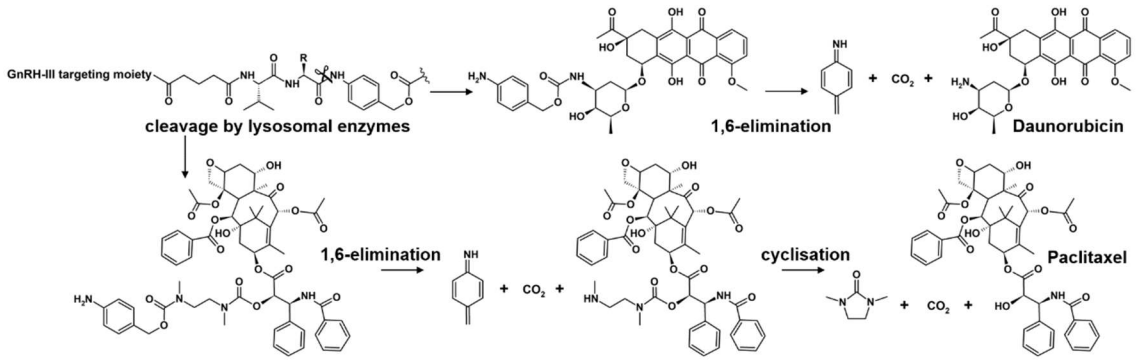

Scheme 5. Proposed mechanism of enzymatical cleavage and subsequent release of daunorubicin and paclitaxel.

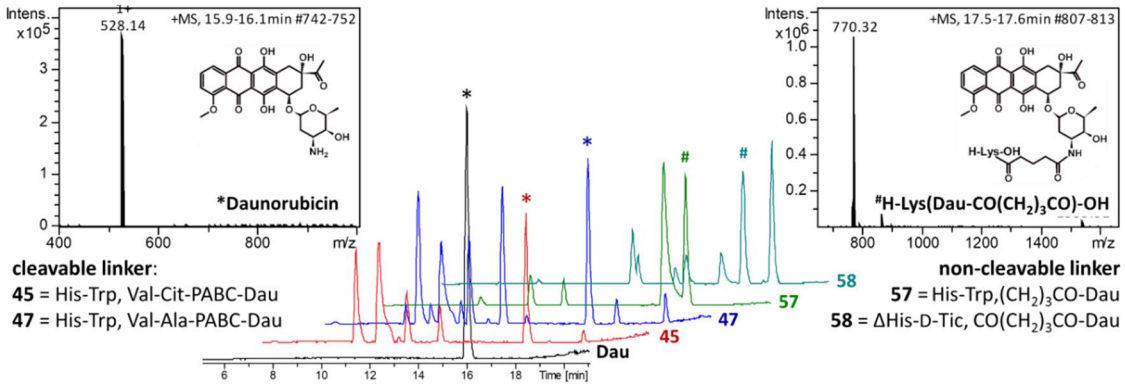

Figure 19. Degradation of the GnRH-III conjugates in presence of lysosomal rat liver homogenate. LC chromatograms of **45**, **47**, **57**, **58** and free Dau (control) after 24 hours degradation and MS spectra of the released *daunorubicin (left) and non-cleavable metabolite, #H-Lys(Dau-CO$(CH_2)_3$CO)-OH (right).

5 minutes incubation. However, both cleavable linkers were successfully proteolyzed by lysosomal enzymes and brought out free Dau within the first hour of incubation which might be of high relevance for the biological activity of the compounds. In general, these data confirm that the releasing strategy of the cathepsin cleavable linkers in combination with the self-immolative PABC-moiety worked very well and could be effectively applied to GnRH-III derivatives. Therefore, it can be assumed that the lower anticancer activity of the conjugates is not related to an inefficient release of the free drug.

Furthermore, also proteolysis of the equivalent PTX-containing GnRH-III conjugates (**49**, **51**, **59**, **60**) in presence of lysosomal enzymes was studied. The obtained degradation profile of the PTX-compounds was quite similar to that of the Dau-conjugates, whereby both cathepsin cleavable linker systems were cleaved with the same efficiency. The diamine-PTX fragment could be already detected for both cleavable compounds after 5 minutes of incubation, while this fragment could not be detected in case of the non-cleavable linker derivatives even after 24 hours of incubation. However, although the diamine-PTX fragment is formed quickly, the release of the free PTX could not be detected within 24 hours under the applied *in vitro* conditions. These findings might serve as an explanation for the similar IC_{50} values of the PTX conjugates and the wide disparity of the biological activity between the free PTX and the conjugates. On the other hand, it can be assumed that the acidic conditions of the experiment which were needed to ensure the activity of the lysosomal enzymes, prevent the cyclisation of the diamine-linker and the release of the free PTX. Considering that the intracellular pH of cancer cells is defined to be $\geq$ 7.4 [405], the nucleophilic attack of the secondary amine towards the carbamate function, followed by the formation of the cyclic urea derivative and the subsequent release of the free PTX (**Scheme 5**), might be much more favorable in the cytosol than in lysosomes. Nevertheless, the obtained results are in line with literature and it could be

shown that the cleavage mechanism by lysosomal enzymes and the release of the PTX-prodrug occurs efficiently, while the formation of the free PTX is the rate limiting step [211,353].

3.1.2.3.3. Radioligand binding studies

The obtained results of the cell viability measurements pointed out that the self-immolative linker-containing GnRH-III-Dau compounds possess a lower anticancer activity than the oxime bond-containing equivalents, while it has been proven that the release of the free Dau occurs efficiently in presence of lysosomal enzymes. In order to better understand this outcome, the receptor binding affinity of the GnRH-III-Dau compound with the highest growth inhibitory activity on A2780 (**48**) and its PTX-containing counterpart (**52**) were studied by the research group of Gábor Halmos. The displacement of [^{125}I]-triptorelin from GnRH-Rs was determined on human pituitary and human prostate cancer tissues, whereby increasing compound concentrations were used. Both compounds bind to the receptors with high affinities in the low nanomolar range, while GnRH unrelated peptides were not able to displace triptorelin. However, in comparison to the best oxime bond-linked GnRH-III-Dau conjugate (**16**), the self-immolative linker Dau conjugate (**48**) exhibits a more than 7-times reduced affinity to the GnRH-receptors (**Table 11**). This might be the reason for the improved anticancer activity of lead-compound **16**. Considering that the equilibrium binding constants of free Dau and H-Lys(Dau=Aoa)-OH differ just by a factor of 1.7 [257], it can be supposed that the decreased receptor affinity of the self-immolative GnRH-Dau conjugates exert a larger influence on the biological activity than the declined DNA binding properties of the smallest Dau-containing metabolite. Interestingly, the PTX-containing compound **52**, has a higher binding affinity than the Dau-equivalent, even if the targeting sequence and the cathepsin cleavage site remain the same. A possible explanation for this observation could be that the incorporation of the additional diamine spacer results in a higher flexibility and provides a longer, more favorable distance between the drug and the

Table 11: Competitive inhibition of [^{125}I][^{6}D-Trp]-GnRH-I binding to membranes of human pituitary and human prostate cancer specimens by GnRH-III-Dau conjugates.

Code	GnRH-III-[^{2}ΔHis-^{3}D-Tic-^{4}Lys(Bu)-^{8}Lys(linker-drug)]	IC_{50} [nM]	
		pituitary	prostate cancer
16	Dau=Aoa	3.53 ± 0.96	2.79 ± 1.24
48	glutaryl-Val-Ala-PABC-Dau	24.77 ± 2.1	20.54 ± 1.46
52	glutaryl-Val-Ala-PABC-diamine-PTX	10.82 ± 1.98	12.73 ± 2.23

all values represent mean ± SE

targeting moiety. Moreover, the inherent properties of the drug in combination with the linker system might also have an impact on the receptor affinity.

3.2. Somatostatin conjugates

Besides GnRH and its derivatives, the hormonal cyclopeptide somatostatin is a promising targeting moiety for the delivery of cytotoxic agents or radionuclides to tumors which overexpress somatostatin receptors [248]. Since the natural tetradecapeptide possesses a very short half-life *in vivo* and induces a variety of biological effects, more stable and selective somatostatin analogs have been developed [154,155,406]. Next to the prominent somatostatin analog octreotide, the tumor selective somatostatin derivatives RC-121 and TT-232 has been used as targeting moieties [206,265,268,277,407–409]. Like octreotide, the octapeptide RC-121 displays a high affinity to SSTR2 and SSTR5, a moderate affinity to SSTR3, and binds only poorly to SSTR1 and SSTR4. In comparison, the heptapeptide TT-232 which varies from RC-121 only by the lack of valine, has been shown to bind selectively to SSTR4 and SSTR1 [161]. In this thesis, the somatostatin analogs RC-121 and TT-232 have been used as homing devices to deliver the classical anticancer agent Dau and its more potent analog pyDau to breast and colon cancer cells, whereby different linker systems have been applied. Furthermore, a new type of somatostatin analogue was designed and used as drug delivery system, in which the intramolecular ring is formed by a thioether bond instead of a disulfide bridge.

3.2.1. 5(6)-Carboxyfluorescein-(FAM)-somatostatin derivatives

Initially, fluorescence labeled somatostatin derivatives have been developed and synthesized to study the influence of structural changes in the targeting peptide on the cellular uptake. Special attention was paid on the effect of a lysosomal cleavable tetrapeptidyl spacer, the presence (RC-121) and absence (TT-232) of Val in the sequence and the modification of the intramolecular disulfide bridge to a thioether bond. The cellular uptake of the compounds was studied by flow cytometry and visualized by CLSM.

3.2.1.1. Synthesis of 5(6)-FAM-somatostatin-derivatives

The 5(6)-carboxyfluorescein (FAM) labeled somatostatin peptides were synthesized by standard Fmoc SPPS as depicted in **Scheme 6**. Two of the disulfide cycled derivatives contain *N*-terminally the lysosomal cleavable tetra-peptidyl linker LRRY and either Val in position 10 (**63**) or not (**64**). Moreover, two equivalent somatostatin compounds without the hydrophilic linker have been synthesized (**61**, **62**). The sequence of the

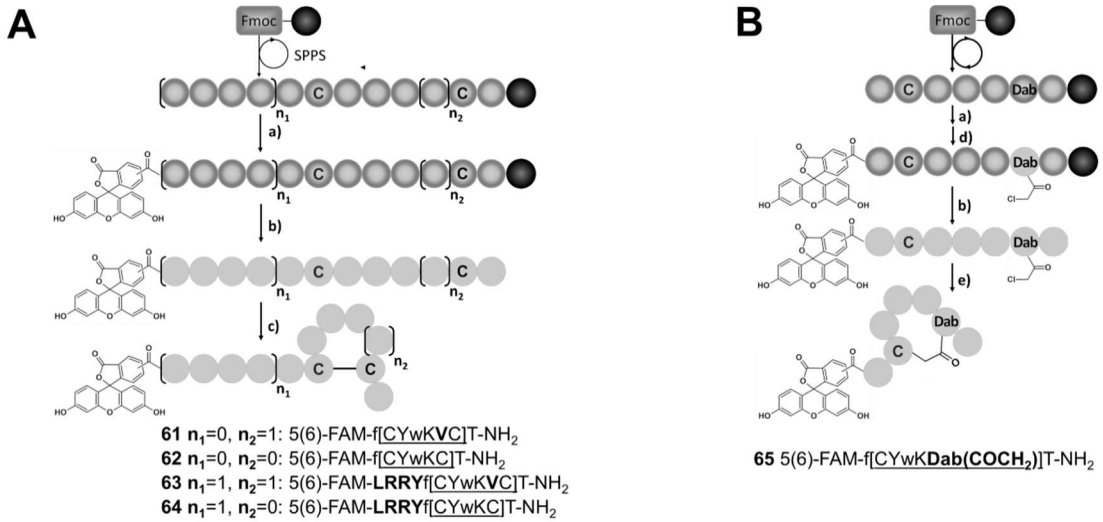

Scheme 6. Synthesis of FAM-somatostatin derivatives. **A**: disulfide bond **B**: thioether (**a**) 5 eq 5(6)-FAM, 5 eq HOBt, 5 eq DIC in DMF, 1.5 h, RT, (**b**) 93% TFA, 2.5% water, 2.5% thioanisole, 1.25% EDT and 0.75% phenol, 3 h, at RT, (**c**) 0.2 mg/mL peptide in 1:19 DMSO:0.1 M Tris-buffer (pH 8.3), (**d**) [1.)] 2% hydrazine in DMF (12 x 5min) [2.)] 5 eq Cl-CH_2-CO-OPcp, 5 eq DIPEA in DMF, 2 h, RT, (**e**) 4 mg/mL.

targeting moiety corresponds to the well known somatostatin derivatives RC-121 (Val; **61**, **63**) and TT-232 (ΔVal; **62**, **64**). For the synthesis, Fmoc-Cys(Trt)-OH was incorporated in the appropriate positions and after peptide chain elongation, FAM was coupled to the *N*-terminus. After cleavage from resin and purification by RP-HPLC, the disulfide bond was formed by air oxidation in alkaline aqueous buffer for several days. The progress was followed by analytical RP-HPLC until the reaction was completed, then the mixture was acidified, freeze dried und purified by preparative RP-HPLC. The synthesis of compound **65** was carried out in a different way, valine was left out and instead of the *C*-terminally localized cysteine, Fmoc-Dab(Dde)-OH was incorporated within the sequence. After main chain assembly, FAM coupling and Dde deprotection, pentachlorophenylchloroacetate (Cl-CH_2-CO-OPcp) was coupled to the free amino group. Afterwards, the peptide was cleaved from resin and purified. The thioether bond formation was carried out in Tris-buffer and subsequently purified by RP-HPLC. The ring size of the cyclic thioether peptide (**65**) corresponds to the ring size of the Val-containing disulfide bridged compounds **61** and **63**. The final FAM-somatostatin analogs were characterized by analytical RP-HPLC and mass spectrometry (**Table 12**, Appendix 10.2.1.1. Figure A48-A52).

Table 12: Chemical characteristics of FAM-somatostatin derivatives.

Code	Sequence	Purity [%]	RP-HPLC R_t [min][a]	ESI-MS MW_{cal} /MW_{exp} [g/mol][b]
61	**FAM**-f[CYwKVC]T-NH_2	≥97	25.15/25.65	1404.56//1404.37
62	**FAM**-f[CYwKC]T-NH_2	≥97	24.22/24.52	1305.43/1305.16
63	**FAM**-LRRY-f[CYwKVC]T-NH_2	>94	24.08/24.25	1993.27/1992.76
64	**FAM**-LRRY-f[CYwKC]T-NH_2	≥95	24.10/24.27	1894.14/1893.78
65	**FAM**-f[CYwK-Dab-($COCH_2$)]T-NH_2	≥95	23.20/23.42	1344.45/1344.30

[a]Column: Macherey-Nagel Nucleosil C18 column (250 mm x 4.6 mm) with 5 µm silica (100 Å pore size); gradient: 0 min 0% B, 5 min 0% B, 30 min 90% B; eluents: 0.1% TFA in water (A) and 0.1% TFA in acetonitrile-water (80:20, v/v) (B); flow rate: 1 mL/min; detection at 220 nm. [b]Bruker Daltonics Esquire 3000+ ion trap mass spectrometer.

3.1.1.2. pH dependent fluorescence properties of 5(6)-FAM-somatostatin-derivatives

Considering that the fluorescence quantum yield of fluorescein and its derivatives depend strongly on the pH value of the environment [410], the fluorescence intensity of the compounds has been measured over a pH range between 4.0 and 7.6 (**Figure 20**). This pH range was chosen due to intracellular pH values of different cellular compartments, like cytosol (pH ≥ 7.4), early endosomes (pH 6.0 - 6.5), late endosomes (pH 5.0 – 6.0) or lysosomes (pH 4.5 – 5.0) [405,411,412]. In accordance with the literature, the fluorescence intensity of the FAM-containing derivatives was higher in neutral-alkaline buffer and reduced in acidic buffer (**Figure 20C**) [413]. This effect is caused by different pH dependent ionic equilibria of the fluorescein moiety. Since the 5(6)-carboxylic function of FAM was used for the coupling to the peptide, it can be considered that the ionization equilibrium is comparable to that of fluorescein (**Figure 20D**). Under alkaline conditions, the phenol, as well as the carboxylic group of the fluorescein are ionized and the dianion species is mainly present. It has been reported that acidification causes first the

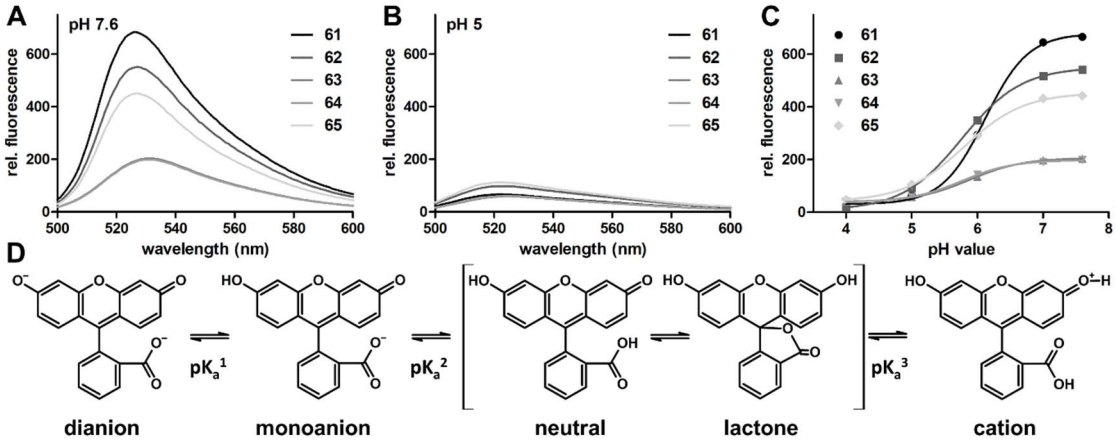

Figure 20. Fluorescence intensity of FAM-somatostatin derivatives **61-65** depending on the pH value. **A**: Fluorescence emission spectra at pH 7.6 (λ_{Ex} = 488 nm), **B**: Fluorescence emission spectra at pH 5 (λ_{Ex} = 488 nm), **C**: Fluorescence intensity depending on the pH (λ_{Ex} = 488 nm, λ_{Em} = 530 nm) - curves obtained by non-linear regression (sigmoidal dose response, R^2 ≥0.9995). **D**: Ionization equilibrium of fluorescein.

protonation of the phenol group, yielding the monoanion ($pK_a^1 \approx 6.4$), followed by formation of the neutral form ($pK_a^2 < 5$), while further acidification is required to produce the cation species ($pK_a^3 \approx 2.1$) [414,415]. Moreover, it could be shown that the fluorescence quantum yield of the dianion form ($\Phi = 0.93$) is much higher than the quantum yield of the monoanion ($\Phi = 0.25$-0.35) and the neutral form ($\Phi = 0.20$-0.25) which provides an explanation for the reduction of the fluorescence intensity of the compounds with decreasing pH [410]. In order to illustrate the pH-related fluorescence properties of the FAM-somatostatin conjugates, the fluorescence maximum ($\lambda_{Ex} = 488$ nm, $\lambda_{Em} = 530$ nm) was plotted against the pH and a sigmoidal fit was performed (**Figure 20C**). This simplified model can be applied by considering different aspects. On the one hand, previous studies pointed out that the cationic form has only a negligible impact on the fluorescence signal at the used conditions, and on the other hand, the fluorescence spectra of the monoanionic and neutral molecule do not differ substantially, since the carboxylic group is not conjugated with the light-absorbing xanthene element of the molecule [410,413]. Therefore, the obtained inflection points which vary between 6.12 and 5.76 represent the mean of pK_a^1 and pK_a^2 and can be considered as overall pK_a^{1-2} of the fluorescence properties defining forms (dianion-neutral) of the fluorescein. Apart from that, the fluorescence measurements exposed that the maximal fluorescence intensity of the LRRY-linker-containing compounds is substantially reduced at pH 7.6 in comparison to the intensity of the FAM-somatostatin derivatives without linker, while the inflection points are in a comparable range. This effect might be caused by non-covalent interaction of the guanidine groups of the arginines and the mono- and dianion form of the fluorophore.

3.1.1.3. Cellular uptake of the bioconjugates by flow cytometry

To study the cellular uptake of the compounds on HT-29 colon cancer and MCF-7 breast cancer cells, flow cytometry studies have been performed by Beáta Biri-Kovács. Initially, the uptake rates of the disulfide bond cycled peptides (**61**-**64**) were determined at different concentrations (6.25, 25 and 100 µM) and compared (**Figure 2**1). The obtained uptake rates of the compounds exhibit the same tendency on both cell lines. In general, the two linker-containing analogs (**63**, **64**) were taken up more efficiently than the classical somatostatin analogs (**61**, **62**). This becomes particularly clear at 25 µM: here at least 93% of living HT-29 cells were FAM positive after treatment with compound **63** and **64**, while only 12.5% and 7.9% reveal the fluorescence signal in case of **61** and **62**. Moreover, the results display that the Val-containing somatostatin derivatives were taken up better

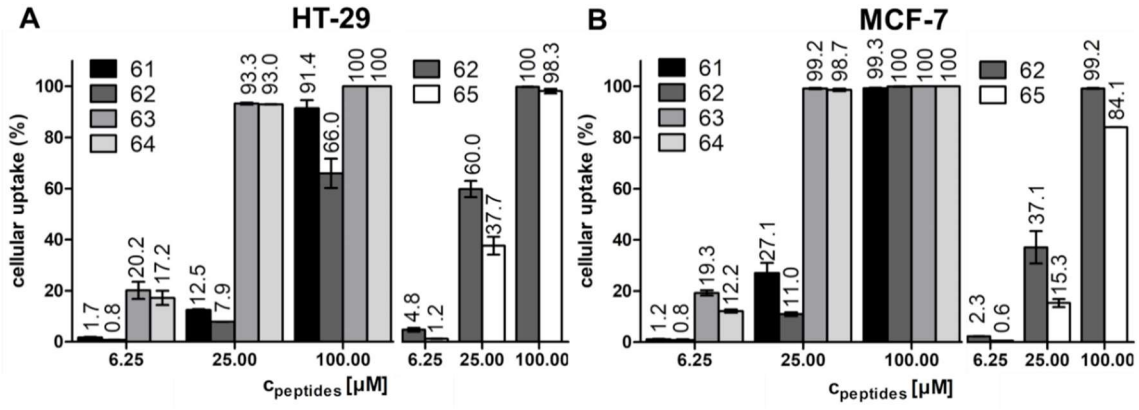

Figure 21. Cellular uptake studies of FAM-somatostatin conjugates after 6 h treatment by flow cytometry on **A**: HT-29 and **B**: MCF-7 cells (individual experiments of compounds **61**-**64** (left) and compounds **62**, **65** (right). Experiments were performed in duplicates. Error bars represent SD.

than the respective ΔVal counterparts. On both cell lines, the LRRY-linker and Val-containing derivative **63** was taken up most efficiently. Furthermore, the cellular uptake of the thioether cycled compound **65** was studied in an individual experiment, thereby the uptake rates were directly compared to that of compound **62**. Both cell lines revealed a similar tendency for the uptake of the two compounds, whereby higher uptake rates could be obtained on HT-29 cells. The results indicate that the disulfide cycled compound were taken up more efficiently than the thioether-containing compound.

3.1.1.4. Confocal laser scanning microscopy (CLSM) studies

Next to the quantitative cellular uptake studies by flow cytometry, CLSM studies have been performed[e] on MCF-7 breast cancer cells to visualize the cellular uptake and the subcellular localization of the somatostatin compounds (**61**-**65**). Considering the results of flow cytometry studies which revealed that more than 80% of living cells had taken up the compounds at 100 µM concentration and six hours of incubation, these conditions were selected for fluorescence microscopy studies. The recorded images of the hydrophilic, cathepsin cleavable linker-containing conjugates **63** and **64** exhibit the fluorescence signal exclusively in the cytosol, while for the compounds without the LRRY-linker (**61**, **62**, **65**) also small cytosolic vesicles could be detected which can be considered as endosomes and/or lysosomes (**Figure 22**, depicted in BestFit mode). Especially, the thioether cycled derivative **65** exposes the fluorescent signal predominantly in small cytosolic compartments. Moreover, the fluorescence intensity of compounds **63** and **64** was strongly enhanced in comparison to the other compounds. Thus, a lower laser energy was used for the image recording. Taking into account that the

[e] All CLSM samples were prepared by Beáta Biri-Kovács and images were recorded by Bálint Szeder

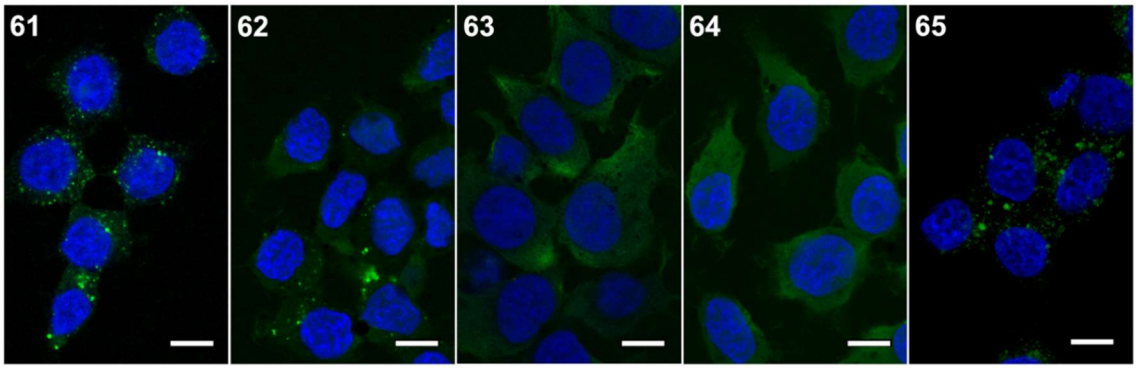

Figure 22. Cellular localization of FAM-somatostatin conjugates **61**-**65** (100 µM, green) on MCF-7 cells visualized by confocal laser scanning microscopy after 6 h incubation. Nuclei were stained by DAPI (blue). Scale bars represent 10 µm.

intact linker-containing compounds **63** and **64** exhibit just a low fluorescence signal in cell-free system, while both cellular experiments showed high fluorescence intensities for these compounds, it can be assumed that the degradation of the FAM-LRRY-linker leads to the liberation of FAM-Leu-OH, which might have more favorable fluorescence properties than the intact FAM-LRRY-compounds. In general, it can be assumed that the direct coupling of the FAM to D-Phe prevent a sufficient degradation of the peptide derivative and the release of small FAM-containing peptide fragment from the lysosome. In case of compound **65**, the resistance towards lysosomal enzymes might be additionally enhanced by the high stability of the intramolecular thioether bond.

3.2.2. Somatostatin-drug conjugates

Based on the results of the FAM-somatostatin derivatives, a variety of somatostatin-drug conjugates have been synthesized and analyzed for their cytostatic effect on human colon and breast cancer cells. Since the incorporation of the LRRY-linker enhanced the cellular uptake of the compounds and provided a sufficient release of the drug or drug metabolites in lysosomes by cathepsins, this peptide spacer was mainly used to connect the drug with the somatostatin peptide. Initially, the same three targeting moiety have been used like in case of the FAM-derivatives, namely RC-121, TT-232 and the novel thioether bridged somatostatin derivative, and the anthracycline Dau was conjugated to an *N*-terminally inserted Aoa-LRRY-linker by oxime bond formation. The peptide carrier of the conjugate which possessed the highest cytostatic effect provides the basis for the development of new somatostatin-drug conjugates, containing either the more potent anticancer agent pyDau or further cleavable linker systems. To examine the influence of pyDau and the linker systems, the antitumor activity of the conjugates was determined and compared.

3.2.2.1. Synthesis of somatostatin-drug conjugates

In general, all somatostatin-drug conjugates were synthesized as described in **Scheme 7**. The targeting peptides were prepared by standard SPPS. In case of the oxime bond-containing conjugates, isopropylidene protected aminooxy acetic acid (>=Aoa-OH) was incorporated at the *N*-terminus of the LRRY-peptide linker. The cyclization of the somatostatin derivatives was carried out in solution by disulfide bond (air oxidation or thallium trifluoroacetate oxidation) or by thioether bond formation. Dau and its more potent relative pyDau were conjugated to the *N*-terminus of the targeting peptide in solution, either by oxime bond formation after isopropylidene deprotection of the >=Aoa, or by coupling of a self-immolative glutaryl-Val-Ala-PABC-Dau linker.

Synthesis of oxime bond-linked somatostatin-Dau and pyDau conjugates

Equivalent to the synthesized FAM-derivatives, two disulfide bridged (with and without Val) and one thioether cycled oxime bond-linked somatostatin-Dau conjugates have been prepared (**66-68, Scheme 7A-B**). The cleavable LRRY-peptide spacer was directly assembled at the *N*-terminus of all three targeting peptides. In case of the disulfide cycled compounds (**66**, **67**), Fmoc-Cys(Trt)-OH was incorporated in the appropriate positions of the sequence. After coupling of >=Aoa-OH, the peptide was cleaved from the resin, purified by RP-HPLC and the disulfide bond was formed by air oxidation, followed by purification. In case of compound **68**, Fmoc-Dab(Dde)-OH was incorporated in position 10 and subsequent to >=Aoa-OH coupling, the Dde-group was cleaved and Cl-CH_2-CO-OPcp was coupled to the ^{10}Dab side chain. Afterwards, the peptide was cleaved from resin, purified and the thioether bond was carried out in alkaline buffer. Subsequent to RP-HPLC purification of the three cyclic peptide, the >=Aoa was deprotected and the compound was purified once more by RP-HPLC. Immediately afterwards, Dau was linked in solution by oxime bond formation and the resulting conjugates were purified again by preparative RP-HPLC. In general, the allover yield of the three oxime bond-linked somatostatin-Dau conjugates (**66-68**) was quite poor (<5%) which was related to various factors. Although the hydrophilic peptide spacer LRRY was included in the sequence, the >=Aoa-containing intermediates, as well as the final Dau-conjugates are poorly soluble under aqueous conditions. This affects not only the disulfide bond formation and purification steps, but also the ligation reaction. Moreover, it turned out that the Aoa-somatostatin derivatives are much more prone to side reactions than the GnRH-III derivatives. In accordance with former studies, mass spectrometric analysis pointed out that the Aoa-unprotected somatostatin compounds react quickly with acetone

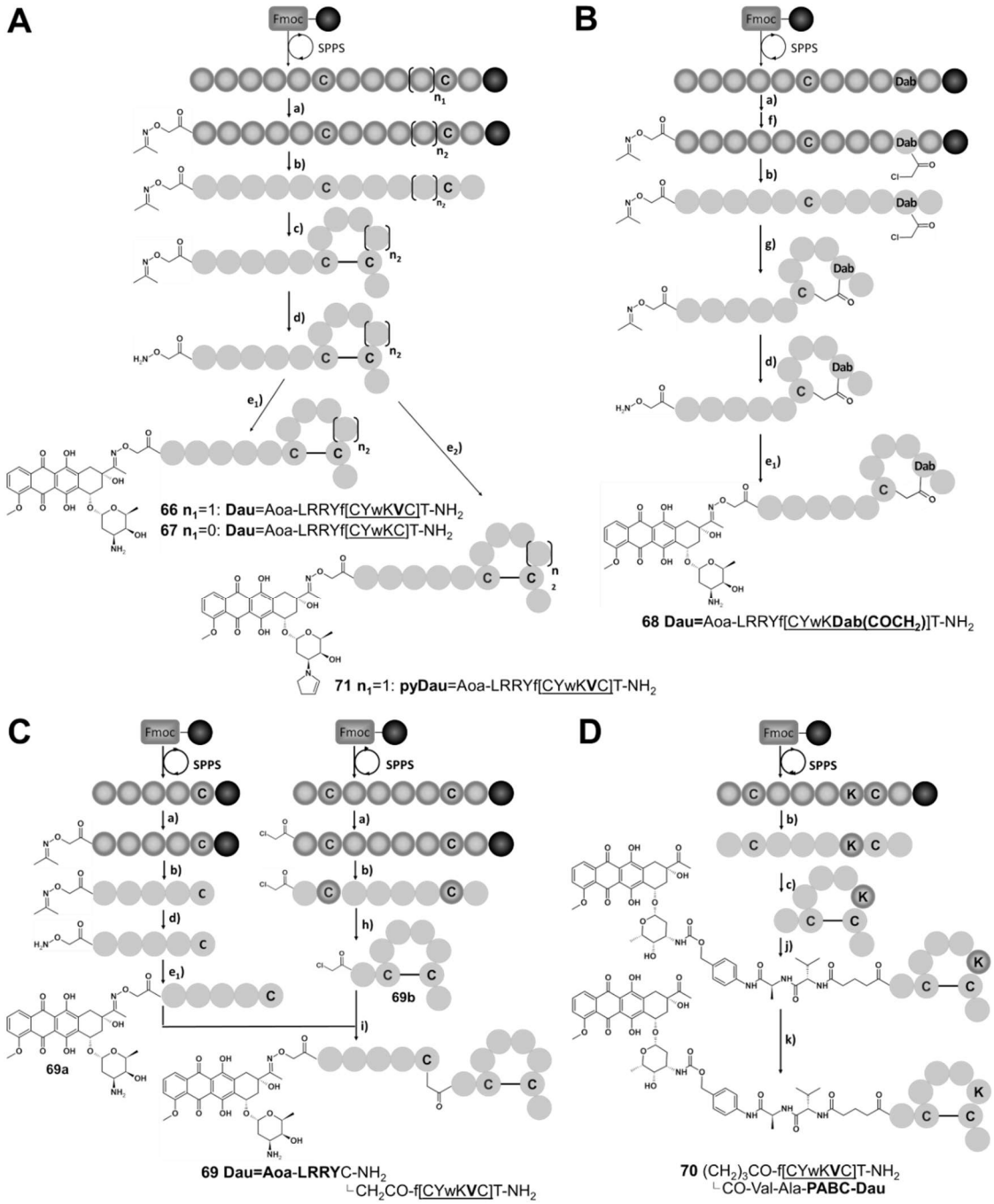

Scheme 7. Synthesis of somatostatin-drug derivatives. **A**: disulfide bridge cyclized and oxime bond-containing Dau/pyDau-conjugates **B**: thioether cyclized and oxime bond-containing Dau-conjugate **C**: disulfide bridge cyclized and thioether linked, oxime bond-containing Dau-conjugate **D**: self-immolative linker-containing-drug conjugate. (**a**) 5 eq >=Aoa, 5 eq HOBt, 5 eq DIC in DMF, 2 h, RT, (**b**) 93% TFA, 2.5% water, 2.5% thioanisole, 1.25% EDT and 0.75% phenol, 3 h, at RT, (**c**) 0.2 mg/mL peptide in 1:19 DMSO:0.1 M Tris-buffer (pH 8.3), (**d**) 5 mg/mL peptide, 1 M H_2N-O-CH_3 in 0.2 M NH_4OAc (pH 5), (**e1**) 10 mg/mL peptide, 1.3 eq Dau in 0.2 M NH_4OAc (pH 5), overnight, RT, (**e2**) 10 mg/mL peptide, 1.3 eq pyDau in 1:1 DMF:H_2O, overnight, 4 °C, (**f**) [1.)] 2% hydrazine in DMF (12 x 5min), [2.)] 5 eq Cl-CH_2-CO-OPcp, 5 eq DIPEA in DMF, 2 h, RT, (**g**) 4 mg/mL peptide in 1:1 DMF:0.1 M Tris-buffer (pH 8.3), 2.5 h, RT, (**h**) 1 eq peptide, 1.2 eq thalium(III) trifluoroacetate, anisole in 4 mL TFA, 5 h, 0 °C, (**i**) 1 eq **69a** and **69b** in 1:1 DMF:0.1 M Tris-buffer (pH 8.3), 2h, RT, (**j**) [1.)] 1 eq **39**, 0.9 eq HATU, 2 eq DIPEA in DMF 30 min, [2.)] 1 eq peptide carrier, overnight, RT, (**k**) 2% hydrazine in DMF, 5 min, RT.

or other carbonyl compound from the environment during RP-HPLC purification and Dau ligation [268].

Next to the oxime bond-linked Dau conjugates, the pyDau-containing counterpart of conjugate **66** was synthesized in a comparable manner yielding compound **71**. PyDau (synthesized from Dau by Kristóf Hegedüs) was freshly purified and in contrast to the Dau conjugate, the ligation was performed at 4 °C to avoid the dimerization of pyDau. The allover yield of conjugate **71** was even 2% lower than the yields of the Dau-conjugates. Next to the above mentioned factors, in this case the retention times of the final product and the isopropylidene reprotected side product were overlapping which leads to an additional reduction of the yield.

With the aim to enable a higher variability of the cleavable linker system, a somatostatin-Dau conjugate was developed, in which the Dau=Aoa-LRRY-linker was conjugated to the RC-121 peptide moiety be thioether bond ligation (**Scheme 7C**). Therefore, the LRRY-linker was synthesized separately by SPPS, whereby Fmoc-Cys(Trt)-OH was inserted at the *C*-terminus of the linker and >=Aoa-OH at the *N*-terminus. After cleavage from resin, >=Aoa deprotection and Dau ligation was performed as described above affording linker **69a**. For the synthesis of the targeting peptide, Fmoc-Cys(Acm)-OH was incorporated in position 2 and 7, and Cl-CH_2-CO-OPcp was coupled at the *N*-terminus. After cleavage from resin and RP-HPLC purification, the deprotection of the cysteines and the disulfide bond formation was carried out simultaneously by thallium trifluoroacetate oxidation, followed by additional RP-HPLC separation of compound **69b** (36% yield). The ligation of **69a** and **69b** was performed in alkaline buffer and the final conjugate **69** was isolated by RP-HPLC (19% yield). The relatively poor yield of the ligation reaction was mainly related to the intermolecular disulfide bond formation of linker **69a** yielding the linker dimer. Since the targeting moiety contains also a disulfide bridge, reducing agents such as dithiothreitol (DTT) or GSH could not be used to avoid the dimerization of the linker. However, this conjugation strategy offers the opportunity to ligate various thiol-containing drug-linker systems to the same targeting moiety. Apart from that, all final oxime bond-linked somatostatin-drug conjugates were characterized by analytical RP-HPLC and ESI-MS (**Table 13**, Appendix 10.2.2.2., Figure A53-56, A58).

Synthesis of self-immolative linker-containing daunorubicin–somatostatin conjugates

As in case of GnRH-III-based DDS, the self-immolative and cathepsin B cleavable linker-containing somatostatin conjugate was synthesized (**Scheme 7D**). Considering that the GnRH-III compounds with the Val-Ala cleavage site exhibit the best antitumor activity, the glutaryl-Val-Ala-PABC-Dau (**39**) linker was conjugated to the RC-121 targeting

sequence by amide bond formation. The self-immolative linker **39** was prepared as described above (3.1.2.1.) in solution. The synthesis of the RC-121 peptide was carried out by SPPS, using Fmoc-Cys(Trt)-OH in position 2 and 7, and Fmoc-Lys(Dde)-OH in position 6. After peptide chain assembly, the peptide was cleaved from resin and purified, followed by disulfide bond formation in solution by air oxidation and additional purification by RP-HPLC. For the conjugation reaction, the appropriate linker was preincubated with HATU and DIPEA to form the activated glutaryl ester and after 30 minutes, the peptide carrier was added. The resulting Dde-protected conjugate could be obtained with 38% yield after RP-HPLC purification. This yield was mainly affected by the poor solubility of the compound in RP-HPLC eluent solution which hampered the purification. In the final step, the Dde group was cleaved in solution and after 10 minutes the reaction mix was purified by RP-HPLC affording conjugate **70** with 50% yield. The relatively short reaction time was necessary, since the cleavage solution affects also the carbamate function of PABC-Dau. Like the other somatostatin-drug conjugates, compound **70** was characterized by analytical RP-HPLC and ESI-MS (**Table 13**, Appendix 10.2.2.1., Figure A57).

Table 13: Chemical characteristics of the somatostatin-drug conjugatess.

Code	Sequence	Purity RP-HPLC [%]	R_t [min][a]	ESI-MS MW_{cal} /MW_{exp} [g/mol][b]
66	**Dau=Aoa**-LRRY-f[CYwKVC]T-NH_2	≥97	23.30	2217.52/2217.45
67	**Dau=Aoa**-LRRY-f[CYwKC]T-NH_2	≥98	22.80	2118.39/2118.30
68	**Dau=Aoa**-LRRY-f[CYwK-Dab-($COCH_2$)]T-NH_2	≥96	22.88	2157.40/2157.02
69	**Dau=Aoa**-LRRYC-NH_2 └CH_2-CO-f-[CYwKVC]T-NH_2	>98	22.93	2377.72./2377.14
70	$(CH_2)_3$-CO-f[CYwKVC]T-NH_2 └CO-(Val-Ala-**PABC-Dau**)	≥96	28.52	1989.22/1988.36
71	**pyDau=Aoa**-LRRY-f[CYwKVC]T-NH_2	≥97	24.27	2269.60/2269.59

[a]Column: Macherey-Nagel Nucleosil C18 column (250 mm x 4.6 mm) with 5 µm silica (100 Å pore size); gradient: 0 min 0% B, 5 min 0% B, 30 min 90% B; eluents: 0.1% TFA in water (A) and 0.1% TFA in acetonitrile-water (80:20, v/v) (B); flow rate: 1 mL/min; detection at 220 nm. [b]Bruker Daltonics Esquire

3.2.2.2. In vitro cytostatic effect of somatostatin-drug conjugates

In order to analyze the *in vitro* cytostatic effect of the somatostatin-drug conjugates on human colon and breast cancer cells, an MTT cell viability assay has been performed. The biological activity of the free drugs was also determined and used as control for a better comparison of the individual experiments. Next to HT-29 colon carcinoma cells, the TNBC cell line MDA-MB-231 has been used instead of estrogen dependent MCF-7 cells, which might encourage upcoming *in vivo* studies, since MCF-7 breast cancer xenograft model strongly depends on exogenous E2 [297,416]. It could be shown that MDA-

MB-231 cells express, like MCF-7, all five STTR, whereby not only SSTR2 and SSTR5 are highly expressed, but also SSTR4 and SSTR1 [417–419]. All synthesized derivatives caused an inhibitory effect on the growth of colon and breast cancer cells, whereby IC_{50} values between 5.43 – 65.44 µM could be obtained on HT-29 cancer cells, and between 9.52 – 30.58 µM on MDA-MB-231 cells (**Table 14**, Appendix 10.2.2.2.). Initially, the three oxime bond-linked somatostatin-Dau conjugates **66**-**68** have been analyzed to gain insight into the efficiency of the targeting moieties. On both cell lines, the RC-121 derived conjugate (**66**) displayed the best cytostatic effect, while the thioether cycled derivative (**68**) which has a similar ring size like compound **66**, revealed a three- to six-times reduced anticancer activity. In contrast, the TT-232 related conjugate **67** exhibits a 12-times lower cytostatic effect on HT-29 cells than compound **66**, but just a 1.7-times reduced activity on MDA-MB-231. This result indicates that MDA-MB-231 cells might express a higher level of STTR4 and/or STTR1 than HT-29 cancer cells. However, considering that compound **66** showed the highest anticancer activity, the RC-121 derived targeting moiety was used to study the influence of linker modification on the cytostatic activity. Thus, the conjugates **69** and **70** have been developed and their anticancer activities were directly compared to compound **66**. Especially, the obtained results of compound **69** indicate that the cytostatic effect is not only influenced be the targeting moiety and the conjugated drug, but also by the ligation method. Although compound **66** and **69** possess the same targeting moiety and the Dau=Aoa-LRRY-linker, the activity of the thioether linked derivative **69** was more than 2.5-times decreased which supports the assumption that the thioether linkage affects the receptor binding and/or the cellular uptake. In case of the self-immolative linker-containing conjugate **70**, the anticancer activity was also slightly reduced in comparison to compound **66**. Considering that the lysosomal cleavage of the self-immolative Val-Ala-PABC-Dau linker facilitates the release of the free drug, while in case of **66** only the Dau=Aoa-Leu-OH metabolite is released, it can be concluded that this linker system has also a negative impact on the receptor binding affinity. A comparable effect has been already observed for the self-immolative GnRH-III-Dau conjugates (see above 3.1.2.3.). Thus, the oxime bond-linked conjugate **66** was confirmed as best somatostatin-Dau analog. Based on these findings, the same linker-containing peptide sequence and ligation method have been used for somatostatin-pyDau conjugate **71**. The cytotoxic effects of compound **71**, as well as of pyDau and the pyDau dimer ($(pyDau)_2$) were studied on HT-29 and MDA-MB-231 human cancer cells (**Table 14**). It could be shown that pyDau exhibits a several orders of magnitude higher cytotoxic effect

than Dau which is in line with comparable studies of pyDox and Dox [243]. Apart from that, during the synthesis of the conjugate, the formation of a dimeric pyDau form could be observed. Previous tandem MS studies indicated that the dimerization occurs by covalent bond formation of two 2-pyrollino moieties yielding a diazacyclodecadiene ring [420]. Unfortunately, the dimerization cannot be avoided at 37 °C which is necessary for the survival of the cells. Thus, the dimeric pyDau was also analyzed for its cytotoxic effect. The monomeric and dimeric forms were separated by RP-HPLC purification, but considering that the dimerization occurs faster under acidic conditions, the presence of the dimeric form could not be fully avoided. Thus, the lyophilized fraction of the monomeric pyDau contains approximately 30% of $(pyDau)_2$. Due to this fact, the obtained IC_{50} value for pyDau represents the activity of a certain mixture of monomeric/dimeric pyDau and cannot be considered as absolute value of the monomeric form. However, a direct comparison with the pure dimeric form supports the conclusion that the dimeric form is less active than the monomeric pyDau, but still provides an adequate potency with IC_{50} values in the low nanomolar range. In comparison to the free pyDau, the somatostatin-pyDau conjugate (**71**) was much more resistant to dimer formation and no dimerization could be detected after oxime bond ligation to the targeting moiety which is in accordance with former findings [420]. Apart from that, the growth inhibitory effect of the pyDau-containing compound **71** was on both cell lines more than 20-times higher than that of the Dau-containing counterpart. Moreover, compound **71** exhibits like the other RC-121 derived conjugates (**66**, **69**, **70**) a similar IC_{50} on both cell lines, indicating that the used HT-29 and MDA-MB-231 cells might express a comparable level of SSTR2 and/or SSTR5.

Table 14: *In vitro* cytostatic effect of somatostatin drug conjugates on HT-29 human colon cancer and MDA-MB-231 human breast cancer cells

Code	Sequence	IC_{50} [µM] HT-29	IC_{50} [µM] MDA-MB-231
Dau		0.07 ± 0.001	0.35 ± 0.02
66	**Dau=Aoa**-LRRY-f[CYwK**V**C]T-NH_2	5.43 ± 0.69	9.52 ± 2.17
67	**Dau=Aoa**-LRRY-f[CYwKC]T-NH_2	65.44 ± 9.38	16.55 ± 1.07
68	**Dau=Aoa**-LRRY-f[CYwK-Dab-($COCH_2$)]T-NH_2	32.33 ± 1.59	30.58 ± 1.35
69	**Dau=Aoa**-LRRYC-NH_2 └CH_2-CO-f[CYwKVC]T-NH_2	24.24 ± 1.14	25.74 ± 3.62
70	(CH_2)$_3$-CO-f[CYwK**V**C]T-NH_2 └CO-(Val-Ala-**PABC-Dau**)	10.95 ± 0.91	12.89 ± 1.32
pyDau		$1.17 \cdot 10^{-3} \pm 0.02 \cdot 10^{-3}$	$1.99 \cdot 10^{-3} \pm 0.04 \cdot 10^{-3}$
$(pyDau)_2$		$4.16 \cdot 10^{-3} \pm 0.09 \cdot 10^{-3}$	$6.33 \cdot 10^{-3} \pm 0.44 \cdot 10^{-3}$
71	**pyDau=Aoa**-LRRY-f[CYwK**V**C]T-NH_2	0.26 ± 0.07	0.28 ± 0.05

all values represent mean ± SE

4. Conclusion and outlook

4.1 GnRH-III-drug conjugates

Oxime bond-linked GnRH-III-Dau conjugates

The results of the 1st set of GnRH-III-Dau conjugates provide a deeper insight into the mechanism of action of the conjugates, and demonstrate that the anticancer activity of drug conjugates is influenced by different factors, whereby not only the stability under physiological conditions, but also the cellular uptake and the release of the drug or active drug-metabolites are of high relevance. All investigated GnRH-III-Dau derivatives display an adequate cytostatic effect on GnRH-R positive HT-29 and MCF-7 cancer cells with IC_{50} values in the low micro-molar range. The well-established lead compound **K2** was determined as most potent candidate of this study revealing the best anticancer-activity and cellular uptake rate on MCF-7 and HT-29 cancer cells in combination with an efficient release of the active drug-metabolite in presence of lysosomal enzymes. In comparison, the six novel GnRH-III-Dau-[^{6}D-Aaa] derivatives exhibit a 3-5 times reduced cytostatic effect depending on different factors which interfere with each other. The main reason for the decline of the biological activity might be the enhanced durability of the compounds within the cancer cell and the corresponding diminished release of the smallest Dau-containing metabolite. This becomes particularly obvious in case of the ^{6}D-Asp bioconjugates **1** and **4**. Both compounds possess slightly enhanced receptor binding affinities and better cellular uptake profiles than the D-Glu derivatives **2** and **5**, while their anticancer activities differ not substantially from each other. Therefore, it can be assumed that the observed larger drug metabolites possess a lower DNA binding affinity than the smallest active metabolite H-Lys(Dau=Aoa)-OH which results in an inferior DNA intercalation, and hence, affects the cell growth inhibitory effect of the compounds. Furthermore, the modification of GnRH-III derivatives by ^{6}D-Aaa incorporation did not cause an improved cellular uptake or receptor binding, while in case of GnRH-I derivatives, a substitution of ^{6}Gly by D-amino acids results in an increased biological activity and receptor affinity, by stabilizing the β-turn conformation of the compounds [100]. Therefore, it can be assumed that the activity of GnRH-I and GnRH-III is not mediated by the same conformational features. This assumption is in line with previous structure related activity studies which indicate that the structure of GnRH-III is more flexible and reveals a relatively ordered extended backbone conformation instead of a GnRH-I-like U-shape [142,143]. Nonetheless, the present results provide clear evidence for a GnRH-R-mediated endocytic pathway of lead compound **K2** which is also

representative for other related GnRH-III-Dau conjugates. In conclusion, it could be confirmed that the GnRH-III-Dau analogs specifically bind the GnRH-receptor on cancer cells which leads to their internalization and a subsequent delivery to lysosomes. After the release of the active Dau-containing metabolites by lysosomal enzymes, the cytotoxic agent gets to its site of action and accumulates in the cell nuclei.

Considering that the sequence modifications of the 1st set of GnRH-III-Dau conjugates did not result in an improved anticancer activity, a 2nd set of GnRH-III conjugates has been designed and synthesized in which the targeting peptide sequence was modified by various amino acid substitutions. Initially, the anticancer activity of the compounds was studied revealing that all 14 novel GnRH-III-Dau conjugates exhibit an adequate *in vitro* cytostatic effect on MCF-7 human breast cancer and HT-29 colon cancer cells. Especially the *N*-terminal modification Glp-D-Tic-Lys(Bu), resulting in compound **16**, leads to an increased inhibition of the cancer cell growth, whereby the inhibitory effect on MCF-7 cancer cells could be enhanced by more than one order of magnitude in comparison to the lead compound **K2**. Due to these promising results, a detailed biochemical characterization of compound **16** was carried out in comparison to **K2** indicating that the *N*-terminal modification leads to improved cellular uptake and an accelerated delivery of the drug to its site of action. Based on the fact that the binding affinity of compound **16** to GnRH-Rs is comparable to **K2** or other high affinity GnRH-R ligands, such as cetrorelix and buserelin, it can be assumed that the receptor-mediated endocytic uptake is not disrupted by the sequence modification. Besides that, lysosomal degradation studies pointed out that the release of the active drug metabolite is not affected, while the compound possesses a high durability in human and mouse plasma which is of high relevance for preclinical studies in tumor-bearing mice. Considering all these findings, the GnRH-III-Dau derivative **16** represents a highly promising candidate for *in vivo* tumor growth inhibition studies. Due to the fact that the tumor growth of MCF-7 breast cancer xenograft model strongly depends on exogenous E2 support [297,416], **16** was also analyzed for its growth inhibitory effect on E2-idependent MDA-MB-231. The new analog showed here, as well an improved growth inhibitory effect which confirms the suitability of MDA-MB-231 breast cancer cells as xenograft model for upcoming *in vivo* studies. Moreover, using MDA-MB-231 for *in vivo* studies would provide valuable information about the potential of our lead compounds on triple negative, but GnRH-R positive breast cancer types. In conclusion, all findings of the present study demonstrate the high

potential of GnRH-Dau-[^{2}ΔHis,^{3}D-Tic,^{4}Lys(Bu),^{8}Lys(Dau=Aoa)] (**16**) as efficient drug delivery system for targeted tumor therapy.

Self-immolative and non-cleavable linker-containing GnRH-III-Dau and -PTX conjugates

Next to the oxime bond-linked GnRH-III-Dau conjugates, novel self-immolative and non-cleavable linker-containing GnRH-III-Dau and PTX conjugates were synthesized and analyzed. For the Dau-conjugates, the amino group of the daunosamine sugar has been used for attachment to the linker, while in case of PTX, the C2'-OH group was used. The cleavable, self-immolative compounds inhibited the cell proliferation of GnRH-R expressing cancer cells in a dose-dependent manner, while the activity of the compounds was clearly reduced on cancer cells which possess a lower GnRH-R expression level. The corresponding IC_{50} values of the Dau-conjugates emphasize that the novel targeting moiety GnRH-III-[^{2}ΔHis-^{3}D-Tic-^{4}Lys(Bu)] has a beneficial impact on the antitumor activity. Moreover, the antiproliferative activity of the non-cleavable control conjugates was strongly decreased which demonstrates the high value of the cathepsin labile linker systems. Apart from that, the present results point out that the applied linker structure was efficiently cleaved by lysosomal enzymes, but the antitumor activity of the conjugates was negatively influenced by other factors. In case of the PTX conjugates, the high stability of the diamine-PTX prodrug might prevent the release of the free drug and affect the activity of the compounds. On the contrary, the release of the free Dau occurs efficiently applying the cathepsin labile and self-immolative linker, but the receptor affinity was dropped down substantially. Nonetheless, the received data demonstrate the high value of GnRH-III-based targeting moieties and the promising characteristic of lysosomal cleavable linker systems, although further optimizations are required.

In direct comparison, the oxime bond-containing lead compound **16** offers various benefits, like a straightforward synthesis, an enhanced cytostatic effect and an improved solubility in aqueous solution. Due to these results, *in vivo* antitumor activity studies of compound **16** and **K2** on tumor bearing mice are ongoing in collaboration with the research group of Dr. József Tóvári (National Institute of Oncology, Budapest). The first preliminary results indicate that single, as well as multiple doses of both compounds are well tolerated by healthy mice, while especially compound **16**, but also **K2**, exhibit significant tumor growth inhibitory effects on orthotopically developed colorectal carcinoma bearing mice, without detectable side effects. Furthermore, initial studies on

breast cancer bearing mice gave clear hints that the antimetastatic activity of conjugates is significantly higher than the activity of free Dau.

4.2. Somatostatin-drug conjugates

Initially, the cellular uptake of fluorescently labeled somatostatin derivatives has been examined. Flow cytometry studies pointed out that all designed FAM-somatostatins were taken up by SSTR expressing MCF-7 and HT-29 human cancer cells, whereby the LRRY-linker-containing conjugates (**63**, **64**) were taken up more efficiently than the compounds without linker (**61**, **62**, **65**). Moreover, the uptake of the RC-121 derived conjugates was enhanced in comparison to the appropriate TT-232 related compound which might be related to a lower SSTR4 receptor level in comparison to the expression of SSTR2 and/or SSTR5. The new somatostatin analog with the thioether bridged cyclic structure was taken up less efficiently, but still revealed an adequate uptake rate on MCF-7 and HT-29 cells. This uptake rate might be enhanced by incorporation of the hydrophilic, cleavable LRRY peptide spacer between the targeting peptide and the cargo. In addition, the results of the CLSM studies indicate that the insertion of the lysosomal cleavable linker ensures the release of the fluorophore-containing small metabolites, and facilitates the escape of these metabolites from the lysosome. Thus, both LRRY-linker-containing somatostatin analogs exposed a strong cytosolic fluorescence signal, while the compounds without linker were predominantly present in cytosolic vesicles. In conclusion, the present study of the FAM-somatostatin conjugates supports and underlines the requirement of a cleavable linker system in case of somatostatin-drug derivatives, since the *N*-terminal D-Phe, which is mainly used as ligation site, might prevent the formation of active drug-metabolites. Apart form that, it could be shown that next to the classical disulfide cycled derivatives, also a thioether cycled somatostatin analog was taken up by SSTR expressing cancer cells which extends the possibilities for the development of somatostatin-based DDSs.

Based on the results of the FAM-labeled somatostatin derivatives, various cleavable linker-containing somatostatin derivatives have been synthesized and analyzed, whereby three different targeting moieties have been used. All evaluated conjugates exhibit an inhibitory effect on the growth of HT-29 colon cancer and MDA-MB-231 breast cancer cells. In accordance with the cellular uptake studies of the FAM-somatostatin analogs, the conjugates with the RC-121 derived peptide moiety displayed a higher anticancer activity than the other conjugates, whereby the oxime bond-linked somatostatin conjugate

66 possesses the highest biological activity of all Dau-conjugates. Moreover, the cytostatic effect of the RC-121 conjugates on HT-29 was comparable to their activity on MDA-MB-231 cells. Due to this, it can be assumed that both cell lines possess a comparable surface expression level of SST2 and/or SST5. In contrast, the cytostatic effect of conjugate **67** which possesses the TT-232 targeting moiety was improved on MDA-MB-231 cells, in comparison to the activity on HT-29 cells. Thus, it can be assumed that the expression level of SST4 and/or SST1 is substantially higher on MDA-MB-231 than on HT-29. However, to gain further information on the exact expression level of the SSTRs and their coincidence on HT-29 and MDA-MB-231 cells, additional studies are necessary. Apart from that, it could be shown that the applied drug-linker system, as well as the linkage itself has an impact on the biological activity of the compounds. This might be related to a decreased SSTR affinity or a reduced cellular uptake of the compounds. Thus, receptor binding studies and further cellular uptake studies might be favorable for a better interpretation of the results. Next to Dau, also 2-pyrrolino-Dau has been conjugated to the best linker-targeting peptide moiety. The obtained IC_{50} value of pyDau conjugate **71** was for both cancer cell lines in the low nanomolar range which evidences the high potency of this Dau derivative. Although the synthesis of the pyDau conjugates is more challenging than the preparation of comparable Dau conjugates, the strong anticancer activity of pyDau-containing somatostatin conjugate (**71**) illustrates the high potential of pyDau-based DDS for targeted cancer therapy.

In summary, it could be shown that GnRH-III, as well as somatostatin analogs are promising targeting moieties for selective cancer therapy. The present results confirm that not only the conjugated drug and the targeting peptide, but also the linker system has a substantial impact on the anticancer activity. In order to further optimize the biological activity of these small molecule drug conjugates, new linker strategies should be investigated which ensure the release of the free drug without affecting the receptor binding affinity. Additionally, the use of anticancer drugs with higher potency than Dau and PXT (e.g. amatoxins or cryptophycins) might enlarge the potential of peptide hormone-based DDS.

5. Experimental section

5.1. Materials and reagents

The following commercially available reagents and solvents were used for the present study, whereby all reagents and solvents were of analytical grade or highest available purity.

5.1.1. Reagents for synthesis and purification

All amino acid derivatives, K-Oxyma Pure®, Rink-Amide MBHA and Ethyl indol AM resin were obtained from Iris Biotech GmBH (Marktredwitz, Germany), Novabiochem®/Merck-Millipore (Darmstadt, Germany) and Bachem (Bubendorf, Switzerland). Boc-aminooxyacetic acid (Boc-Aoa-OH), aminooxyacetic acid, scavengers, coupling agents (1-hydroxybenzotriazole hydrate (HOBt), *N,N'*-diisopropylcarbodiimide (DIC)), and cleavage reagents (triisopropylsilane (TIS), 1,2-ethanedithiole (EDT), thioanisole, phenol, piperidine, 1,8-diazabicyclo[5.4.0]undec-7-ene (DBU), trifluoroacetic acid (TFA)), diisopropylethylamine (DIPEA), methanol (MeOH), *tert*-butanol, *n*-butyric anhydride, hydrochloric acid (HCl) and solvent for RP-HPLC acetonitrile (MeCN) were purchased from Sigma-Aldrich Kft (Budapest, Hungary). Daunorubicin hydrochloride was provided from IVAX (Budapest, Hungary). *N*,*N*-dimethylformamide (DMF), dichloromethane (DCM) and diethyl ether (Et_2O) were purchased from Molar Chemicals Kft (Budapest, Hungary).

5.1.2. Reagents for cell culturing and cell biology experiments

DMEM, HPMI, RPMI-1640, Fetal Bovine Serum (FBS), L-glutamine, Penicillin-Streptomycin (Pen-Strep), sodium pyruvate, PBS, trypsin and EDTA solutions were purchased from Lonza (Basel, Switzerland). Non-essential amino acids (NEAA), Mowiol® 4–88 mounting medium, diamidine-2-phenylindole dihydrochloride (DAPI), paraformaldehyde and Tox-8 (resazurin-based *in vitro* toxicology assay kit) were obtained from Sigma-Aldrich Kft. MCF-7 human breast adenocarcinoma cells (ATCC: HTB-22), HT-29 human colon adenocarcinoma cells (ATCC: HTB-38), MDA-MB-231 (ATCC: HTB-26) breast adenocarcinoma cells were obtained from ATCC (Manassas, USA). 6-, 24- and 96-well plates were obtained from Sarstedt, (Nürnbrecht, Germany). Glycine, Tris, SDS, NaCl, EDTA, Tween-20, AcOH, MeOH and EtOH absolute (99.7%) HiPerSolv CHROMANORM, ammonium-sulphate-14-18-hydrate and ortho phosphoric acid were obtained from VWR Prolabo® chemicals (Leuven, Belgium). Tricine, bromophenol blue, Coomassie Brilliant Blue were purchased from amresco® (Solon,

Ohio, USA). Acrylamide (2x) and *N*,*N*'-methylene bisacrylamide (2x) were received from SERVA Electrophoresis GmbH (Heidelberg, Germany). Glycerol anhydrous BioChemica, Triton® X-100 Molecular Biology grade BC, TCEP hydrochloride BioChemia BC and nonfat dried milk powder were obtained from AppliChem Panreac (Darmstadt, Germany). APS and β-mercaptoethanol were purchased from G-Biosciences® (St. Louis, MO, USA). Apart from that, alamarBlue reagent® (Thermo Scientific, Waltham, MA, USA), MTT reagent (Duchefa Biochemie, Harlem, Netherland), TEMED (TCI chemicals, Tokyo, Japan), protease inhibitor cocktail set III (Merck Calbiochem®), PVDF membrane Immobilon®-P 0.45 µm (Merck Millipore), Extra Thick Western Blotting Filter Paper (Thermo Scientific), PageRuler^{TM} prestained Protein Ladder (product number $^{\#}$26616, Thermo Scientific), cover glasses (thickness 1, Assistant, Karl Hecht GmbH & Co KG, Sondheim/Rhön, Germany), microscopy slides (VWR International, Debrecen, Hungary), anti-GnRH-R antibody (Proteintech, Rosemant, IL, USA, catalog number: 19950-1AP, produced in rabbit), secondary anti-rabbit-horseradish peroxidase (HRP) antibody (Santa Cruz Biotechnology, Dallas, TX, USA, sc-2004, produced in goat), anti-actin primary antibody (Santa Cruz Biotechnology, sc-1616, produced in goat) and anti-goat-HRP secondary antibody (Santa Cruz Biotechnology, sc-2354, produced in mouse) were used for the appropriate experiments.

5.1.3. Reagents for *in vitro* stability and degradation of drug-conjugates

The rat liver lysosomal homogenate was prepared as previously described [257] and protein concentration was determined with Qubit Protein Assay Kit (Thermo Scientific). Human and mice plasma was collected, isolated and provided from the research group of Dr. József Tóváry at National Institute of Oncology in Budapest (OOI). Water for chromatography (LC-MS Grade) LiChrosolv®, MeCN hypergrade for LC-MS LiChrosolv®, formic and acetic acid 98% - 100% for LC-MS LiChropur®, NH_4OAc and NaOAc were obtained form Merck Millipore.

5.2. Methods

5.2.1. Synthesis and purification

5.2.1.1. General synthesis protocols

Solid-phase peptide synthesis (SPPS)

Peptides were prepared manually by SPPS according to Fmoc/tBu chemistry on a Rink-Amide MBHA resin (0.73 mmol/g coupling capacity) or on a Fmoc-Ethyl-Indole AM resin (0.94 mmol/g coupling capacity). The derivatives were synthesized by the following

protocol. The resin was washed with DMF (4 times 1 min), followed by Fmoc deprotection with 2% piperidine, 2% DBU in DMF (4 times; 2 + 2 + 5 + 10 min). For the coupling reaction, 3 eq of α-Fmoc-protected amino acid derivative, 3 eq DIC and 3 eq HOBt in DMF were used (60 min).

Dde cleavage and butyrylation of ^{4}Lys (GnRH-conjugates)

After peptide chain elongation, the Dde group of Lys was cleaved with 2% hydrazine in DMF (12 x 5 min) and the resin-bound peptide was washed with DMF (5 x 1 min). In the next step, the butyrylation of the α-NH_2 amino group was performed with 3 eq butyric anhydride and 3 eq DIPEA in DMF (2 h).

Mtt cleavage

The Mtt group of ^{8}Lys was removed by using 2% TFA in DCM (6 x 5 min). The peptidyl resin was neutralized with 10% DIPEA in DCM (3 x 5 min).

Coupling of isopropylidene-aminooxyacetic acid (>=Aoa-OH)

The coupling reaction was carried out with 5 eq >=Aoa-OH, 5 eq K-Oxyma Pure® and 5 eq HOBt in DMF for 2 hours.

Deprotection of the side chain protecting groups and simultaneous cleavage of the peptide from the resin – GnRH-III peptide carriers (DP1)

The GnRH-III peptidyl-resin was dried in desiccator for at least 3 hours or washed with Et_2O (3 x 2 min) and then treated with 95% TFA, 2.5% TIS and 2.5% water (v/v/v) in the presence of 10 eq free aminooxyacetic acid as 'carbonyl capture' reagent for 2 h, at RT [268]. Peptides were precipitated with ice-cold Et_2O, centrifuged, washed 3 times with fresh Et_2O, dissolved in water-MeCN (0.1% TFA) 4:1 (v/v) and lyophilized.

Deprotection of the side chain protecting groups and simultaneous cleavage of the peptide from the resin – Somatostatin peptide carriers (DP2)

The somatostatin peptidyl-resin was dried in desiccator for at least 3 hours or washed with Et_2O (3 x 2 min) and then treated with 93% TFA, 2.5% water, 2.5% thioanisole, 1.25% EDT and 0.75% phenol (v/v/v/v/w) for 3 h, at RT. Peptides were precipitated with ice-cold Et_2O, centrifuged, washed 3 times with fresh Et_2O, dissolved in water:*tert*-butanol (0.1% TFA) 1:4 (v/v) and lyophilized.

Disulfide formation by air oxidation

After purification of the crude somatostatin derivatives by RP-HPLC and lyophilization, 0.2 mg/mL peptides were dissolved in 5% DMSO and 95% 0.1 M Tris-buffer (pH 8.3) and stirred for 1-4 days at RT. Reaction process was controlled by analytical RP-HPLC

and ESI-MS. When the reaction was completed, the pH of reaction mixture was adjusted to pH 5 with 6 M HCl, followed by freeze-drying and purification by preparative RP-HPLC.

Isopropylidene deprotection

To remove the isopropylidene protecting group of the >=Aoa-moiety, the compound was dissolved in 0.2 M NH_4OAc solution (pH 5), containing 1 M of methoxylamine to a concentration of 5 mg/mL. The reaction was stirred at RT for one-two hour. Reaction process was controlled by analytical RP-HPLC. When the reaction was completed, the reaction mixture was purified by RP-HPLC. Product-containing fractions were evaporated and used for Dau ligation.

Ligation of daunorubicin – oxime bond formation

The oxime bond formation was carried out in 0.2 M ammonium acetate buffer (pH 5.0), at a peptide concentration of 10 mg/mL and 1.3 eq Dau [256]. The reaction mixtures were stirred overnight at RT and then purified by RP-HPLC.

Coupling of pentachlorophenyl-chloroacetat (Cl-CH_2-CO-OPcp)

For the on-resin coupling, 5 eq of Cl-CH_2-CO-OPcp were dissolved in DMF (3 mL) and 5 eq DIPEA were added. After 2 h, the resin was washed with DMF (4 times 1 min) and prepared for TFA cleavage.

Fmoc-deprotection in solution

The compound of interest was dissolved in 2 mL DMF and 5 eq piperidine was added. Solution was stirred for 2 h at RT. DMF was evaporated under high vacuum. Remains were triturated with Et_2O and the precipitate was isolated by centrifugation.

Boc-deprotection in solution

The compound of interest was dissolved in 1.5 mL DCM/TFA (2:1, v/v) and stirred for 45 min, followed by evaporation and purification by preparative RP-HPLC.

5.2.1.2. Purification

Semipreparative and preparative RP-HPLC

System I

For purification, a KNAUER 2501 HPLC system (H. Knauer, Bad Homburg, Germany) was used either with a preparative Phenomenex (Torrance, CA, USA) Luna® C18(2) column (100 Å, 10 µm, 250 mm x 21.2 mm) (**a**), or with a semipreparative column: Phenomenex Jupiter® C4 column (300 Å, 10 µm, 250 mm x 10 mm) (**b**), or Phenomenex

Proteo® C18 column (90 Å, 10 µm, 250 mm x 10 mm) (**c**). Linear gradient elution with eluent A (0.1% TFA in water) and eluent B (0.1% TFA in MeCN/H_2O (80:20, v/v)) was used at a flow rate of 15 mL/min for preparative and 4 mL for semipreparative RP-HPLC. Peaks were detected at 220 or 280 nm.

System II

For purification, the Thermo Fisher Scientific HPLC system Dionex Ultimate 3000 was used, equipped with Dionex RS variable wavelength Detector and a semipreparative RP-HPLC Waters Atlantis column (100 Å, 5 µm, 100 mm x 19 mm). Linear gradient elution with eluent A (0.1% TFA in water) and eluent B (0.1% TFA in MeCN) was used at a flow rate of 10 mL/min. Peaks were detected at 220 and 280 nm.

Flash-chromatography

For flash-chromatography, Chromagel 60 ACC (40-63 µm) silica gel and a column with 20 mm diameter was used and filled up to 200 mm column height.

5.2.1.3. Synthesis of GnRH-III-drug conjugates

5.2.1.3.1. Synthesis of oxime bond-linked daunorubicin–GnRH-III conjugates

Synthesis of 1st set of GnRH-III-Dau-conjugates – modification in position 6

The synthesis of GnRH-III–[(^{4}Lys(Bu)/^{4}Ser, ^{6}Aaa, ^{8}Lys(Dau=Aoa)] (**K1**, **K2**, **1-6**) conjugates was carried out on a Fmoc-Rink-Amid-MBHA resin (200 mg per conjugate) using protected amino acid derivatives and orthogonal lysine protecting groups. Fmoc-Lys(Mtt)-OH was incorporated in position 8 and either Fmoc-Ser(tBu)-OH (**K1**, **1-3**) or Fmoc-Lys(Dde)-OH (**K2**, **4-6**) was incorporated in position 4. Initially after peptide chain elongation, the Dde group was removed first and ^{4}Lys was butyrylated. In the following, the Mtt group was cleaved and Boc-Aoa-OH was coupled. After cleavage from resin (DP1), the crude compounds were purified by preparative RP-HPLC (system Ia: 0 min 5% B; 5 min 5% B; 10 min 20% B, 50 min 80% B). Product-containing fractions were combined and eluent was evaporated. The remaining colorless oil was directly used for Dau ligation and purified by preparative RP-HPLC (system I-a: 0 min 15% B; 5 min 15% B; 10 min 30% B, 50 min 80% B).

Synthesis of 2nd set of GnRH-III-Dau-conjugates – advanced sequence modification

*Synthesis of GnRH-III-Dau conjugates **7-12** and **14-18***

SPPS of GnRH-III compounds were carried out on a Fmoc-Rink-Amid-MBHA resin (200 mg per conjugate) using appropriate protected amino acid derivatives and orthogonal lysine protecting groups for position 4 and 8. The synthesis and purification of the

compounds was performed in the same manner as described for the 1st set of GnRH-III-Dau-conjugates (see above), whereby coupling time of Fmoc-D-Tic-OH was extended up to two hours and compound **16** was additionally purified by semipreparative RP-HPLC (system I-b: 0 min 20% B; 5 min 20% B, 50 min 50% B)

*Synthesis of GnRH-III-Dau conjugates **13** and **20***

The synthesis of **13** and **20** were performed on Fmoc-Ethyl-Indole AM resin (200 mg per compound). The first amino acid was allowed to react for two hours. Further synthesis steps were carried out as described for conjugates **7**-**12** and **14**-**18**.

*Synthesis of GnRH-III-Dau conjugate **19***

The following modified synthetic route was used to avoid the side reaction on methyl ester which occurred during the Dde deprotection with 2% hydrazine solution. Bioconjugate **19** was prepared by manual SPPS according to Fmoc/tBu chemistry on a Rink-Amide MBHA resin (300 mg). Fmoc-Lys(Mtt)-OH was incorporated in position 8 and on-resin synthesis was continued. After coupling of Fmoc-His(Trt)-OH in position 5, the Mtt group was removed and >=Aoa-OH was coupled to the side chain of ^{8}Lys using two times 10 eq K-Oxima pure®, 10 eq DIC and 10 eq HOBt in DMF (RT, 2 h). The coupling reaction was repeated twice, followed by blockage of the remaining unreacted ε-NH_2 with 5% acetic anhydride and 10% DIPEA in DMF (v/v/v) for 30 min. Then main chain synthesis was carried out till the end by using Fmoc-Lys(Mtt)-OH also in position 4. Afterwards, the Mtt group was deprotected after and ^{4}Lys was butyrylated followed by TFA-cleavage (DP1). The crude compound was purified by preparative RP-HPLC (0 min 5% B; 5 min 5% B; 10 min 20% B, 50 min 80% B) and lyophilized. In the next step, the >=Aoa moiety was deprotected and subsequently separated by RP-HPLC (see above). Appropriate fractions were evaporated and directly used for Dau ligation. The reaction mixture was purified by RP-HPLC (system I-a: 0 min 15% B; 5 min 15% B; 10 min 35% B, 50 min 70% B).

5.2.1.3.2. Synthesis of self-immolative linker-containing GnRH-III-Dau and -PTX conjugates

Synthesis of self-immolative linker

Fmoc-Val-OSu (**21**)

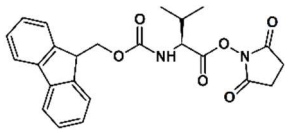

MW: 436.46 Da
m = 5.219 g (93%)

Fmoc-Val-OH (4 g, 12.85 mmol, 1 eq) and HOSu (1.48 g, 12.85 mmol, 1 eq) were dissolved in dry THF (35 mL) under nitrogen atmosphere at 15 °C. DCC (2.65 g, 12.85 mmol, 1 eq) was dissolved in dry THF (7 mL), added dropwise within 30 min and stirred at RT for further 24 hours. The reaction mixture was separated by suction filtration and the filtrate was evaporated. To remove further impurities, the product was resolved in 50 mL DCM and extracted with 50 mL saturated $NaHCO_3$ and 50 mL brine. The organic layer was dried with Na_2SO_4. The filtrate was evaporated affording Fmoc-Val-OSu as a white foam.

^{1}H NMR (400 MHz, $CDCl_3$/CD_3OD): δ = 7.80 (d, *J* = 7.48 Hz, 2H), 7.63 (d, *J* = 7.19 Hz, 2H), 7.45 (t, *J* = 7.37 Hz, 2H), 7.36 (t, *J* = 7.53 HZ, 2H), 4.73 (m, 1H), 4.48 (d, *J* = 6.66 HZ, 2H), 4.29 (t, *J* = 7.03 Hz, 1H), 2.87 (s, 4H), 2.41 (m, 1H), 1.11 (m, 6H).

Fmoc-Val-Cit-OH (**22**)

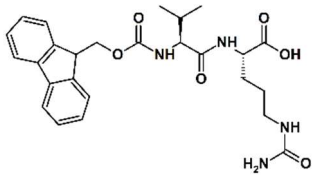

MW: 496.56 Da
m = 2.244 g (77%)

L-citrulline (1.082 g, 6.175 mmol, 1.05 eq) and $NaHCO_3$ (0.519 g, 6.175, 1.05 eq) were dissolved in 15 mL water. **21** (2.567 g, 5.88 mmol, 1 eq) was dissolved in 15 mL DME and added to the aqueous solution. THF (10 mL) was added and the reaction was stirred overnight. 50 mL of 15% citric acid was added and extracted with 10% isopropanol/ EtOAc (v/v) (3 x 50 mL). Combined organic layer was washed with water (3 x 30 mL) and brine (2 x 50 mL) and dried with Na_2SO_4. The filtrate was evaporated and the remaining solid was triturated in 60 mL Et_2O and sonicated for 45 min. Filtration yielded Fmoc-Val-Cit-OH (**22**) as white solid.

^{1}H NMR (400 MHz, CD_3OD): δ = 7.82 (d, *J* = 7.58 Hz, 2H), 7.69 (d, *J* = 6.98 Hz, 2H), 7.43 (t, *J* = 7.48 Hz, 2H), 7.38 (t, *J* = 7.38 Hz, 2H), 7.19 (d, J = 8.4, 1H), 4.48-4.31 (m, 3H), 4.25 (t, *J* = 6.9 Hz, 1H), 3.96 (t, *J* = 7.80, 1H), 3.12 (t, *J* = 6.72 Hz, 2H), 2.07 (m, 1H), 1.93 (m, 1H), 1.72 (m, 1H), 1.63-1.50 (m, 2H), 1.00 (m, 6H).

Fmoc-Val-Cit-PAB-OH (**23**)

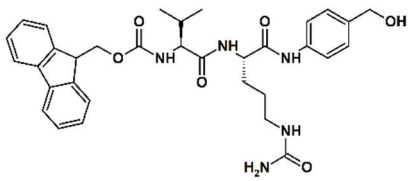

MW: 601.69 Da
m = 1.0181 g (84%)

Compound **22** (1 g, 2.015 mmol, 1 eq) and PAB-OH (0.5 g, 4.03 mmol, 2 eq) were dissolved in 30 mL DCM:MeOH (2:1, v/v). EEDQ was added and the reaction was stirred

in the dark under N_2 atmosphere (overnight at RT). The solvent was removed by evaporation and the remaining solid was triturated in 40 mL Et_2O and sonicated for 45 min. Filtration yielded Fmoc-Val-Cit-PAB-OH (**23**) as yellow solid.

^{1}H NMR (400 MHz, DMSO-d_6): δ = 9.97 (s, 1H), 8.10 (d, *J* = 7.64 HZ, 1H), 7.90 (d, J = 7.49 Hz, 2H), 7.75 (t, J = 7.8 Hz, 2H), 7.56 (d, *J* = 8.35 Hz, 2H), 7.42 (m, 2H), 7.33 (t, *J* = 7.42 Hz, 2H), 7.24 (d, *J* = 8.4 Hz, 2H), 5.97 (t, *J* = 5.86 Hz, 1H), 5.40 (s, 2H), 5.09 (t, *J* = 5.75, 1H), 4.46-4.39 (m, 3H), 4.36-4.19 (m, 3H), 3.94 (dd, *J* = 7.13, 6.91 Hz, 1H), 3.07-2.87 (m, 2H), 1.99 (m 1H), 1.69 (m, 1H), 1.59 (m, 1H), 1.50-1.32 (m, 2H); 0.87 (m, 6H).

Fmoc-Val-Cit-PABC-Pnp (**24**)

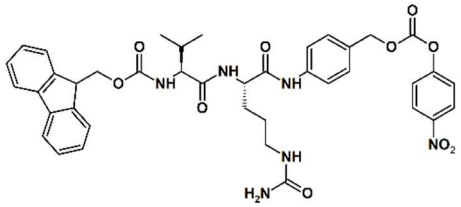

MW: 766.80 Da
m = 0.490 g (78%)

Compound **23** (490 mg, 0.814 mmol, 1eq) was dissolved in 5 mL DMF under N_2 atmosphere and bis-Pnp carbonate (496 mg, 1.63 mmol, 2 eq) was added, followed by addition of DIPEA (215 µL, 1.23 mmol, 1.5 eq). Reaction mixture was stirred for 3 hours at RT. DMF was removed by high vacuum evaporation. Remaining solid was triturated with 15 mL Et_2O and sonicated for 40 min. Filtration afforded Fmoc-Val-Cit-PAB-Pnp (**24**) as yellow solid.

^{1}H NMR (400 MHz, DMSO-d_6): δ = 10.14 (s, 1H), 8.32 (d, *J* = 9.2 Hz, 2H), 8.15 (d, *J* = 7.56 Hz, 1H), 7.90 (d, *J* = 7.49 Hz, 2H), 7.75 (t, *J* = 7.66 Hz, 2H), 7.65 (d, *J* = 8.43 Hz, 2H), 7.58 (d, J = 9.18 Hz, 2H), 7.42 (m, 2H), 7.33 (t, *J* = 7.56 2 H), 5.98 (t, *J* = 5.72 Hz, 1H), 5.42 (s, 2H), 5.25 (s, 2H),4.43 (m, 1H),4.33-4.17 (m, 3H), 3.94 (dd, 7.02, 7.10) 1H), 3.09-2.87 (m, 2H), 2.00 (m, 1H), 1.70 (m, 1H), 1.61 (m, 1H), 1.51 (m, 2H), 0.87 (m, 6H).

Fmoc-Val-Cit-PABC-Dau (**25**)

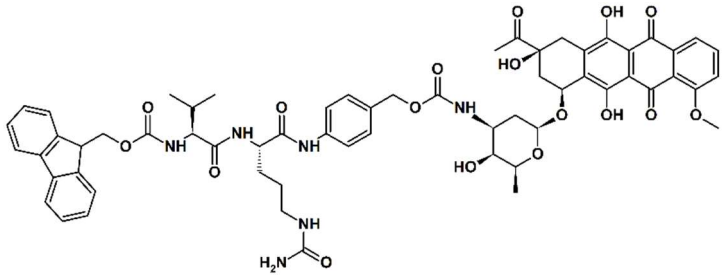

MW: 1155.21 Da
m = 35 mg (47%)

Dau (38 mg, 0.072 mmol, 1.1 eq) was dissolved in 1.5 mL dry DMF. Compound **24** (50 mg, 0.0652 mmol, 1 eq) was added, followed by addition of DIPEA (17.1 µL, 0.0978

mmol, 1.5 eq). Reaction was stirred overnight at RT under N_2 atmosphere. Then 70 mL EtOAc was added and organic phase was extracted with 1 M $KHSO_4$ (2 x 10 mL), sat. $NaHCO_3$ (2 x 10 mL) and 10 mL brine. The organic layer was dried with Na_2SO_4 and concentrated. The red solid was dissolved in DCM:MeOH (9:1, v/v), filtrated and purified by flash-chromatography (eluents: initially 6:3:1, then 7:2:1 EtOAc/hexane/MeOH, followed by 9:1 DCM/MeOH). Combined product-containing fractions were evaporated affording Fmoc-Val-Cit-PABC-Dau (**25**) as a red solid.

ESI-MS: MW_{cal}: 1155.21, found $[M+H]^+$ = 1155.63, $[M+Na]^+$= 1177.53, $[M-H]^-$ = 1153.31

Glutaryl-Val-Cit-PABC-Dau (**27**)

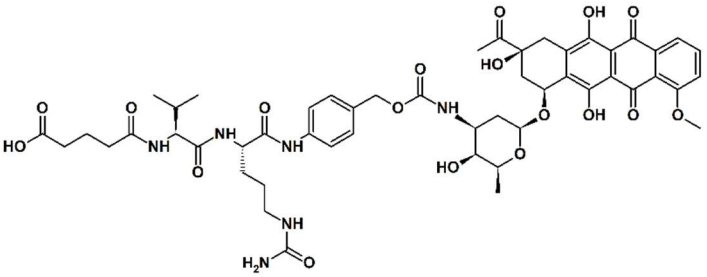

MW: 1047.07 Da
m = 10.3 mg (38%)

Fmoc-group of compound **25** (35 mg, 0.0303 mmol) was removed as described above and H-Val-Cit-PABC-Dau (**26**) was resolved in dry DMF (2 mL). Glutaric anhydride (6.91 mg, 0.0606 mmol, 2 eq) was dissolved in dry DMF (106 µL) and added, followed by addition of DIPEA (10.6 µL, 0.0606 mmol, 2 eq). The reaction was stirred at RT for 2 hours, then DMF was evaporated under high vacuum and remaining red solid was dissolved in MeCN/water and purified by semipreparative RP-HPLC (system II, gradient 10% B to 90% B in 12 min). Product **27**-containing fractions were combined and freeze-dried.

ESI-MS: MW_{cal}: 1047.07, found $[M+Na]^+$= 1069.50, $[M-H]^-$ = 1045.72

N-(Boc)-N,N'-dimethylethylenediamine (**28**)

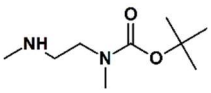

MW: 188.27 Da

N,N'-dimethylethylenediamine (1.5 g ≙ 1.86 mL (ρ = 0.807 g/mL), 17.02 mmol, 3 eq) was dissolved under N_2 atmosphere in dry DCM (20 mL) and cooled to 0 °C. Boc_2O was dissolved in dry DCM (10 mL) and added very slowly (dropping funnel). The reaction was stirred overnight, then solvent was evaporated and EtOAc (100 mL) were added. Organic phase was washed with water (2 x 20 mL) and brine (2 x 20 mL), dried with Na_2SO_4 and filtrate was concentrated *in vacuo* offering **28** as a pale yellow oil.

^{1}H NMR (400 MHz, $CDCl_3$): δ = 3.36 (bs, 2H), 2.90 (s, 3H), 2.77 (bs, 1H), 2.49 (s, 3H), 1.87 (bs, 2H), 1.48 (s, 9H).

N-(Boc)-N'-(H-Val-Cit-PABC)- N,N'-dimethylethylenediamine (**29**)

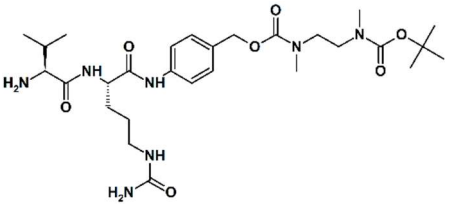

MW: 593.72 Da
m = 107 mg (55.3%)

Compound **24** (250 mg, 0.326 mmol, 1 eq) was dissolved in 1.5 mL dry DMF under N_2 atmosphere. The solution was cooled to 0 °C and compound **28** (solution of 159 mg in 1 mL DMF, 0.815 mmol, 2.5 eq) was added, followed by addition of DIPEA (142 µL, 0.815 mmol, 2.5 eq). Reaction warmed up slowly and stirred overnight at RT. EtOAc (100 mL) was added and washed with 0.5 M $KHSO_4$ (2 x 30 mL), sat. $NaHCO_3$ (2 x 20 mL) and brine (1 x 30 mL). The $KHSO_4$ phase was basified with 10 M NaOH to pH 9 and extracted with EtOAc (2 x 50 mL). The organic layer was washed with brine and dried with Na_2SO_4 and concentrated (yellow oil).

ESI-MS: MW_{cal}: 593.72, found $[M+H]^+$ = 595.33, $[M+Na]^+$= 617.45, $[M-H]^-$ = 592.26

N-(Boc)-N'-(glutaryl-Val-Cit-PABC)- N,N'-dimethylethylenediamine (**30**)

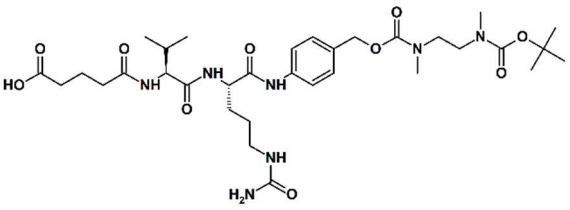

MW: 707.81 Da
m = 47 mg (37%)

Compound **29** (107 mg, 0.1802 mmol, 1 eq) was solved in 2 mL DMF. Glutaric anhydride (61.7 mg, 0.541 mmol, 3 eq) was added, followed by addition of DIPEA (95 µL, 0.541 mmol, 3 eq) and the reaction was stirred at RT for 4 hours. The solution was concentrated under high vacuum and EtOAc (100 mL) was added. The organic phase was washed with 1 M $KHSO_4$ (2 x 20 mL) and brine (2 x 10 mL), dried with Na_2SO_4 and evaporated. The remained solid was dissolved in 2 mL DCM/MeOH (9:1, v/v) and purified by flash-chromatography (eluent was stepwise changed from 95:5 to 80:20 DCM/MeOH + 0.1% AcOH). Combined fractions were concentrated *in vacuo* and an oily product-AcOH mixture remained which could be separated by semipreparative RP-HPLC (system II; 10% B to 100% B in 12 min). Product **30**-containing fractions were combined and freeze-dried.

ESI-MS: MW_{cal}: 707.81, found $[M+Na]^+$= 730.84, $[M-H]^-$ = 706.77

2'-(4-Nitrophenoxycarbonyl)paclitaxel (**31**)

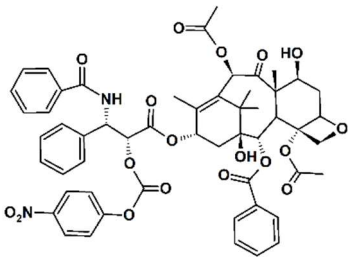

MW: 1019.0092 Da
m = 70.5 mg (55%)

PTX (107 mg, 0.1253 mmol, 1 eq) was dissolved in dry DCM (2.5 mL) under N_2 atmosphere at RT. Pyridine was added (30 µL, 0.3759 mmol, 3 eq) and cooled down to -50 °C. Pnp-chloroformate was dissolved in 1 mL dry DCM and added dropwise. After 20 min, the reaction mixture was warmed up to -20 °C and the reaction progress was controlled by TLC (eluent: 4:6 hexane/EtOAc). After 4 hours, the reaction was stopped by adding EtOAc (70 mL) and washed with 1 M $KHSO_4$ (2 x 10 mL) and brine (2 x 10 mL). The organic layer was dried and concentrated, followed by purification *via* flash chromatography (eluent was stepwise changed from 6:4 to 3:7 hexane/EtOAc). Combined fractions were evaporated yielding **31** (white solid).

ESI-MS: MW_{cal}: 1019.01, found $[M+Na]^+$= 1041.64, $[M-H]^-$ = 706.77.

N-[carbonyl-(2'-PTX)-N'-(glutaryl-Val-Cit-PABC)- N,N'-dimethylethylenediamine (**33**)

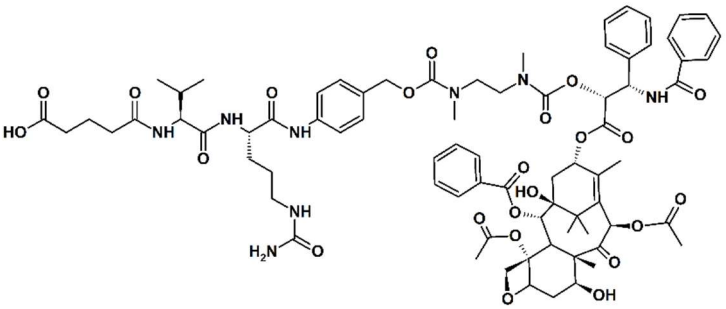

MW: 1487.60 Da
m = 12.8 mg (57%)

Boc-group of compound **30** (12 mg, 0.0169 mmol) was cleaved and the product was purified by RP-HPLC (system I-a, 0 min 10% B; 5 min 10% B; 10 min 20% B, 50 min 80% B) and lyophilized. The obtained *N*-(glutaryl-Val-Cit-PABC)-*N*,*N*'-dimethylethylenediamine (**32**) (9.2 mg, 0.01513 mmol, 1 eq) was dissolved in dry DMF and activated PTX (**31)** (19.8 mg, 0.01943 mmol, 1.3 eq) was added, followed by addition of DIPEA (10.5 µL, 0.06058 mmol, 4 eq). The reaction was stirred for 24 hours at RT and purified by preparative RP-HPLC (system I-a, 0 min 15% B; 5 min 15% B; 10 min 30% B, 50 min 100% B).

ESI-MS: MW_{cal}: 1487.60, found $[M+H]^+$ = 1487.93

Fmoc-Val-Ala-OH (**34**)

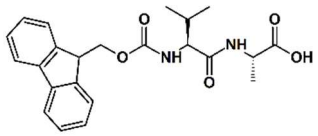

MW: 410.46 Da
m = 0.954 g (64%)

L-alanine (0.337 g, 3.78 mmol, 1.1 eq) and $NaHCO_3$ (0.317 g, 3.78, 1.01 eq) were dissolved in 15 mL water. Compound **21** (1.48 g, 3.44 mmol, 1 eq) was dissolved in 15 mL DME and added to the aqueous solution. THF (10 mL) was added and the reaction mixture was stirred overnight. 50 mL of 15% citric acid was added and extracted with 10% isopropanol/EtOAc (v/v) (2 x 50 mL). Combined organic layer was washed with water (3 x 30 mL) and brine (2 x 50 mL) and dried with Na_2SO_4. The filtrate was evaporated and the remaining solid was triturated in 60 mL Et_2O and sonicated for 45 min. Filtration yielded Fmoc-Val-Ala-OH (**34**) as white solid.

^{1}H NMR (400 MHz, CD_3OD): δ = 7.81 (d, *J* = 7.51 Hz, 2H), 7.69 (d, *J* = 7.43 Hz, 2H), 7.40 (t, *J* = 7.50 Hz, 2H), 7.32 (t, *J* = 7.50 Hz, 2H), 7.16 (d, *J* = 8.4, 1H), 4.45-4.34 (m, 3H), 4.25 (t, *J* = 6.9 Hz, 1H), 3.99 (t, *J* = 7.76, 1H), 2.07 (m, 1H), 1.42 (d, *J* = 7.2 Hz, 3H), 0.98 (m, 6H).

Fmoc-Val-Ala-PAB-OH (**35**)

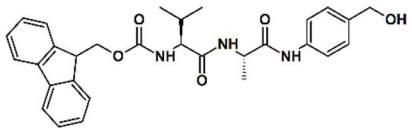

MW: 515.60 Da
m = 1.142 g (95%)

Compound **34** (0.954 g, 2.325 mmol, 1 eq) and PAB-OH (0.575 g, 4.65 mmol, 2 eq) were dissolved in 30 mL DCM:MeOH (2:1, v/v). EEDQ was added and the reaction was stirred in the dark under N_2 atmosphere (overnight at RT). The solvent was removed by evaporation and the remaining solid was triturated in 40 mL Et_2O and sonicated for 45 min. Filtration yielded Fmoc-Val-Ala-PAB-OH (**35**) as yellow solid.

^{1}H NMR (400 MHz, DMSO-d_6): δ = 9.93 (s, 1H), 8.17 (d, *J* = 7.06 HZ, 1H), 7.90 (d, *J* = 7.50 Hz, 2H), 7.75 (t, J = 7.20 Hz, 2H), 7.54 (d, *J* = 8.46 Hz, 2H), 7.43 (m, 3H), 7.33 (t, *J* = 7.35 Hz, 2H), 7.24 (d, *J* = 8.4 Hz, 2H), 5.10 (t, *J* = 5.62, 1H), 4.48-4.39 (m, 3H), 4.35-4.20 (m, 3H), 3.91 (dd, *J* = 7.31, 7.27 Hz, 1H), 1.99 (m 1H), 1.31 (d, *J* = 7.08 Hz, 3H); 0.88 (m, 6H).

Fmoc-Val-Ala-PABC-Pnp (**36**)

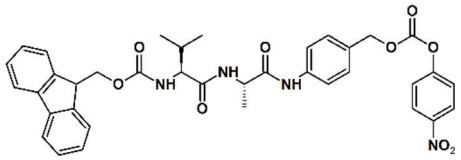

MW: 680.70 Da
m = 527 mg (65%)

Compound **35** (614 mg, 1.2 mmol, 1eq) was dissolved in 5 mL DMF under N_2 atmosphere and bis-Pnp carbonate (743.5 mg, 2.4 mmol, 2 eq) was added, followed by addition of DIPEA (427 µL, 2.4 mmol, 2 eq). Reaction mixture was stirred overnight at RT. DMF was removed by high vacuum evaporation. The remaining solid was triturated with 15 mL Et_2O and sonicated for 40 min. Filtration afforded Fmoc-Val-Ala-PAB-Pnp (**36**) as yellow solid.

^{1}H NMR (400 MHz, DMSO-d_6): δ = 10.10 (s, 1H), 8.32 (d, *J* = 8.56 Hz, 2H), 8.15 (d, *J* = 6.27 Hz, 1H), 7.90 (d, *J* = 7.14 Hz, 2H), 7.75 (t, *J* = 6.27 Hz, 2H), 7.65 (d, *J* = 7.93 Hz, 2H), 7.58 (d, J = 8.49 Hz, 2H), 7.42 (m, 2H), 7.33 (t, *J* = 7.00 2 H), 5.25 (s, 2H), 4.44 (t, *J* = 6.61, 1H), 4.36-4.18 (m, 3H), 3.93 (m, 1H), 2.12-1.94 (m, 1H), 1.33 (d, *J* = 6.48 Hz, 3H), 0.88 (m, 6H).

Fmoc-Val-Ala-PABC-Dau (**37**)

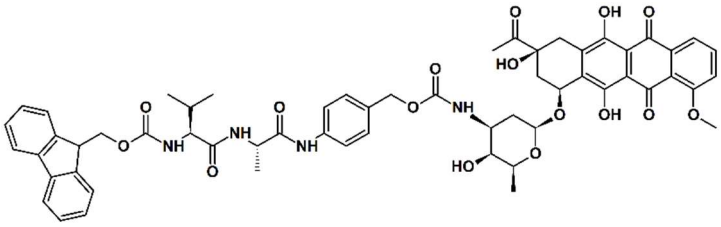

MW: 1069.11 Da
m = 22.2 mg (34%)

Dau (32.4 mg, 0.0615 mmol, 1 eq) was dissolved in 2 mL dry DMF. Then compound **36** (62.8 mg, 0.0922 mmol, 1.5 eq) was added, followed by addition of DIPEA (20 µL, 0.115 mmol, 1.9 eq). Reaction was stirred overnight at RT under N_2 atmosphere. Then 70 mL EtOAc was added and organic phase was extracted with 1 M $KHSO_4$ (2 x 10 mL), sat. $NaHCO_3$ (2 x 10 mL) and 10 mL brine. The organic layer was dried with Na_2SO_4 and concentrated. The red solid was dissolved in DCM:MeOH (9:1, v/v), filtrated and purified by flash-chromatography (eluents: 7:2:1 EtOAc/hexane/MeOH, followed by 9:1 DCM/MeOH). Combined product-containing fractions were evaporated affording Fmoc-Val-Ala-PABC-Dau (**37**) as a red solid.

ESI-MS: MW_{cal}: 1069.11, found $[M+Na]^+$= 1092.04, $[M-H]^-$ = 1068.22

Glutaryl-Val-Ala-PABC-Dau (**39**)

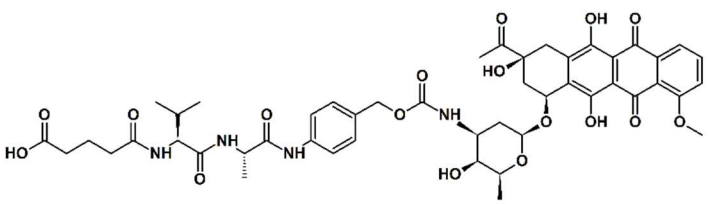

MW: 960.97 Da
m = 13.3 mg (65%)

Fmoc-group of **37** (22.2 mg, 0.0211 mmol) was removed as described above and H-Val-Ala-PABC-Dau (**38**) was resolved in dry DMF (1.5 mL). Glutaric anhydride (64.8 mg,

0.0422 mmol, 2 eq) was dissolved in dry DMF (68 µL) and added, followed by addition of DIPEA (7.4 µL, 0.0422 mmol, 2 eq). The reaction was stirred overnight at RT, then DMF was evaporated under high vacuum and the remaining red solid was dissolved in MeCN/water and purified by semipreparative RP-HPLC (system II, gradient 10% B to 100% B in 16 min). Product **39**-containing fractions were combined and freeze-dried.
ESI-MS: MW_{cal}: 960.97, found, $[M-H]^-$ = 959.45

N-(Boc)-N'-(Fmoc-Val-Ala-PABC)- N,N'-dimethylethylenediamine (**40**)

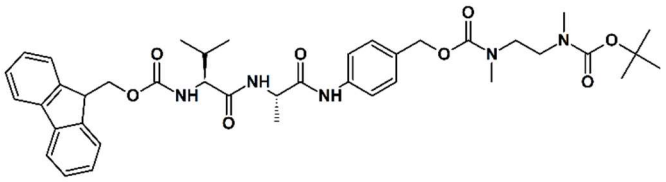

MW: 729.86 Da
m = 106 mg (66%)

Compound **36** (150 mg, 0.2204 mmol, 1 eq) was dissolved in 10 mL THF under N_2 atmosphere. The solution was cooled to 0 °C and **28** (solution of 104 mg in 2 mL THF, 0.551 mmol, 2.5 eq) was added, followed by addition of DIPEA (96 µL, 0.551 mmol, 2.5 eq). Reaction was warmed up slowly and stirred overnight at RT. EtOAc (70 mL) was added and washed with 1 M $KHSO_4$ (2 x 30 mL), sat. $NaHCO_3$ (4 x 15 mL) and brine (1 x 30 mL). The organic layer dried with Na_2SO_4 concentrated and purified by flash-chromatography (eluent was stepwise changed from 100% DCM to 4% MeOH in DCM. Product-containing fractions were combined and evaporation provided **40** as a yellow solid.
ESI-MS: MW_{cal}: 729.86, found $[M+Na]^+$= 752.89

N-(Boc)-N'-(glutaryl-Val-Ala-PABC)- N,N'-dimethylethylenediamine (**41**)

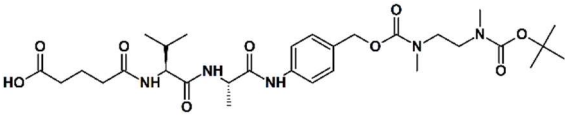

MW: 621.7223 Da
m = 24 mg (47%)

Fmoc-group of **40** (60.6 mg, 0.0830 mmol) was deprotected and resolved in 2 mL DMF. Glutaric anhydride (18.9 mg, 0.1660 mmol, 2 eq) was added, followed by addition of DIPEA (29 µL, 0.1661 mmol, 2 eq) and the reaction was stirred overnight at RT. The solution was concentrated under high vacuum and EtOAc (35 mL) was added. The organic phase was washed with 1 M $KHSO_4$ (2 x 7 mL) and brine (1 x 10 mL), dried with Na_2SO_4 and evaporated. The remained solid was dissolved in 2 mL DCM/MeOH (9:1, v/v) and purified by flash-chromatography (eluent was stepwise changed from 100% DCM to 10% MeOH in DCM + 0.1% AcOH). Combined fractions were concentrated *in vacuo* and product-AcOH mixture remained which could be separated by semipreparative

RP-HPLC (system II; 10% B to 100% B in 12 min). Product **41**-containing fractions were combined and freeze-dried.

ESI-MS: MW_{cal}: 621.72, found $[M+Na]^+$= 645.29, $[M-H]^-$ = 620.74

N-[carbonyl-(2'-PTX)]-N'-(glutaryl-Val-Ala-PABC)- N,N'-dimethylethylenediamine (**42**)

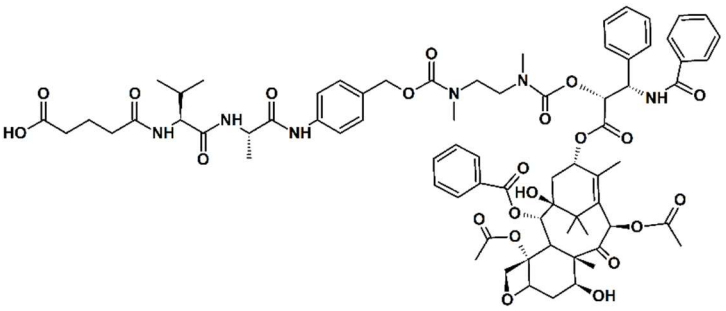

MW: 1401.5068 Da
m = 7.6 mg (70%)

Boc-group of **41** (12 mg, 0.0183 mmol) was cleaved and the product was purified by semipreparative RP-HPLC (system I, 0 min 10% B; 5 min 10% B; 10 min 20% B, 50 min 80% B) and lyophilized. The obtained *N*-(glutaryl-Val-Ala-PABC)-*N*,*N*'-dimethylethylene diamine (4 mg product, 0.0077 mmol, 1 eq) was dissolved in dry DMF and activated PTX (**31**) (12.3 mg, 0.01207 mmol, 1.6 eq) was added, followed by addition of DIPEA (5.3 µL, 0.0307 mmol, 4 eq). The reaction was stirred for 24 hours at RT and purified by preparative RP-HPLC (system I-a, 0 min 15% B; 5 min 15% B; 10 min 30% B, 50 min 100% B).

ESI-MS: MW_{cal}: 1401.51, found $[M+H]^+$= 1401.85, $[M-H]^-$ = 1400.91

Synthesis of self-immolative GnRH-III-drug conjugates

Synthesis of peptide carriers (**43** and **44**)

Synthesis of <Glp-His-Trp-Lys(Bu)-His-Asp-Trp-Lys-Pro-Gly-NH_2 (**43**) and <Glp-D-Tic-Lys(Bu)-His-Asp-Trp-Lys-Pro-Gly-NH_2 (**44**) were carried out on a Fmoc-Rink-Amid-MBHA resin (200 mg per carrier) using appropriate protected amino acid derivatives and Fmoc-Lys(Mtt)-OH was incorporated in position 4 and Fmoc-Lys(Boc)-OH. After peptide chain elongation, Mtt group was cleaved and ^{4}Lys was butyrylated. After cleavage from resin (DP1), the crude compounds were purified by preparative RP-HPLC (system I-a: 0 min 5% B; 5 min 5% B; 10 min 20% B, 50 min 80% B). Product-containing fractions were combined and eluent was evaporated.

Conjugation reaction of linker and peptide carrier -general protocol

Drug-linker **(**1 eq) was dissolved in 1 mL dry DMF. HATU (0.9 eq) and DIPEA (2 eq) were added and stirred for 30 min. Then peptide carrier (1 eq) was added and stirred

overnight at RT. DMF was evaporated and the final conjugate was purified.

Synthesis of self-immolative daunorubicin–GnRH-III conjugates **(45-48)**

The conjugation was performed as described above, using Dau-linker **27** or **39** and peptide carrier **43** or **44.** The final conjugates were purified by semipreparative RP-HPLC (system II, 10% B to 100% B in 12 min). In **Table 15**, the appropriate amount of starting material and the obtained yield of conjugation product are summarized. The structures of the final self-immolative linker-containing GnRH-III conjugates are depicted in **Scheme 8**.

Table 15: Ligation reaction. The linker (1 eq) was preactivated with HATU (0.9 eq) and DIPEA (2 eq) for 30 min, then peptide (1 eq) was added and reaction mixture was stirred for 24 hours.

Starting material						**Product**			
glutaryl-X-PABC-Dau-Linker				**Peptide (1 eq)**		**Conjugates**			
Code	**Linker**	**[mg]**	**[µmol]**	**Code**		**Code**	**MW_{cal}**	**Yield**	**[mg]**
27	Val-Cit	3.28	3.1	**43**	[^{2}His-^{3}Trp]	**45**	2399.568	70%	3.9
27	Val-Cit	5.00	4.78	**44**	[$^2\Delta$His-^{3}D-Tic]	**46**	2235.40	62%	6.0
39	Val-Ala	5.00	5.20	**43**	[^{2}His-^{3}Trp]	**47**	2313.47	70%	7.5
39	Val-Ala	5.00	5.20	**44**	[$^2\Delta$His-^{3}D-Tic]	**48**	2149.31	65%	6.6

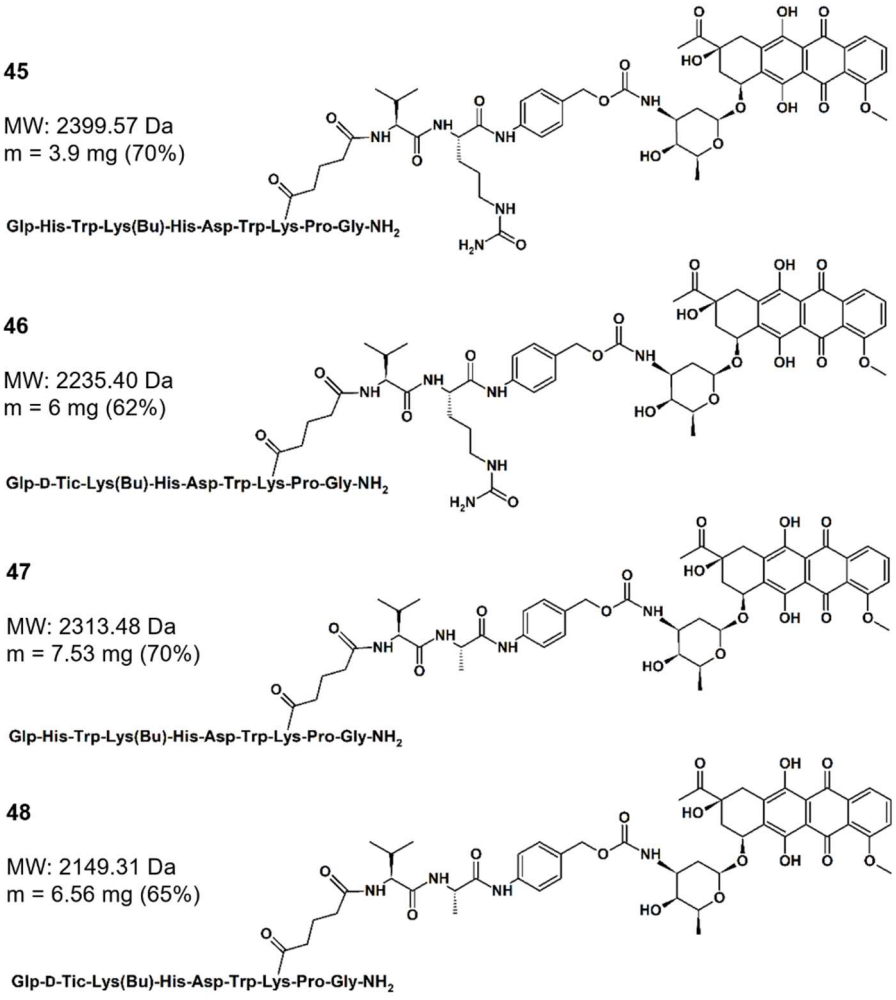

Scheme 8. Structure of self-immolative GnRH-III-daunorubicin conjugates **(45-48)**

*Synthesis of self-immolative paclitaxel–GnRH-III conjugates (**49-52**)*

The conjugation was performed as defined above, using PTX-linker **33** or **42** and peptide carrier **43** or **44.** The conjugates were purified by semipreparative RP-HPLC (system I-c, 0 min 20% B; 10 min 20% B; 15 min 35% B, 55 min 100% B). In **Table 16**, the appropriate amount of educts and the obtained yield of conjugation products are summarized. The structures of the self-immolative GnRH-III-PTX conjugates are shown in **Scheme 9**.

Table 16: Ligation reaction. The linker (1 eq) was preactivated with HATU (0.9 eq) and DIPEA (2 eq) for 30 min, then peptide (1 eq) was added and reaction mixture was stirred for 24 hours.

Starting material						**Product**			
glutaryl-X-PABC-PTX-Linker				**Peptide**		**Conjugates**			
Code	**X**	**[mg]**	**[µmol]**	**Code**		**Code**	**MW_{cal}**	**Yield**	**[mg]**
33	Val-Cit	5.20	3.50	**43**	[^{2}His-^{3}Trp]	**49**	2840.10	84%	7.1
33	Val-Cit	5.00	4.78	**44**	[^{2}ΔHis-^{3}D-Tic]	**50**	2675.66	62%	6.0
42	Val-Ala	5.00	5.20	**43**	[^{2}His-^{3}Trp]	**51**	2754.01	70%	7.5
42	Val-Ala	5.00	5.20	**44**	[^{2}ΔHis-^{3}D-Tic]	**52**	2589.84	65%	6.6

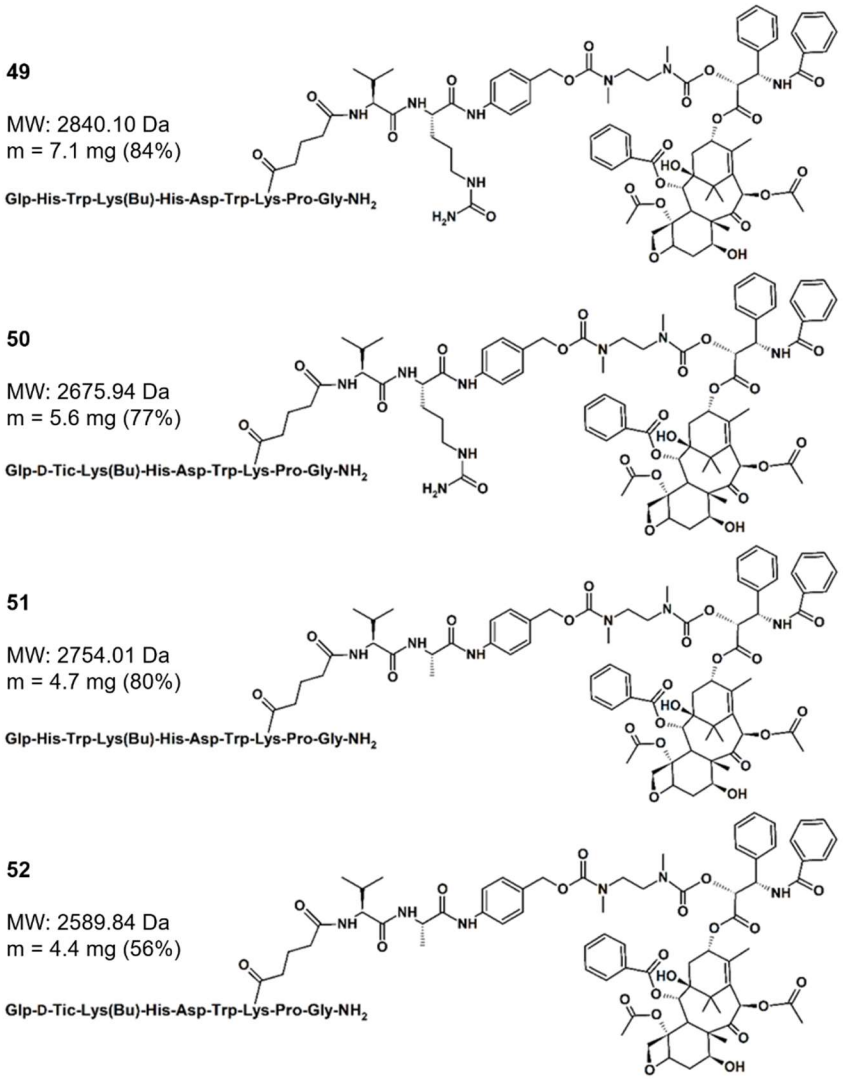

Scheme 9. Structure of self-immolative GnRH-III-paclitaxel conjugates **(49-52)**

Synthesis of non-cleavable linker

Glutaryl-Dau (**53**)

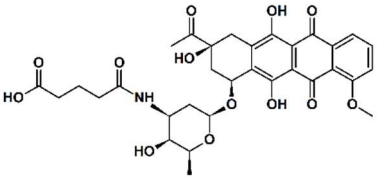

MW: 641.62 Da
m = 31.2 mg (65%)

Dau (25.33 mg, 0.22 µmol) was dissolved in 2 mL dry DMF, glutaric anhydride (and DIPEA were added and stirred at RT for 3 h. The mixture was acidified with TFA and linker **53** was purified by preparative RP-HPLC (system I-a, 0 min 15% B; 5 min 15% B; 10 min 30% 20, 50 min 80% B).

ESI-MS: MW_{cal}: 641.62, found $[M+H]^+$ = 642.08, $[M-H]^-$ = 640.25, $[M-TFA]^-$ = 754.37

N-Boc-N'-(glutaryl)- N,N'-dimethylethylenediamine linker (**54**)

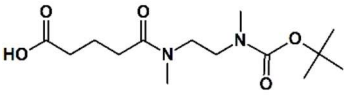

MW: 302.37 Da
m = 176 mg (83%)

Intermediate **28** (198 mg, 1.05 mmol, 1.5 eq) was dissolved in 1.5 mL dry DMF. Glutaric anhydride (80 mg, 0.70 mmol, 1 eq) and DIPEA (240 µL, 1.4 mmol, 2 eq) were added and stirred at RT for 6 h. Then EtOAc was added (50 mL) and was washed with 1 M $KHSO_4$ (4 x 10 mL) and brine (2 x 10 mL). The organic layer was dried with Na_2SO_4 and concentrated by evaporation. Compound **54** was used for the next step without further purification.

ESI-MS: MW_{cal}: 302.37, found $[M+H]^+$ = 303.27, $[M-H]^-$ = 301.19

N-[carbonyl-(2'-PTX)]-N'-(glutaryl)- N,N'-dimethylethylenediamine linker (**56**)

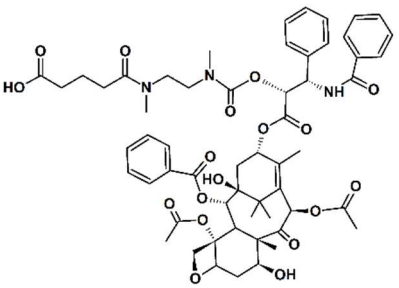

MW: 1082.15 Da
m = 5.6 mg (75%)

Boc-group of compound **54** (100 mg, 1.031 mmol) was removed and *N*-(glutaryl)-*N*,*N*'-dimethylethylenediamine was obtained as a dark-brown oil (**55**). Compound **55** (1.6 mg, 0.0079 mmol, 1.15 eq) was directly used and dissolved in dry DMF (0.5 mL). Activated PTX (**31**) (7 mg, 0.0069 mmol 1 eq) was also dissolved in dry DMF (0.5 mL) added to **55**, followed by addition of DIPEA (36 µL, 0.207 mmol, 30 eq, pH 8-9). The reaction mixture was stirred overnight at RT. Mixture was acidified with TFA and linker **56** was

purified by semipreparative RP-HPLC (system I-c, 0 min 20% B; 10 min 20% B; 15 min 35% 20, 55 min 100% B).

ESI-MS: MW_{cal}: 1082.15, found $[M+H]^+$ = 1082.68, $[M-H]^-$ = 1081.92, $[M-TFA]^-$ = 1194.84

Synthesis of non-cleavable GnRH-III-drug conjugates

*Synthesis of non-cleavable GnRH-III-daunorubicin conjugates (**57, 58**)*

The conjugation was performed as described above, using Dau-linker **53** and peptide carrier **43** or **44.** The final conjugates were purified by semipreparative RP-HPLC (system I-c, 0 min 15% B; 10 min 15% B; 15 min 30% 20, 55 min 80% B). In **Table 17**, the appropriate amount of starting material and the obtained yield of conjugation product are summarized. The structures of the final non-cleavable linker-containing GnRH-III-Dau conjugates are depicted in **Scheme 10**.

Table 17: Ligation reaction. Linker (1 eq) was preactivated with HATU (0.9 eq) and DIPEA (2 eq) for 30 min, then peptide (1 eq) was added and reaction mixture was stirred for 24 hours.

Starting material					**Product**			
Glutaryl-Dau-Linker			**Peptide**		**Conjugates**			
Code	**[mg]**	**[µmol]**	**Code**		**Code**	**MW_{cal}**	**Yield**	**[mg]**
53	5.00	7.80	**43**	[^{2}His-^{3}Trp]	**57**	1994.120	52%	7.3
53	5.00	7.80	**44**	[^{2}ΔHis-^{3}D-Tic]	**58**	1829.955	50%	6.5

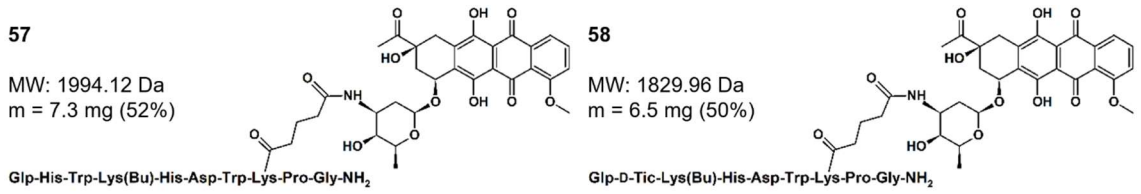

Scheme 10. Structure of non-cleavable GnRH-III-daunorubicin conjugates (**57**, **48**)

*Synthesis of non-cleavable paclitaxel–GnRH-III conjugates (**59-60**)*

The conjugation was performed as described above, using PTX-linker **56** and peptide carrier **43** or **44.** The final conjugates were purified by semipreparative RP-HPLC (system I-c, 0 min 20% B; 10 min 20% B; 15 min 30% 20, 55 min 90% B). In **Table 18** the appropriate amount of starting material and the obtained yield of conjugation product are summarized. The structures of the final non-cleavable linker-containing GnRH-III-Dau conjugates are shown in **Scheme 11**.

Table 18: Ligation reaction. Linker (1 eq) was preactivated with HATU (0.9 eq) and DIPEA (2 eq) for 30 min, then peptide (1 eq) was added and reaction mixture was stirred for 24 hours.

Starting material					Product			
Glutaryl-diamine-PTX-Linker			Peptide		Conjugates			
Code	[mg]	[µmol]	Code		Code	MW_{cal}	Yield	[mg]
56	2.60	2.40	**43**	[^{2}His-^{3}Trp]	**59**	2434.652	53%	2.8
56	2.60	2.40	**44**	[$^2\Delta$His-^{3}D-Tic]	**60**	2270.487	65%	3.2

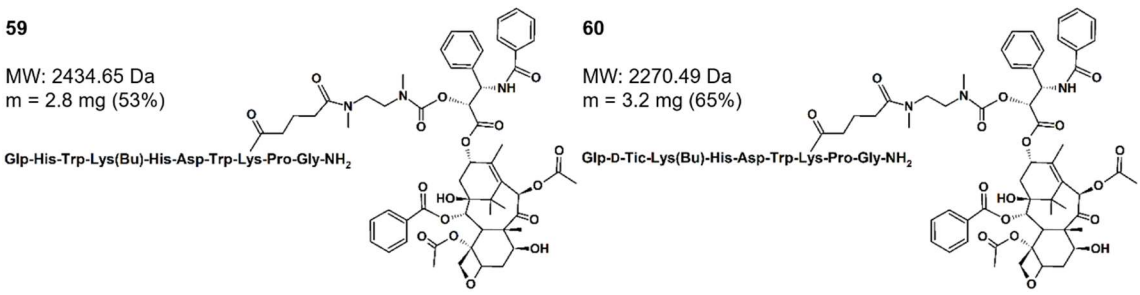

Scheme 11. Structure of non-cleavable GnRH-III-paclitaxel conjugates (**59, 60**)

5.2.1.4. Synthesis of somatostatin-drug conjugates

5.2.1.4.1. Synthesis of 5(6)-Carboxyfluorescein–somatostatin conjugates (**61-65**)

*Synthesis of FAM-somatostatin conjugates **61-64***

Peptide synthesis was performed on a Fmoc-Rink-Amid-MBHA resin (250 mg per peptide), whereby Fmoc-Cys(Trt)-OH was incorporated at the appropriate positions and FAM (5 eq) was coupled to the *N*-terminus (RT, 1.5 h). Afterwards, peptides were cleaved from resin (DP2, see 5.2.1.1.) and purified by preparative RP-HPLC (system 1-a: 0 min 15% B; 5 min 15% B; 10 min 35% B, 50 min 80% B). After lyophilization, formation of the intramolecular disulfide bridge was carried out by air oxidation (see 5.2.1.1.), followed by RP-HPLC purification (system 1-a: 0 min 15% B; 5 min 15% B; 10 min 35% B, 50 min 80% B).

*Synthesis of FAM-somatostatin conjugate **65***

Compound **65** was synthesized on a Fmoc-Rink-Amid-MBHA resin (200 mg) and appropriate protected amino acids were used for SPPS. Fmoc-Dab(Dde)-OH was incorporated in position 10 and FAM (5 eq) was coupled to the *N*-terminus. After peptide chain elongation, the Dde group was cleaved (12 x 5 min with 2% hydrazine in DMF (v/v)), followed by coupling of Cl-CH_2-CO-OPcp. In the next step, the peptide was cleaved from the resin (DP2) and purified by RP-HPLC (system I: 0 min 15% B; 5 min 15% B; 10 min 35% B, 50 min 80% B). Cyclisation was carried out by intramolecular thioether bond formation, whereby the peptide (20 mg) was dissolved in DMF (500 µL) and added dropwise to 4.5 mL Tris-buffer (0.1 M, pH 8.3). The reaction was stirred

overnight at RT. The reaction mixture was purified (RP-HPLC system I-a: 0 min 15% B; 5 min 15% B; 10 min 35% B, 50 min 80% B) and freeze-dried.

5.2.1.4.2. Synthesis of oxime bond-linked daunorubicin–somatostatin conjugates

*Synthesis of somatostatin conjugates **66** and **67***

The syntheses of somatostatin conjugates **66** and **67** were carried out on a Fmoc-Rink-Amid-MBHA resin (250 mg per conjugate) using appropriate protected amino acids, whereby Fmoc-Cys(Trt)-OH was incorporated in position 6 and 11 (**66**) or 10 (**67**). >=Aoa-OH was coupled to the *N*-terminus and after peptide chain elongation, peptides were cleaved from the resin (DP2, see 5.2.1.1.), the crude compounds were purified by preparative RP-HPLC (system I-a: 0 min 15% B; 5 min 15% B; 10 min 35% B, 50 min 70% B) and freeze-dried. Then intramolecular disulfide bond was formed by air oxidation (5.2.1.1.) and purified by preparative RP-HPLC (system I-a: 0 min 15% B; 5 min 15% B; 10 min 35% B, 50 min 65% B). Afterwards, the >=Aoa moiety was deprotected, followed by further separation by RP-HLPC (system 1-a: 0 min 15% B; 5 min 15% B; 10 min 35% B, 50 min 65% B). Appropriate fractions were immediately evaporated and directly used for Dau ligation. The reaction mixture was purified by RP-HPLC (system 1-a: 0 min 15% B; 5 min 15% B; 10 min 40% B, 50 min 70% B) and freeze-dried.

*Synthesis of somatostatin conjugate **68***

The synthesis of **68** was performed on a Fmoc-Rink-Amid-MBHA resin (200 mg) and appropriate protected amino acids were used for SPPS. Fmoc-Dab(Dde)-OH was incorporated in position 10 and >=Aoa-OH was coupled to the *N*-terminus. After peptide chain elongation, the Dde group was cleaved (12 x 5 min with 2% hydrazine in DMF (v/v)), followed by coupling of Cl-CH_2-CO-OPcp. In the next step, the peptide was cleaved from the resin (DP2) and purified by RP-HPLC (system I: 0 min 15% B; 5 min 15% B; 10 min 35% B, 50 min 80% B). Cyclisation was carried by intramolecular thioether bond formation, whereby the peptide (40 mg) was dissolved stepwise in 1:1 DMF/Tris-buffer (0.1 M, pH 8.3) to a final volume of 10 mL. The reaction was stirred at RT and monitored by analytical RP-HPLC. The reaction mixture was purified after 2.5 hours (RP-HPLC system I-c: 0 min 15% B; 5 min 15% B; 10 min 25% B, 50 min 75% B) and freeze-dried. Afterwards, the isopropylidene group was cleaved and Dau ligation was performed after purification and evaporation. The final conjugate **68** was obtained after additional purification by RP-HPLC and lyophilization.

*Synthesis of somatostatin conjugates **69***

For the preparation of somatostatin conjugates **69**, the peptide linker Dau=Aoa-Leu-Arg-Arg-Tyr-Cys-NH_2 (**69a**) and the targeting moiety Cl-CH_2-CO-D-Phe-[Cys-Tyr-D-Trp-Lys-Val-Cys]-Thr-NH_2 (**69b**) were synthesized. SPPS was carried out on a Fmoc-Rink-Amid-MBHA resin (250 mg per peptide) using propriate protected amino acids. Fmoc-Cys(Trt)-OH was used for linker **69a** and Fmoc-Cys(Acm)-OH was incorporated in position 2 and 7 of **69b**. Cl-CH_2-CO-OPcp was coupled to the *N*-terminus of **69b**.

The linker **69a** was cleaved from the resin by procedure DP1 and purified by preparative RP-HPLC (system I-a: 0 min 15% B; 5 min 15% B; 10 min 30% B, 50 min 70% B). Then the isopropyliden group was cleaved and the linker was purified (RP-HPLC system I-a: 0 min 15% B; 5 min 15% B; 10 min 30% B, 50 min 70% B), followed by Dau ligation in solution and additional purification. After lyophilization, **69a** was obtained as a red solid.

The peptide moiety **69b** was cleaved from the resin by DP2 and purified (RP-HPLC system I-a: 0 min 20% B; 5 min 20% B; 10 min 40% B, 50 min 70% B). The intramolecular disulfide bridge formation of Acm protected **69b** (20 mg, 0.0158 mmol, 1 eq) was carried out with thalium(III) trifluoroacetate (10.3 mg, 0.019 mmol, 1.2 eq) and anisole (200 µL) in 4 mL TFA at 0 °C. After 5 hours, Et_2O (20 mL) was added and TFA/Et_2O solution was evaporated. Afterwards, the peptide was precipitated with fresh ice-cooled Et_2O (40 mL), centrifuged, washed with fresh Et_2O (3 x 30 mL), dissolved in water-MeCN (0.1% TFA) 4:1 (v/v) lyophilized and purified (RP-HPLC system I-a: 0 min 20% B; 5 min 20% B; 10 min 40% B, 50 min 70% B). **69b**-containing fractions were combined and lyophilized (white solid).

For the ligation by intermolecular thioether bond formation, peptide **69b** (5 mg, 4.5 µmol, 1 eq) was dissolved in 1 mL DMF and 1mL Tris-buffer (0.1 M, pH 8.3) and the linker **69a** was added stepwise (5.75 mg, 4.5 µmol, 1 eq). The reaction was stirred at RT and monitored by analytical RP-HPLC. After 2 hours, the reaction mixture was purified (RP-HPLC system I-a: 0 min 20% B; 5 min 20% B; 10 min 40% B, 50 min 70% B) and freeze-dried.

5.2.1.4.2. Synthesis of self-immolative linker-containing daunorubicin–somatostatin conjugates

*Synthesis of somatostatin conjugate **70***

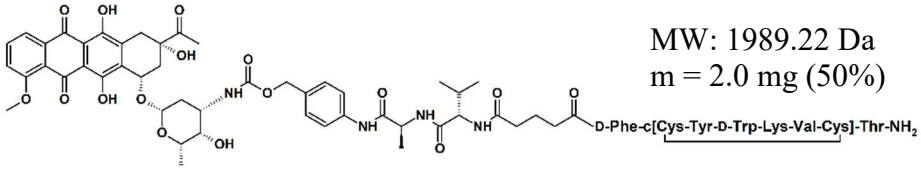

MW: 1989.22 Da
m = 2.0 mg (50%)

For the synthesis of conjugate **70**, the targeting moiety D-Phe-Cys-Tyr-D-Trp-Lys(Dde)-Val-Cys-Thr-NH_2 was prepared by SPPS and cleaved from resin by DP2. Then the intramolecular disulfide bridge was formed by air oxidation as described above, followed by purification.

Linker **39** (5 mg, 5.2 µmol, 1 eq) was dissolved in 1 mL dry DMF. HATU (2 mg, 5.2 µmol, 1 eq) and DIPEA (1.8 µL, 10.4 µmol, 2 eq) were added and stirred for 30 min. Then targeting peptide (7.6 mg, 6.2 µmol, 1.2 eq) was added and stirred overnight at RT. DMF was evaporated and the conjugate was purified by semipreparative RP-HPLC (system I-b: 0 min 15% B; 5 min 15% B; 10 min 25% B, 80 min 80% B) and lyophilized (**70(Dde)** m = 4.3 mg (38%)). To obtain conjugate **70**, the Dde group of the lysine was deprotected in solution by treatment with 2% hydrazine in DMF (v/v). After 10 min, the reaction mixture was separated by RP-HPLC (system I-b: 0 min 15% B; 5 min 15% B; 10 min 25% B, 80 min 80% B), followed by freeze-drying.

5.2.1.4.3. Synthesis of oxime bond-linked pyrrolino-daunorubicin–somatostatin conjugates

*Synthesis of somatostatin conjugate **71***

For the synthesis of somatostatin conjugate **71**, the same peptide precursor was used as for conjugate **66**. After disulfide bond formation, the >=Aoa moiety was deprotected and at the same time, pyDau was freshly purified (RP-HPLC system I-b: (0 min 15% B; 5 min 15% B; 10 min 25% B, 50 min 80% B). The pyDau-containing fractions were stored on ice and meanwhile the deprotected somatostatin peptide was purified (system I-a: 0 min 15% B; 5 min 15% B; 10 min 35% B, 50 min 65% B). The product-containing fractions were combined with pyDau fractions and evaporated together. Afterwards, 3 mL DMF/water (1:1, v/v) was added and the reaction was stirred overnight at 4 °C. The mixture was purified by RP-HPLC (system-I-C: 0 min 10% B; 5 min 10% B; 10 min 20% B, 50 min 60% B) and freeze-dried.

5.2.2. Analytical methods

5.2.2.1. Reverse-phase high-performance liquid chromatography RP-HPLC

A Knauer 2501 HPLC system was used to prove the purity of the compounds. As a stationary phase, either a Phenomenex Luna C18 column (100 Å, 5 µm, 250 mm x 4.6 mm) (**a**), a Macherey-Nagel Nucleosil C18 column (100 Å, 5µm, 250 mm x 4.6 mm) (**b**) or a Vydac 214TP5 C4 column (300 Å, 5 µm, 250 mm x 4.6 mm) (**c**) was used. A linear gradient elution (**a**: 0 min 0% B; 5 min 0% B; 50 min 90%, **b**: 0 min 0% B; 5 min 0% B; 30 min 90%, **c**: 0 min 0% B; 5 min 0% B; 40 min 90%) was used at a flow rate of 1 mL/min with eluent A (0.1% TFA in water) and eluent B (0.1% TFA in MeCN/H_2O (80:20, v/v)). Peaks were detected at 220 nm.

5.2.2.2. Mass spectrometry

Electrospray ionization (ESI) mass spectrometric analyses were performed on an Esquire 3000+ ion trap mass spectrometer (Bruker Daltonics, Bremen, Germany). Spectra were acquired in the 50–2500 *m/z* range. Samples were dissolved in a mixture of MeCN/water (1:1, v/v) and 0.1% formic acid.

Liquid chromatography-mass spectrometry (LC-MS) was carried out on the same ESI mass spectrometer used with an Agilent 1100 HPLC system and a diode array detector (Agilent, Waldbronn, Germany). A Supelco C18 column (150 mm x 2.1 mm, 3 µm) (Hesperia, CA, USA) was used with a linear gradient from 2–70% B in 25 min (eluent A: H_2O + 0.1% HCOOH; eluent B: MeCN/H_2O (80:20) + 0.1% HCOOH at a flow rate of 0.2 mL/min) to separate the peptides. Spectra were recorded in positive ion mode in the 100–2500 *m/z* range

5.2.2.3. Thin layer chromatography

To monitor reaction by analytical thin-layer chromatography (TLC), silica gel 60 F254 pre-coated glass plates (0.25 mm thickness) or aluminum sheets were used. Detection of spots was accomplished by irradiation with a UV lamp at 254 nm and/or staining with a pancaldi or ninhydrin solution.

5.2.2.4. NMR

Proton NMR spectra were recorded on a spectrometer operating at 400.16 MHz. Proton chemical shifts are reported in ppm (δ) with the solvent reference relative to tetramethylsilane (TMS) employed as the internal standard ($CDCl_3$ δ = 7.26 ppm; CD_2Cl_2, δ = 5.32 ppm; $[D]_6$ DMSO, δ = 2.50 ppm; CD_3OD, δ = 3.33 ppm). The following

abbreviations are used to describe spin multiplicity: s = singlet, d = doublet, t = triplet, q = quartet, m = multiplet, bs = broad signal, dd = doublet of doublet.

5.2.3. Cell culturing and cell biology experiments

5.2.3.1. Cell culturing

MCF-7 human breast adenocarcinoma cells were cultured in DMEM supplemented with 10% (v/v) Fetal Bovine Serum (FBS), L-glutamine (2 mM), non-essential amino acids (NEAA), sodium pyruvate (1 mM) and 1% Penicillin-Streptomycin. A2780 human ovarian cancer, HT-29 human colon cancer and Panc-1 human pancreatic cancer cells, were maintained in RPMI-1640, supplied with 10% FBS, L-glutamine and 1% Penicillin-Streptomycin. MDA-MB-231 breast adenocarcinoma cells were cultured in DMEM, supplemented with 10% FBS and 1% Penicillin-Streptomycin. Cells were maintained in plastic culture dishes at 37 °C with a humidified atmosphere, containing 5% CO_2/95% air.

5.2.3.2. Cell viability assay

Oxime bond-linked daunorubicin–GnRH-III conjugates[f]

5 x 10^3 cells per well were seeded to 96-well plates in 100 µL complete cell medium. After 24 h, plates were centrifuged (216 x g, 5 min), 50 µL complete medium was removed and 50 µL FBS-free medium was added. Then cells were treated with 100 µL bioconjugate-solution dissolved in serum-free medium (concentration range 0.068–150 µM, control wells were treated with serum-free medium). On the next day, plates were centrifuged (216 x g, 5 min) and 150 µL medium was taken out and replaced by serum-free medium. This step was repeated, followed by adding of 150 µL complete medium and incubation for 48 h. The cell viability was determined by adding 20 µL alamarBlue solution to each well and additional incubation of 2-3 hours. A Symulti-mode microplate reader (Synergy H2, BioTek, Winooski, VT, USA) was used for fluorescence detection (λ_{Ex} = 570 and λ_{Em} = 620 nm). Experiments were performed at least twice, using four parallels per concentration. The cell viability (and IC_{50} values) was calculated with GraphPadPrism using a nonlinear regression (sigmoidal dose–response).

Self-immolative linker-containing GnRH-III-Dau and -PTX conjugates

5 x 10^3 cells per well were seeded to 96-well plates in 100 µL complete cell medium. After 24 h, complete medium was removed and cells were treated with 200 µL

[f] Performed by Beáta Biri-Kovács (MTA-ELTE Research Group of Peptide Chemistry, ELTE Budapest)

bioconjugate-solution in serum-free medium (concentration range 0.0032–50 μM, control wells were treated with serum-free medium). Medium was taken out after 6 h treatment (PTX-conjugates) or 24 h (Dau-conjugates), replaced by complete medium and incubation was continued. To determine cell viability, the medium was removed after 72 h and 100 μL resazurin solution (10% Tox-8 in FBS-free medium) was added to each well, followed by additional incubation of 2-3 hours. A Tecan infinite 200 pro microplate reader (Tecan Group Ltd., Zürich, Switzerland) was used for fluorescence detection (λ_{Ex} = 560 and λ_{Em} = 590 nm). Experiments were performed at least twice, using three parallels per concentration. The cell viability (and IC_{50} values) was calculated with GraphPadPrism using a nonlinear regression (sigmoidal dose–response).

Somatostatin-drug conjugates

5 x 10^3 cells per well were seeded to 96-well plates in 100 μL complete cell medium. After 24 h, cells were treated with 100 μL bioconjugate-solution in serum-free medium (concentration range 0.0032–100 μM or 0,0016-50μM, control wells were treated with serum-free medium). On the next day, incomplete medium was removed and replaced by 200 μL complete medium and cells were incubated for further 48 h. The cell viability was determined by adding 20 μL MTT solution (5 mg/mL) to each well and the plate was incubated for additional 2-3 hours. A Bio-Rad 550 microplate reader (Hercules, California, U.S.A.) was used for fluorescence detection (λ_{Abs} = 570 nm). Experiments were performed at least twice, using three parallels per concentration. The cell viability (and IC_{50} values) was calculated with GraphPadPrism using a nonlinear regression (sigmoidal dose–response).

5.2.3.3. Flow cytometry studies[g]

To study the cellular uptake of the bioconjugates, cells were seeded (10^5 cells/well) in complete cell medium to 24-well plates (1 mL/well). On the next day, plates were centrifuged (216 x g, 5 min) and 950 μL medium was removed. Cells were treated with the conjugates (3.125 to 50 μM) in 250 μL serum-free medium. After 6 h, plates were centrifuged (216 x g, 5 min) and cells were washed with 500 μL HPMI medium. After centrifugation, HPMI was completely removed and cells were detached with trypsin-EDTA solution (10 min, 37 °C). Trypsinization was stopped by adding 850 μL HPMI/10% FBS. The cells were suspended, transferred to FACS-tubes and centrifuged at 216 x g for 5 min at 4 °C. Afterwards, the supernatant was removed and the cells were

[g] Studies of 1st set of oxime-linked GnRH-III-Dau conjugates were performed by Beáta Biri-Kovács

resuspended in 250 µL HPMI medium. To detect the intracellular fluorescence intensity (that is proportional to the cellular uptake), samples were analyzed by a BD LSR II flow cytometer (BD Bioscience, Franklin Lakes, NJ, USA). At least 5000 cells per sample were measured and the fluorescence signal was detected by using the phycoerythrin (PE) standard filter (λ_{Ex} = 488 nm, λ_{EM} = 562-588 nm). The obtained data were analyzed by FACSDiVa (BD Bioscience) 5.0 software.

5.2.3.4. Confocal laser scanning microscopy (CLSM) studies[hi]

To study the subcellular localization, 10^5 cells/per well were seeded in 1 mL complete cell medium to 24-well plates which contained cover glasses (thickness 1). After one day, the plates were centrifuged (216 x g, 5 min) and supernatant was removed, the treatment was performed with 250 µL peptide solution by using either different concentrations (10, 40 and 160 µM) or various time-points of 40 µM of bioconjugate (**K2**: 1, 5 10, 30 minutes and 1, 2, 3, 6 hours; **16**: 5, 15, 30, 60 seconds and 5, 10, 15, 30, 60 minutes) in serum-free medium for different time points. Afterwards, cells were washed twice with PBS and fixed by 4% paraformaldehyde for 20 min at 37 °C. To stain the nuclei, the samples were washed three times with PBS and incubated for 15 min with 250 µL DAPI, (0.2 µg/mL, dissolved in PBS) in the dark. After three times washing, cover glasses were mounted to microscopy slides by Mowiol® 4–88 mounting medium and dried overnight. In case of lysosomal co-localization study, lysosomes were stained in living cells before 5 min treatment with **K2** (40 µM) by CytoPainter lysosomal staining Kit, according to the manufacturer's instructions. Confocal microscopy studies were performed on a Zeiss LSM 710 system (Carl Zeiss Microscopy GmbH, Jena, Germany) with a 40X oil objective and ZEN Lite (Carl Zeiss Microscopy GmbH) software was used for image processing.

5.2.3.5. Western blot analysis

Cell lysis

To determine GnRH-receptor expression, western blot analysis was performed on whole cell lysates. Cells (10^6 cells/well) were seeded in 3 mL complete medium to six-well plates. After 24 h, the cells were washed two times with PBS and treated with 500 µL trypsin-EDTA (10 min, 37 °C). Then 5 mL complete medium was added and cells were suspended, followed by centrifugation (216 x g, 5 min). The supernatant was removed, 1

[h] Samples for CLSM were prepared by Beáta Biri-Kovács
[i] CLSM-images were recorded by Bálint Szeder

mL PBS was added and cells were centrifuged again. The remaining cell pellet was treated with 100-150 µL lysis buffer (50 mM Tris pH 7.4, 150 mM NaCl, 2 mM EDTA, 1% Triton-X 100 and Protease Inhibitor Cocktail). Samples were smoothly shaken at 4 °C for 30 min, followed by 30 min centrifugation at 16,000 x g. Total protein quantity of the supernatant was measured with the Qubit Protein Assay Kit.

SDS gel electrophoresis

Cell lysates of interest were adjusted to equal protein concentration. Afterwards, SDS-sample buffer was added to cell lysate (1:1, v/v), denaturated (95 °C, 5 min) and 25 µL were loaded to 10% Tris-tricine gel and gel electrophoresis was performed according to literature (130-150 mV) [421].

Western blot

After electrophoresis, the gel was incubated for 15 min in blotting buffer (25 mM Tris, 192 mM glycine, 20% MeOH, 1% SDS, pH 8.3). Meanwhile, the PVDF membrane was soaked 1 min in 100% MeOH, 2 min in water and 10 min in blotting buffer. Afterwards, the gel and the membrane were interposed between filter papers and a wet western blot was performed in transfer buffer at 350 mA (Bio-Rad system). Then the membrane was blocked for 1 h at RT with 4% milk powder in TBST (20 mM Tris, 150 mM NaCl, 0.1% Tween-20, pH 7.5). To detect the GnRH receptor, an anti-GnRH-R antibody was diluted in 4% milk powder in TBST (1:1000) and incubated at 4 °C overnight. On the next day, the blot was washed with TBST (4 x 15 min) and an anti-rabbit-HRP secondary antibody was added in 4% milk powder in TBST for 1 h (1:3000). After washing with TBS (2 x 3 min), the chemiluminescence was detected by adding 4 mL ECL Substrate (Western Lightning Plus-ECL, PerkinElmer, Waltham, MA, USA) onto the membrane and incubated for 1 min. The GnRH-R bound antibodies were detected using a Bio-Rad molecular Imager® (ChemoDoc^{TM} XRS+, Hercules, California, USA). After detection of the GnRH-R, the membrane was stripped with mild stripping buffer (0.2 M glycine, 0.1% SDS, 1% Tween-20, pH 2.2) (2 x 5 min) and washed with TBS (10 min) and TBST (10 min). Then the membrane was blocked again and actin was detected as a loading control by an anti-actin primary antibody (Santa Cruz Biotechnology, sc-1616, produced in goat, 1:2000) and anti-goat-HRP secondary antibody (Santa Cruz Biotechnology, sc-2354, produced in mouse, 1:3000) using the same protocol as for GnRH-R detection.

5.2.3.6. Radioligand binding studies[j]

Ligand competition assays with radiolabeled triptorelin[k] were performed to evaluate the binding affinity of GnRH-III derivatives to GnRH-receptors on human pituitary and human prostate cancer cells as reported earlier [264,303,304,422]. Tissue samples of human prostate cancer cells were obtained from a patient at the time of initial surgical treatment and normal human pituitary tissue (anterior lobe) was derived by autopsy. All subjects gave their informed consent for inclusion before they participated in the study. The collection and the use of these specimens for these studies were conducted in accordance with the Declaration of Helsinki and approved by the local Institutional Ethics Committee (UD REC/IEC 4831-2017). Cell membrane homogenates were prepared as previously described [264,303,304,423]. Triptorelin was radioiodinated as described in the literature by chloramine-T method and purified by RP-HPLC [264,303,304,424]. The binding affinities of the nonradio-labeled GnRH-III bioconjugates to GnRH-RI were determined by displacement of [^{125}I]-GnRH-I-[^{6}D-Trp] in an *in vitro* ligand competition assay [264,303,304,422]. Membrane homogenates which contained 50–160 mg protein were incubated in duplicate or triplicate with 60–80,000 cpm [^{125}I]-GnRH-I-[^{6}D-Trp] and increasing concentration (1 pM–1 μM) of nonradioactive bioconjugates as competitive binders in 150 mL binding buffer. To determine the protein concentration by the method of Bradford, a Bio-Rad protein assay kit was used. The LIGAND-PC computerized curve-fitting software of Munson and Rodbard was used to determine the receptor binding characteristics and IC_{50} values [264,303,304,422].

5.2.4. *In vitro* stability and degradation of drug-conjugates

5.2.4.1. Stability in cell culture medium

The bioconjugates were dissolved in water to a concentration of 2.5 mg/mL followed by dilution with serum free cell culture medium to a bioconjugate concentration of 0.5 mg/mL. The mixtures were incubated at 37 °C for 24 h and samples of 50 μL were directly monitored by RP-HPLC at time points 0 h, 1 h, 2 h, 6 h and 24 h.

5.2.4.2. Degradation of drug-conjugates in presence of rat liver lysosomal homogenate

The bioconjugates were dissolved in water to a concentration of 5 μg/μL. The reaction was carried out in 0.2 M NaOAc buffer (pH 5), with an identical concentration of bioconjugate and rat liver lysosomal homogenate (0.25 μg/μL). The reaction mixtures

[j] Performed by Prof. Gábor Halmos and co-workers (Department of Biopharmacy, University of Debrecen)
[k] radioiodinated triptorelin was produced by Dr. János Gardi (1st Department of Internal Medicine, University of Szeged)

were incubated at 37 °C and aliquots of 15 µL were taken at 5 min, 1 h, 2 h, 4 h, 8 h and 24 h and quenched with 2 µL of acetic acid. The analysis of the samples was performed by LC–MS.

3.2.4.3. Plasma stability of drug-conjugates

The conjugates were dissolved in water and diluted with human plasma (90%) to a final concentration of 10 µM. The mixture was incubated at 37 °C and aliquots were taken after 0.5, 1, 2, 4, 8 and 24 h. To quench the reaction, 10 µL of acetic acid was added. Large human plasma proteins were excluded using ultra centrifugal filters with a cut-off of 10 kDa. The lower molecular weight fractions were analyzed by LC-MS. As controls, 90% plasma plus 10% water and 10 µM of bioconjugate in 100% water were incubated and analyzed in the same manner.

6. Summary

Targeted tumor therapy is a valuable treatment option for cancer to overcome the drawbacks of classical chemotherapy. Since many cancer cells overexpress receptors for the peptide hormones GnRH and SST, their ligands can be used as homing devices to deliver cytotoxic drugs selectively to cancer cells which reduce harmful side-effects to healthy tissue. Hence, the present thesis is focused on the synthesis and evaluation of novel GnRH-III and SST-drug conjugates.

Many GnRH-III-Dau conjugates have been developed and systematically refined in our research group. To achieve an improved antitumor activity of oxime bond-linked GnRH-III compounds, 20 novel conjugates with modified peptide sequence were prepared. The *in vitro* cytostatic effect of these compounds was studied on GnRH-R expressing cancer cells and compared to our lead compound. The bioconjugate GnRH-III-[^{2}ΔHis-^{3}D-Tic-^{4}Lys(Bu),^{8}Lys(Dau=Aoa)]) displayed a highly improved antitumor activity. Moreover, cellular uptake and localization studies, stability analysis in plasma and lysosomal enzymes, as well as receptor binding studies have been carried out, revealing the high potential of this compound for targeted tumor therapy.

Based on these results, additional GnRH-III-drug conjugates were developed using the two best targeting moieties. The anticancer drugs PTX and Dau were attached to the peptides using cathepsin B cleavable, self-immolative linkers. For a better comparison, non-cleavable counterparts were also synthesized. Cell viability studies on human cancer cells verified the growth inhibitory effect of the cleavable GnRH-III derivatives. Moreover, the drug releasing concept of the linker systems could be validated by lysosomal degradation studies.

Besides, somatostatin-drug conjugates were synthesized and analyzed. Initially, the potential of different targeting moieties has been studied. Hence, carboxyfluorescein labeled derivatives were established to determine the cellular uptake of the compounds. Due to the results, corresponding oxime bond-linked Dau-conjugates were synthesized and the cytostatic effect was studied on SSTR expressing cancer cells. The best targeting moiety was used to analyze the impact of diverse linker systems on the anticancer activity. The best candidate consists of the RC-121 carrier and the drug linker Dau=Aoa-LRRY. To further improve the antitumor activity, the highly potent anticancer drug 2-pyrrolino-daunorubicin was used instead of Dau affording conjugate pyDau=Aoa-LRRY-RC-121 which possesses a strong *in vitro* anticancer activity with an IC_{50} value in the nanomolar

range. This somatostatin conjugate represents a highly promising candidate for targeted cancer therapy.

Our results confirm the high potential of compound **16** and **71** for selective cancer therapy which underlines the great value of GnRH-III and SST-drug conjugates for targeted tumor therapy.

.

7. Acknowledgements

On this occasion, I would like to express my gratefulness to all people who supported me within the last 4 years and made it possible to achieve this goal.

First of all, I would like to thank my supervisor, Professor Dr. Gábor Mező for selecting me as a PhD candidate and giving me the opportunity to work on this fascinating research topic. Moreover, I would like to thank him for the warm welcome in the research group and his big support at any time of the four years. During this time, his strong commitment and patience helped me to cope with every scientific, administrative or language challenge. There was not a single problem which could not be solved by his competence and expertise.

My special thank goes to Dr. Beáta Biri-Kovács for her strong support and commitment during the whole PhD period. Her energy and enthusiasm helped me so much to make progress with my research project and was an important contribution. She introduced me to the world of cell culturing and experiments, performed many valuable studies, helped me to solve every problem which occurred and always cheered me up in the right moments. She was not only the best collaborator you could ask for, but also became a good friend.

I am especially grateful to my good friend and colleague Andrea Angelo Pierluigi Tripodi. It is impossible to find enough words to thank him for his strong support in the last years. It was a great adventure and amazing experience that we shared. With his unbelievable kindness and helpfulness, he supported me and he helped me so much to overcome all difficulties and bad moments. We always considered us as a team and he is the best team mate you can get. I will always remember the nice and enjoyable time in ‘our’ laboratory and the precious moments outside the working place. I am already missing him a lot!

I would like to express my special thanks to all collaborators who helped me with the experiments in the cell culture laboratory. My special thanks go to Dr. Szilvia Bősze who always helped me with the experiments, answered every questions and facilitated valuable solutions for my problems. Moreover, I would like to thank Dr. Rita Oláhné Szabó and Dr. Ildikó Szabó for her help in the cell culture laboratory.

I would like to thank Dr. Gitta Schlosser for all her support and guidance in mass spectrometry. She always took some time for my questions and experiments, even in the busiest moments and especially in the last weeks when I had to finish my PhD project.

Apart from that I would like to thanks all the other members from the Research Group of Peptide Chemistry for the excellent working environment and the great time in Budapest. I

especially thank Kata Nóra Enyedi and Lilla Pethő who helped and advised me when I had some problems and who measured plenty of MS samples within the first year.

Moreover, I am very grateful to Dr. József Tóvári and all members of the research group. My special thanks go to the coworkers who were involved in the *in vivo* experiments related to my PhD topic. In particular, I would like to Ivan Ranđelović for all his big help and support, as well as for introducing me to the cell culture laboratory and always finding the possibility to share the cell culture facilities. He is one of the kindest and most helpful person I have ever met. Besides, I want to thank Bence Kapuvári for the great collaboration.

I would also like to express my thanks to all employees of Heidelberg Pharma and the great three months. I particularly want to thank Professor Dr. Andreas Pahl, Dr. Christoph Müller and Dr. Torsten Hechler for the strong support and their expertise. Moreover, I am very thankful to Barbara Korsak, Francesca Gallo and Nicole Straube for the warm welcome, providing me a very nice work environment and offering me their help.

I am also very grateful to Professor Dr. Cesare Gennari from the Department of Organic Chemistry (University of Milan) and all members of the research group who supported and encouraged me within the three months in Milan. A special thank goes to Ariana Pina and Mattia Cettolin, but also to all the other *ragazzi* who supported me during this period and filled it with great memories.

I would like to express my gratitude to Professor Dr. Ines Neundorf from the Department of Chemistry (University of Cologne) and all members of the research group for the great help and friendly welcome. In particular I want to thank Annika Klimpel for her strong support and her exceptional helpfulness. Without her, my time in Cologne would not be as great as it was. Moreover, I am especially grateful to my good friend and collaborator Lucia Feni for the valuable collaboration and her big help with the CPPs and our 'love-peptide'. It is my special wish to thank her for being so fantastic and wonderfully crazy. I am so happy that I met her and that we experienced all the great moments, including the special and stupid adventure in Rimini.

Moreover, I would like to thank all members of the European Training Network MAGICBULLET. In particularly I want to express my appreciation to Professor Dr. Norbert Sewald and Dr. Marcel Frese from the University of Bielefeld for the excellent organization of the network and the strong support within the four years. In addition, I would like to thank all members of his research group for the nice collaboration which arose during the last years. My special thanks go to Adina Noémi Borbély for all her

efforts and commitment of our shared project, as well as for her very friendly and helpful manner. Moreover, I would also like to thank Eduard Figueras Agustí for all his valuable remarks and for the great experiences together in Milan.

I want to thank Professor Dr. László Kőhidai for giving me the opportunity to work in the laboratories. In addition, I am thankful to all members of the research group for their support and helpfulness.

I want to thank the work of Professor Dr. Gábor Halmos and all coworkers who performed the receptor binding studies and supported me with valuable data. Besides, I would like to thank Dr. János Gardi who produced and provided the radioiodinated triptorelin.

My thanks go to Bálint Szeder and Professor Dr. László Buday for supporting my project and recording the excellent confocal microscopy images.

I would like to thank Kristóf Hegedüs who produced and provided the 2-pyrrolino-daunorubicin.

Ganz besonders möchte ich mich bei all meinen Freunden und meiner Familie bedanken, die trotz der großen Entfernung immer für mich da waren and mich immer unterstütz haben, mich in den richtigen Momenten aufgeheitert und abgelenkt haben, aber mir auch die Zeit and Ruhe gelassen haben, die notwendig war um dieses Ziel zu erreichen.

Ganz besonders möchte ich mich bei Christian Henze bedanken, der seit vier Jahren immer für mich da ist und trotz der Entfernung nicht aufgehört hat an uns zu glauben und mir so viel Vertrauen entgegengebracht hat. Der bereit war mich überall besuchen zu kommen und der fast jeden Tag mit mir telefoniert hat, um sich meine großen und kleinen Sorgen geduldig anzuhören. Es ist nicht leicht, jemanden zu finden, der zugleich Freund, Partner und hilfreicher Berater ist. Ohne diesen Rückhalt wäre dies alles undenkbar gewesen. Danke für alles was war, ist und noch sein wird!

Nicht zuletzt gebührt meinen Eltern der wohl größte Dank, da sie mich bei all meinen Wegen unterstützt haben. Egal ob zu Hause, in der Schule, der Lehre, im späteren Beruf, oder während der Zeit des Abiturs, des Studiums und natürlich auch wahrend des Promotionsstudiums, sie waren und sind immer für mich da und haben mich nach Kräften unterstützt. Ich hoffe sehr, dass sich das niemals ändern wird. Ohne meine Eltern wäre all dies nicht möglich gewesen and ich möchte mich besonders für all die finanzielle, sowie seelische und moralische Unterstützung bedanken, die sie mir all die Jahre entgegengebracht haben.

Finally, I would like to express my appreciation to all institutions and organizations who provided the financial support for my PhD project and related research.

This work was supported by the European Union's Horizon 2020 research and innovation program under the Marie Sklodowska-Curie Grant No 642004, and by the National Research, Development and Innovation Office under grant NKFIH K119552 and NVKP_16-1-2016-0036. Financial resources for the western blot detection system were provided by MedInProt. These studies were also supported by grant (VEKOP-2.3.3-15-2017-00020) from the European Union and the State of Hungary, co-financed by the European Regional Development Fund.

8. Publication list

8.1. Research articles

Publications in frame of the PhD project

Schuster, S.; Biri-Kovács, B.; Szeder, B.; Farkas, V.; Buday, L.; Szabó, Z.; Halmos, G.; Mező, G. Synthesis and in vitro biochemical evaluation of oxime bond-linked daunorubicin–GnRH-III conjugates developed for targeted drug delivery. *Beilstein J. Org. Chem*. **2018**, *14*, 756–771. [doi:10.3762/bjoc.14.64]

Schuster, S.; Biri-Kovács, B.; Szeder, B.; Buday, L.; Gardi, J.; Szabó, Z.; Halmos, G.; Mező, G. Enhanced In Vitro Antitumor Activity of GnRH-III-Daunorubicin Bioconjugates Influenced by Sequence Modification. *Pharmaceutics.* **2018**, *10*(4), 223-242. [doi:10.3390/pharmaceutics10040223]

Further publications

Schuster, S.; Roessler, C.; Meleshin, M.; Zimmermann, P.; Simic, Z.; Kambach, C.; Schiene-Fischer, C.; Steegborn, C.; Hottiger, M.O.; Schutkowski, M. A continuous sirtuin activity assay without any coupling to enzymatic or chemical reactions. *Sci Rep*. **2016**, *6*, 22643. [doi:10.1038/srep22643]

8.2. Conference proceedings

Schuster, S.; Biri-Kovács, B.; Borbély, A.; Sewald, N.; Neundorf, I.; Gennari, C.;, Mező, G. Synthesis and biochemical evaluation of GnRH-III drug conjugates. *In: Patrick B. Timmons, Chandralal M. Hewage, Michal Lebl (eds) Proceedings of 35th European Peptide Symposium*. **2018**. 80-83

Schuster, S.; Biri-Kovács, B.; Mező, G. Influence of sequence modification in GnRH-III on the efficiency of tumour targeting. *In: A. Beck-Sickinger, K. Mörl, K. Bellmann-Sickert, S. Els-Heindl, U. Diederichsen (eds.) Proceedings of 34th European Peptide Symposium*. **2017**. 167-168

8.3. Conference participations

Synthesis and biochemical characterization of GnRH-III drug conjugates.

Schuster, S.; Biri-Kovács, B.; Neundorf, I.; Gennari, C.;, Mező, G. *Chemistry towards Biology (CTB9)*, **September 2019**, Budapest – Hungary, oral presentation

Synthesis and biochemical evaluation of GnRH-III drug conjugates.

Schuster, S.; Biri-Kovács, B.; Borbély, A.; Sewald, N.; Neundorf, I.; Gennari, C.; Mező, G. *35th European Peptide Symposium,* **August 2018**, Dublin – Ireland, oral presentation

Synthesis and biochemical evaluation of oxime bond-linked daunorubicin-GnRH-III conjugates.
Schuster, S.; Biri-Kovács, B.; Mező, G. *RiminiPeptides2018*, **June 2018**, Rimini – Italy, oral presentation

Effect of GnRH-III peptide-drug bio-conjugates on tumor growth *in vitro* and *in vivo.*
Ranđelović, I.; **Schuster, S.**; Kapuvári, B.; Mező, G.; Tóvári, J. *RiminiPeptides2018*, **June 2018**, Rimini – Italy, oral presentation given by Ivan Ranđelović

Development and biochemical characterization of self-immolative linker-containing GnRH-III-drug conjugates.
Schuster, S.; Gennari, C.; Neundorf, I.; Mező, G. *RiminiPeptides2018*, **June 2018**, Rimini – Italy, poster presentation

Development of novel GnRH-III-based drug delivery systems as potential anticancer drugs.
Schuster, S.; Biri-Kovács, B.; Szeder, B.; Buday, L.; Gennari, C.; Mező, G. *Hungarian Peptide Symposium*, **May 2017**, Balatonszemes – Hungary, oral presentation

Influence of sequence modification in GnRH-III on the efficiency of tumour targeting.
Schuster, S.; Biri-Kovács, B.; Mező, G. *34th European Peptide Symposium,* **September 2016**, Leipzig – Germany, poster appetizer (3 minutes presentation) & poster presentation

Influence of sequence modification in GnRH-III on the efficiency of tumour targeting.
Schuster, S.; Biri-Kovács, B.; Mező, G. *15th Naples Workshop on Bioactive Peptides,* **June 2016**, Naples – Italy, oral presentation

Influence of sequence modification in GnRH-III on the efficiency of tumor targeting.
Schuster, S.; Biri-Kovács, B.; Mező, G. *Hungarian Peptide Symposium*, **May 2016**, Balatonszemes – Hungary, oral presentation

9. References

[1] "Non communicable diseases," can be found under https://www.who.int/news-room/fact-sheets/detail/noncommunicable-diseases, **n.d.**

[2] "WHO | Cancer," can be found under http://www.who.int/cancer/en/, **n.d.**

[3] F. Bray, J. Ferlay, I. Soerjomataram, R. L. Siegel, L. A. Torre, A. Jemal, *CA. Cancer J. Clin.* **2018**, *68*, 394–424.

[4] S. BW, W. CP, *World Cancer Report 2014*, **n.d.**

[5] D. Belpomme, P. Irigaray, A. J. Sasco, J. A. Newby, V. Howard, R. Clapp, L. Hardell, *Int. J. Oncol.* **2007**, *30*, 1037–1049.

[6] P. Kanavos, *Ann. Oncol. Off. J. Eur. Soc. Med. Oncol.* **2006**, *17 Suppl 8*, viii15–viii23.

[7] "What Is Cancer?," can be found under https://www.cancer.gov/about-cancer/understanding/what-is-cancer, **2007**.

[8] D. Hanahan, R. A. Weinberg, *Cell* **2000**, *100*, 57–70.

[9] D. Hanahan, R. A. Weinberg, *Cell* **2011**, *144*, 646–674.

[10] S. Negrini, V. G. Gorgoulis, T. D. Halazonetis, *Nat. Rev. Mol. Cell Biol.* **2010**, *11*, 220–228.

[11] J. J. Salk, E. J. Fox, L. A. Loeb, *Annu. Rev. Pathol.* **2010**, *5*, 51–75.

[12] J. Korkola, J. W. Gray, *Curr. Opin. Genet. Dev.* **2010**, *20*, 4–14.

[13] H. F. Dvorak, *N. Engl. J. Med.* **1986**, *315*, 1650–1659.

[14] F. Pagès, J. Galon, M.-C. Dieu-Nosjean, E. Tartour, C. Sautès-Fridman, W.-H. Fridman, *Oncogene* **2010**, *29*, 1093–1102.

[15] D. G. DeNardo, P. Andreu, L. M. Coussens, *Cancer Metastasis Rev.* **2010**, *29*, 309–316.

[16] S. I. Grivennikov, F. R. Greten, M. Karin, *Cell* **2010**, *140*, 883–899.

[17] B.-Z. Qian, J. W. Pollard, *Cell* **2010**, *141*, 39–51.

[18] A. E. Karnoub, R. A. Weinberg, *Breast Dis.* **2006**, *26*, 75–85.

[19] J. E. Long, M. J. Wongchenko, D. Nickles, W.-J. Chung, B. Wang, J. Riegler, J. Li, Q. Li, W. Sandoval, J. Eastham-Anderson, et al., *Cell Death Differ.* **2019**, 1.

[20] L. Wyld, R. A. Audisio, G. J. Poston, *Nat. Rev. Clin. Oncol.* **2015**, *12*, 115–124.

[21] V. T. DeVita, E. Chu, *Cancer Res.* **2008**, *68*, 8643–8653.

[22] B. A. Chabner, T. G. Roberts, *Nat. Rev. Cancer* **2005**, *5*, 65–72.

[23] M. Baumann, M. Krause, J. Overgaard, J. Debus, S. M. Bentzen, J. Daartz, C. Richter, D. Zips, T. Bortfeld, *Nat. Rev. Cancer* **2016**, *16*, 234–249.

[24] R. Baskar, K. A. Lee, R. Yeo, K.-W. Yeoh, *Int. J. Med. Sci.* **2012**, *9*, 193–199.

[25] W. S. Halsted, *Ann. Surg.* **1894**, *20*, 497–555.

[26] A. Urruticoechea, R. Alemany, J. Balart, A. Villanueva, F. Viñals, G. Capellá, *Curr. Pharm. Des.* **2010**, *16*, 3–10.

[27] S. Puhalla, S. Bhattacharya, N. E. Davidson, *Mol. Oncol.* **2012**, *6*, 222–236.

[28] E. D. Crawford, *Rev. Urol.* **2004**, *6*, S3–S11.

[29] I. H. Abdulkareem, I. B. Zurmi, *Niger. J. Clin. Pract.* **2012**, *15*, 9–14.

[30] F. Labrie, A. Bélanger, V. Luu-The, C. Labrie, J. Simard, L. Cusan, J. Gomez, B. Candas, *Endocr. Rev.* **2005**, *26*, 361–379.

[31] B. M. Evers, D. Parekh, C. M. Townsend, J. C. Thompson, *Ann. Surg.* **1991**, *213*, 190–198.

[32] C. Sawyers, *Nature* **2004**, *432*, 294–297.

[33] V. V. Padma, *BioMedicine* **2015**, *5*, 19.

[34] Z.-R. Lu, P. Qiao, *Mol. Pharm.* **2018**, *15*, 3603–3616.

[35] C. G. Drake, E. J. Lipson, J. R. Brahmer, *Nat. Rev. Clin. Oncol.* **2014**, *11*, 24–37.

[36] J. W. Hadden, *Int. J. Immunopharmacol.* **1999**, *21*, 79–101.

[37] R. E. Hardy, E. V. Ikpeazu, *J. Natl. Med. Assoc.* **1989**, *81*, 518–523.
[38] E. Frei, K. Antman, B. Teicher, P. Eder, L. Schnipper, *J. Clin. Oncol.* **1989**, *7*, 515–526.
[39] M. Verma, *J. Pers. Med.* **2012**, *2*, 1–14.
[40] O. of the Commissioner, "Press Announcements - FDA approves first cancer treatment for any solid tumor with a specific genetic feature," can be found under https://www.fda.gov/NewsEvents/Newsroom/PressAnnouncements/ucm560167.htm, **n.d.**
[41] K. Gao, D. Wang, Y. Huang, *Cancer Inform.* **2018**, *17*, 1176935118805398.
[42] W. Goldberg, E. London, *Dermatol Z 190310457–62* **n.d.**
[43] R. F. Mould, *Curr. Oncol.* **2007**, *14*, 118–122.
[44] L. G. Larsson, *Acta Oncol. Stockh. Swed.* **1995**, *34*, 1011–1015.
[45] *J. Int. Comm. Radiat. Units Meas.* **2010**, *10*, NP-NP.
[46] D. Schulz-Ertner, H. Tsujii, *J. Clin. Oncol. Off. J. Am. Soc. Clin. Oncol.* **2007**, *25*, 953–964.
[47] C.-M. C. Ma, R. L. Maughan, *Med. Phys.* **2006**, *33*, 571–573.
[48] B. R. Thomadsen, J. F. Williamson, M. J. Rivard, A. S. Meigooni, *Med. Phys.* **2008**, *35*, 4708–4723.
[49] M. J. Rivard, J. L. M. Venselaar, L. Beaulieu, *Med. Phys.* **2009**, *36*, 2136–2153.
[50] T. Barwick, L. Bretsztajn, K. Wallitt, D. Amiras, A. Rockall, C. Messiou, *Br. J. Radiol.* **2019**, *92*, 20180768.
[51] M. Pasler, V. Hernandez, N. Jornet, C. H. Clark, *Phys. Imaging Radiat. Oncol.* **2018**, *5*, 76–84.
[52] G. C. Barnett, C. M. L. West, A. M. Dunning, R. M. Elliott, C. E. Coles, P. D. P. Pharoah, N. G. Burnet, *Nat. Rev. Cancer* **2009**, *9*, 134–142.
[53] S. Bhide, C. Nutting, *BMC Med.* **2010**, *8*, 25.
[54] R. S. Lee, J. Batke, L. Weir, N. Dea, C. G. Fisher, *J. Spine Surg.* **2018**, *4*, 368–373.
[55] Y. Wang, W. Deng, N. Li, S. Neri, A. Sharma, W. Jiang, S. H. Lin, *Front. Pharmacol.* **2018**, *9*, DOI 10.3389/fphar.2018.00185.
[56] R. de Haan, D. Pluim, B. van Triest, M. van den Heuvel, H. Peulen, D. van Berlo, J. George, M. Verheij, J. H. M. Schellens, C. Vens, *Radiother. Oncol.* **2018**, *126*, 443–449.
[57] J. Chen, T. Su, Y. Lin, B. Wang, J. Li, J. Pan, C. Chen, *Clin. Transl. Oncol.* **2018**, *20*, 411–419.
[58] C. Yang, K. Bromma, W. Sung, J. Schuemann, D. Chithrani, *Cancers* **2018**, *10*, 150.
[59] P. Ehrlich, *Frankf. Ztg. Handel. Zweites Morgenbl. 51* **n.d.**
[60] G. Androutsos, *J. BUON Off. J. Balk. Union Oncol.* **2004**, *9*, 485–491.
[61] F. Stern, *Angew. Chem. Int. Ed.* **2004**, *43*, 4254–4261.
[62] P. Ehrlich, **1910**.
[63] P. Valent, B. Groner, U. Schumacher, G. Superti-Furga, M. Busslinger, R. Kralovics, C. Zielinski, J. M. Penninger, D. Kerjaschki, G. Stingl, et al., *J. Innate Immun.* **2016**, *8*, 111–120.
[64] B. Witkop, *Proc. Am. Philos. Soc.* **1999**, *143*, 540–557.
[65] S. Farber, L. K. Diamond, R. D. Mercer, R. F. Sylvester, J. A. Wolff, *N. Engl. J. Med.* **1948**, *238*, 787–793.
[66] K. Strebhardt, A. Ullrich, *Nat. Rev. Cancer* **2008**, *8*, 473–480.
[67] L. M. Meyer, F. R. Miller, M. J. Rowen, G. Bock, J. Rutzky, *Acta Haematol.* **1950**, *4*, 157–167.
[68] V. V. Shah, E. J. Lin, S. P. Reddy, J. J. Wu, in *Ther. Sev. Psoriasis* (Eds.: J.J. Wu, S.R. Feldman, M.G. Lebwohl), Elsevier, **2016**, pp. 37–48.

[69] "Methotrexate," can be found under https://www.cancer.gov/about-cancer/treatment/drugs/methotrexate, **2008**.
[70] G. D. Weinstein, *Ann. Intern. Med.* **1977**, *86*, 199–204.
[71] C. Wagener, C. Stocking, O. Müller, *Cancer Signaling, Enhanced Edition: From Molecular Biology to Targeted Therapy*, John Wiley & Sons, **2017**.
[72] "Mechlorethamine," can be found under https://www.drugbank.ca/drugs/DB00888, **n.d.**
[73] A. Polavarapu, J. A. Stillabower, S. G. W. Stubblefield, W. M. Taylor, M.-H. Baik, *J. Org. Chem.* **2012**, *77*, 5914–5921.
[74] V. Goede, B. Eichhorst, K. Fischer, C.-M. Wendtner, M. Hallek, *Leuk. Lymphoma* **2015**, *56*, 1585–1592.
[75] S. Dasari, P. B. Tchounwou, *Eur. J. Pharmacol.* **2014**, *0*, 364–378.
[76] J. D. Watson, F. H. C. Crick, *Nature* **1953**, *171*, 737.
[77] C. Heidelberger, N. K. Chaudhuri, P. Danneberg, D. Mooren, L. Griesbach, R. Duschinsky, R. J. Schnitzer, E. Pleven, J. Scheiner, *Nature* **1957**, *179*, 663.
[78] D. B. Longley, D. P. Harkin, P. G. Johnston, *Nat. Rev. Cancer* **2003**, *3*, 330–338.
[79] P. G. Corrie, *Medicine (Baltimore)* **2008**, *36*, 24–28.
[80] C. Gründker, G. Emons, *Front. Endocrinol.* **2017**, *8*, 187.
[81] M. Di Marco, R. Di Cicilia, M. Macchini, E. Nobili, S. Vecchiarelli, G. Brandi, G. Biasco, *Oncol. Rep.* **2010**, *23*, 1183–1192.
[82] A. Vincent, J. Herman, R. Schulick, R. H. Hruban, M. Goggins, *The Lancet* **2011**, *378*, 607–620.
[83] K. A. Sauter, L. J. Wood, J. Wong, M. Iordanov, B. E. Magun, *Cancer Biol. Ther.* **2011**, *11*, 1008–1016.
[84] K. K. Kwok, E. C. Vincent, J. N. Gibson, in *Pharmacol. Ther. Dent. Seventh Ed.* (Eds.: F.J. Dowd, B.S. Johnson, A.J. Mariotti), Mosby, **2017**, pp. 530–562.
[85] J. V. McGowan, R. Chung, A. Maulik, I. Piotrowska, J. M. Walker, D. M. Yellon, *Cardiovasc. Drugs Ther.* **2017**, *31*, 63–75.
[86] R. C. Donehower, *The Oncologist* **1996**, *1*, 240–243.
[87] S. Kokkali, E.-S. Tripodaki, M. Drizou, D. Stefanou, E. Magou, D. Zylis, M. Kapiris, D. Nasi, C. Georganta, A. Ardavanis, *In Vivo* **2018**, *32*, 653–657.
[88] D. D. Von Hoff, T. Ervin, F. P. Arena, E. G. Chiorean, J. Infante, M. Moore, T. Seay, S. A. Tjulandin, W. W. Ma, M. N. Saleh, et al., *N. Engl. J. Med.* **2013**, *369*, 1691–1703.
[89] A. Vogel, F. Kullmann, V. Kunzmann, S.-E. Al-Batran, H. Oettle, R. Plentz, J. Siveke, C. Springfeld, H. Riess, *Oncol. Res. Treat.* **2015**, *38*, 596–603.
[90] D. H. Ahn, K. Krishna, M. Blazer, J. Reardon, L. Wei, C. Wu, K. K. Ciombor, A. M. Noonan, S. Mikhail, T. Bekaii-Saab, *Ther. Adv. Med. Oncol.* **2017**, *9*, 75–82.
[91] R. D. Winefield, R. A. Entwistle, T. B. Foland, G. H. Lushington, R. H. Himes, *ChemMedChem* **2008**, *3*, 1844–1847.
[92] C. Villanueva, F. Bazan, S. Kim, M. Demarchi, L. Chaigneau, A. Thiery-Vuillemin, T. Nguyen, L. Cals, E. Dobi, X. Pivot, *Drugs* **2011**, *71*, 1251–1258.
[93] W. G. Nelson, H. B. Carter, T. L. DeWeese, E. S. Antonarakis, M. A. Eisenberger, in *Abeloffs Clin. Oncol. Fifth Ed.* (Eds.: J.E. Niederhuber, J.O. Armitage, J.H. Doroshow, M.B. Kastan, J.E. Tepper), Content Repository Only!, Philadelphia, **2014**, pp. 1463-1496.e9.
[94] G. T. Beatson, *Trans. Medico-Chir. Soc. Edinb.* **1896**, *15*, 153–179.
[95] A. K. Shiau, D. Barstad, P. M. Loria, L. Cheng, P. J. Kushner, D. A. Agard, G. L. Greene, *Cell* **1998**, *95*, 927–937.
[96] A. V. Schally, A. Arimura, Y. Baba, R. M. G. Nair, H. Matsuo, T. W. Redding, L. Debeljuk, W. F. White, *Biochem. Biophys. Res. Commun.* **1971**, *43*, 393–399.

[97] P. M. Conn, W. F. Crowley, *Annu. Rev. Med.* **1994**, *45*, 391–405.
[98] P. Limonta, M. Montagnani Marelli, S. Mai, M. Motta, L. Martini, R. M. Moretti, *Endocr. Rev.* **2012**, *33*, 784–811.
[99] G. Mezo, in *Amino Acids Pept. Proteins*, **2013**, pp. 203–252.
[100] R. P. Millar, *Anim. Reprod. Sci.* **2005**, *88*, 5–28.
[101] S. C. Sealfon, H. Weinstein, R. P. Millar, *Endocr. Rev.* **1997**, *18*, 180–205.
[102] D. H. Coy, J. A. Vilchez-Martinez, E. J. Coy, A. V. Schally, *J. Med. Chem.* **1976**, *19*, 423–425.
[103] J. J. Nestor, T. L. Ho, R. A. Simpson, B. L. Horner, G. H. Jones, G. I. McRae, B. H. Vickery, *J. Med. Chem.* **1982**, *25*, 795–801.
[104] M. Fujino, T. Fukuda, S. Shinagawa, S. Kobayashi, I. Yamazaki, *Biochem. Biophys. Res. Commun.* **1974**, *60*, 406–413.
[105] W. Wiegelmann, H. G. Solbach, H. K. Kley, E. Nieschlag, K. H. Rudorff, H. L. Krüskemper, *Horm. Res.* **1976**, *7*, 1–10.
[106] A. S. Dutta, B. J. Furr, M. B. Giles, B. Valcaccia, A. L. Walpole, *Biochem. Biophys. Res. Commun.* **1978**, *81*, 382–390.
[107] A. M. Padula, *Anim. Reprod. Sci.* **2005**, *88*, 115–126.
[108] G. Mezo, M. Manea, *Expert Opin. Ther. Pat.* **2009**, *19*, 1771–1785.
[109] A. Schultze-Mosgau, G. Griesinger, C. Altgassen, S. von Otte, D. Hornung, K. Diedrich, *Expert Opin. Investig. Drugs* **2005**, *14*, 1085–1097.
[110] C. Chen, D. Wu, Z. Guo, Q. Xie, G. J. Reinhart, A. Madan, J. Wen, T. Chen, C. Q. Huang, M. Chen, et al., *J. Med. Chem.* **2008**, *51*, 7478–7485.
[111] M. Ezzati, B. R. Carr, *Womens Health Lond. Engl.* **2015**, *11*, 19–28.
[112] "Drugs@FDA: FDA Approved Drug Products," can be found under https://www.accessdata.fda.gov/scripts/cder/daf/index.cfm?event=overview.process&varApplNo=210450, **n.d.**
[113] A. Nagy, A. V. Schally, *Biol. Reprod.* **2005**, *73*, 851–859.
[114] O. Taratula, O. B. Garbuzenko, A. M. Chen, T. Minko, *J. Drug Target.* **2011**, *19*, 900–914.
[115] A. V. Schally, G. Srkalovic, B. Szende, T. W. Redding, T. Janaky, A. Juhasz, E. Korkut, R. Z. Cai, K. Szepeshazi, S. Radulovic, *J. Steroid Biochem. Mol. Biol.* **1990**, *37*, 1061–1067.
[116] W. R. Miller, W. N. Scott, R. Morris, H. M. Fraser, R. M. Sharpe, *Nature* **1985**, *313*, 231–233.
[117] C. Gründker, A. R. Günthert, S. Westphalen, G. Emons, *Eur. J. Endocrinol.* **2002**, *146*, 1–14.
[118] P. Limonta, R. M. Moretti, M. Montagnani Marelli, M. Motta, *Front. Neuroendocrinol.* **2003**, *24*, 279–295.
[119] R. M. Moretti, M. Monagnani Marelli, J. C. van Groeninghen, M. Motta, P. Limonta, *Endocr. Relat. Cancer* **2003**, *10*, 161–167.
[120] M. Montagnani Marelli, R. M. Moretti, J. Januszkiewicz-Caulier, M. Motta, P. Limonta, *Curr. Cancer Drug Targets* **2006**, *6*, 257–269.
[121] T. Yano, J. Pinski, S. Radulovic, A. V. Schally, *Proc. Natl. Acad. Sci. U. S. A.* **1994**, *91*, 1701–1705.
[122] L. W. T. Cheung, A. S. T. Wong, *FEBS J.* **2008**, *275*, 5479–5495.
[123] W.-K. So, J.-C. Cheng, S.-L. Poon, P. C. K. Leung, *FEBS J.* **2008**, *275*, 5496–5511.
[124] C. Gründker, G. Emons, *Reprod. Biol. Endocrinol. RBE* **2003**, *1*, 65.
[125] R. P. Millar, A. J. Pawson, K. Morgan, E. F. Rissman, Z.-L. Lu, *Front. Neuroendocrinol.* **2008**, *29*, 17–35.

[126] D. Dondi, P. Limonta, R. M. Moretti, M. M. Marelli, E. Garattini, M. Motta, *Cancer Res.* **1994**, *54*, 4091–4095.
[127] C. Gründker, P. Völker, G. Emons, *Endocrinology* **2001**, *142*, 2369–2380.
[128] R. M. Moretti, M. M. Marelli, D. Dondi, A. Poletti, L. Martini, M. Motta, P. Limonta, *J. Clin. Endocrinol. Metab.* **1996**, *81*, 3930–3937.
[129] S. S. Kakar, W. E. Grizzle, J. D. Neill, *Mol. Cell. Endocrinol.* **1994**, *106*, 145–149.
[130] A. Imai, T. Ohno, K. Iida, T. Fuseya, T. Furui, T. Tamaya, *Gynecol. Oncol.* **1994**, *55*, 144–148.
[131] R. P. Millar, Z.-L. Lu, A. J. Pawson, C. A. Flanagan, K. Morgan, S. R. Maudsley, *Endocr. Rev.* **2004**, *25*, 235–275.
[132] R. P. Millar, A. J. Pawson, *Endocrinology* **2004**, *145*, 3590–3593.
[133] R. B. White, J. A. Eisen, T. L. Kasten, R. D. Fernald, *Proc. Natl. Acad. Sci. U. S. A.* **1998**, *95*, 305–309.
[134] C. Gründker, A. R. Günthert, R. P. Millar, G. Emons, *J. Clin. Endocrinol. Metab.* **2002**, *87*, 1427–1430.
[135] M. M. Montagnani, R. M. Moretti, S. Mai, J. Januszkiewicz-Caulier, M. Motta, P. Limonta, *J. Clin. Endocrinol. Metab.* **2009**, *94*, 1761–1767.
[136] S. A. Sower, Y. C. Chiang, S. Lovas, J. M. Conlon, *Endocrinology* **1993**, *132*, 1125–1131.
[137] S. Lovas, I. Pályi, B. Vincze, J. Horváth, M. Kovács, I. Mezö, G. Tóth, I. Teplán, R. F. Murphy, *J. Pept. Res. Off. J. Am. Pept. Soc.* **1998**, *52*, 384–389.
[138] M. Kovács, B. Vincze, J. E. Horváth, J. Seprődi, *Peptides* **2007**, *28*, 821–829.
[139] M. Kovacs, J. Seprodi, M. Koppan, J. E. Horvath, B. Vincze, I. Teplan, B. Flerko, *J. Neuroendocrinol.* **2002**, *14*, 647–655.
[140] M. Fekete, S. Bajusz, K. Groot, V. J. Csernus, A. V. Schally, *Endocrinology* **1989**, *124*, 946–955.
[141] I. Mezö, S. Lovas, I. Pályi, B. Vincze, A. Kálnay, G. Turi, Z. Vadász, J. Seprödi, M. Idei, G. Tóth, et al., *J. Med. Chem.* **1997**, *40*, 3353–3358.
[142] E. V. Pappa, A. A. Zompra, Z. Diamantopoulou, Z. Spyranti, G. Pairas, F. N. Lamari, P. Katsoris, G. A. Spyroulias, P. Cordopatis, *Biopolymers* **2012**, *98*, 525–534.
[143] G. Mező, A. Czajlik, M. Manea, A. Jakab, V. Farkas, Z. Majer, E. Vass, A. Bodor, B. Kapuvári, M. Boldizsár, et al., *Peptides* **2007**, *28*, 806–820.
[144] K. Zarogoulidis, E. Eleftheriadou, T. Kontakiotis, G. Gerasimou, P. Zarogoulidis, I. Sapardanis, G. Galaktidou, L. Sakkas, A. Gotzamani-Psarrakou, N. Karatzas, *Lung Cancer Amst. Neth.* **2012**, *76*, 84–88.
[145] A. Arimura, J. B. Fishback, *Neuroendocrinology* **1981**, *33*, 246–256.
[146] P. Rorsman, M. O. Huising, *Nat. Rev. Endocrinol.* **2018**, *14*, 404–414.
[147] O. Keskin, S. Yalcin, *OncoTargets Ther.* **2013**, *6*, 471–483.
[148] L. P. Shen, R. L. Pictet, W. J. Rutter, *Proc. Natl. Acad. Sci.* **1982**, *79*, 4575–4579.
[149] G. Tulipano, S. Schulz, *Eur. J. Endocrinol.* **2007**, *156*, S3–S11.
[150] K. Sharma, C. B. Srikant, *Int. J. Cancer* **1998**, *76*, 259–266.
[151] P. Dasgupta, *Pharmacol. Ther.* **2004**, *102*, 61–85.
[152] "Somatuline® Depot (lanreotide) for GEP-NETs & Carcinoid Syndrome," can be found under https://www.somatulinedepot.com/gn/, **n.d.**
[153] C. Bruns, I. Lewis, U. Briner, G. Meno-Tetang, G. Weckbecker, *Eur. J. Endocrinol.* **2002**, *146*, 707–716.
[154] R. Z. Cai, B. Szoke, R. Lu, D. Fu, T. W. Redding, A. V. Schally, *Proc. Natl. Acad. Sci. U. S. A.* **1986**, *83*, 1896–1900.
[155] A. V. Schally, *Cancer Res.* **1988**, *48*, 6977–6985.

[156] M. Goomann, X. Jiang, J. Igarashi, H. Li, T.-A. Tran, R.-H. Mattern, in *Pept. Sci. — Present Future Proc. 1st Int. Pept. Symp.* (Ed.: Y. Shimonishi), Springer Netherlands, Dordrecht, **2002**, pp. 342–345.
[157] G. Kéri, I. Mezo, Z. Vadasz, A. Horvath, M. Idei, T. Vántus, A. Balogh, G. Bokonyi, T. Bajor, I. Teplan, et al., *Pept. Res.* **1993**, *6*, 281–288.
[158] G. Kéri, J. Erchegyi, A. Horváth, I. Mezõ, M. Idei, T. Vántus, A. Balogh, Z. Vadász, G. Bökönyi, J. Seprõdi, et al., *Proc. Natl. Acad. Sci. U. S. A.* **1996**, *93*, 12513–12518.
[159] A. Steták, P. Csermely, A. Ullrich, G. Kéri, *Biochem. Biophys. Res. Commun.* **2001**, *288*, 564–572.
[160] J.-U. Lee, R. Hosotani, M. Wada, R. Doi, T. Koshiba, K. Fujimoto, Y. Miyamoto, S. Tsuji, S. Nakajima, M. Hirohashi, et al., *Eur. J. Cancer Oxf. Engl. 1990* **2002**, *38*, 1526–1534.
[161] Z. Helyes, E. Pintér, J. Szolcsányi, *Drugs Future* **2005**, *30*, 558–566.
[162] L. Dai, J. Liu, Z. Luo, M. Li, K. Cai, *J. Mater. Chem. B* **2016**, *4*, 6758–6772.
[163] H. Gharwan, H. Groninger, *Nat. Rev. Clin. Oncol.* **2016**, *13*, 209–227.
[164] J. Zhang, P. L. Yang, N. S. Gray, *Nat. Rev. Cancer* **2009**, *9*, 28–39.
[165] H. M. Shepard, P. Jin, D. J. Slamon, Z. Pirot, D. C. Maneval, *Handb. Exp. Pharmacol.* **2008**, 183–219.
[166] "FDA Approval Trastuzumab," can be found under https://www.accessdata.fda.gov/drugsatfda_docs/appletter/1998/trasgen092598L.pdf, **1998**.
[167] J. Baselga, J. Albanell, M. A. Molina, J. Arribas, *Semin. Oncol.* **2001**, *28*, 4–11.
[168] M. X. Sliwkowski, J. A. Lofgren, G. D. Lewis, T. E. Hotaling, B. M. Fendly, J. A. Fox, *Semin. Oncol.* **1999**, *26*, 60–70.
[169] R. Nahta, F. J. Esteva, *Breast Cancer Res.* **2006**, *8*, 215.
[170] Y. Izumi, L. Xu, E. di Tomaso, D. Fukumura, R. K. Jain, *Nature* **2002**, *416*, 279.
[171] K. S. Klos, X. Zhou, S. Lee, L. Zhang, W. Yang, Y. Nagata, D. Yu, *Cancer* **2003**, *98*, 1377–1385.
[172] X.-F. Wen, G. Yang, W. Mao, A. Thornton, J. Liu, R. C. Bast, X.-F. Le, *Oncogene* **2006**, *25*, 6986–6996.
[173] F. R. Wilson, M. E. Coombes, Q. Wylie, M. Yurchenko, C. Brezden-Masley, B. Hutton, B. Skidmore, C. Cameron, *Syst. Rev.* **2017**, *6*, 196.
[174] H. Kaplon, J. M. Reichert, *mAbs* **2019**, *11*, 219–238.
[175] G. Mathe, L. O. C. Tran Ba, J. Bernard, *Comptes Rendus Hebd. Seances Acad. Sci.* **1958**, *246*, 1626–1628.
[176] K. Tsuchikama, Z. An, *Protein Cell* **2018**, *9*, 33–46.
[177] G. Köhler, C. Milstein, *Nature* **1975**, *256*, 495.
[178] C. H. Ford, C. E. Newman, J. R. Johnson, C. S. Woodhouse, T. A. Reeder, G. F. Rowland, R. G. Simmonds, *Br. J. Cancer* **1983**, *47*, 35–42.
[179] R. V. J. Chari, M. L. Miller, W. C. Widdison, *Angew. Chem. Int. Ed Engl.* **2014**, *53*, 3796–3827.
[180] H. E. Chadd, S. M. Chamow, *Curr. Opin. Biotechnol.* **2001**, *12*, 188–194.
[181] G. P. Smith, *Science* **1985**, *228*, 1315–1317.
[182] N. Lonberg, D. Huszar, *Int. Rev. Immunol.* **1995**, *13*, 65–93.
[183] P. F. Bross, J. Beitz, G. Chen, X. H. Chen, E. Duffy, L. Kieffer, S. Roy, R. Sridhara, A. Rahman, G. Williams, et al., *Clin. Cancer Res. Off. J. Am. Assoc. Cancer Res.* **2001**, *7*, 1490–1496.
[184] F. R. Appelbaum, I. D. Bernstein, *Blood* **2017**, *130*, 2373–2376.
[185] P. M. LoRusso, D. Weiss, E. Guardino, S. Girish, M. X. Sliwkowski, *Clin. Cancer Res.* **2011**, *17*, 6437–6447.

[186] S. M. Horwitz, R. H. Advani, N. L. Bartlett, E. D. Jacobsen, J. P. Sharman, O. A. O'Connor, T. Siddiqi, D. A. Kennedy, Y. Oki, *Blood* **2014**, *123*, 3095–3100.
[187] N. M. Okeley, J. B. Miyamoto, X. Zhang, R. J. Sanderson, D. R. Benjamin, E. L. Sievers, P. D. Senter, S. C. Alley, *Clin. Cancer Res.* **2010**, *16*, 888–897.
[188] M. S. K. Sutherland, R. J. Sanderson, K. A. Gordon, J. Andreyka, C. G. Cerveny, C. Yu, T. S. Lewis, D. L. Meyer, R. F. Zabinski, S. O. Doronina, et al., *J. Biol. Chem.* **2006**, *281*, 10540–10547.
[189] I. Schechter, A. Berger, *Biochem. Biophys. Res. Commun.* **1967**, *27*, 157–162.
[190] G. D. Lewis Phillips, G. Li, D. L. Dugger, L. M. Crocker, K. L. Parsons, E. Mai, W. A. Blättler, J. M. Lambert, R. V. J. Chari, R. J. Lutz, et al., *Cancer Res.* **2008**, *68*, 9280–9290.
[191] A. D. Ricart, *Clin. Cancer Res.* **2011**, *17*, 6417–6427.
[192] *ADC Rev.* **n.d.**
[193] R. Dixit, Ph.D, DABT, *ADC Rev.* **2019**.
[194] J. P. Stephan, K. R. Kozak, W. L. T. Wong, *Bioanalysis* **2011**, *3*, 677–700.
[195] J. R. Junutula, H. Raab, S. Clark, S. Bhakta, D. D. Leipold, S. Weir, Y. Chen, M. Simpson, S. P. Tsai, M. S. Dennis, et al., *Nat. Biotechnol.* **2008**, *26*, 925–932.
[196] J. R. Junutula, K. M. Flagella, R. A. Graham, K. L. Parsons, E. Ha, H. Raab, S. Bhakta, T. Nguyen, D. L. Dugger, G. Li, et al., *Clin. Cancer Res. Off. J. Am. Assoc. Cancer Res.* **2010**, *16*, 4769–4778.
[197] S. Bhakta, H. Raab, J. R. Junutula, *Methods Mol. Biol. Clifton NJ* **2013**, *1045*, 189–203.
[198] P. Hofl, *ADC Rev.* **2016**.
[199] M. P. Deonarain, *Drug Discov. Today Technol.* **2018**, *30*, 47–53.
[200] K. Fosgerau, T. Hoffmann, *Drug Discov. Today* **2015**, *20*, 122–128.
[201] M. Hagimori, Y. Fuchigami, S. Kawakami, *Chem. Pharm. Bull. (Tokyo)* **2017**, *65*, 618–624.
[202] L. Raibaut, O. El Mahdi, O. Melnyk, *Top. Curr. Chem.* **2015**, *363*, 103–154.
[203] L. R. Malins, R. J. Payne, *Curr. Opin. Chem. Biol.* **2014**, *22*, 70–78.
[204] L. Di, *AAPS J.* **2014**, *17*, 134–143.
[205] S. P. Shirmardi, M. Gandomkar, M. G. Maragheh, M. Shamsaei, *Cancer Biother. Radiopharm.* **2011**, *26*, 309–316.
[206] A. V. Schally, A. Nagy, *Life Sci.* **2003**, *72*, 2305–2320.
[207] C. Dubuc, R. Langlois, F. Bénard, N. Cauchon, K. Klarskov, P. Tone, J. E. van Lier, *Bioorg. Med. Chem. Lett.* **2008**, *18*, 2424–2427.
[208] C. A. Fischer, S. Vomstein, T. L. Mindt, *Pharmaceuticals* **2014**, *7*, 662–675.
[209] T. W. Moody, S. A. Mantey, T. K. Pradhan, M. Schumann, T. Nakagawa, A. Martinez, J. Fuselier, D. H. Coy, R. T. Jensen, *J. Biol. Chem.* **2004**, *279*, 23580–23589.
[210] A. Raposo Moreira Dias, A. Pina, A. Dal Corso, D. Arosio, L. Belvisi, L. Pignataro, M. Caruso, C. Gennari, *Chem. – Eur. J.* **2017**, *23*, 14410–14415.
[211] A. Dal Corso, M. Caruso, L. Belvisi, D. Arosio, U. Piarulli, C. Albanese, F. Gasparri, A. Marsiglio, F. Sola, S. Troiani, et al., *Chem. – Eur. J.* **2015**, *21*, 6921–6929.
[212] R. Colombo, M. Mingozzi, L. Belvisi, D. Arosio, U. Piarulli, N. Carenini, P. Perego, N. Zaffaroni, M. De Cesare, V. Castiglioni, et al., *J. Med. Chem.* **2012**, *55*, 10460–10474.
[213] U. Piarulli, A. R. M. Dias, L. Bodero, A. Martins, D. Arosio, S. Gazzola, L. Belvisi, L. Pignataro, C. Steinkühler, A. D. Corso, et al., *ChemMedChem* **2019**, DOI 10.1002/cmdc.201900049.

[214] P. López Rivas, C. Müller, C. Breunig, T. Hechler, A. Pahl, D. Arosio, L. Belvisi, L. Pignataro, A. Dal Corso, C. Gennari, *Org. Biomol. Chem.* **2019**, DOI 10.1039/c9ob00617f.
[215] L. Bodero, P. López Rivas, B. Korsak, T. Hechler, A. Pahl, C. Müller, D. Arosio, L. Pignataro, C. Gennari, U. Piarulli, *Beilstein J. Org. Chem.* **2018**, *14*, 407–415.
[216] A. Pina, A. Dal Corso, M. Caruso, L. Belvisi, D. Arosio, S. Zanella, F. Gasparri, C. Albanese, U. Cucchi, I. Fraietta, et al., *ChemistrySelect* **2017**, *2*, 4759–4766.
[217] D. Lorusso, G. Scambia, G. Amadio, A. di Legge, A. Pietragalla, R. De Vincenzo, V. Masciullo, M. Di Stefano, G. Mangili, G. Citterio, et al., *Br. J. Cancer* **2012**, *107*, 37–42.
[218] K. N. Enyedi, S. Tóth, G. Szakács, G. Mező, *PloS One* **2017**, *12*, e0178632.
[219] A. A. P. Tripodi, S. Tóth, K. N. Enyedi, G. Schlosser, G. Szakács, G. Mező, *Beilstein J. Org. Chem.* **2018**, *14*, 911–918.
[220] A. Corti, M. Fiocchi, F. Curnis, in *-Gener. Ther. Technol. Immune-Mediat. Inflamm. Dis.* (Ed.: P. Mina-Osorio), Springer International Publishing, Cham, **2017**, pp. 101–122.
[221] R. Lin, A. G. Cheetham, P. Zhang, Y. Lin, H. Cui, *Chem. Commun.* **2013**, *49*, 4968–4970.
[222] A. G. Cheetham, P. Zhang, Y. Lin, L. L. Lock, H. Cui, *J. Am. Chem. Soc.* **2013**, *135*, 2907–2910.
[223] M. Lelle, C. Freidel, S. Kaloyanova, I. Tabujew, A. Schramm, M. Musheev, C. Niehrs, K. Müllen, K. Peneva, *Eur. J. Med. Chem.* **2017**, *130*, 336–345.
[224] L. Feni, Improving Cargo Delivery in Cancer Therapy with the Help of Cell-Penetrating Peptides, Dissertation, **2019**.
[225] L. Ma, C. Wang, Z. He, B. Cheng, L. Zheng, K. Huang, *Curr. Med. Chem.* **2017**, *24*, 3373–3396.
[226] A. Scomparin, S. Salmaso, A. Eldar-Boock, D. Ben-Shushan, S. Ferber, G. Tiram, H. Shmeeda, N. Landa-Rouben, J. Leor, P. Caliceti, et al., *J. Control. Release Off. J. Control. Release Soc.* **2015**, *208*, 106–120.
[227] X. Zhao, H. Li, R. J. Lee, *Expert Opin. Drug Deliv.* **2008**, *5*, 309–319.
[228] A. E. Machulkin, Y. A. Ivanenkov, A. V. Aladinskaya, M. S. Veselov, V. A. Aladinskiy, E. K. Beloglazkina, V. E. Koteliansky, A. G. Shakhbazyan, Y. B. Sandulenko, A. G. Majouga, *J. Drug Target.* **2016**, *24*, 679–693.
[229] J. Roy, T. X. Nguyen, A. K. Kanduluru, C. Venkatesh, W. Lv, P. V. N. Reddy, P. S. Low, M. Cushman, *J. Med. Chem.* **2015**, *58*, 3094–3103.
[230] J. Marinello, M. Delcuratolo, G. Capranico, *Int. J. Mol. Sci.* **2018**, *19*, 3480.
[231] X. Xu, H. L. Persson, D. R. Richardson, *Mol. Pharmacol.* **2005**, *68*, 261–271.
[232] S. Bajusz, T. Janaky, V. J. Csernus, L. Bokser, M. Fekete, G. Srkalovic, T. W. Redding, A. V. Schally, *Proc. Natl. Acad. Sci. U. S. A.* **1989**, *86*, 6313–6317.
[233] S. Bajusz, T. Janaky, V. J. Csernus, L. Bokser, M. Fekete, G. Srkalovic, T. W. Redding, A. V. Schally, *Proc. Natl. Acad. Sci. U. S. A.* **1989**, *86*, 6318–6322.
[234] T. Janáky, A. Juhász, S. Bajusz, V. Csernus, G. Srkalovic, L. Bokser, S. Milovanovic, T. W. Redding, Z. Rékási, A. Nagy, *Proc. Natl. Acad. Sci. U. S. A.* **1992**, *89*, 972–976.
[235] S. R. Milovanovic, E. Monje, K. Szepeshazi, S. Radulovic, A. Schally, *J. Cancer Res. Clin. Oncol.* **1993**, *119*, 273–278.
[236] A. Nagy, A. V. Schally, P. Armatis, K. Szepeshazi, G. Halmos, M. Kovacs, M. Zarandi, K. Groot, M. Miyazaki, A. Jungwirth, et al., *Proc. Natl. Acad. Sci. U. S. A.* **1996**, *93*, 7269–7273.

[237] S. Westphalen, G. Kotulla, F. Kaiser, W. Krauss, G. Werning, H. P. Elsasser, A. Nagy, K. D. Schulz, C. Grundker, A. V. Schally, et al., *Int. J. Oncol.* **2000**, *17*, 1063–1072.
[238] A. V. Schally, *Horm. Metab. Res. Horm. Stoffwechselforschung Horm. Metab.* **2008**, *40*, 315–322.
[239] A. V. Schally, A. Nagy, *Trends Endocrinol. Metab. TEM* **2004**, *15*, 300–310.
[240] J. Engel, G. Emons, J. Pinski, A. V. Schally, *Expert Opin. Investig. Drugs* **2012**, *21*, 891–899.
[241] "Aeterna Zentaris Announces that ZoptEC Phase 3 Clinical Study of Zoptrex™ Did Not Achieve its Primary Endpoint," can be found under https://www.businesswire.com/news/home/20170501005409/en/Aeterna-Zentaris-Announces-ZoptEC-Phase-3-Clinical, **2017**.
[242] A. Nagy, A. Plonowski, A. V. Schally, *Proc. Natl. Acad. Sci.* **2000**, *97*, 829–834.
[243] A. Nagy, P. Armatis, A. V. Schally, *Proc. Natl. Acad. Sci. U. S. A.* **1996**, *93*, 2464–2469.
[244] J. Stepankova, M. Studenovsky, J. Malina, J. Kasparkova, B. Liskova, O. Novakova, K. Ulbrich, V. Brabec, *Biochem. Pharmacol.* **2011**, *82*, 227–235.
[245] M. Koppán, A. Nagy, A. V. Schally, A. Plonowski, G. Halmos, J. M. Arencibia, K. Groot, *The Prostate* **1999**, *38*, 151–158.
[246] A. Stangelberger, A. V. Schally, A. Nagy, K. Szepeshazi, C. A. Kanashiro, G. Halmos, *The Prostate* **2006**, *66*, 200–210.
[247] G. Keller, A. V. Schally, T. Gaiser, A. Nagy, B. Baker, G. Halmos, J. B. Engel, *Eur. J. Cancer* **2005**, *41*, 2196–2202.
[248] G. Mező, M. Manea, *Expert Opin. Drug Deliv.* **2010**, *7*, 79–96.
[249] S. Aggarwal, M. W. Ndinguri, R. Solipuram, N. Wakamatsu, R. P. Hammer, D. Ingram, W. Hansel, *Int. J. Cancer* **2011**, *129*, 1611–1623.
[250] T. Karampelas, O. Argyros, N. Sayyad, K. Spyridaki, C. Pappas, K. Morgan, G. Kolios, R. P. Millar, G. Liapakis, A. G. Tzakos, et al., *Bioconjug. Chem.* **2014**, *25*, 813–823.
[251] M. Pribylova, M. Dvorakova, V. Hanusova, I. Nemethova, L. Skalova, T. Vanek, *Int. J. Pharm.* **2011**, *415*, 175–180.
[252] C. Wang, Y. Ma, S. Feng, K. Liu, N. Zhou, *J. Pept. Sci.* **2015**, *21*, 569–576.
[253] I. Pályi, B. Vincze, S. Lovas, I. Mező, J. Pató, A. Kálnay, G. Turi, D. Gaál, R. Mihalik, I. Péter, et al., *Proc. Natl. Acad. Sci. U. S. A.* **1999**, *96*, 2361–2366.
[254] G. Mezo, M. Manea, I. Szabí, B. Vincze, M. Kovács, *Curr. Med. Chem.* **2008**, *15*, 2366–2379.
[255] P. Schlage, G. Mezo, E. Orbán, S. Bosze, M. Manea, *J. Control. Release Off. J. Control. Release Soc.* **2011**, *156*, 170–178.
[256] I. Szabó, M. Manea, E. Orbán, A. Csámpai, S. Bősze, R. Szabó, M. Tejeda, D. Gaál, B. Kapuvári, M. Przybylski, et al., *Bioconjug. Chem.* **2009**, *20*, 656–665.
[257] E. Orbán, G. Mezo, P. Schlage, G. Csík, Z. Kulić, P. Ansorge, E. Fellinger, H. M. Möller, M. Manea, *Amino Acids* **2011**, *41*, 469–483.
[258] M. Manea, J. Tóvári, M. Tejeda, Á. Schulcz, B. Kapuvári, B. Vincze, G. Mező, *Anticancer. Drugs* **2012**, *23*, 90–97.
[259] M. Manea, U. Leurs, E. Orbán, Z. Baranyai, P. Öhlschläger, A. Marquardt, Á. Schulcz, M. Tejeda, B. Kapuvári, J. Tóvári, et al., *Bioconjug. Chem.* **2011**, *22*, 1320–1329.
[260] B. Kapuvári, R. Hegedüs, Á. Schulcz, M. Manea, J. Tóvári, A. Gacs, B. Vincze, G. Mező, *Invest. New Drugs* **2016**, *34*, 416–423.
[261] U. Leurs, E. Lajkó, G. Mező, E. Orbán, P. Öhlschläger, A. Marquardt, L. Kőhidai, M. Manea, *Eur. J. Med. Chem.* **2012**, *52*, 173–183.

[262] U. Leurs, G. Mező, E. Orbán, P. Öhlschläger, A. Marquardt, M. Manea, *Biopolymers* **2012**, *98*, 1–10.
[263] R. Hegedüs, A. Pauschert, E. Orbán, I. Szabó, D. Andreu, A. Marquardt, G. Mező, M. Manea, *Biopolymers* **2015**, *104*, 167–177.
[264] R. Hegedüs, M. Manea, E. Orbán, I. Szabó, É. Kiss, É. Sipos, G. Halmos, G. Mező, *Eur. J. Med. Chem.* **2012**, *56*, 155–165.
[265] A. Nagy, A. V. Schally, G. Halmos, P. Armatis, R. Z. Cai, V. Csernus, M. Kovács, M. Koppán, K. Szepesházi, Z. Kahán, *Proc. Natl. Acad. Sci. U. S. A.* **1998**, *95*, 1794–1799.
[266] S. Seitz, A. V. Schally, A. Treszl, A. Papadia, F. Rick, L. Szalontay, K. Szepeshazi, O. Ortmann, G. Halmos, F. Hohla, et al., *Anticancer. Drugs* **2009**, *20*, 553.
[267] S. Seitz, A. V. Schally, S. Gluck, F. Rick, L. Szalontay, F. Hohla, A. Papadia, F. Köster, O. Ortmann, S. Buchholz, *J. Clin. Oncol.* **2009**, *27*, 619–619.
[268] G. Mezö, I. Szabó, I. Kertész, R. Hegedüs, E. Orbán, U. Leurs, S. Bösze, G. Halmos, M. Manea, *J. Pept. Sci. Off. Publ. Eur. Pept. Soc.* **2011**, *17*, 39–46.
[269] C. M. Huang, Y. T. Wu, S. T. Chen, *Chem. Biol.* **2000**, *7*, 453–461.
[270] X. Chen, X.-Y. Zhang, Y. Shen, L.-L. Fan, M.-L. Ren, Y.-P. Wu, *Oncotarget* **2016**, *7*, 83451–83461.
[271] M. Huo, Q. Zhu, Q. Wu, T. Yin, L. Wang, L. Yin, J. Zhou, *J. Pharm. Sci.* **2015**, *104*, 2018–2028.
[272] T. Yin, Q. Wu, L. Wang, L. Yin, J. Zhou, M. Huo, *Mol. Pharm.* **2015**, *12*, 3020–3031.
[273] M. L. Sun, J. M. Wei, X. W. Wang, L. Li, P. Wang, M. Li, C. H. Yi, *Exp. Oncol.* **2007**, *29*, 186–191.
[274] H. Shen, D. Hu, J. Du, X. Wang, Y. Liu, Y. Wang, J. Wei, D. Ma, P. Wang, L. Li, *Eur. J. Pharmacol.* **2008**, *601*, 23–29.
[275] Y. Zhang, H. Zhang, X. Wang, J. Wang, X. Zhang, Q. Zhang, *Biomaterials* **2012**, *33*, 679–691.
[276] N. Zheng, W. Dai, H. Zhang, X. Wang, J. Wang, X. Zhang, K. Wang, J. Li, Q. Zhang, *J. Drug Target.* **2015**, *23*, 67–78.
[277] M. Lelle, S. Kaloyanova, C. Freidel, M. Theodoropoulou, M. Musheev, C. Niehrs, G. Stalla, K. Peneva, *Mol. Pharm.* **2015**, *12*, 4290–4300.
[278] T. Liu, T. Jia, X. Yuan, C. Liu, J. Sun, Z. Ni, J. Xu, X. Wang, Y. Yuan, *Int. J. Nanomedicine* **2016**, *11*, 2235–2250.
[279] H.-Y. Zhang, W.-Q. Xu, Y. Zheng, E. Omari-Siaw, Y. Zhu, X. Cao, S.-S. Tong, J. Yu, X. Xu, *Oncotarget* **2016**, *7*, 86326–86338.
[280] P. Beck, H. Cui, J. D. Hegemann, M. A. Marahiel, A. Krüger, M. Groll, *ChemMedChem* **2015**, *10*, 1969–1973.
[281] M. Barrio, J. Czernin, S. Fanti, V. Ambrosini, I. Binse, L. Du, M. Eiber, K. Herrmann, W. P. Fendler, *J. Nucl. Med.* **2017**, *58*, 756–761.
[282] "FDA approval of NETSPOT," can be found under https://www.accessdata.fda.gov/drugsatfda_docs/label/2018/208547s011lbl.pdf, **n.d.**
[283] "FDA approval of Lutathera," can be found under https://www.accessdata.fda.gov/drugsatfda_docs/label/2018/208700s000lbl.pdf, **n.d.**
[284] I. Szabó, S. Bősze, E. Orbán, É. Sipos, G. Halmos, M. Kovács, G. Mező, *J. Pept. Sci. Off. Publ. Eur. Pept. Soc.* **2015**, *21*, 426–435.
[285] S. Fister, A. R. Günthert, B. Aicher, K. W. Paulini, G. Emons, C. Gründker, *Cancer Res.* **2009**, *69*, 6473–6481.
[286] G. F. Walker, R. Ledger, I. G. Tucker, *Int. J. Pharm.* **2001**, *216*, 77–82.

[287] M. Brudel, U. Kertscher, H. Berger, B. Mehlis, *J. Chromatogr. A* **1994**, *661*, 55–60.
[288] L. Polgár, *Handb. Proteolytic Enzym.* **2013**, 1773–1784.
[289] V. Turk, V. Stoka, O. Vasiljeva, M. Renko, T. Sun, B. Turk, D. Turk, *Biochim. Biophys. Acta BBA - Proteins Proteomics* **2012**, *1824*, 68–88.
[290] V. Turk, B. Turk, D. Turk, *EMBO J.* **2001**, *20*, 4629–4633.
[291] I. Klemenčič, A. K. Carmona, M. H. S. Cezari, M. A. Juliano, L. Juliano, G. Gunčar, D. Turk, I. Križaj, V. Turk, B. Turk, *Eur. J. Biochem.* **2000**, *267*, 5404–5412.
[292] D. K. Nägler, R. Ménard, T. Sulea, in *Handb. Proteolytic Enzym. Third Ed.* (Eds.: N.D. Rawlings, G. Salvesen), Academic Press, **2013**, pp. 1839–1844.
[293] J. S. Mort, in *Handb. Proteolytic Enzym. Third Ed.* (Eds.: N.D. Rawlings, G. Salvesen), Academic Press, **2013**, pp. 1784–1791.
[294] H. Kirschke, in *Handb. Proteolytic Enzym. Third Ed.* (Eds.: N.D. Rawlings, G. Salvesen), Academic Press, **2013**, pp. 1795–1800.
[295] M. Ruutu, B. Johansson, R. Grenman, K. Syrjänen, S. Syrjänen, *Anticancer Res.* **2004**, *24*, 2627–2631.
[296] G. Kaur, J. M. Dufour, *Spermatogenesis* **2012**, *2*, 1–5.
[297] C. Gründker, C. Föst, S. Fister, N. Nolte, A. R. Günthert, G. Emons, *Breast Cancer Res.* **2010**, *12*, R49.
[298] C. Gründker, A. R. Günthert, M. Hellriegel, G. Emons, *Eur. J. Endocrinol.* **2004**, *151*, 619–628.
[299] C. Gründker, P. Völker, F. Griesinger, A. Ramaswamy, A. Nagy, A. V. Schally, G. Emons, *Am. J. Obstet. Gynecol.* **2002**, *187*, 528–537.
[300] P. Limonta, M. Manea, *Cancer Treat. Rev.* **2013**, *39*, 647–663.
[301] R. M. Moretti, M. Montagnani Marelli, J. C. Van Groeninghen, P. Limonta, *J. Clin. Endocrinol. Metab.* **2002**, *87*, 3791–3797.
[302] K. Szepeshazi, A. V. Schally, G. Halmos, *Int. J. Oncol.* **2007**, *30*, 1485–1492.
[303] Halmos Gabor, Arencibia José M., Schally Andrew V., Davis Rodney, Bostwick David G., *J. Urol.* **2000**, *163*, 623–629.
[304] B. Rozsa, M. Nadji, A. V. Schally, B. Dezso, T. Flasko, G. Toth, M. Mile, N. L. Block, G. Halmos, *The Prostate* **2011**, *71*, 445–452.
[305] J. D. Neill, J. C. Sellers, L. C. Musgrove, L. W. Duck, *Mol. Cell. Endocrinol.* **1997**, *127*, 143–154.
[306] S. Gangadharan, A. A. Karande, *Biomed. Res. J.* **2014**, *1*, 71.
[307] E. Lajkó, S. Spring, R. Hegedüs, B. Biri-Kovács, S. Ingebrandt, G. Mező, L. Kőhidai, *Beilstein J. Org. Chem.* **2018**, *14*, 2495–2509.
[308] M. Fujino, S. Shinagawa, I. Yamazaki, S. Kobayashi, M. Obayashi, T. Fukuda, R. Nakayama, W. F. White, R. H. Rippel, *Arch. Biochem. Biophys.* **1973**, *154*, 488–489.
[309] J. R. Chenault, D. D. Kratzer, R. A. Rzepkowski, M. C. Goodwin, *Theriogenology* **1990**, *34*, 81–98.
[310] K. Herédi-Szabó, J. Lubke, G. Toth, R. F. Murphy, S. Lovas, *Peptides* **2005**, *26*, 419–422.
[311] A. A. Zompra, V. Magafa, F. N. Lamari, A. Nikolopoulou, B. Nock, T. Maina, G. A. Spyroulias, N. K. Karamanos, P. Cordopatis, *J. Pept. Res.* **2005**, *66*, 57–64.
[312] H. Yao, G. He, S. Yan, C. Chen, L. Song, T. J. Rosol, X. Deng, *Oncotarget* **2016**, *8*, 1913–1924.
[313] E. Orbán, M. Manea, A. Marquadt, Z. Bánóczi, G. Csík, E. Fellinger, S. Bősze, F. Hudecz, *Bioconjug. Chem.* **2011**, *22*, 2154–2165.

[314] F. O. Müller, J. Terblanchè, R. Schall, R. V. Z. Smit, T. Tucker, K. Marais, G. Groenewoud, H. C. Porchet, M. Weiner, D. Hawarden, *Br. J. Clin. Pharmacol.* **1997**, *44*, 335–341.
[315] J. J. L. Oberyé, B. M. J. L. Mannaerts, H.-J. Kleijn, C. J. Timmer, *Fertil. Steril.* **1999**, *72*, 1001–1005.
[316] "Triptorelin," can be found under https://www.drugbank.ca/drugs/DB06825, **n.d.**
[317] E. Kaliste-Korhonen, K. Tuovinen, O. Hänninen, *Hum. Exp. Toxicol.* **1996**, *15*, 972–978.
[318] G. M. Dubowchik, M. A. Walker, *Pharmacol. Ther.* **1999**, *83*, 67–123.
[319] Y. V. Kovtun, V. S. Goldmacher, *Cancer Lett.* **2007**, *255*, 232–240.
[320] G. M. Dubowchik, R. A. Firestone, L. Padilla, D. Willner, S. J. Hofstead, K. Mosure, J. O. Knipe, S. J. Lasch, P. A. Trail, *Bioconjug. Chem.* **2002**, *13*, 855–869.
[321] M. P. Deonarain, G. Yahioglu, I. Stamati, A. Pomowski, J. Clarke, B. M. Edwards, S. Diez-Posada, A. C. Stewart, *Antibodies* **2018**, *7*, 16.
[322] M. Barok, H. Joensuu, J. Isola, *Breast Cancer Res.* **2014**, *16*, DOI 10.1186/bcr3621.
[323] M. Barok, M. Tanner, K. Köninki, J. Isola, *Breast Cancer Res. BCR* **2011**, *13*, R46.
[324] M. Skwarczynski, Y. Hayashi, Y. Kiso, *J. Med. Chem.* **2006**, *49*, 7253–7269.
[325] J. Rautio, H. Kumpulainen, T. Heimbach, R. Oliyai, D. Oh, T. Järvinen, J. Savolainen, *Nat. Rev. Drug Discov.* **2008**, *7*, 255–270.
[326] R. Duncan, *Nat. Rev. Cancer* **2006**, *6*, 688–701.
[327] C. A. Blencowe, A. T. Russell, F. Greco, W. Hayes, D. W. Thornthwaite, *Polym. Chem.* **2011**, *2*, 773–790.
[328] G. M. Dubowchik, S. Radia, *Tetrahedron Lett.* **1997**, *38*, 5257–5260.
[329] G. M. Dubowchik, H. Dalton King, K. Pham-Kaplita, *Tetrahedron Lett.* **1997**, *38*, 5261–5264.
[330] P. L. Carl, P. K. Chakravarty, J. A. Katzenellenbogen, *J. Med. Chem.* **1981**, *24*, 479–480.
[331] F. M. H. de Groot, H. J. Broxterman, H. P. H. M. Adams, A. van Vliet, G. I. Tesser, Y. W. Elderkamp, A. J. Schraa, R. J. Kok, G. Molema, H. M. Pinedo, et al., *Mol. Cancer Ther.* **2002**, *1*, 901–911.
[332] A. Younes, U. Yasothan, P. Kirkpatrick, *Nat. Rev. Drug Discov.* **2012**, *11*, 19–20.
[333] Y. Liu, K. M. Bajjuri, C. Liu, S. C. Sinha, *Mol. Pharm.* **2012**, *9*, 168–175.
[334] C. for D. E. and Research, "Postmarket Drug Safety Information for Patients and Providers - Brentuximab Vedotin (marketed as Adcetris) Information," can be found under https://www.fda.gov/Drugs/DrugSafety/PostmarketDrugSafetyInformationforPatientsandProviders/ucm287672.htm, **n.d.**
[335] J. A. Francisco, C. G. Cerveny, D. L. Meyer, B. J. Mixan, K. Klussman, D. F. Chace, S. X. Rejniak, K. A. Gordon, R. DeBlanc, B. E. Toki, et al., *Blood* **2003**, *102*, 1458–1465.
[336] S. O. Doronina, B. E. Toki, M. Y. Torgov, B. A. Mendelsohn, C. G. Cerveny, D. F. Chace, R. L. DeBlanc, R. P. Gearing, T. D. Bovee, C. B. Siegall, et al., *Nat. Biotechnol.* **2003**, *21*, 778–784.
[337] S. Cazzamalli, E. Figueras, L. Pethő, A. Borbély, C. Steinkühler, D. Neri, N. Sewald, *ACS Omega* **2018**, *3*, 14726–14731.
[338] D. U. Chimmanamada, E. Kostik, D. Vutukuri, W. Ying, J. Zhang, *Hsp90 Inhibitor Drug Conjugates*, **2019**, US20190060473A1.
[339] D. Zhou, J. Casavant, E. I. Graziani, H. He, J. Janso, F. Loganzo, S. Musto, N. Tumey, C. J. O'Donnell, R. Dushin, *Bioorg. Med. Chem. Lett.* **2019**, *29*, 943–947.

[340] R. P. Lyon, T. D. Bovee, S. O. Doronina, P. J. Burke, J. H. Hunter, H. D. Neff-LaFord, M. Jonas, M. E. Anderson, J. R. Setter, P. D. Senter, *Nat. Biotechnol.* **2015**, *33*, 733–735.
[341] M. Abdollahpour-Alitappeh, M. Lotfinia, N. Bagheri, K. S. Sepehr, M. Habibi-Anbouhi, F. Kobarfard, S. Balalaie, A. Foroumadi, G. Abbaszadeh-Goudarzi, K. Abbaszadeh-Goudarzi, et al., *J. Cell. Physiol.* **2019**, *234*, 2693–2704.
[342] A. C. Tiberghien, J.-N. Levy, L. A. Masterson, N. V. Patel, L. R. Adams, S. Corbett, D. G. Williams, J. A. Hartley, P. W. Howard, *ACS Med. Chem. Lett.* **2016**, *7*, 983–987.
[343] P. W. Howard, L. Masterson, A. Tiberghien, J. A. Flygare, J. L. Gunzner, P. Polakis, A. Polson, H. E. Raab, S. D. Spencer, *Pyrrolobenzodiazepines and Conjugates Thereof*, **2011**, WO2011130598A1.
[344] S. C. Jeffrey, M. T. Nguyen, J. B. Andreyka, D. L. Meyer, S. O. Doronina, P. D. Senter, *Bioorg. Med. Chem. Lett.* **2006**, *16*, 358–362.
[345] F. Bryden, C. Martin, S. Letast, E. Lles, I. Viéitez-Villemin, A. Rousseau, C. Colas, M. Brachet-Botineau, E. Allard-Vannier, C. Larbouret, et al., *Org. Biomol. Chem.* **2018**, *16*, 1882–1889.
[346] N. Jain, S. W. Smith, S. Ghone, B. Tomczuk, *Pharm. Res.* **2015**, *32*, 3526–3540.
[347] A. H. Staudacher, M. P. Brown, *Br. J. Cancer* **2017**, *117*, 1736–1742.
[348] A. P. Singh, S. Sharma, D. K. Shah, *J. Pharmacokinet. Pharmacodyn.* **2016**, *43*, 567–582.
[349] Z. Meng, Q. Lv, J. Lu, H. Yao, X. Lv, F. Jiang, A. Lu, G. Zhang, *Int. J. Mol. Sci.* **2016**, *17*, DOI 10.3390/ijms17050796.
[350] X. Zhang, X. Li, Q. You, X. Zhang, *Eur. J. Med. Chem.* **2017**, *139*, 542–563.
[351] A. Safavy, J. A. Bonner, H. W. Waksal, D. J. Buchsbaum, G. Y. Gillespie, M. B. Khazaeli, R. Arani, D.-T. Chen, M. Carpenter, K. P. Raisch, *Bioconjug. Chem.* **2003**, *14*, 302–310.
[352] G. M. Dubowchik, K. Mosure, J. O. Knipe, R. A. Firestone, *Bioorg. Med. Chem. Lett.* **1998**, *8*, 3347–3352.
[353] F. M. H. de Groot, W. J. Loos, R. Koekkoek, L. W. A. van Berkom, G. F. Busscher, A. E. Seelen, C. Albrecht, P. de Bruijn, H. W. Scheeren, *J. Org. Chem.* **2001**, *66*, 8815–8830.
[354] K. Hochdörffer, K. Abu Ajaj, C. Schäfer-Obodozie, F. Kratz, *J. Med. Chem.* **2012**, *55*, 7502–7515.
[355] Y. Meyer, J.-A. Richard, B. Delest, P. Noack, P.-Y. Renard, A. Romieu, *Org. Biomol. Chem.* **2010**, *8*, 1777–1780.
[356] I. Ranđelović, S. Schuster, B. Kapuvári, G. Mező, Tóvári, Józseph, *Unpubl. Data* **n.d.**
[357] A. H. J. Wang, G. Ughetto, G. J. Quigley, A. Rich, *Biochemistry* **1987**, *26*, 1152–1163.
[358] Y. G. Gao, Y. C. Liaw, Y. K. Li, G. A. van der Marel, J. H. van Boom, A. H. Wang, *Proc. Natl. Acad. Sci. U. S. A.* **1991**, *88*, 4845–4849.
[359] C. A. Frederick, L. D. Williams, G. Ughetto, G. A. van der Marel, J. H. van Boom, A. Rich, A. H. Wang, *Biochemistry* **1990**, *29*, 2538–2549.
[360] D. J. Wagener, P. H. de Mulder, J. A. Wils, *Ann. Oncol. Off. J. Eur. Soc. Med. Oncol.* **1994**, *5 Suppl 3*, 81–86.
[361] B. Liu, E. D. Staren, T. Iwamura, H. E. Appert, J. M. Howard, *J. Surg. Res.* **2001**, *99*, 179–186.
[362] S. Kiuchi, S. Ikeshita, Y. Miyatake, M. Kasahara, *Exp. Mol. Pathol.* **2015**, *98*, 41–46.

[363] S. Chand, K. O'Hayer, F. F. Blanco, J. M. Winter, J. R. Brody, *Int. J. Biol. Sci.* **2016**, *12*, 273–282.
[364] D. Li, K. Xie, R. Wolff, J. L. Abbruzzese, *The Lancet* **2004**, *363*, 1049–1057.
[365] L. Stern, N. Giese, T. Hackert, O. Strobel, P. Schirmacher, K. Felix, M. M. Gaida, *J. Cancer* **2018**, *9*, 711–725.
[366] "Prognosis - Hirshberg Foundation for Pancreatic Cancer Research," can be found under http://pancreatic.org/pancreatic-cancer/about-the-pancreas/prognosis/, **n.d.**
[367] "Survival Rates for Pancreatic Cancer," can be found under https://www.cancer.org/cancer/pancreatic-cancer/detection-diagnosis-staging/survival-rates.html, **n.d.**
[368] D. W. Miller, M. Fontain, C. Kolar, T. Lawson, *Cancer Lett.* **1996**, *107*, 301–306.
[369] D. W. Miller, E. V. Batrakova, A. V. Kabanov, *Pharm. Res.* **1999**, *16*, 396–401.
[370] G. J. Zaman, M. J. Flens, M. R. van Leusden, M. de Haas, H. S. Mülder, J. Lankelma, H. M. Pinedo, R. J. Scheper, F. Baas, H. J. Broxterman, *Proc. Natl. Acad. Sci. U. S. A.* **1994**, *91*, 8822–8826.
[371] S. P. Cole, K. E. Sparks, K. Fraser, D. W. Loe, C. E. Grant, G. M. Wilson, R. G. Deeley, *Cancer Res.* **1994**, *54*, 5902–5910.
[372] L. M. Breuninger, S. Paul, K. Gaughan, T. Miki, A. Chan, S. A. Aaronson, G. D. Kruh, *Cancer Res.* **1995**, *55*, 5342–5347.
[373] Z.-S. Chen, T. Furukawa, T. Sumizawa, K. Ono, K. Ueda, K. Seto, S.-I. Akiyama, *Mol. Pharmacol.* **1999**, *55*, 921–928.
[374] S. Okada, Y. Sakata, S. Matsuno, M. Kurihara, Y. Sasaki, Y. Ohashi, T. Taguchi, *Br. J. Cancer* **1999**, *80*, 438–443.
[375] N. Gebbia, V. Gebbia, *Eur. J. Cancer* **1996**, *32*, 1822–1823.
[376] B. Liu, E. Staren, T. Iwamura, H. Appert, J. Howard, *World J. Gastroenterol.* **2001**, *7*, 855–859.
[377] B. Jachez, R. Nordmann, F. Loor, *J. Natl. Cancer Inst.* **1993**, *85*, 478–483.
[378] A. H. Dantzig, R. L. Shepard, J. Cao, K. L. Law, W. J. Ehlhardt, T. M. Baughman, T. F. Bumol, J. J. Starling, *Cancer Res.* **1996**, *56*, 4171–4179.
[379] C. O. Cardarelli, I. Aksentijevich, I. Pastan, M. M. Gottesman, *Cancer Res.* **1995**, *55*, 1086–1091.
[380] S. H. Jang, M. G. Wientjes, J. L.-S. Au, *J. Pharmacol. Exp. Ther.* **2001**, *298*, 1236–1242.
[381] L. O'Driscoll, N. Walsh, A. Larkin, J. Ballot, W. S. Ooi, G. Gullo, R. O'Connor, M. Clynes, J. Crown, S. Kennedy, *Anticancer Res.* **2007**, *27*, 2115–2120.
[382] C. Dumontet, G. E. Duran, K. A. Steger, L. Beketic-Oreskovic, B. I. Sikic, *Cancer Res.* **1996**, *56*, 1091–1097.
[383] M. J. Schibler, F. Cabral, *J. Cell Biol.* **1986**, *102*, 1522–1531.
[384] M. Kavallaris, C. A. Burkhart, S. B. Horwitz, *Br. J. Cancer* **1999**, *80*, 1020–1025.
[385] M. Kavallaris, D. Y. Kuo, C. A. Burkhart, D. L. Regl, M. D. Norris, M. Haber, S. B. Horwitz, *J. Clin. Invest.* **1997**, *100*, 1282–1293.
[386] S. Mozzetti, C. Ferlini, P. Concolino, F. Filippetti, G. Raspaglio, S. Prislei, D. Gallo, E. Martinelli, F. O. Ranelletti, G. Ferrandina, et al., *Clin. Cancer Res.* **2005**, *11*, 298–305.
[387] S. Ranganathan, C. A. Benetatos, P. J. Colarusso, D. W. Dexter, G. R. Hudes, *Br. J. Cancer* **1998**, *77*, 562–566.
[388] J. Du, B. Li, Y. Fang, Y. Liu, Y. Wang, J. Li, W. Zhou, X. Wang, *BMC Cancer* **2015**, *15*, 536.
[389] K. M. Lee, D. Cao, A. Itami, P. M. Pour, R. H. Hruban, A. Maitra, M. M. Ouellette, *Histopathology* **2007**, *51*, 539–546.

[390] E. Crivellato, L. Candussio, A. M. Rosati, F. Bartoli-Klugmann, F. Mallardi, G. Decorti, *J. Histochem. Cytochem.* **2002**, *50*, 731–734.
[391] L. Feni, I. Neundorf, in *Pept. Pept.-Based Biomater. Their Biomed. Appl.* (Eds.: A. Sunna, A. Care, P.L. Bergquist), Springer International Publishing, Cham, **2017**, pp. 279–295.
[392] M. Kristensen, D. Birch, H. Mørck Nielsen, *Int. J. Mol. Sci.* **2016**, *17*, DOI 10.3390/ijms17020185.
[393] A. Bolhassani, B. S. Jafarzade, G. Mardani, *Peptides* **2017**, *87*, 50–63.
[394] A. Mickan, D. Sarko, U. Haberkorn, W. Mier, *Curr. Pharm. Biotechnol.* **2014**, *15*, 200–209.
[395] J. D. Ramsey, N. H. Flynn, *Pharmacol. Ther.* **2015**, *154*, 78–86.
[396] A. D. Frankel, C. O. Pabo, *Cell* **1988**, *55*, 1189–1193.
[397] M. Green, P. M. Loewenstein, *Cell* **1988**, *55*, 1179–1188.
[398] D. Derossi, A. H. Joliot, G. Chassaing, A. Prochiantz, *J. Biol. Chem.* **1994**, *269*, 10444–10450.
[399] A. Prochiantz, *Curr. Opin. Neurobiol.* **1996**, *6*, 629–634.
[400] I. Neundorf, R. Rennert, J. Hoyer, F. Schramm, K. Löbner, I. Kitanovic, S. Wölfl, *Pharmaceuticals* **2009**, *2*, 49–65.
[401] S. Richter, V. Bouvet, M. Wuest, R. Bergmann, J. Steinbach, J. Pietzsch, I. Neundorf, F. Wuest, *Nucl. Med. Biol.* **2012**, *39*, 1202–1212.
[402] A. Gronewold, M. Horn, I. Ranđelović, J. Tóvári, S. Muñoz Vázquez, K. Schomäcker, I. Neundorf, *Chemmedchem* **2017**, *12*, 42–49.
[403] Z. Zheng, H. Aojula, D. Clarke, *J. Drug Target.* **2010**, *18*, 477–487.
[404] H. Zhang, Y. G. Gao, G. A. van der Marel, J. H. van Boom, A. H. Wang, *J. Biol. Chem.* **1993**, *268*, 10095–10101.
[405] B. A. Webb, M. Chimenti, M. P. Jacobson, D. L. Barber, *Nat. Rev. Cancer* **2011**, *11*, 671–677.
[406] W. Bauer, U. Briner, W. Doepfner, R. Haller, R. Huguenin, P. Marbach, T. J. Petcher, null Pless, *Life Sci.* **1982**, *31*, 1133–1140.
[407] J. Peng, X. Qi, Y. Chen, N. Ma, Z. Zhang, J. Xing, X. Zhu, Z. Li, Z. Wu, *J. Drug Target.* **2014**, *22*, 428–438.
[408] A. Zou, M. Huo, Y. Zhang, J. Zhou, X. Yin, C. Yao, Q. Zhu, M. Zhang, J. Ren, Q. Zhang, *J. Pharm. Sci.* **2012**, *101*, 627–640.
[409] I. Tóth, J. P. Malkinson, N. S. Flinn, B. Drouillat, A. Horváth, J. Erchegyi, M. Idei, A. Venetianer, P. Artursson, L. Lazorova, et al., *J. Med. Chem.* **1999**, *42*, 4010–4013.
[410] M. M. Martin, L. Lindqvist, *J. Lumin.* **1975**, *10*, 381–390.
[411] Y. Liu, W. Wang, J. Yang, C. Zhou, J. Sun, *Asian J. Pharm. Sci.* **2013**, *8*, 159–167.
[412] J. C. Weddell, P. I. Imoukhuede, *Integr. Biol.* **2017**, *9*, 464–484.
[413] R. Ohgaki, Y. Teramura, D. Hayashi, L. Quan, S. Okuda, S. Nagamori, M. Takai, Y. Kanai, *Sci. Rep.* **2017**, *7*, 17484.
[414] H. Diehl, *Talanta* **1989**, *36*, 413–415.
[415] L. Ferrari, L. Rovati, P. Fabbri, F. Pilati, *Sensors* **2013**, *13*, 484–499.
[416] B. Vincze, I. Pályi, D. Daubner, T. Kremmer, I. Számel, I. Bodrogi, J. Sugár, J. Seprődi, I. Mező, I. Teplán, et al., *J. Steroid Biochem. Mol. Biol.* **1991**, *38*, 119–126.
[417] H. L. Watt, U. Kumar, *Cancer Cell Int.* **2006**, *6*, 5.
[418] Z. Kahán, A. Nagy, A. V. Schally, F. Hebert, B. Sun, K. Groot, G. Halmos, *Int. J. Cancer* **1999**, *82*, 592–598.
[419] B. Karaca, M. Degirmenci, A. Ozveren, H. Atmaca, E. Bozkurt, B. Karabulut, U. A. Sanli, R. Uslu, *Cancer Chemother. Pharmacol.* **2015**, *75*, 1273–1280.

[420] Y. Altrichter, Targeting Tumoral GnRH Receptors with Peptides: Applications to the Development of Drug Delivery Systems and Receptor Detection Methods, Master thesis, **2015**.
[421] H. Schägger, *Nat. Protoc.* **2006**, *1*, 16–22.
[422] S. Schuster, B. Biri-Kovács, B. Szeder, V. Farkas, L. Buday, Z. Szabó, G. Halmos, G. Mező, *Beilstein J. Org. Chem.* **2018**, *14*, 756–771.
[423] G. Halmos, J. L. Wittliff, A. V. Schally, *Cancer Res.* **1995**, *55*, 280–287.
[424] W. M. Hunter, F. C. Greenwood, *Nature* **1962**, *194*, 495–496.

10. Appendix

10.1. GnRH-drug conjugates

10.1.1. 1st set of oxime-linked GnRH-III-Dau conjugates

10.1.1.1. RP-HPLC profile and ESI-ion trap mass spectrum

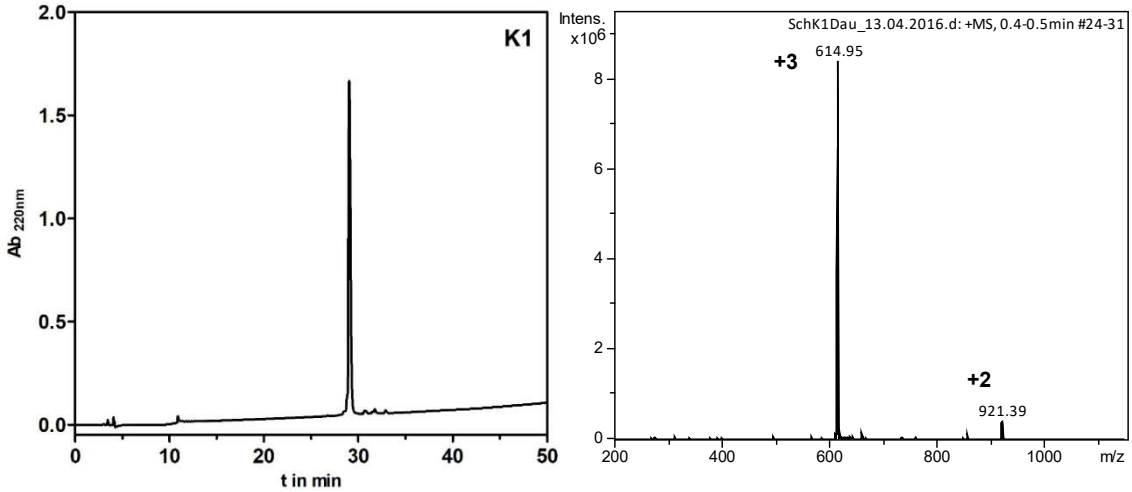

Figure A1. RP-HPLC profile and ESI-ion trap mass spectrum of GnRH-III-[^{4}Ser, ^{8}Lys(Dau=Aoa)] (**K1**) MW_{cal} /MW_{exp} = 1841.89/1841.85g/mol).

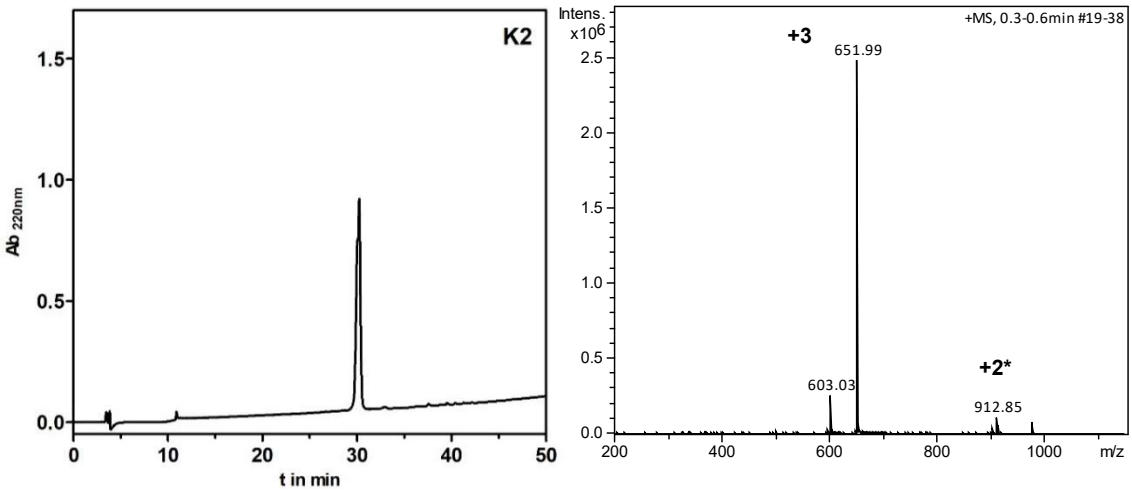

Figure A2. RP-HPLC profile and ESI-ion trap mass spectrum of GnRH-III-[^{4}Lys(Bu), ^{8}Lys(Dau=Aoa)] (**K2**) (MW_{cal} /MW_{exp} = 1953.07/1952.97 g/mol).

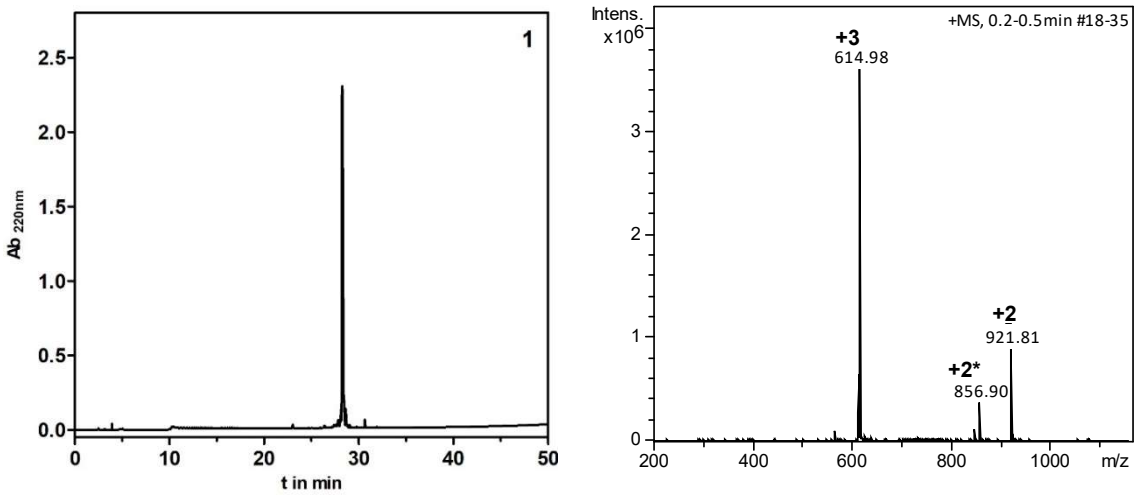

Figure A3. RP-HPLC profile and ESI-ion trap mass spectrum of GnRH-III-[^{4}Ser, ^{6}D-Asp ^{8}Lys(Dau=Aoa)] (**1**) (MW_{cal} /MW_{exp} = 1841.89/1841.60 g/mol).

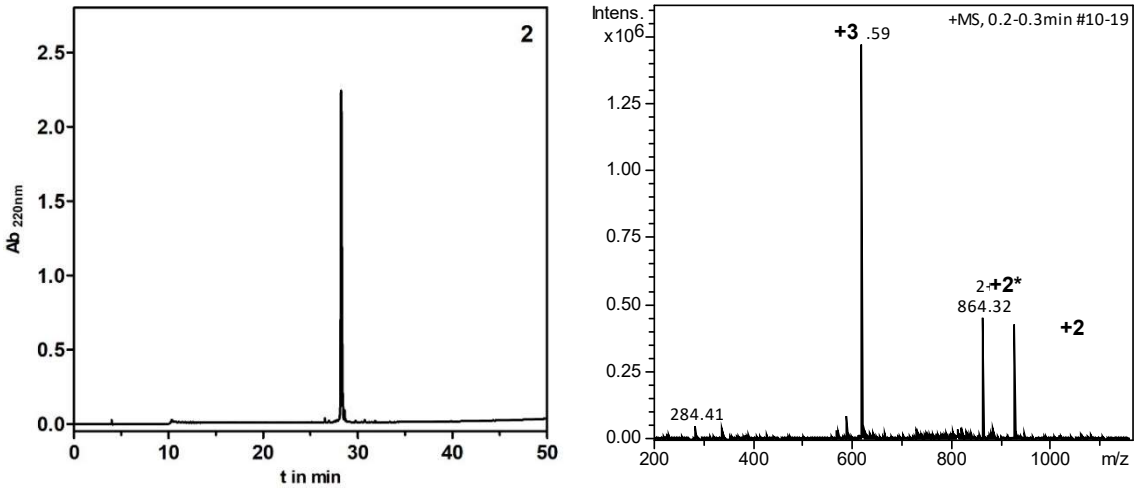

Figure A4. RP-HPLC profile and ESI-ion trap mass spectrum of GnRH-III-[^{4}Ser, ^{6}D-Glu ^{8}Lys(Dau=Aoa)] (**2**) (MW_{cal} /MW_{exp} = 1855.91/1855.70 g/mol).

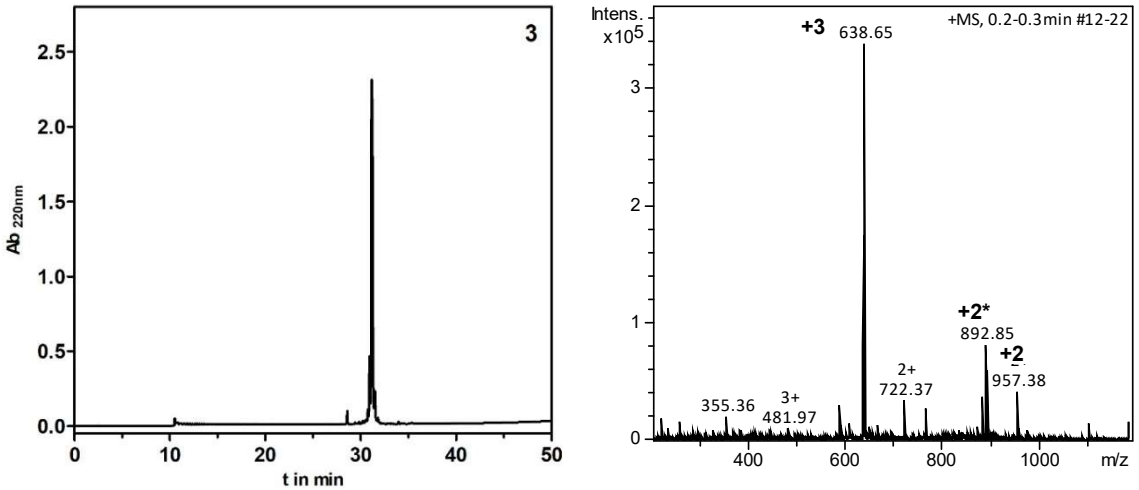

Figure A5. RP-HPLC profile and ESI-ion trap mass spectrum of GnRH-III-[^{4}Ser, ^{6}D-Trp ^{8}Lys(Dau=Aoa)] (**3**) (MW_{cal} /MW_{exp} = 1913.01/1912.80 g/mol).

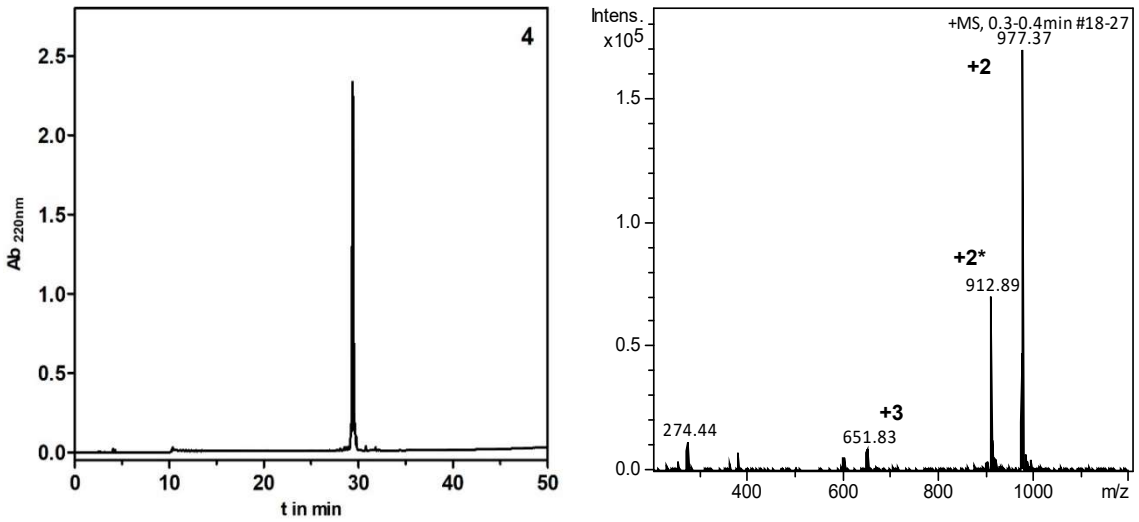

Figure A6. RP-HPLC profile and ESI-ion trap mass spectrum of GnRH-III-[^{4}Lys(Bu), ^{6}D-Asp, ^{8}Lys(Dau=Aoa)] (**4**) (MW_{cal} /MW_{exp} = 1953.07/1952.90 g/mol).

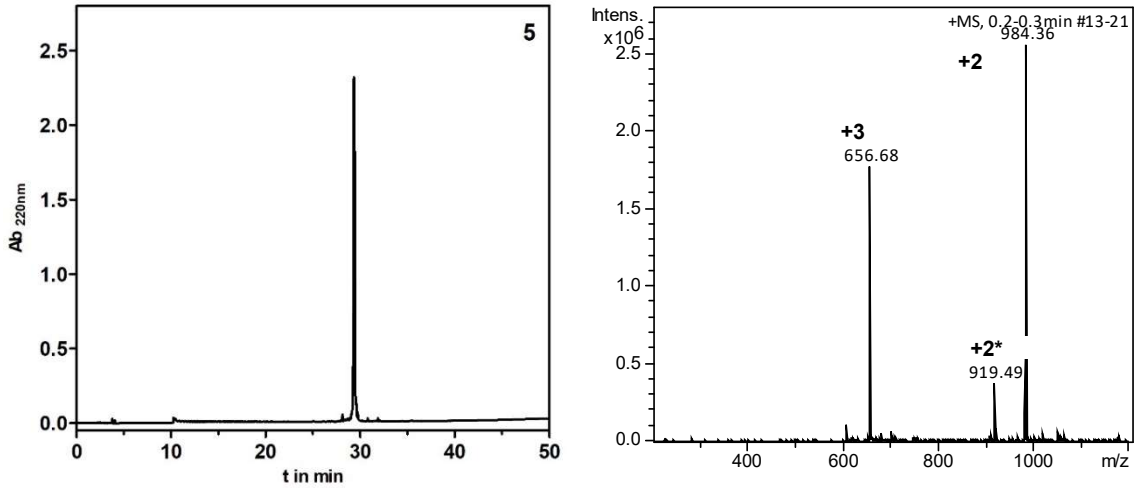

Figure A7. RP-HPLC profile and ESI-ion trap mass spectrum of GnRH-III-[^{4}Lys(Bu), ^{6}D-Glu, ^{8}Lys(Dau=Aoa)] (**5**) (MW_{cal} /MW_{exp} = 1966.93/1966.70 g/mol).

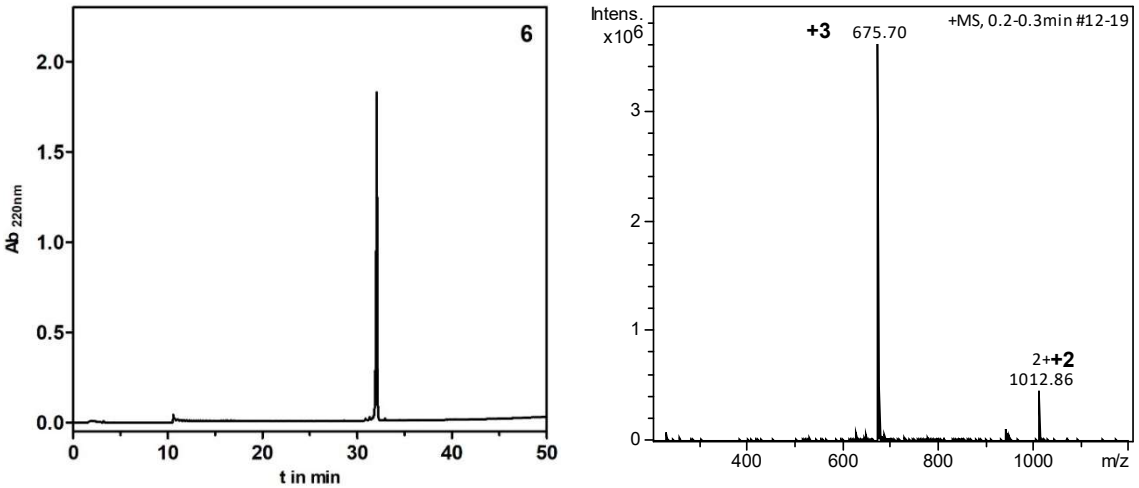

Figure A8. RP-HPLC profile and ESI-ion trap mass spectrum of GnRH-III-[^{4}Lys(Bu), ^{6}D-Trp, ^{8}Lys(Dau=Aoa)] (**6**) (MW_{cal} /MW_{exp} = 2024.03/2023.70 g/mol).

10.1.1.2. Lysosomal degradation in presence of rat liver lysosomal homogenate

Table A1. Fragments of 1st set of GnRH-III-Dau conjugates produced by rat liver homogenate

Code	Compound	Fragment	MW_{cal}/MW_{exp}
K1	[^{8}Lys(Dau=Aoa)]	<EHWSHDWK(Dau=Aoa)PG-NH_2	1841.89/1841.66
		<EHWSHDWK(Dau=Aoa)P-OH	1785.82/1785.27
		<EHWSHDWK(Dau=Aoa)-OH	1688.70/1688.69
		H-WSHDWK(Dau=Aoa)-OH	1440.49/1439.78
		H-HDWK(Dau=Aoa)PG-NH_2	1320.36/139.83
		H-HDWK(Dau=Aoa)-OH	1167.18/1166.87
		H-K(Dau=Aoa)PG-NH_2	881.94/881.39
		H-K(Dau=Aoa)P-OH	825.86/825.35
		H-K(Dau=Aoa)-OH	728.75/728.34
		<EHWSH-OH	676.68/676.23
		<EHWS-OH	539.54/539.32
		<EHW-OH	452.46/452.32
		H-DW-OH	319.12/319.28
1	[^{6}D-Asp, ^{8}Lys(Dau=Aoa)]	<EHWSHdWK(Dau=Aoa)PG-NH_2	1841.89/1841.63
		<EHWSHdWK(Dau=Aoa)P-OH	1785.82/1785.63
		<EHWSHdWK(Dau=Aoa)-OH	1688.70/1688.44
		H-WSHdWK(Dau=Aoa)PG-NH_2	1593.65/1593.61
		H-WSHdWK(Dau=Aoa)-OH	1440.49/1440.45
		H-SHdWK(Dau=Aoa)-OH	1254.26/1253.83
2	[^{6}D-Glu, ^{8}Lys(Dau=Aoa)]	<EHWSHeWK(Dau=Aoa)PG-NH_2	1855.90/1855.67
		<EHWSHeWK(Dau=Aoa)P-OH	1799.87/1799.79
		<EHWSHeWK(Dau=Aoa)-OH	1702.76/1701.85
		H-WSHeWK(Dau=Aoa)PG-NH_2	1607.70/1607.63
		H-WSHeWK(Dau=Aoa)-OH	1454.51/1453.91
		H-SHeWK(Dau=Aoa)-OH	1268.30/1267.75
		H-K(Dau=Aoa)-OH	728.75/728.33
3	[^{6}D-Trp, ^{8}Lys(Dau=Aoa)]	<EHWSHwWK(Dau=Aoa)PG-NH_2	1913.04/1912.79
		<EHWSHwWK(Dau=Aoa)P-OH	1856.941856.64
		<EHWSHwWK(Dau=Aoa)-OH	1759.85/1759.61
		H-WSHwWK(Dau=Aoa)-OH	1511.61/1511.58
		H-SHwWK(Dau=Aoa)PG-NH_2	1478.58/1477.79
		H-SHwWK(Dau=Aoa)-OH	1325.40/1324.04
		H-wWK(Dau=Aoa)-OH	1101.18/1101.01
		H-K(Dau=Aoa)-OH	728.75/728.34
		<EHWSHwW-OH	1049.12/1049.06
K2	[^{4}Lys(Bu), ^{8}Lys(Dau=Aoa)]	<EHWK(Bu)HDWK(Dau=Aoa)PG-NH_2	1953.07/1952.79
		<EHWK(Bu)HDWK(Dau=Aoa)-OH	1799.92/1799.69
		H-HDWK(Dau=Aoa)PG-NH_2	1320.36/1319.95
		H-HDWK(Dau=Aoa)-OH	1167.18/1166.91
		H-K(Dau=Aoa)PG-NH_2	881.94/881.44
		H-K(Dau=Aoa)P-OH	825.86/825.40
		H-K(Dau=Aoa)-OH	728.75/728.37
		<EHWK(Bu)HD-OH	902.96/902.84
		<EHWK(Bu)-OH	650.73/650.71
		<EHW-OH	452.46/452.31
		H-DW-OH	319.32/319.27
4	[^{4}Lys(Bu), ^{6}D-Asp, ^{8}Lys(Dau=Aoa)]	<EHWK(Bu)HdWK(Dau=Aoa)PG-NH_2	1953.07/1952.79
		<EHWK(Bu)HdWK(Dau=Aoa)P-OH	1897.03/1896.90
		<EHWK(Bu)HdWK(Dau=Aoa)-OH	1799.92/1799.81
		H-WK(Bu)HdWK(Dau=Aoa)-OH	1551.67/1551.59
		H-K(Bu)HdWK(Dau=Aoa)PG-NH_2	1518.65/1517.88
		H-K(Bu)HdWK(Dau=Aoa)-OH	1365.46/1364.92
		H-HdWK(Dau=Aoa)-OH	1167.18/1166.90
		<EHWK(Bu)-OH	650.73/650.43
		<EHW-OH	452.46/452.3

5	[^{4}Lys(Bu), ^{6}D-Glu, ^{8}Lys(Dau=Aoa)]	<EHWK(Bu)HeWK(Dau=Aoa)PG-NH_2	1967.13/1966.82
		<EHWK(Bu)HeWK(Dau=Aoa)P-OH	1911.06/1910.81
		<EHWK(Bu)HeWK(Dau=Aoa)-OH	1813.94/1813.70
		H-WK(Bu)HeWK(Dau=Aoa)-OH	1565.70/1565.13
		H-HeWK(Dau=Aoa)-OH	1181.22/1180.67
		H-K(Bu)HeWK(Dau=Aoa)-OH	1379.49/1378.93
		<EHW-OH	452.46/452.31
6	[^{4}Lys(Bu), ^{6}D-Trp, ^{8}Lys(Dau=Aoa)]	<EHWK(Bu)HwWK(Dau=Aoa)PG-NH_2	2024.22/2024.25
		<EHWK(Bu)HwWK(Dau=Aoa)P-OH	1968.16/1967.84
		<EHWK(Bu)HwWK(Dau=Aoa)-OH	1871.04/1870.50
		<EHWK(Bu)HwW-OH	1160.30/1160.21
		H-K(Bu)HwWK(Dau=Aoa)-OH	1436.59/1436.24
		H-HwWK(Dau=Aoa)-OH	1238.32/1232.04
		H-K(Dau=Aoa)-OH	728.75/728.33
		<EHWK(Bu)-OH	650.73/650.43
		H-HwW-OH	527.58/527.37

10.1.1.3. In vitro cytostatic effect – Dose response curves

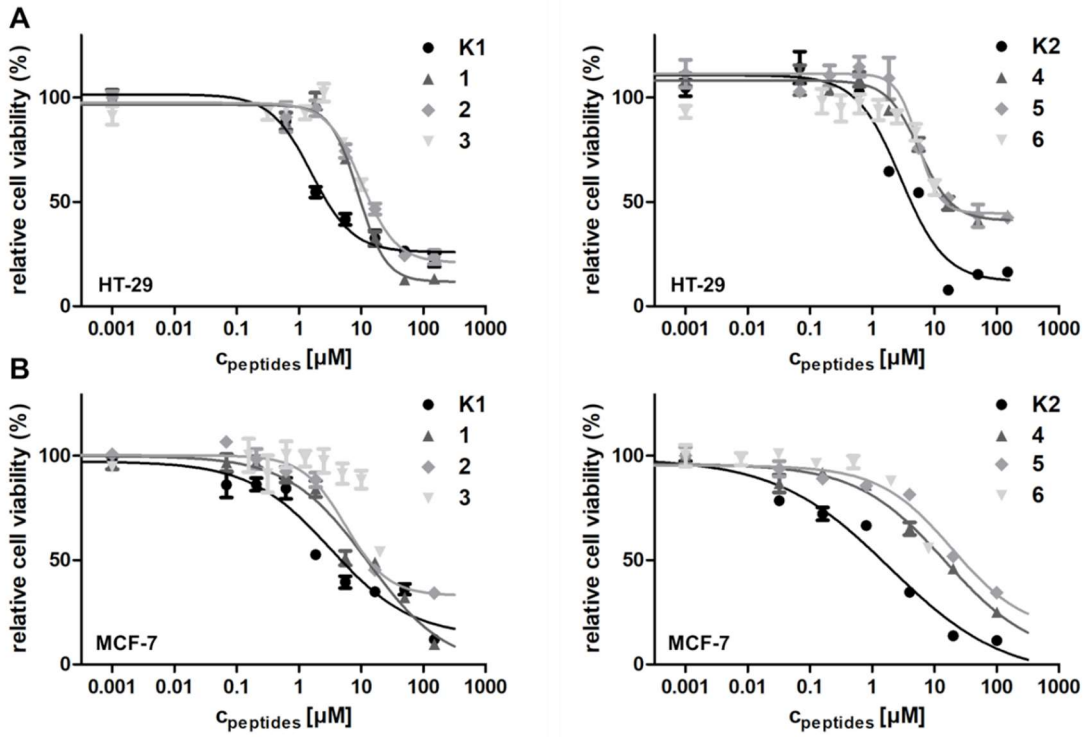

Figure A9. Cytostatic effect of 1st set of GnRH-III conjugate on **A**: HT-29 and **B:** MFC-7 human cancer cells after 72 h (24 h treatment and an additional 48 h incubation). Curves obtained by non-linear regression (sigmoidal dose response, error bars represent the standard deviation of four parallels, the measurements were repeated twice).

10.1.1.4. Confocal laser scanning microscopy studies

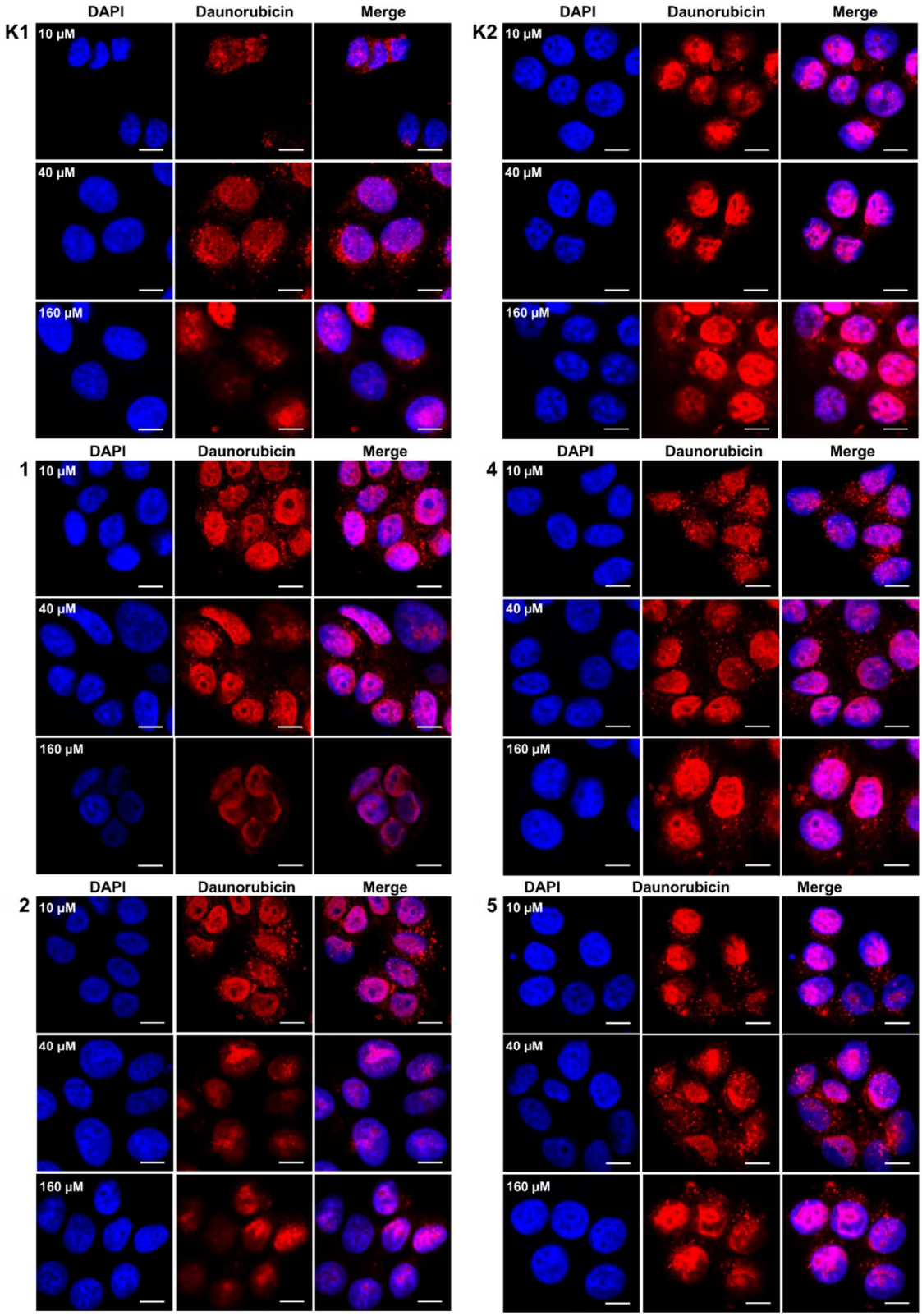

Figure A10. Cellular uptake of 1st set of bioconjugate **K1**, **K2**, **1**, **2**, **4** and **5** at 10 µM, 40 µM and 100 µM visualized by confocal laser scanning microscopy (scale bars represent 10 µm).

10.1.2. 2nd set of oxime-linked GnRH-III-Dau conjugates

10.1.2.1. RP-HPLC profile and ESI-ion trap mass spectrum

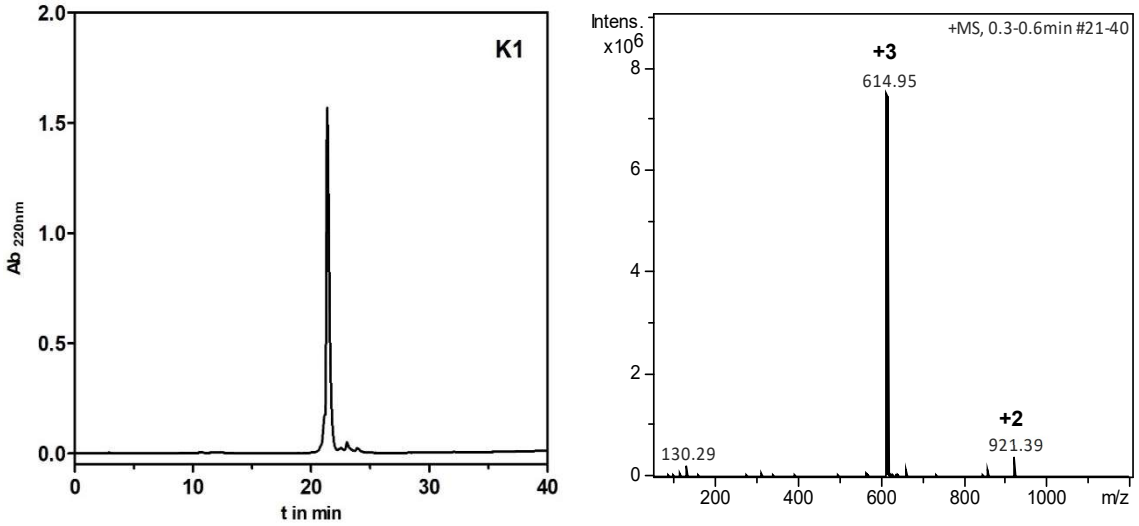

Figure A11. RP-HPLC profile and ESI-ion trap mass spectrum of GnRH-III-[^{4}Ser, ^{8}Lys(Dau=Aoa)] (**K1**) (MW_{cal} /MW_{exp} = 1841.89/1841.85g/mol).

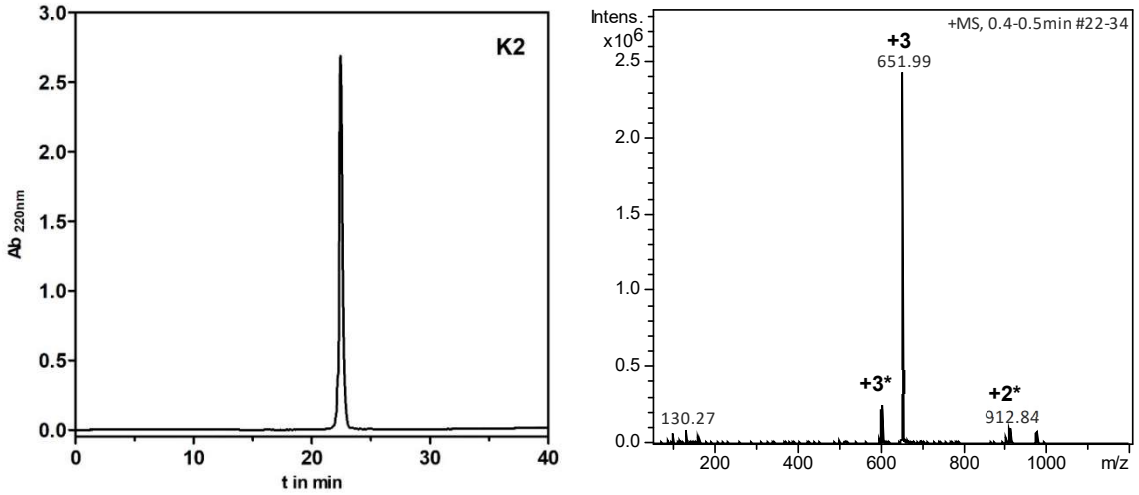

Figure A12. RP-HPLC profile and ESI-ion trap mass spectrum of GnRH-III-[^{4}Lys(Bu), ^{8}Lys(Dau=Aoa)] (**K2**) (MW_{cal} /MW_{exp} = 1953.07/1952.97 g/mol).

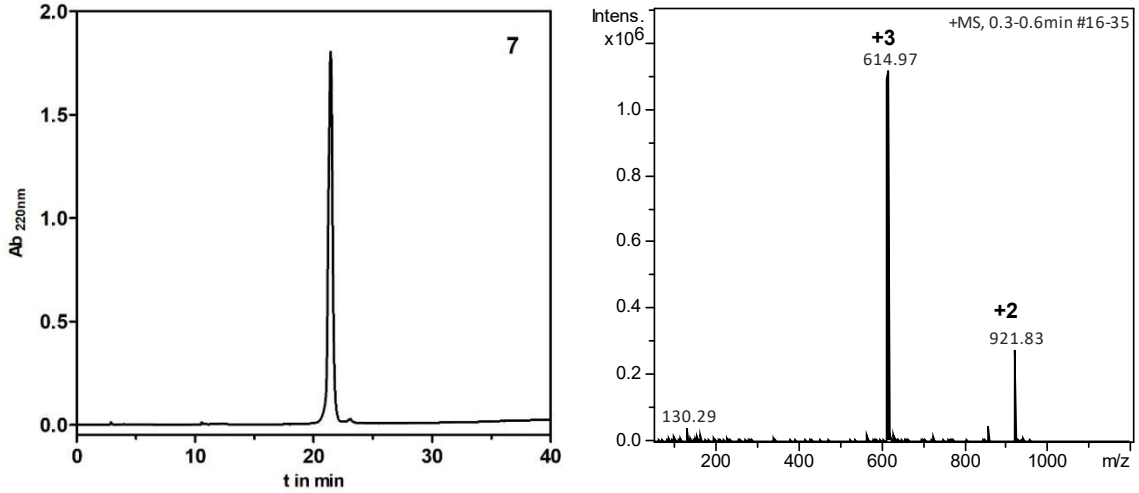

Figure A13. RP-HPLC profile and ESI-ion trap mass spectrum of GnRH-III-[^{3}Trp, ^{8}Lys(Dau=Aoa)] (**7**) (MW_{cal} /MW_{exp} = 1841.89/1841.91 g/mol).

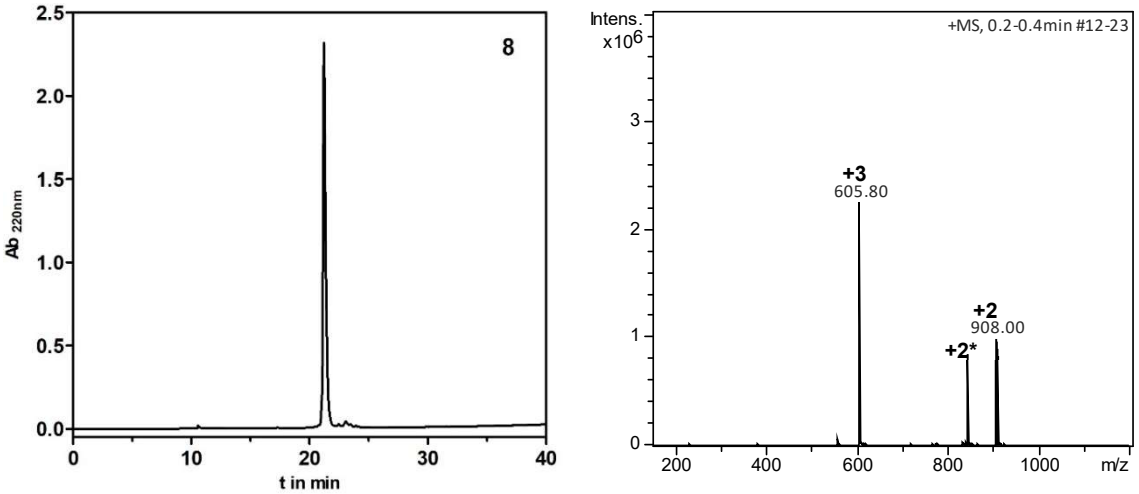

Figure A14. RP-HPLC profile and ESI-ion trap mass spectrum of GnRH-III-[^{3}Tic, ^{8}Lys(Dau=Aoa)] (**8**) (MW_{cal} /MW_{exp} = 1814.86/1814.40 g/mol).

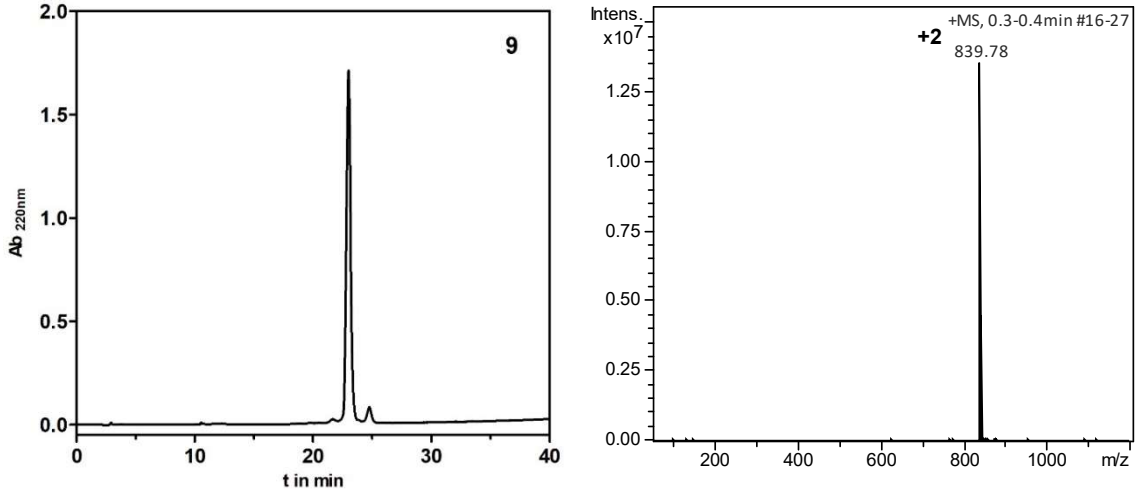

Figure A15. RP-HPLC profile and ESI-ion trap mass spectrum of GnRH-III-[^{2}ΔHis, ^{3}D-Tic, ^{8}Lys(Dau=Aoa)] (**9**) (MW_{cal} /MW_{exp} = 1677.72/1677.56 g/mol).

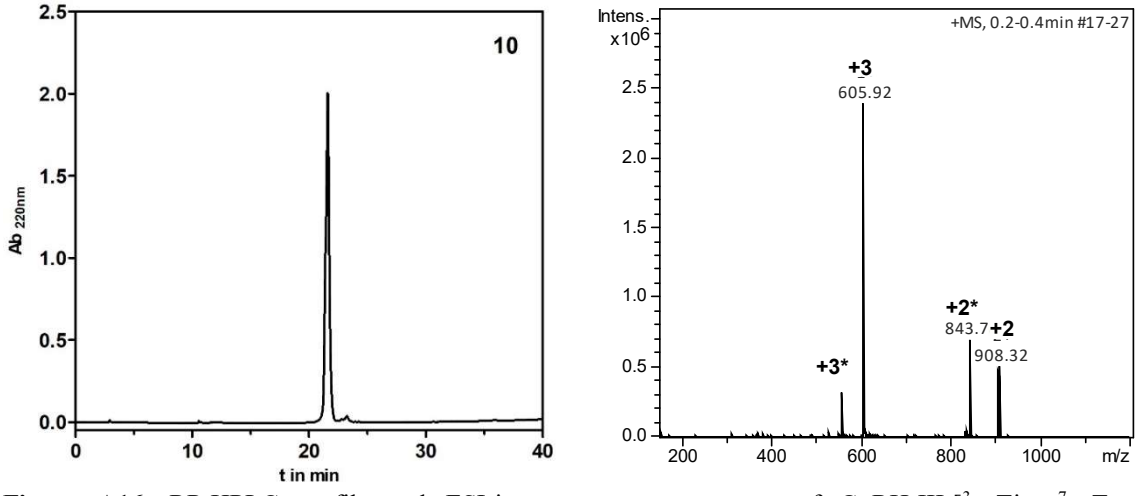

Figure A16. RP-HPLC profile and ESI-ion trap mass spectrum of GnRH-III-[^{3}D-Tic, ^{7}D-Trp. ^{8}Lys(Dau=Aoa)] (**10**) (MW_{cal} /MW_{exp} = 1814.86/1814.64 g/mol).

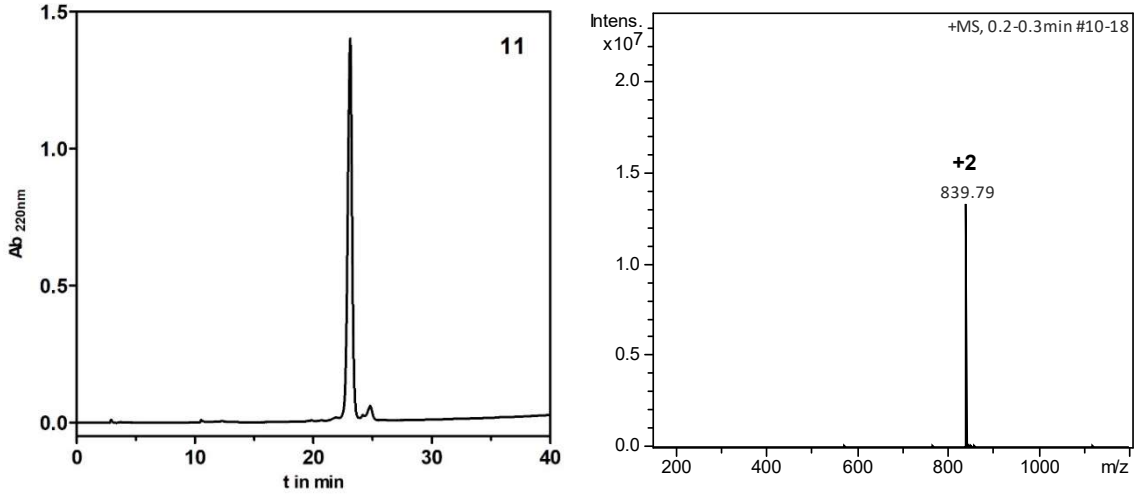

Figure A17. RP-HPLC profile and ESI-ion trap mass spectrum of GnRH-III-[^{2}ΔHis, ^{3}D-Tic, ^{7}D-Trp, ^{8}Lys(Dau=Aoa)] (**11**) (MW_{cal} /MW_{exp} = 1677.72/1677.58 g/mol).

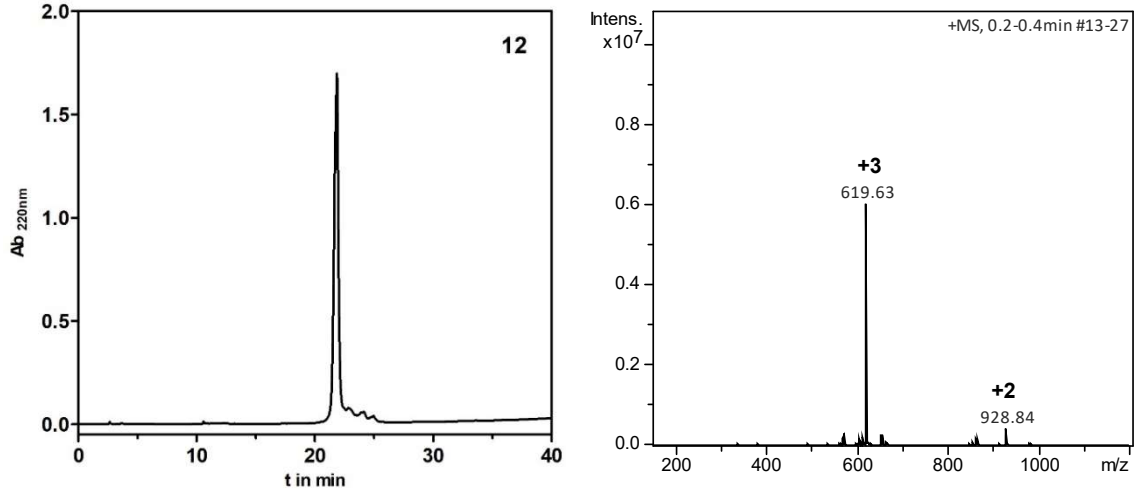

Figure A18. RP-HPLC profile and ESI-ion trap mass spectrum of GnRH-III-[^{6}Asp(OMe), ^{8}Lys(Dau=Aoa)] (**12**) (MW_{cal} /MW_{exp} = 1855.91/1855.68 g/mol).

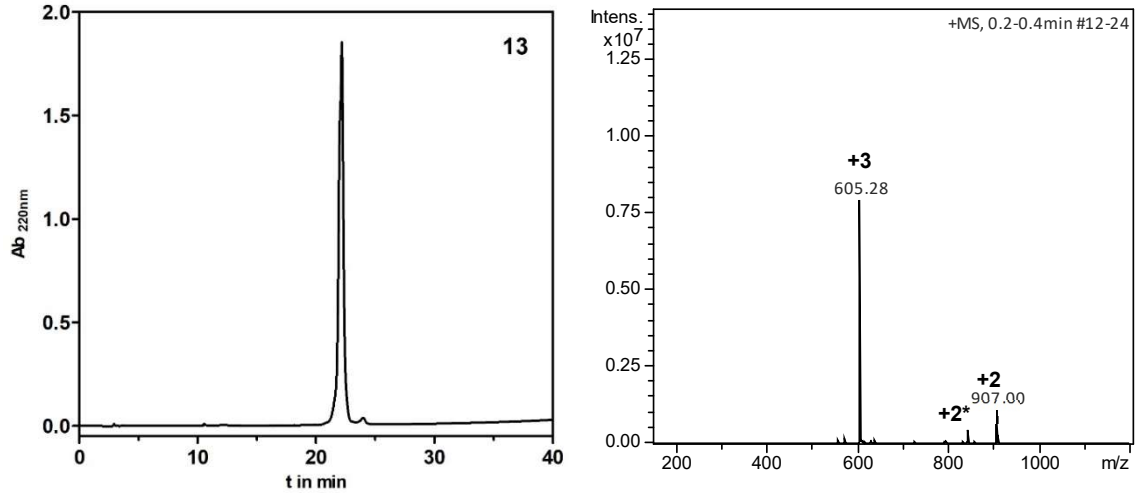

Figure A19. RP-HPLC profile and ESI-ion trap mass spectrum of GnRH-III-[^{8}Lys(Dau=Aoa), ^{10}ΔGly-NH-Et] (**13**) (MW_{cal} /MW_{exp} = 1812.88/1812.84 g/mol).

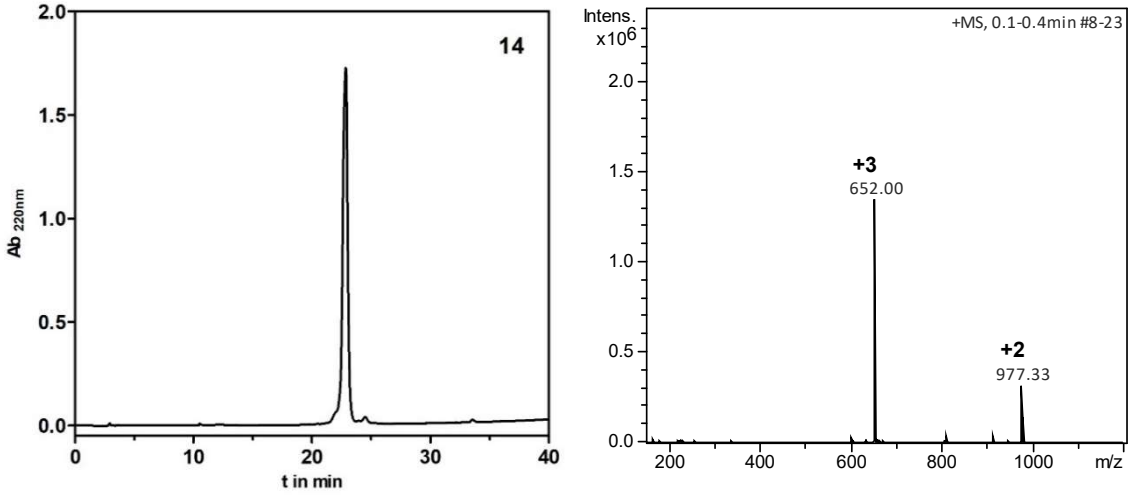

Figure A20. RP-HPLC profile and ESI-ion trap mass spectrum of GnRH-III-[^{3}D-Trp, ^{4}Lys(Bu), ^{8}Lys(Dau=Aoa)] (**14**) (MW_{cal} /MW_{exp} = 1953.07/1953.00 g/mol).

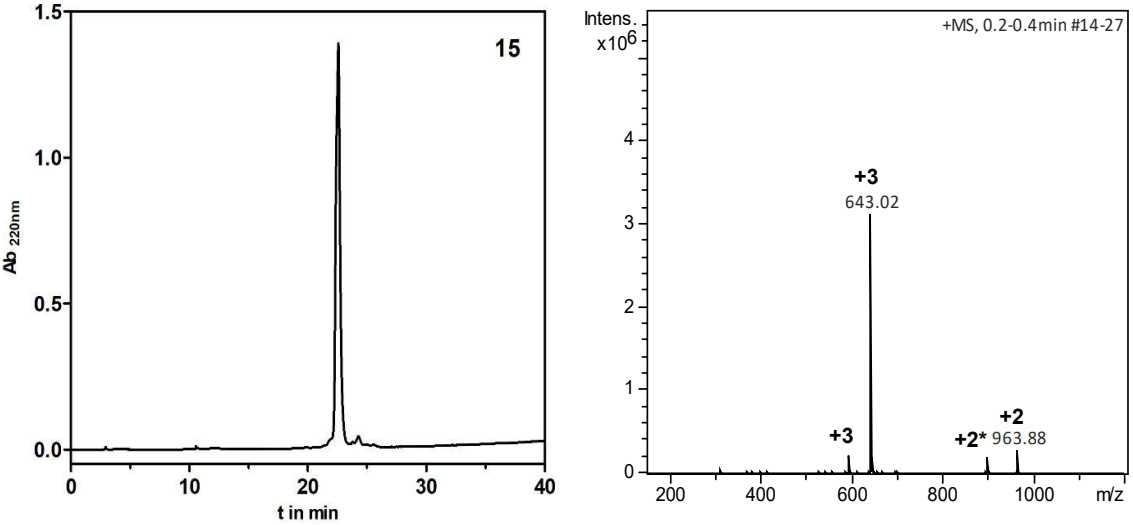

Figure A21. RP-HPLC profile and ESI-ion trap mass spectrum of GnRH-III-[^{3}D-Tic, ^{4}Lys(Bu), ^{8}Lys(Dau=Aoa)] (**15**) (MW_{cal} /MW_{exp} = 1926.05/1926.06 g/mol).

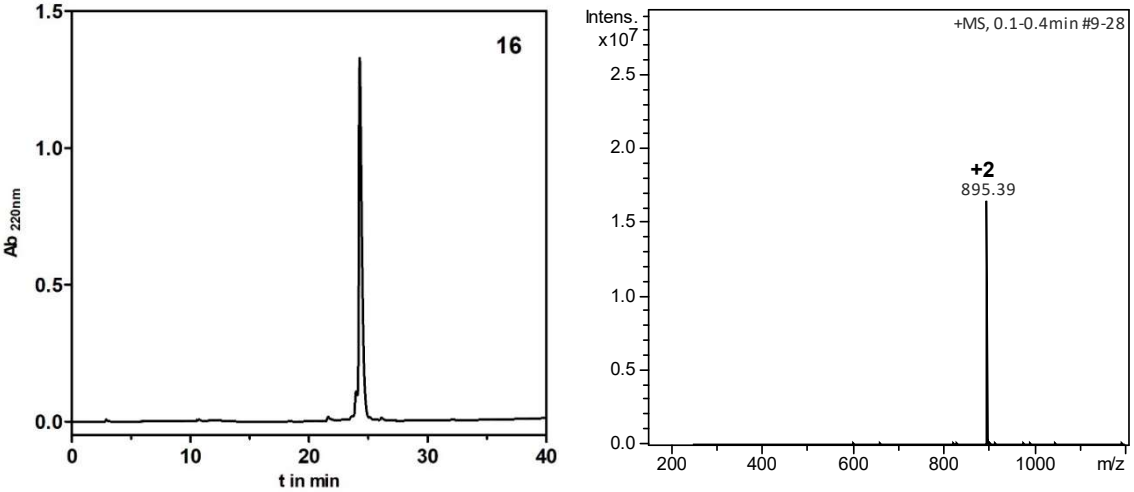

Figure A22. RP-HPLC profile and ESI-ion trap mass spectrum of GnRH-III-[^{2}ΔHis, ^{3}D-Tic, ^{4}Lys(Bu), ^{8}Lys(Dau=Aoa)] (**16**) (MW_{cal} /MW_{exp} = 1788.91/1788.78 g/mol).

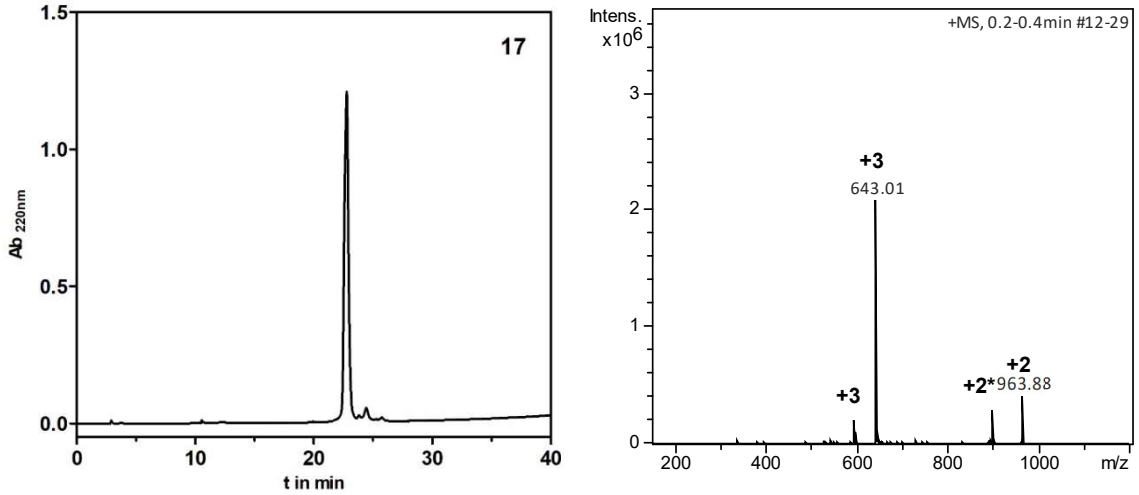

Figure A23. RP-HPLC profile and ESI-ion trap mass spectrum of GnRH-III-[, ^{3}D-Tic, ^{4}Lys(Bu), ^{7}D-Trp, ^{8}Lys(Dau=Aoa)] (**17**) (MW_{cal} /MW_{exp} = 1926.05/1926.03 g/mol).

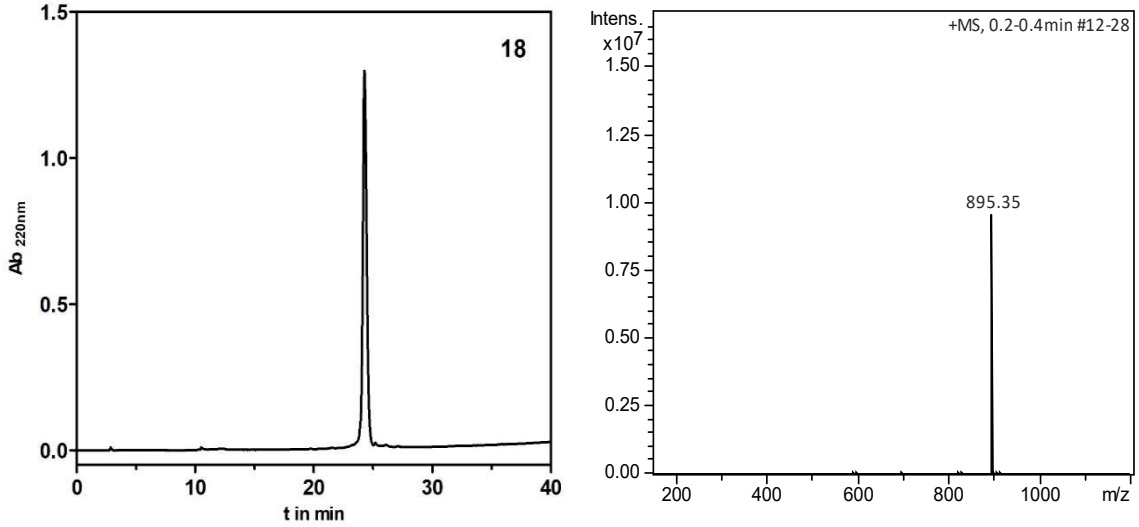

Figure A24. RP-HPLC profile and ESI-ion trap mass spectrum of GnRH-III-[^{2}ΔHis, ^{3}D-Tic, ^{4}Lys(Bu), ^{7}D-Trp, ^{8}Lys(Dau=Aoa)] (**18**) (MW_{cal} /MW_{exp} = 1788.91/1788.70 g/mol).

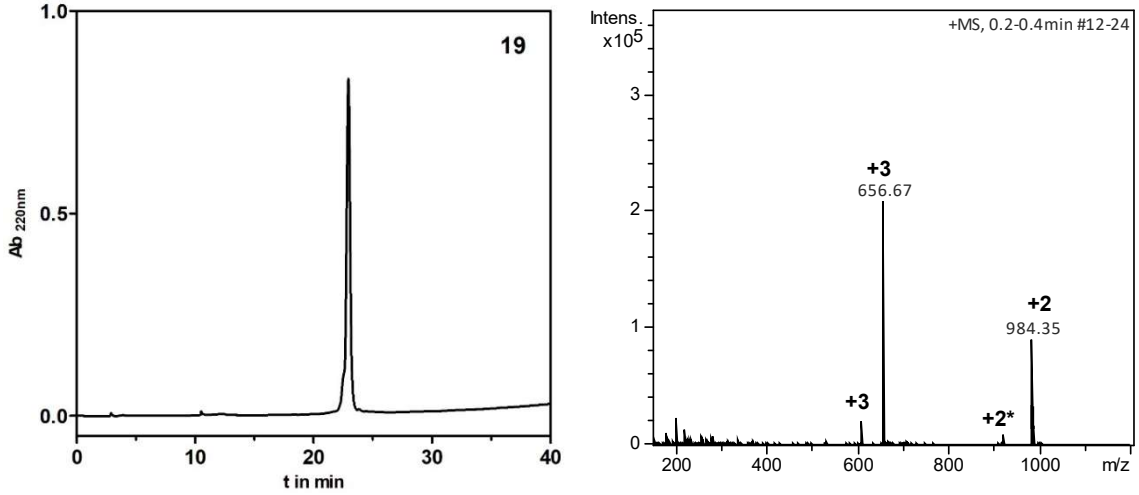

Figure A25. RP-HPLC profile and ESI-ion trap mass spectrum of GnRH-III-[^{4}Lys(Bu), ^{6}Asp(OMe), ^{8}Lys(Dau=Aoa)] (**19**) (MW_{cal} /MW_{exp} = 1967.10/1967.01 g/mol).

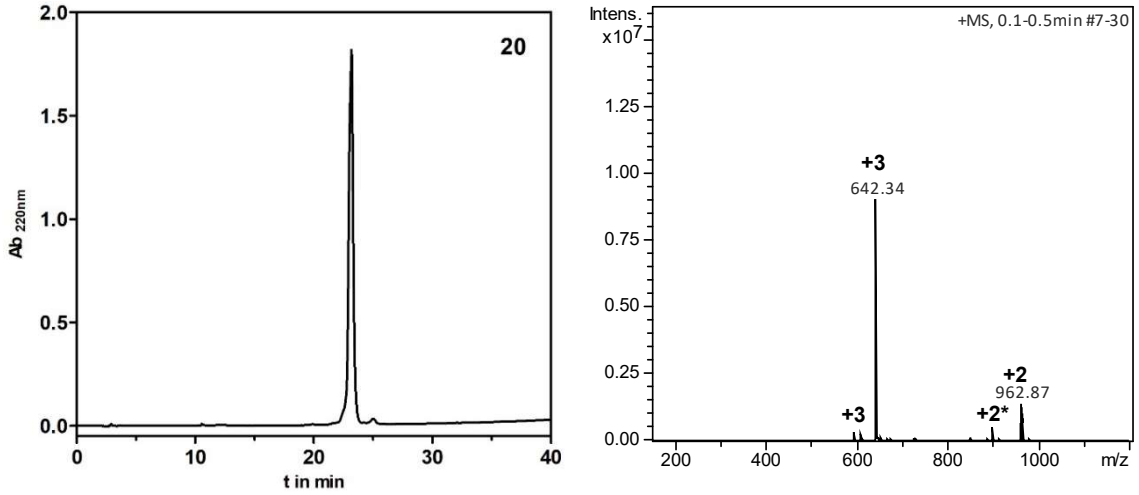

Figure A26. RP-HPLC profile and ESI-ion trap mass spectrum of GnRH-III-[^{8}Lys(Dau=Aoa), ^{10}ΔGly-NH-Et] (**20**) (MW_{cal} /MW_{exp} = 1924.07/1924.02 g/mol).

10.1.2.2. In vitro cytostatic effect – Dose response curves

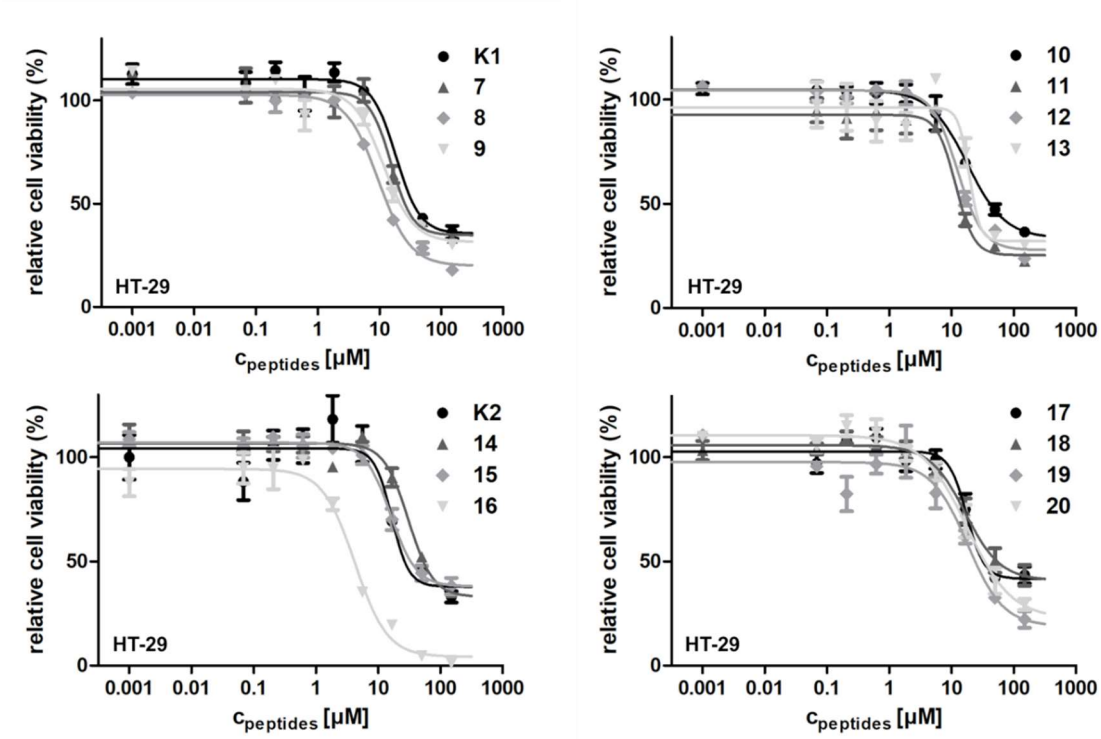

Figure A27. Cytostatic effect of 2nd set of GnRH-III conjugate on HT-29 human cancer cells after 72 h (24 h treatment and an additional 48 h incubation). Curves obtained by non-linear regression (sigmoidal dose response, error bars represent the standard deviation of four parallels, the measurements were repeated twice).

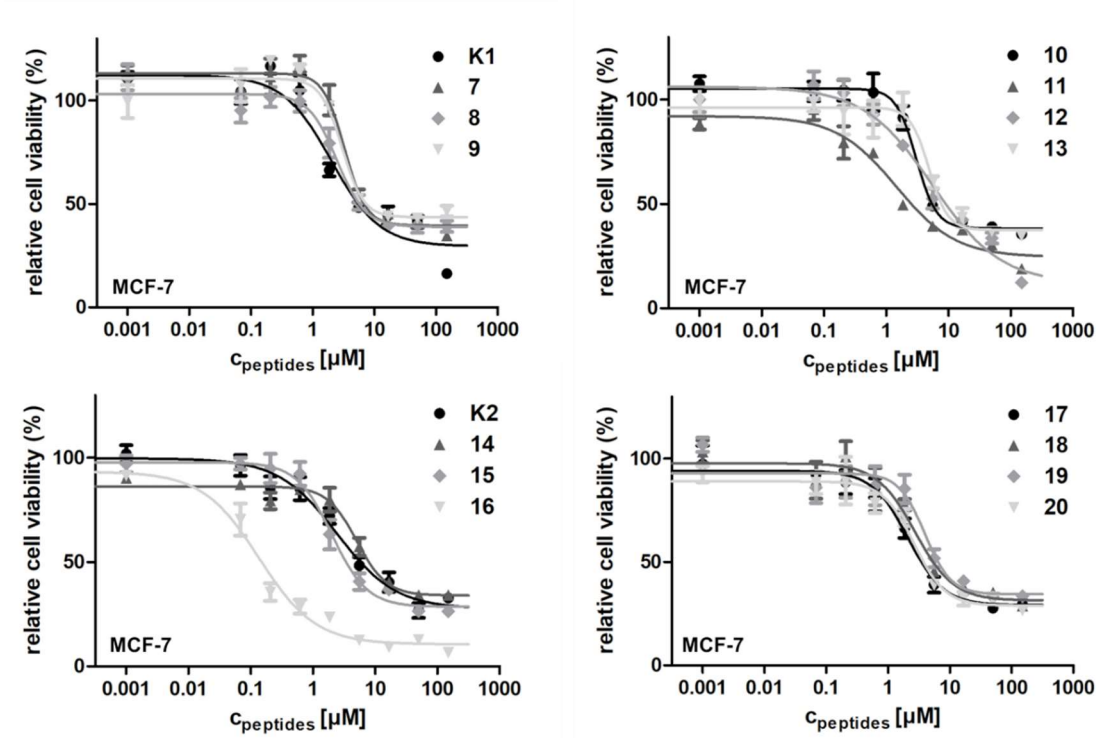

Figure A28. Cytostatic effect of 2nd set of GnRH-III conjugate on MCF-7 human cancer cells after 72 h (24 h treatment and an additional 48 h incubation). Curves obtained by non-linear regression (sigmoidal dose response, error bars represent the standard deviation of four parallels, the measurements were repeated twice).

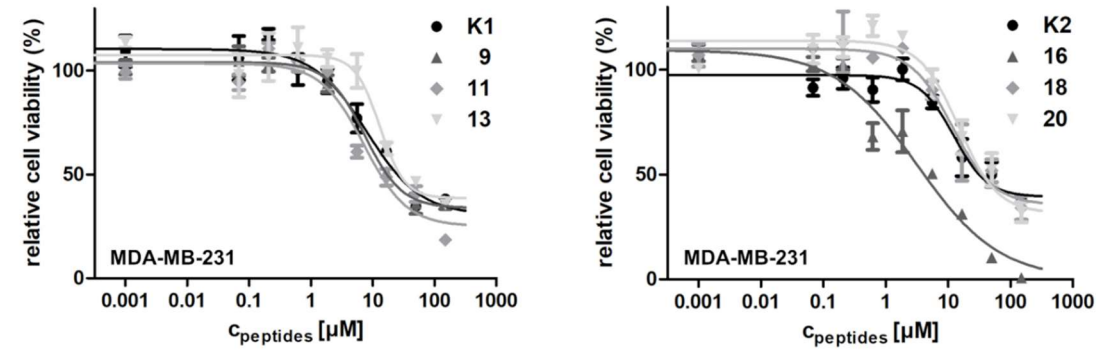

Figure A29. Cytostatic effect of 2nd set of GnRH-III conjugate on MDA-MB-231 human cancer cells after 72 h (24 h treatment and an additional 48 h incubation). Curves obtained by non-linear regression (sigmoidal dose response, error bars represent the standard deviation of four parallels, the measurements were repeated twice).

10.1.2.3. Western blot studies

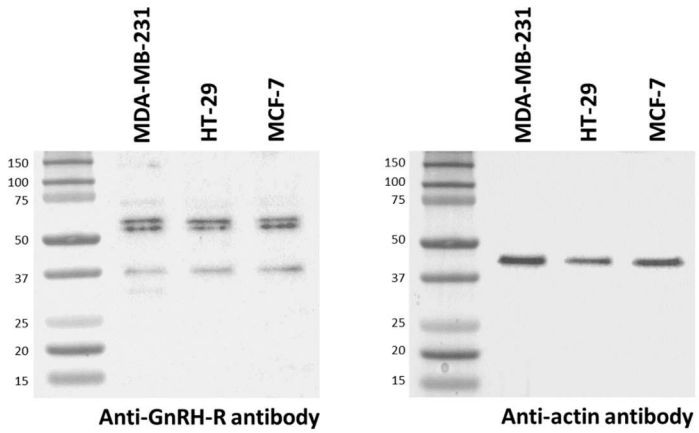

Figure A30. Western blot performed on whole cell lysates of MDA-MB-231, HT-29 and MCF-7 cancer cells. Anti-GnRH-R antibody (Proteintech, 19950-1AP) (left) was used to detect GnRH-R. Actin expression was evaluated as loading control (Santa Cruz Biotechnology, sc-1616 (right). Band at 38 kDa represents the full length human GnRH-R; the signals at higher molecular weight (55-70 kDa) are assumed to be glycosylated forms of the receptor.

10.1.2.4. Plasma stability

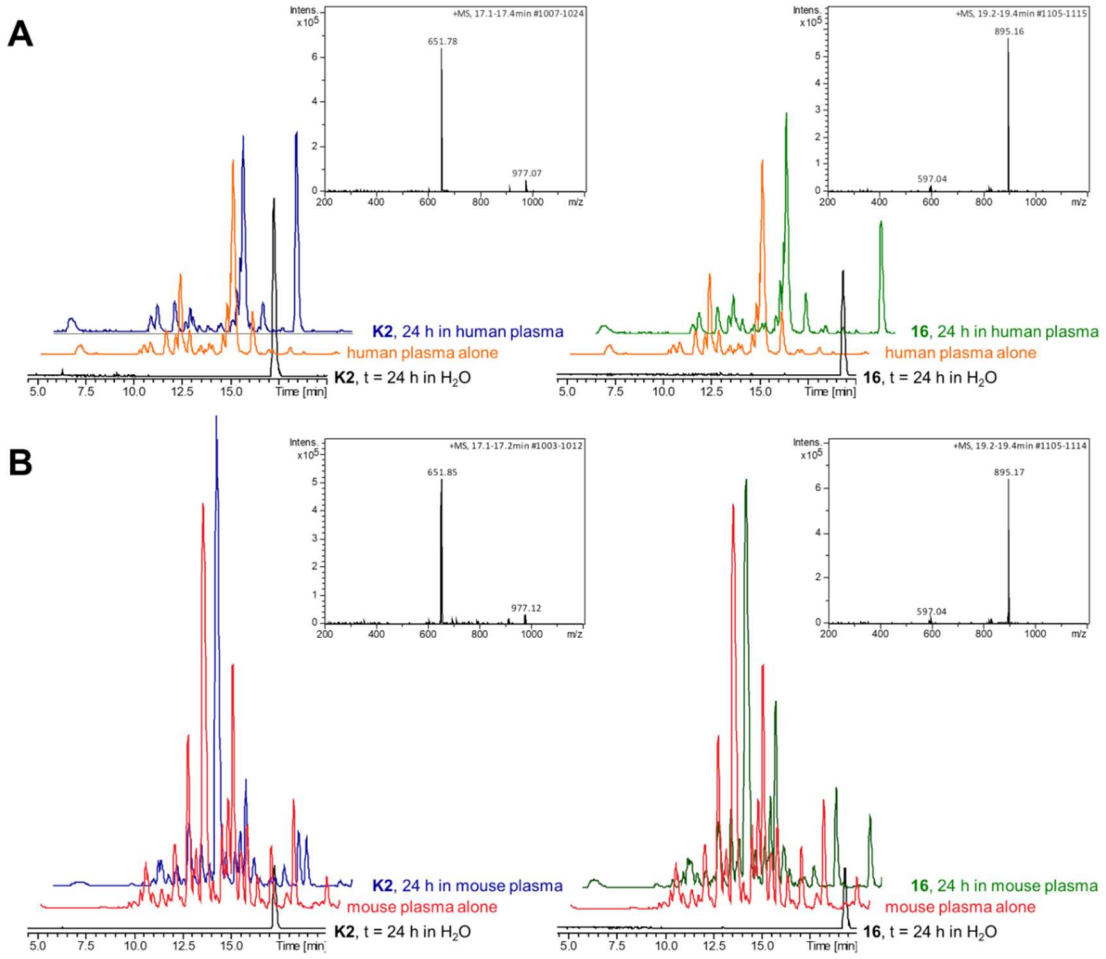

Figure A31. Stability of the bioconjugates **K2** and **16** in human plasma. LC-MS chromatogram of human plasma and the conjugates after 24 h incubation at 37 °C in H_2O or in human plasma plus the corresponding MS compound spectra.

10.1.2.5. Lysosomal degradation in presence of rat liver lysosomal homogenate

Table A2. Fragments of GnRH-III-Dau conjugates **K2** and **16** produced by rat liver homogenate

Code	Compound	Fragment	MW_{cal}/MW_{exp}
K2	[^{4}Lys(Bu),	<EHWK(Bu)HDWK(Dau=Aoa)PG-NH_2	1953.07/1952.79
	^{8}Lys(Dau=Aoa)]	<EHWK(Bu)HDWK(Dau=Aoa)-OH	1799.92/1799.69
		H-HDWK(Dau=Aoa)PG-NH_2	1320.36/1319.95
		H-HDWK(Dau=Aoa)-OH	1167.18/1166.91
		H-K(Dau=Aoa)PG-NH_2	881.94/881.44
		H-K(Dau=Aoa)P-OH	825.86/825.40
		H-K(Dau=Aoa)-OH	728.75/728.37
		<EHWK(Bu)HD-OH	902.96/902.84
		<EHWK(Bu)-OH	650.73/650.71
		<EHW-OH	452.46/452.31
		H-DW-OH	319.32/319.27
16	[^{2}ΔHis, ^{3}D-Tic, ^{4}Lys(Bu),	<E-D-Tic-K(Bu)HDWK(Dau=Aoa)PG-NH_2	1788.91/1788.33
	^{8}Lys(Dau=Aoa)]	<E-D-Tic-K(Bu)HDWK(Dau=Aoa)-OH	1635.72/1635.22
		<E-D-Tic-K(Bu)HDW-OH	925.00/924.32
		<E-D-Tic-K(Bu)HD-OH	738.78/738.26
		<E-D-Tic-K(Bu)H-OH	623.70/623.29
		<E-D-Tic-K(Bu)-OH	486,56/486.90
		H-K(Dau=Aoa)P-OH	825.86/825.40
		H-K(Dau=Aoa)-OH	728.75/728.37

10.1.2.6. Radioligand binding studies

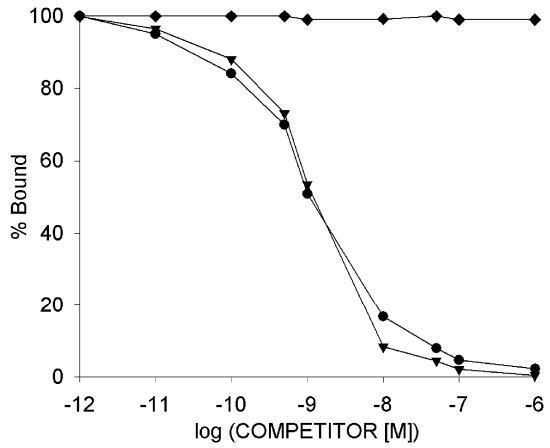

Figure A32. Representative displacement of [^{125}I]-GnRH-I-[^{6}D-Trp] binding to membrane fractions of human prostate cancer specimens by increasing concentrations of GnRH-III conjugates **16** (●) and **K2** (▼). Other unrelated peptides, like somatostatin, human growth hormone and epidermal growth factor (♦) did not displace the radioligand. Each point represents mean of duplicate or triplicate determinations.

10.1.3. Self-immolative and non-cleavable linker-containing GnRH-III-Dau and -PTX conjugates

10.1.3.1. RP-HPLC profile and ESI-ion trap mass spectrum

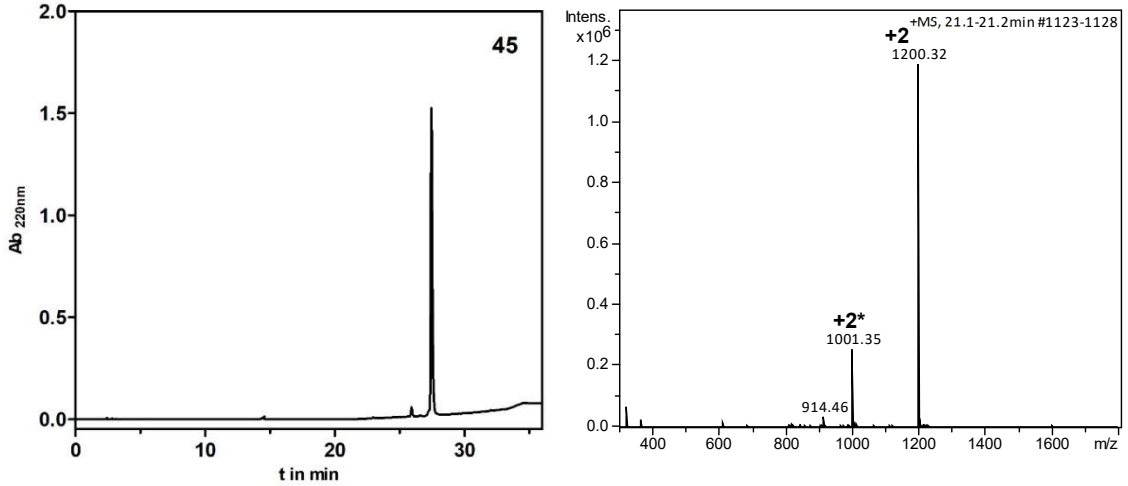

Figure A33. RP-HPLC profile and ESI-ion trap mass spectrum of GnRH-III-[^{2}His-^{3}Trp,^{8}Lys(glutaryl-Val-Cit-PABC-Dau)] conjugate (**45**) (MW_{cal} /MW_{exp} = 2399.57/2398.63 g/mol).

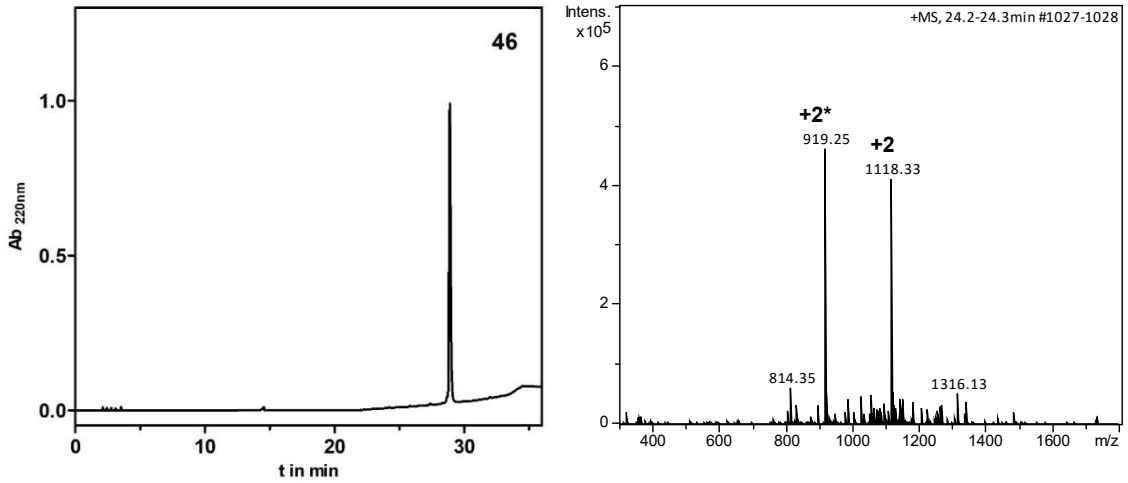

Figure A34. RP-HPLC profile and ESI-ion trap mass spectrum of GnRH-III-[^{2}ΔHis-^{3}D-Tic,^{8}Lys(glutaryl-Val-Cit-PABC-Dau)] conjugate (**46**) (MW_{cal} /MW_{exp} = 2235.40/2234.45 g/mol).

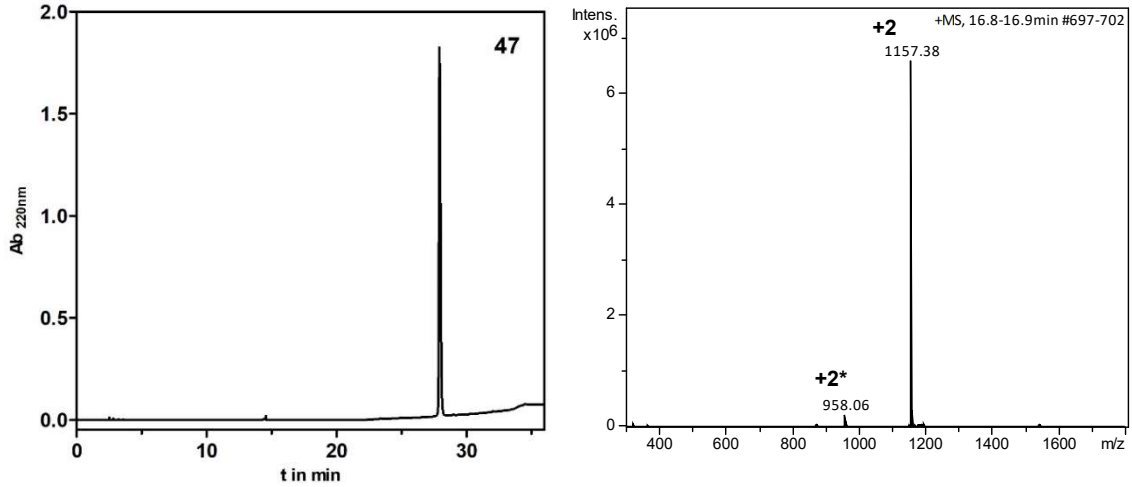

Figure A35. RP-HPLC profile and ESI-ion trap mass spectrum of GnRH-III-[^{2}His-^{3}Trp,^{8}Lys(glutaryl-Val-Ala-PABC-Dau)] conjugate (**47**) (MW_{cal} /MW_{exp} = 2235.40/2234.45 g/mol).

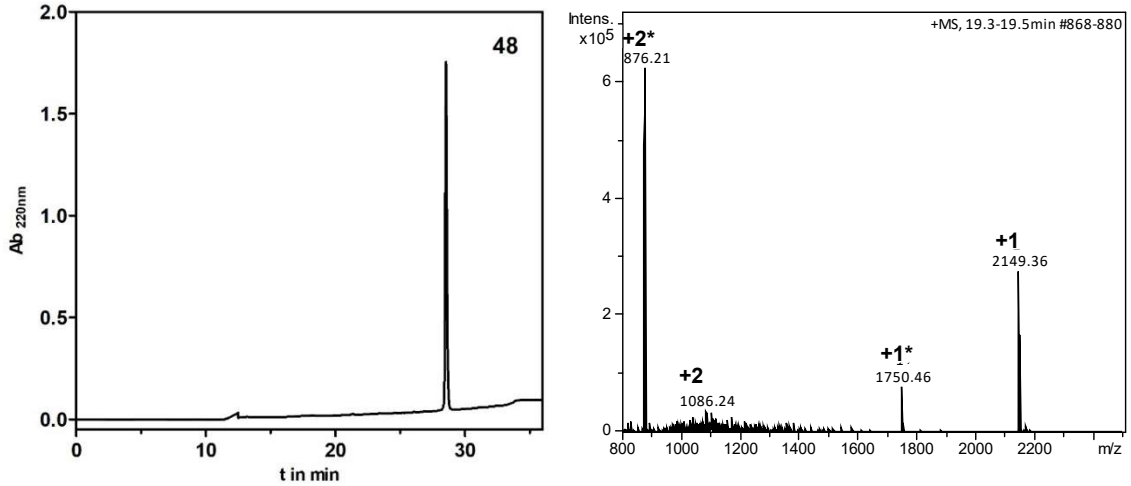

Figure A36. RP-HPLC profile and ESI-ion trap mass spectrum of GnRH-III-[^{2}ΔHis-^{3}D-Tic, ^{8}Lys(glutaryl-Val-Cit-PABC-Dau conjugate (**48**) (MW_{cal} /MW_{exp} = 2149.31/2148.35 g/mol).

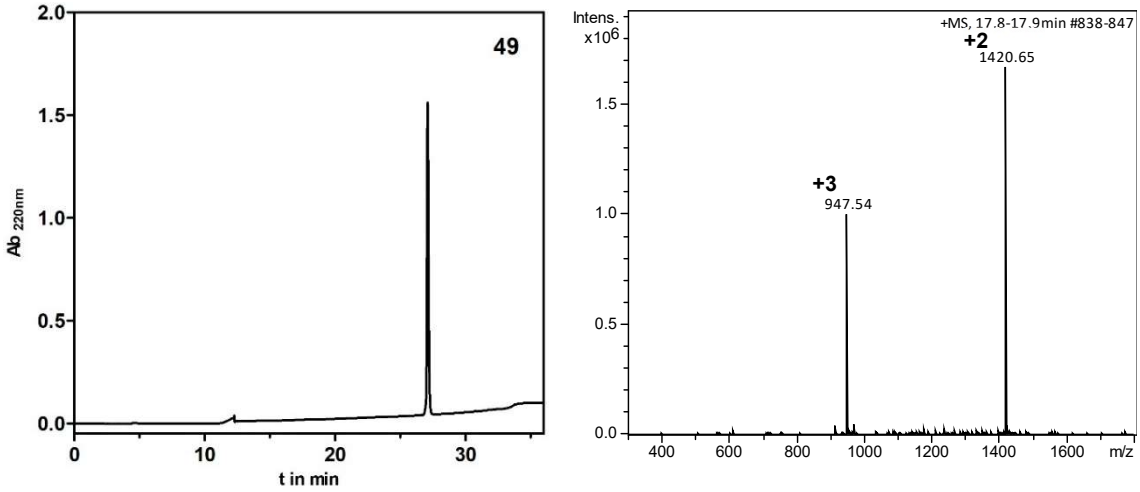

Figure A37. RP-HPLC profile and ESI-ion trap mass spectrum of GnRH-III-[^{2}His-^{3}Trp,^{8}Lys(glutaryl-Val-Cit-PABC-diamine-PTX)] conjugate (**49**) (MW_{cal} /MW_{exp} = 2840.10/2839.30 g/mol).

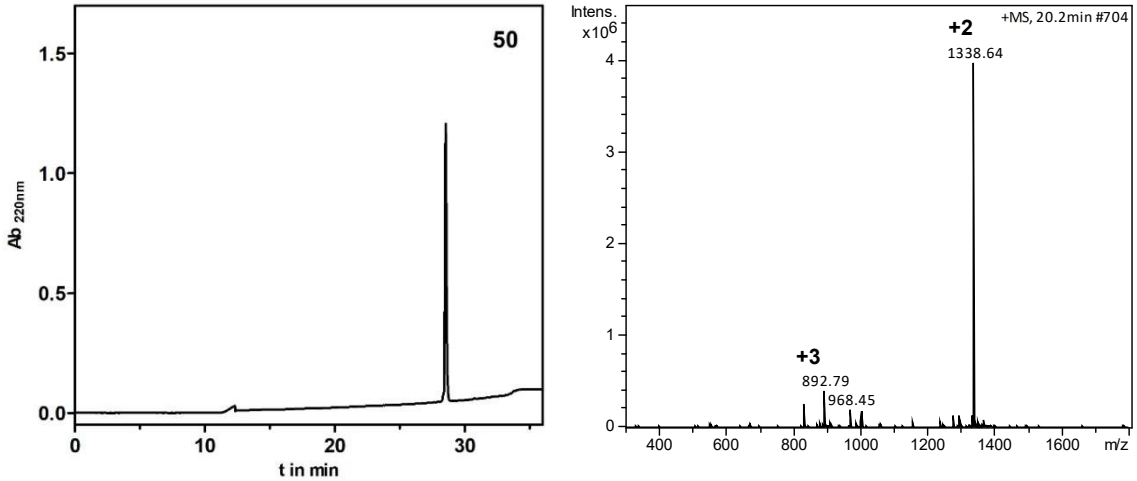

Figure A38. RP-HPLC profile and ESI-ion trap mass spectrum of GnRH-III-[^{2}ΔHis-^{3}D-Tic,^{8}Lys(glutaryl-Val-Cit-PABC-diamine-PTX)] conjugate (**50**) (MW_{cal} /MW_{exp} = 2675.66/2675.28 g/mol).

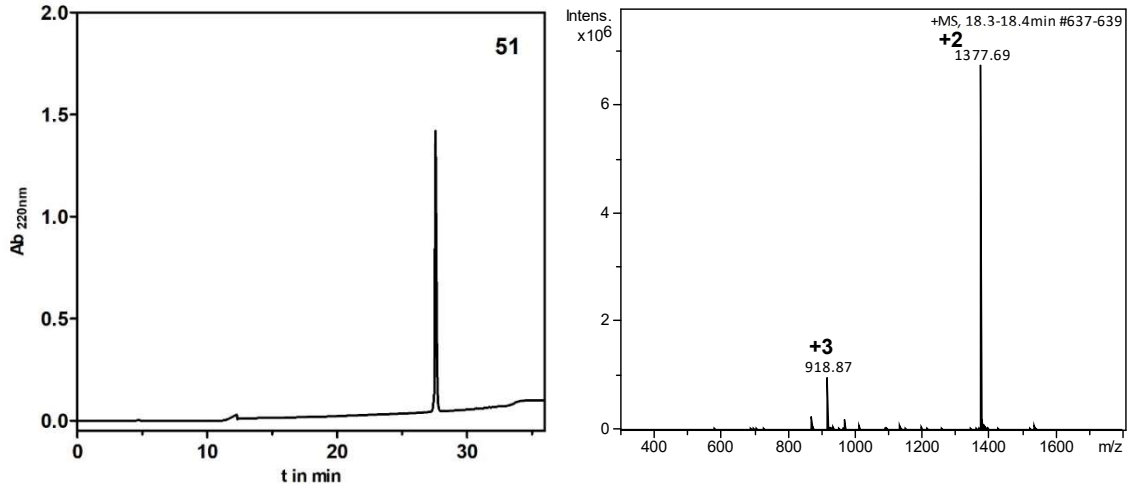

Figure A39. RP-HPLC profile and ESI-ion trap mass spectrum of GnRH-III-[^{2}His-^{3}Trp,^{8}Lys(glutaryl-Val-Ala-PABC-diamine-PTX)] conjugate (**51**) (MW_{cal} /MW_{exp} = 2754.01/2753.38 g/mol).

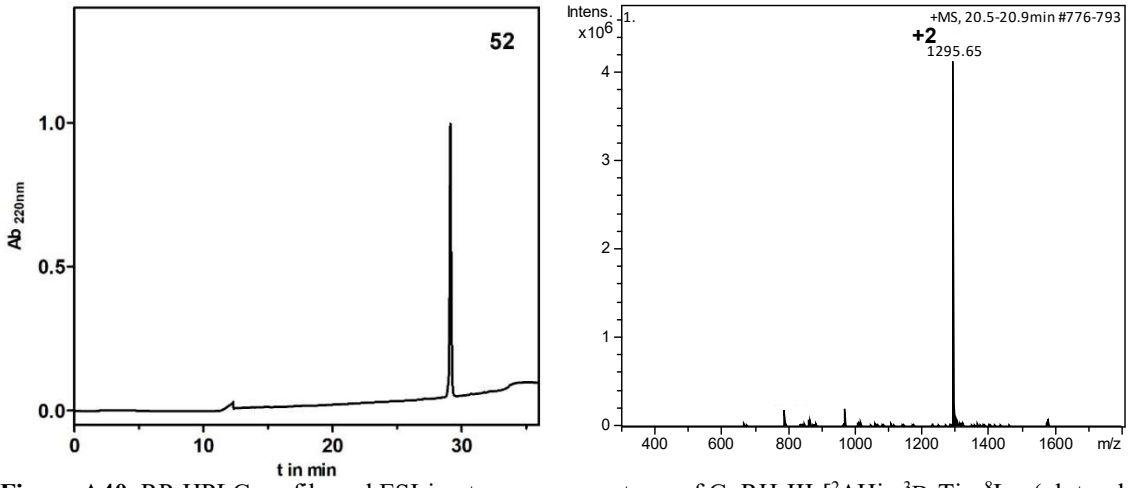

Figure A40. RP-HPLC profile and ESI-ion trap mass spectrum of GnRH-III-[^{2}ΔHis-^{3}D-Tic, ^{8}Lys(glutaryl-Val-Cit-PABC-diamine-PTX)] conjugate (**52**) (MW_{cal} /MW_{exp} = 2589.84/2589.30 g/mol).

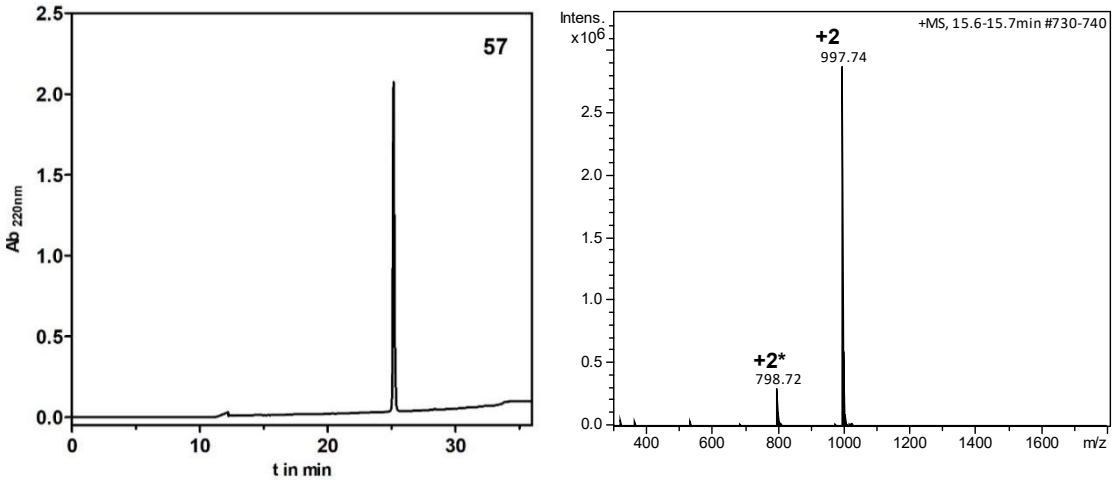

Figure A41. RP-HPLC profile and ESI-ion trap mass spectrum of GnRH-III-[^{2}His-^{3}Trp,^{8}Lys(glutaryl-Dau)] conjugate (**57**) (MW_{cal} /MW_{exp} = 1994.12/1993.48 g/mol).

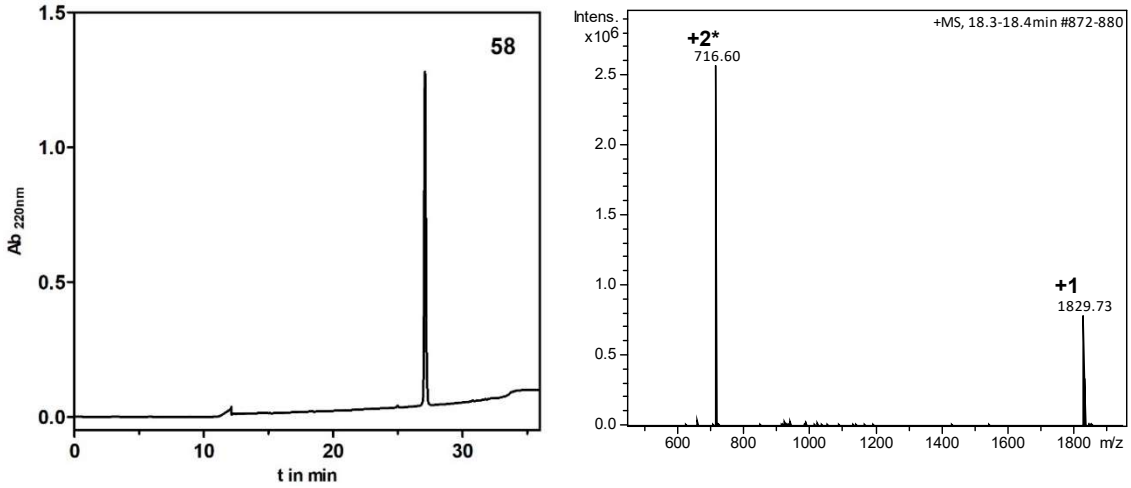

Figure A42. RP-HPLC profile and ESI-ion trap mass spectrum of GnRH-III-[^{2}ΔHis-^{3}D-Tic,^{8}Lys(glutaryl-Dau)] conjugate (**58**) (MW_{cal} /MW_{exp} = 1829.95/1829.75 g/mol).

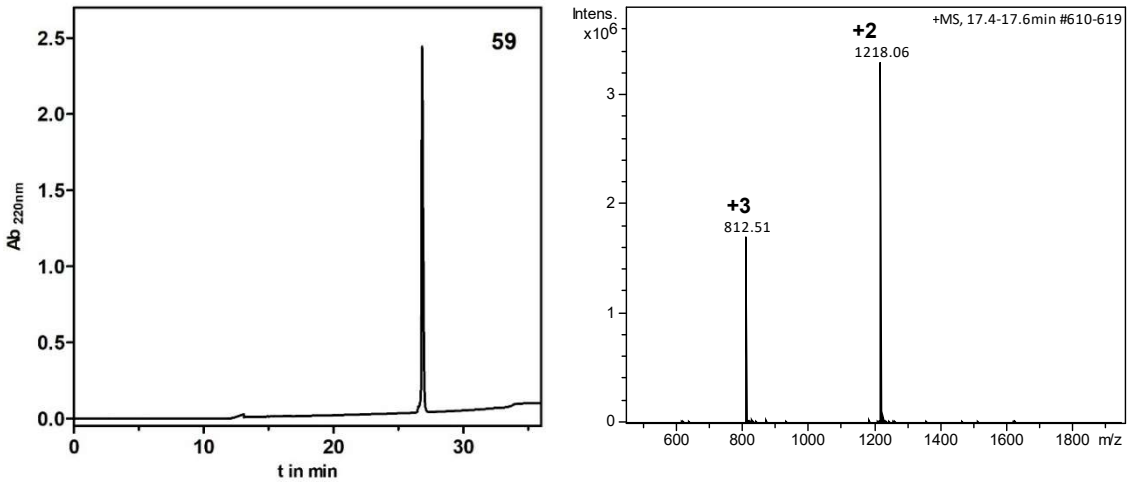

Figure A43. RP-HPLC profile and ESI-ion trap mass spectrum of GnRH-III-[^{2}His-^{3}Trp,^{8}Lys(glutaryl-diamine-PTX)] conjugate (**59**) (MW_{cal} /MW_{exp} = 2434.65/2434.12 g/mol).

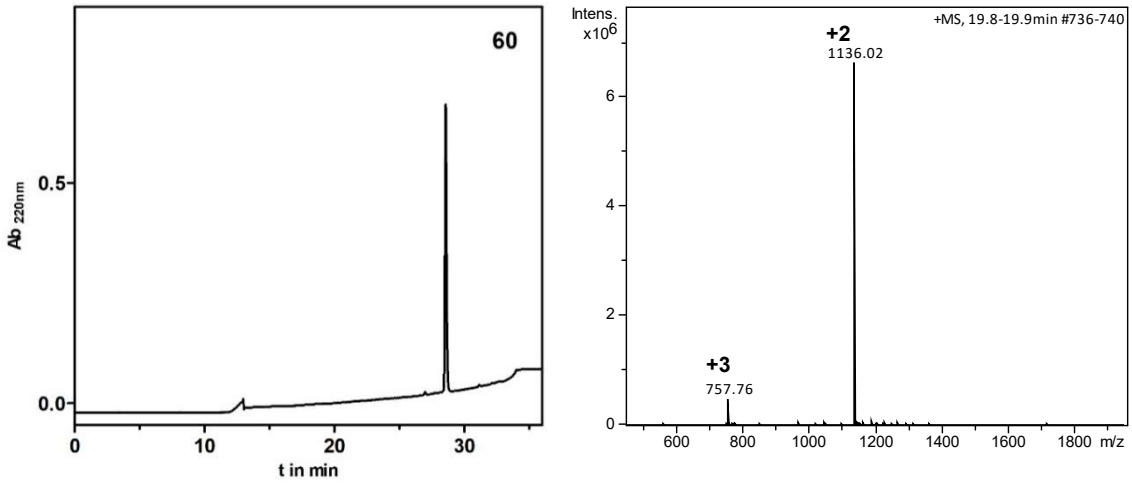

Figure A44. RP-HPLC profile and ESI-ion trap mass spectrum of GnRH-III-[^{2}ΔHis-^{3}D-Tic, ^{8}Lys(glutaryl-diamine-PTX)] conjugate (**60**) (MW_{cal} /MW_{exp} = 2270.49/2270.04 g/mol).

10.1.3.2. In vitro cytostatic effect – Dose response curves

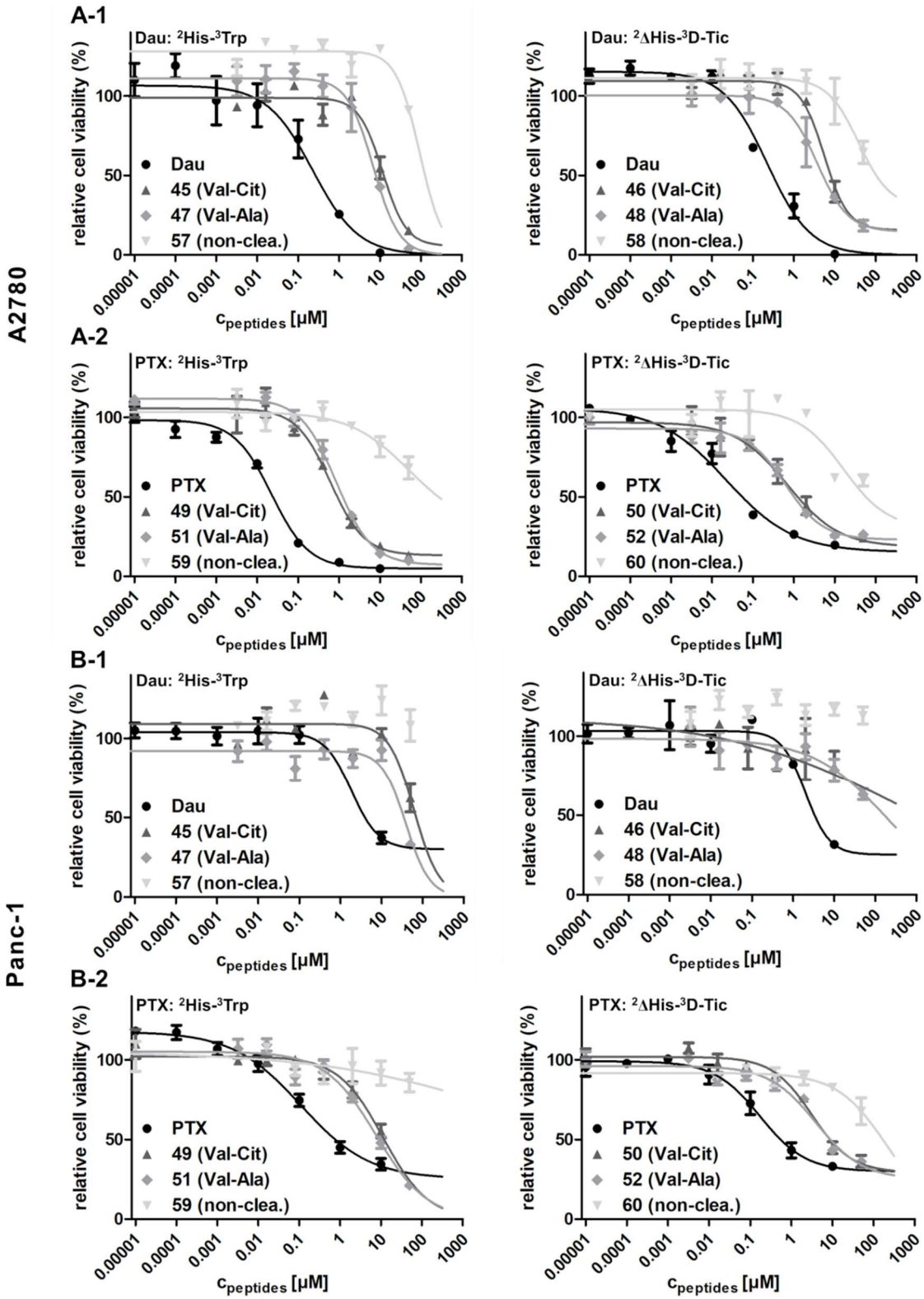

Figure A45. Cytostatic effect of self-immolative and non-cleavable linker-containing GnRH-III conjugate on **A:** A2780 and **B:** Panc-1 human cancer cells. **1**: Dau conjugates after 72 h (24 h treatment, additional 48 h incubation). **2:** PTX conjugates after 72 h (6 h treatment, additional 66 h incubation). Curves obtained by non-linear regression (sigmoidal dose response, error bars represent the standard deviation of three parallels, the measurements were repeated twice).

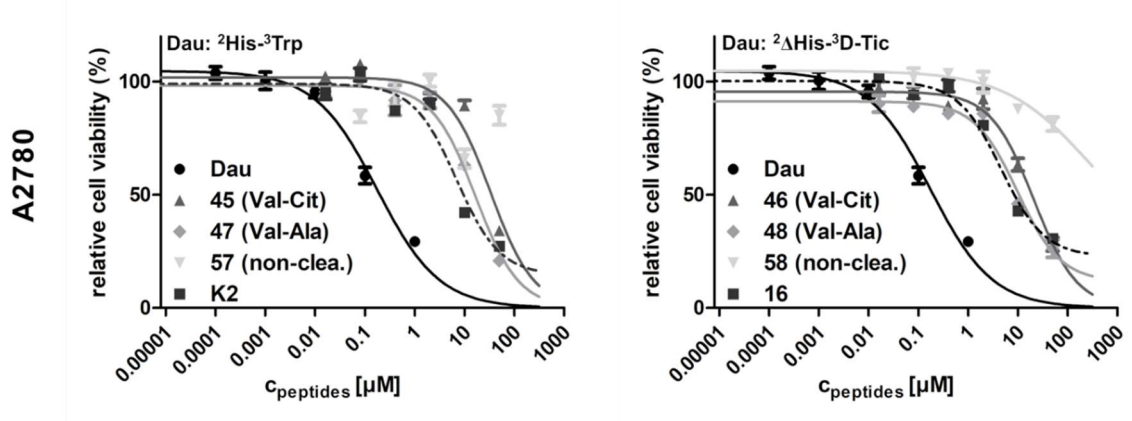

Figure A46. Cytostatic effect of self-immolative and non-cleavable linker-containing GnRH-III-Dau conjugates on A2780 in comparison to the oxime bond-containing GnRH-III compounds **K2** and **16** after 72 h (6 h treatment, additional 66 h incubation). Curves obtained by non-linear regression (sigmoidal dose response, error bars represent the standard deviation of three parallels, the measurements were repeated twice).

10.1.3.3. Lysosomal degradation in presence of rat liver lysosomal homogenate

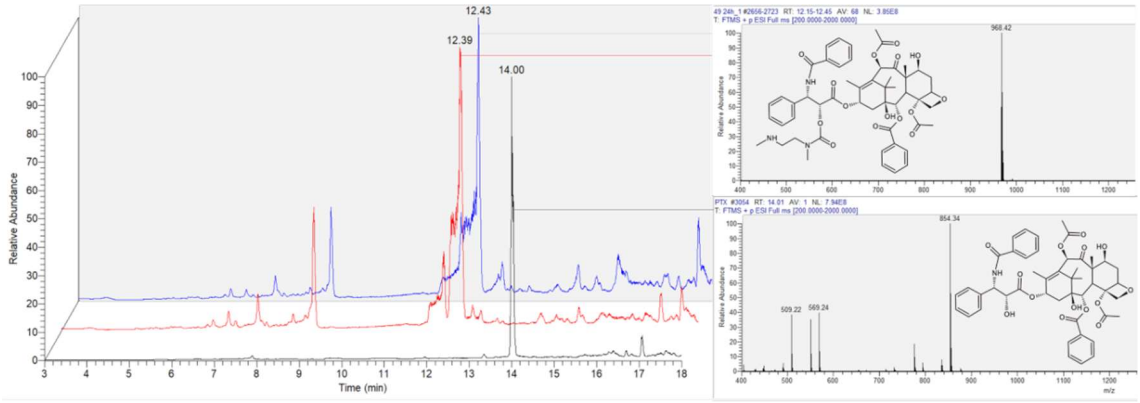

Figure A47. Degradation of the GnRH-III-PTX conjugates in presence of lysosomal rat liver homogenate. LC chromatograms of PTX (black), **49** (red) and **51** (blue) after 24 h degradation and MS spectra of the released PTX prodrug and free PTX.

10.2. Somatostatin conjugates

10.2.1. FAM-somatostatin derivatives

10.2.1.1. RP-HPLC profile and ESI-ion trap mass spectrum

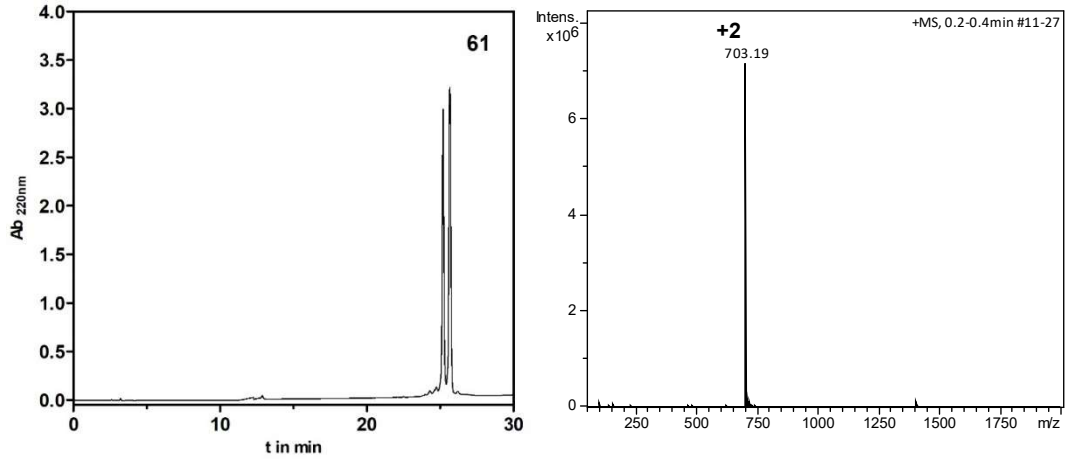

Figure A48. RP-HPLC profile and ESI-ion trap mass spectrum of FAM-somatostatin derivative (**61**) (MW_{cal} /MW_{exp} = 1404.56//1404.37 g/mol).

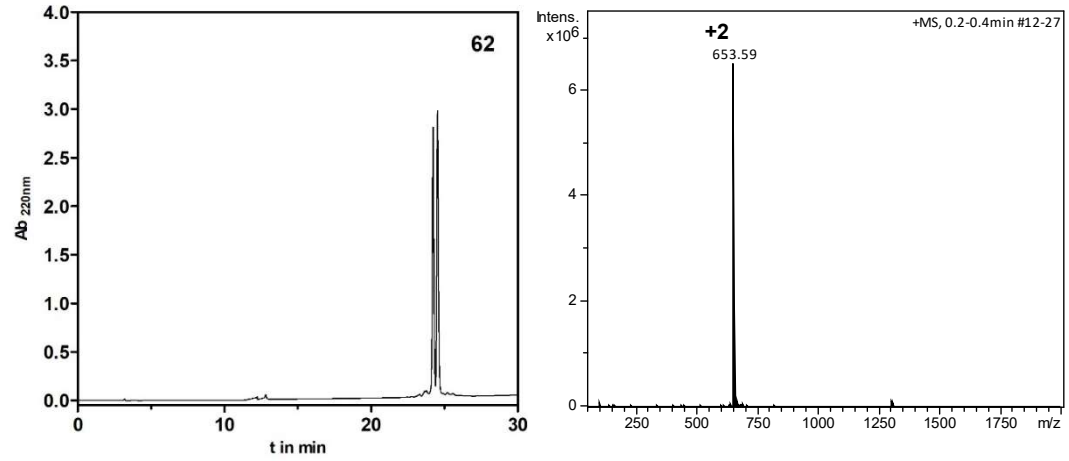

Figure A49. RP-HPLC profile and ESI-ion trap mass spectrum of FAM-somatostatin derivative (**62**) (MW_{cal} /MW_{exp} = 1305.43/1305.16 g/mol).

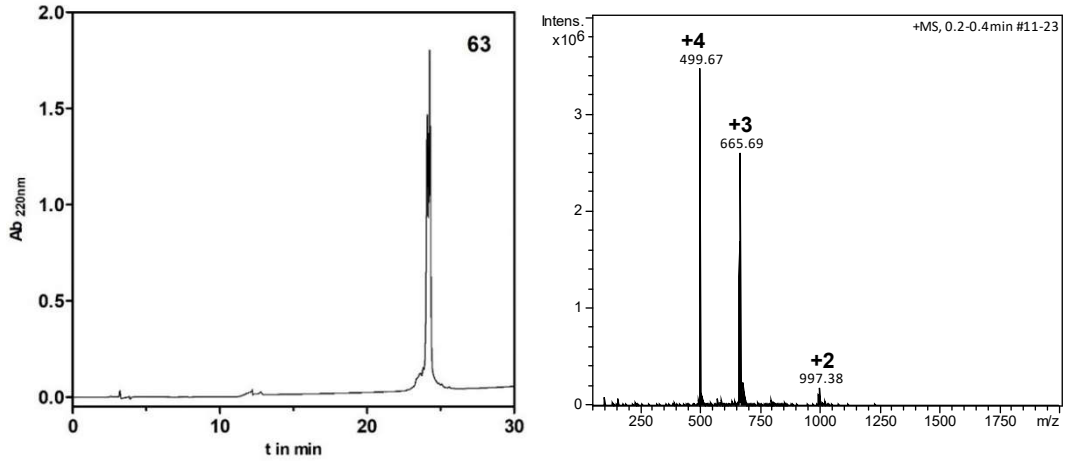

Figure A50. RP-HPLC profile and ESI-ion trap mass spectrum of FAM-somatostatin derivative (**63**) (MW_{cal} /MW_{exp} = 1993.27/1992.76 g/mol).

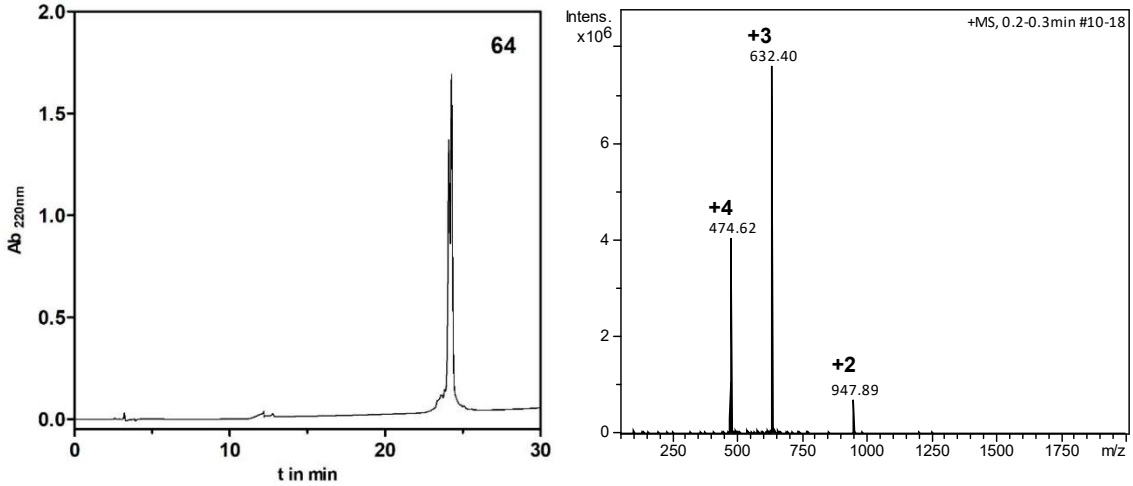

Figure A51. RP-HPLC profile and ESI-ion trap mass spectrum of FAM-somatostatin derivative (**64**) (MW_{cal} /MW_{exp} = 1894.14/1893.78 g/mol).

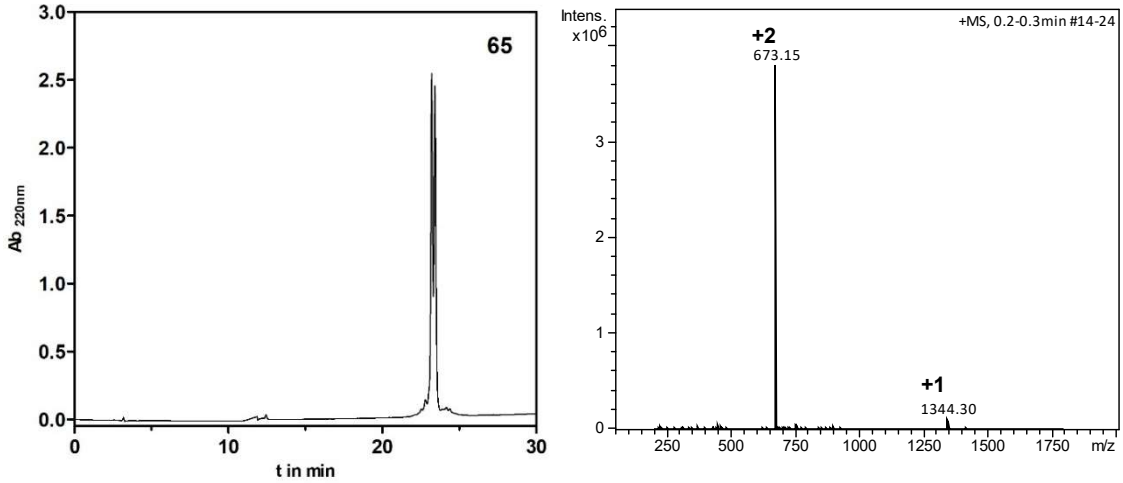

Figure A52. RP-HPLC profile and ESI-ion trap mass spectrum of FAM-somatostatin derivative (**65**) (MW_{cal} /MW_{exp} = 1344.45/1344.3 g/mol).

10.2.2. Somatostatin-drug conjugates

10.2.2.1. RP-HPLC profile and ESI-ion trap mass spectrum

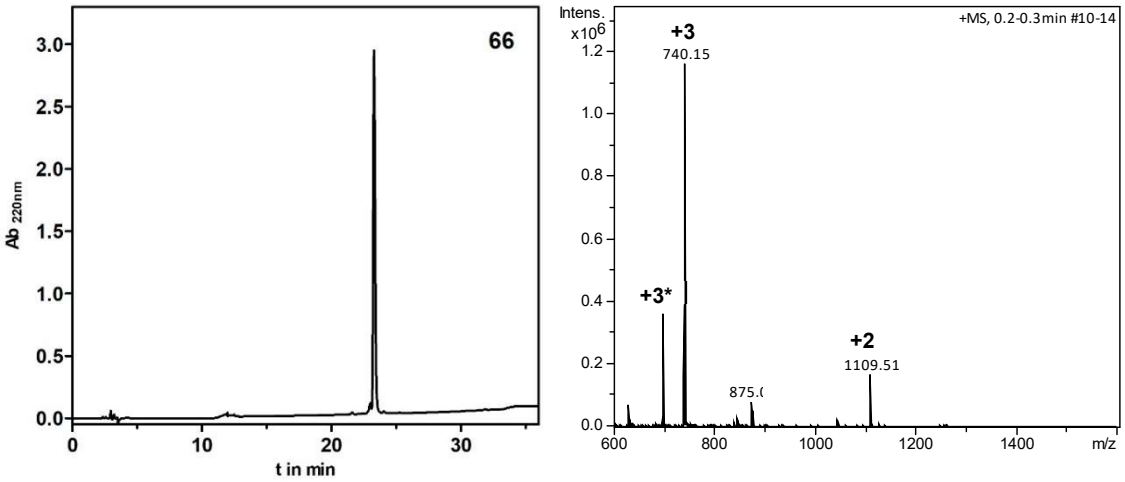

Figure A53. RP-HPLC profile and ESI-ion trap mass spectrum of somatostatin-Dau conjugate (**66**) (MW_{cal} /MW_{exp} = 2217.52/2217.45 g/mol).

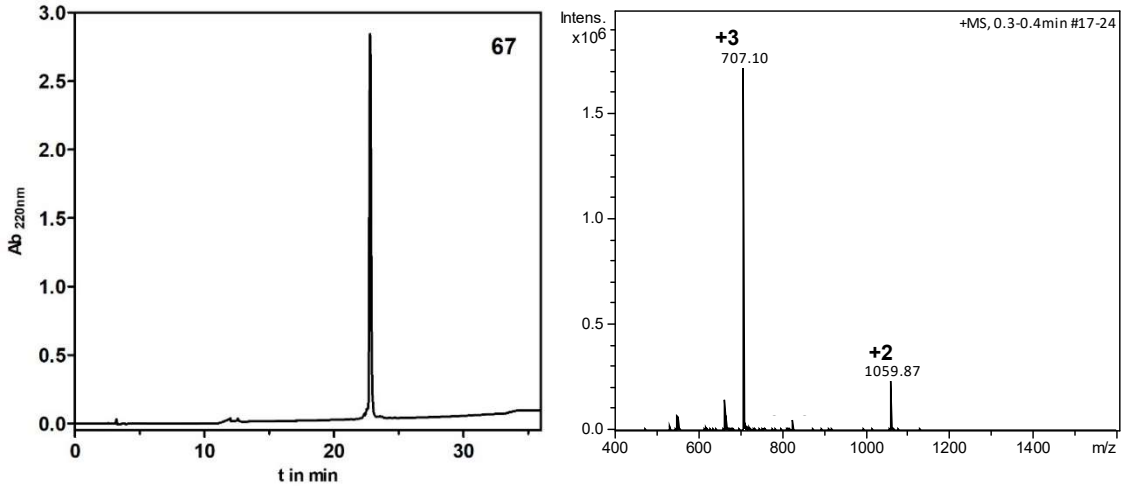

Figure A54. RP-HPLC profile and ESI-ion trap mass spectrum of somatostatin-Dau conjugate (**67**) (MW_{cal} /MW_{exp} = 2118.39/2118.30 g/mol).

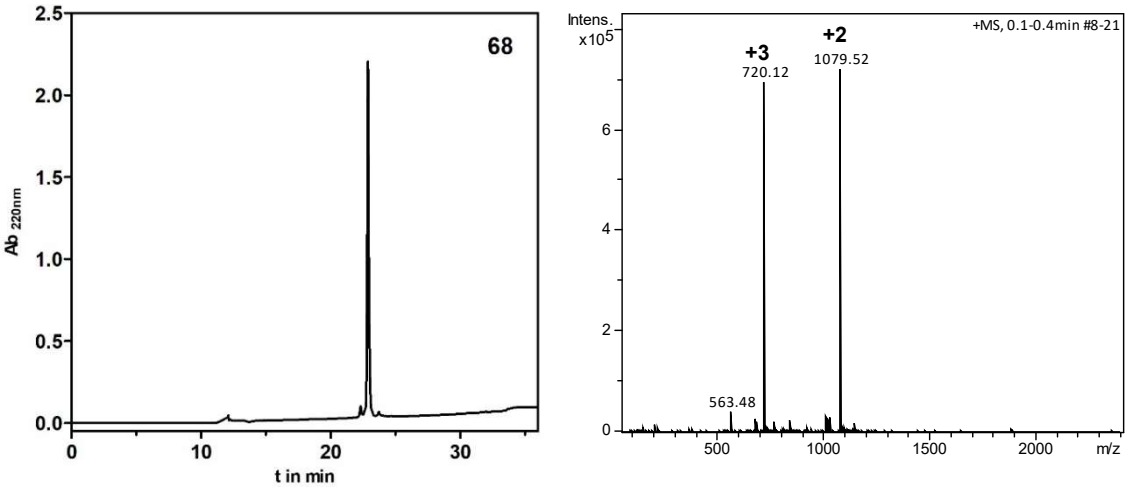

Figure A55. RP-HPLC profile and ESI-ion trap mass spectrum of somatostatin-Dau conjugate (**68**) (MW_{cal} /MW_{exp} = 2157.40/2157.02 g/mol).

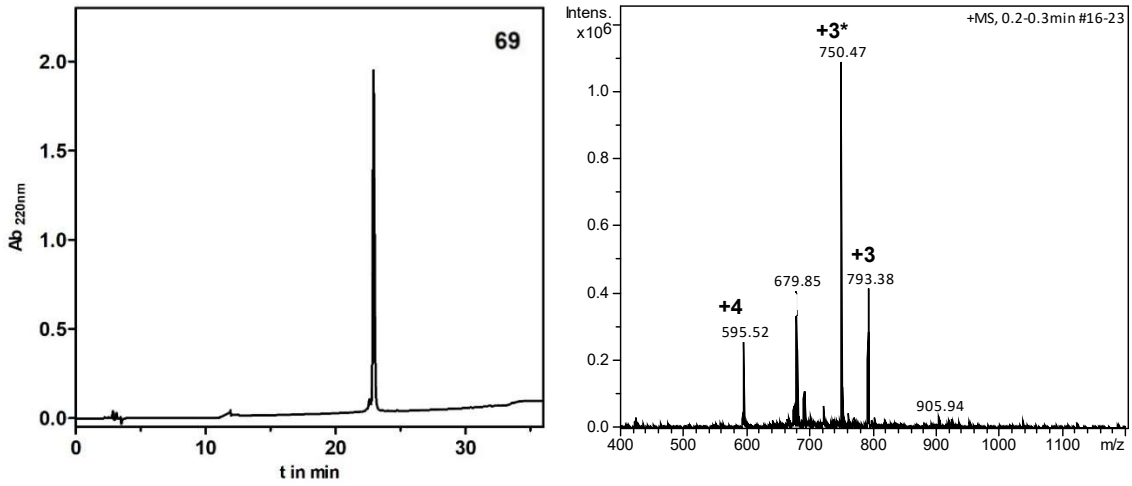

Figure A56. RP-HPLC profile and ESI-ion trap mass spectrum of somatostatin-Dau conjugate (**69**) (MW_{cal} /MW_{exp} = 2377.72./2377.14 g/mol).

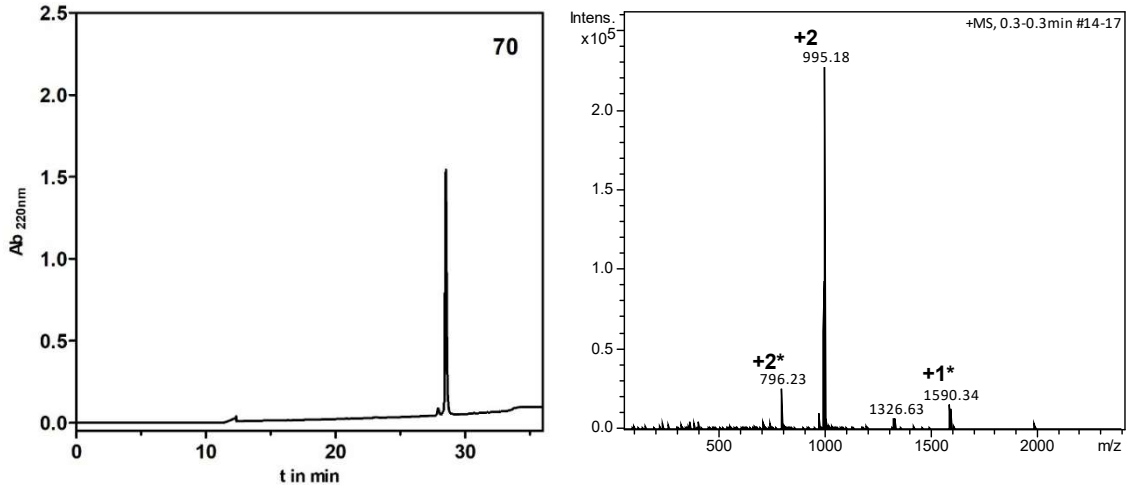

Figure A57. RP-HPLC profile and ESI-ion trap mass spectrum of somatostatin-Dau conjugate (**70**) (MW_{cal} /MW_{exp} = 1989.22/1988.36 g/mol).

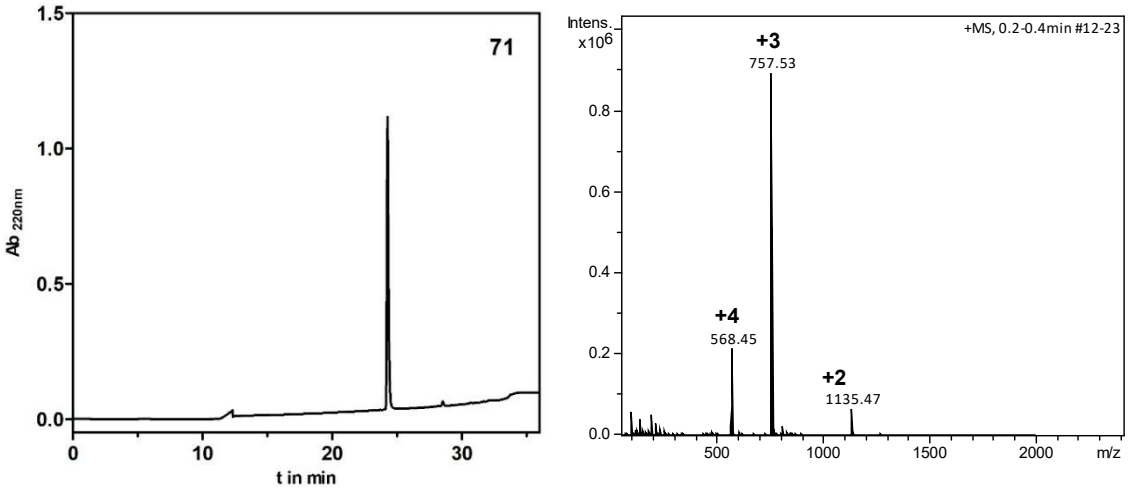

Figure A58. RP-HPLC profile and ESI-ion trap mass spectrum of somatostatin-pyDau conjugate (**71**) (MW_{cal} /MW_{exp} = 2269.60/2269.59 g/mol).

10.2.2.2. In vitro cytostatic effect – Dose response curves

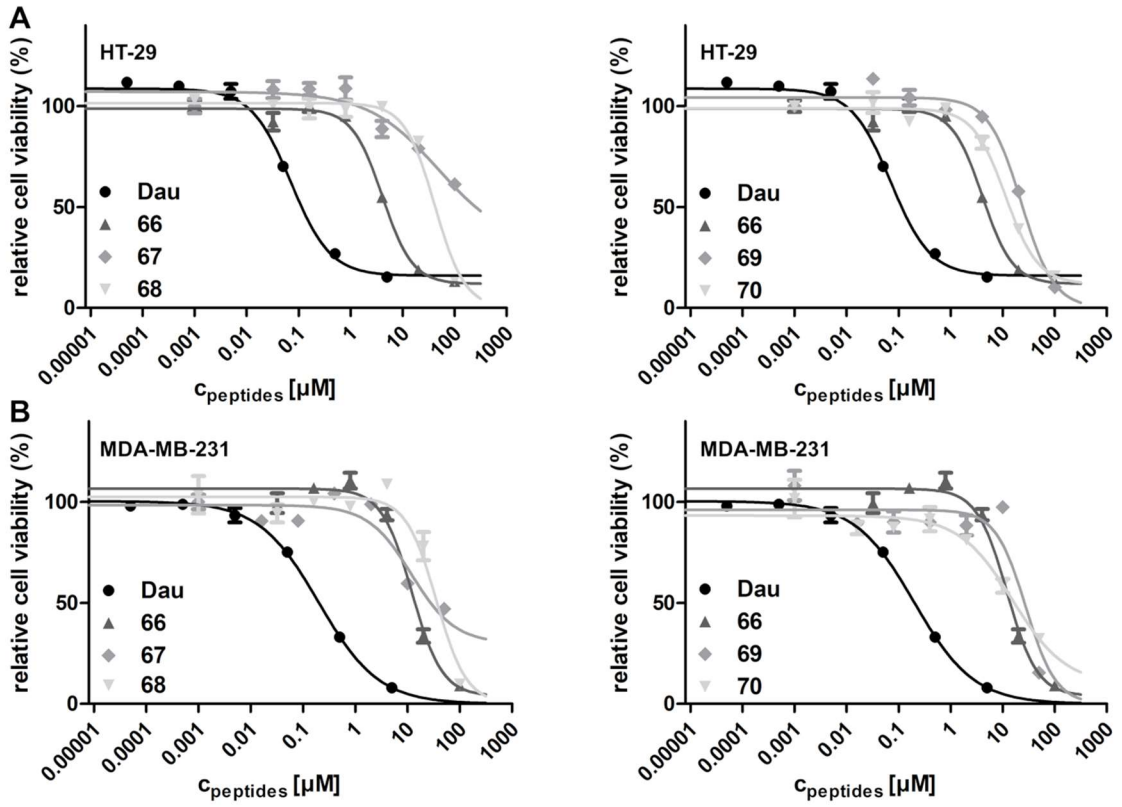

Figure A59. Cytostatic effect of somatostatin-Dau conjugates (**66**-**70**) on **A:** HT-29 and **B:** MDA-MB-231 human cancer cells after 72 h (24 h treatment, additional 48 h incubation). Curves obtained by non-linear regression (sigmoidal dose response, error bars represent the standard deviation of three parallels, the measurements were repeated thrice).

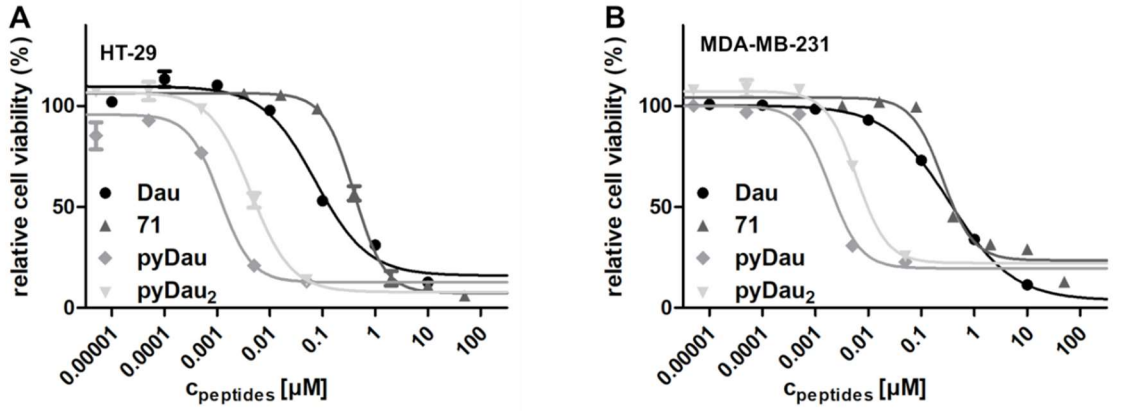

Figure A60. Cytostatic effect of somatostatin-pyDau conjugate **71** on **A:** HT-29 and **B:** MDA-MB-231 human cancer cells after 72 h (24 h treatment, additional 48 h incubation) in comparison to daunorubicin (Dau), pyrrolino-daunorubicin (pyDau) and its dimer ($pyDau_2$). Curves obtained by non-linear regression (sigmoidal dose response, error bars represent the standard deviation of three parallels, the measurements were repeated thrice).

EÖTVÖS LORÁND UNIVERSITY
DECLARATION FORM
for disclosure of a doctoral dissertation

I. The data of the doctoral dissertation:

Name of the author: Schuster Sabine
MTMT-identifier: 10064373
Title and subtitle of the doctoral dissertation: Synthesis of GnRH and Somatostatin Cytotoxic Drug Conjugates
DOI-identifier[72]: 10.15476/ELTE.2019.098
Name of the doctoral school: School of Chemistry
Name of the doctoral programme: Synthetic Chemistry, Materials Science and Biomolecular Chemistry
Name and scientific degree of the supervisor: Prof. Dr. Mező Gábor, Head of the Research Group of Peptide Chemistry
Workplace of the supervisor: Department of Organic Chemistry, Research Group of Peptide Chemistry, Eötvös Loránd University

II. Declarations

1. As the author of the doctoral dissertation,[73]
a) I agree to public disclosure of my doctoral dissertation after obtaining a doctoral degree in the storage of ELTE Digital Institutional Repository. I authorize the administrator of the Department of Doctoral, Habilitational and International Affairs of the Dean's Office of the facultry of Science to upload the dissertation and the abstract to ELTE Digital Institutional Repository, and I authorize the administrator to fill all the declarations that are required in this procedure.
b) I request to defer public disclosure to the University Library and the ELTE Digital Institutional Repository until the date of announcement of the patent or protection. For details, see the attached application form;[74]
c) I request in case the doctoral dissertation contains qualified data pertaining to national security, to disclose the doctoral dissertation publicly to the University Library and the ELTE Digital Institutional Repository ensuing the lapse of the period of the qualification process.;[75]
d) I request to defer public disclosure to the University Library and the ELTE Digital Institutional Repository, in case there is a publishing contract concluded during the doctoral procedure or up until the award of the degree. However, the bibliographical data of the work shall be accessible to the public. If the publication of the doctoral dissertation will not be carried out within a year from the award of the degree subject to the publishing contract, I agree to the public disclosure of the doctoral dissertation and abstract to the University Library and the ELTE Digital Institutional Repository.[76]
2. As the author of the doctoral dissertation, I declare that
a) the doctoral dissertation and abstract uploaded to the ELTE Digital Institutional Repository are entirely the result of my own intellectual work and as far as I know, I did not infringe anyone's intellectual property rights.;
b) the printed version of the doctoral dissertation and the abstract are identical with the doctoral dissertation files (texts and diagrams) submitted on electronic device.
3. As the author of the doctoral dissertation, I agree to the inspection of the dissertation and the abstract by uploading them to a plagiarism checker software.

Budapest, ……, 20…

……

Signature of dissertation author

72 Filled by the administrator of the faculty offices.
73 The relevant part shall be underlined.
74 Submitting the doctoral dissertation to the Disciplinary Doctoral Council, the patent or protection application form and the request for deferment of public disclosure shall also be attached.
75 Submitting the doctoral dissertation, the notarial deed pertaining to the qualified data shall also be attached.
76 Submitting the doctoral dissertation, the publishing contract shall also be attached.